

University of Alberta

The Synthesis of Rhodium Catalyst-Organic Frameworks for Isomerization and
Continuous-Flow Hydrogenation Reactions

by

Elizabeth Gail Corkum

A thesis submitted to the Faculty of Graduate Studies and Research
in partial fulfillment of the requirements for the degree of

Doctor of Philosophy

Department of Chemistry

©Elizabeth Gail Corkum
Fall 2013
Edmonton, Alberta

Permission is hereby granted to the University of Alberta Libraries to reproduce single copies of this thesis and to lend or sell such copies for private, scholarly or scientific research purposes only.

Where the thesis is converted to, or otherwise made available in digital form, the University of Alberta will advise potential users of the thesis of these terms.

The author reserves all other publication and other rights in association with the copyright in the thesis and, except as herein before provided, neither the thesis nor any substantial portion thereof may be printed or otherwise reproduced in any material form whatsoever without the author's prior written permission.

Abstract

The development of immobilized asymmetric catalysts is of vital importance as it would allow for easy catalyst recovery from the reaction mixture and reuse. One strategy for immobilization involves the synthesis of insoluble polymer-supported catalysts. Most polymeric catalysts are made by polymerizing a chiral ligand, or grafting the ligand to a polymer support, followed by metallation of the ligand sites. The resulting catalysts are often plagued by poor activity and reusability due to incomplete metallation, limited access to catalytic active sites and metal leaching. The Bergens group developed a method where a ruthenium metal-containing monomer (MCM) is directly polymerized by alternating ring-opening metathesis polymerization (altROMP) and deposited on insoluble barium salts. The resulting catalyst-organic frameworks (COFs) exhibited remarkable reuse with no drop in activity or selectivity and no detectable ruthenium leaching. This dissertation describes the extension of the altROMP methodology to rhodium-BINAP containing catalysts and their use in the intramolecular cycloisomerization of 1,6-enynes, solvent-free allylic alcohol isomerizations and continuous-flow olefin hydrogenations.

The altROMP of MCMs $[\text{RhCl}((R)\text{-}5,5'\text{-dinatorimido-BINAP})]_2$ (**I**) and $[\text{Rh}(\text{NBD})((R)\text{-}5,5'\text{-dinatorimido-BINAP})](\text{SbF}_6)$ (**II**), with cyclooctene as a spacer monomer, and with $\text{RuCl}_2(\text{CHPh})(\text{PCy}_3)_2$ as the ROMP catalyst,

gave two novel rhodium-BINAP COFs, **Ia** and **Ila** respectively, that were subsequently deposited on BaSO₄ or Ba-L-tartrate.

Framework **Ia** sustained up to six reuses and provided the highest TONs to date (up to 890), with no drop in enantioselectivity (95-99.9% *ee*), in the cycloisomerization of 1,6-enynes. As well, a key intermediate in the production of pharmaceutical (+)-pilocarpine was afforded in >99.9% *ee*. Framework **Ia** also provided the highest TONs to date (up to 38,000) for the rhodium catalyzed isomerization of secondary allylic alcohols with catalyst loadings as low as 0.0025 mol%. In both cases, the COF proved to be more active and selective than the parent homogeneous catalyst. Framework **Ila** proved to be highly active in the continuous-flow hydrogenation of a variety of olefin-containing substrates and sustained up to 55,700 TOs over a period of 30 days in the H-Cube® continuous-flow reactor. As well, in a preliminary study, >99.9% *ee* was obtained in the continuous-flow hydrogenation of itaconic acid by framework **Ia**.

Acknowledgements

I would like to thank my supervisor Steve for providing me with an innovative and challenging research project for my graduate program. I greatly appreciate the numerous discussions we had and the guidance you provided.

To Sonja Francis and Jeremy John... we started this journey together in 2008 as the newest members of the Bergens group and it seems only right that we are finishing it together. I love you both and am so grateful for your friendship and support.

To my good friend and coworker Michael Hass, you have been an integral part of my life, both in and out of the lab. I will always cherish our all-you-can-eat sushi dates and your advice regarding which designer purse I absolutely must buy. You truly are an amazing person and I am so happy to have you in my life.

To the past members of the Bergens group, Dr. Matthew Markiewicz, Dr. Satoshi Takebayashi and Andrew Sullivan, I am extremely grateful for all of your advice and guidance during the good times and the more frustrating times. Thank you so much for listening!

To the current members of the Bergens group, Suneth Kalapugama, Rasu Loorthuraja and Austin Penner, you have all been amazing to work with and made coming to work every day a real joy. I wish you all the best of luck in your research.

To Dr. Jason Cooke, I am so thankful for your advice and support. I found our numerous discussions truly motivating and inspiring and I would like to thank you for helping me conquer many obstacles throughout the later stages of my grad school career.

I would like to thank Dr. Rod Wasylishen and Guy Bernard for their help with the solid state NMR analysis and spectral acquisition and Dr. John Duke for performing the neutron activation analysis study. It was a pleasure working with all of you.

I am extremely grateful for the expertise and experience of the support staff in the NMR Laboratory, Analytical and Instrumentation Laboratory, Electronics and Machine Shops, Glassblowing Shop, Chemical Stores and Receiving, and Purchasing. I would like to extend a special thanks to Wayne Moffat and Dieter Starke whose contributions have been innumerable and integral to my research.

I would like to thank all of my friends back home and in Alberta for their support, especially Brent Rudyk and Greg Kaufman. I am grateful for all of the experiences and memories that we created and I can't wait until we are all reunited once more.

I am so extremely thankful for my loving and supportive family without which none of this would have been possible. To Ben, Chris and Ashley, thanks for always being there for me and providing many much needed distractions. To my mom and dad, thanks for all of the encouragement throughout this process. I love you both so much and

could not have done this without you. To Sharon, Eric, Lillian and Mike, you have been the best home away from home I could have asked for and made me feel like family from day one. You all have a special place in my heart.

To Teague... where do I begin. I can't even put into words how thankful I am for your love and support. You have been my rock, my shoulder to cry on, my greatest supporter and best friend. I love you so much and can't wait to begin the next chapter of our lives together.

I would like to extend a special thank you to Dr. Anna Jordan. You were always in my corner and had my best interests at heart. Thank you so much for being my confidant, mentor and friend.

Table of Contents

Chapter		Page
1	Introduction	
	The importance of enantiopure compounds	1
	Asymmetric catalysis and the need to immobilize	2
	Benefits of immobilization and methods used	5
	Polymer-supported catalysts	7
	Pioneering work by Grubbs and Kagan	8
	Polymer-supported BINAP systems	11
	Grafting to polystyrene	11
	Copolymerization	20
	Alternating ROMP assembly	28
	Research objectives	32
	References	33

2	Polymer-Supported Rhodium-BINAP Catalyst-Organic Frameworks Synthesized by Ring-Opening Metathesis Polymerization	
	Introduction	40
	Section A: Ring-opening metathesis polymerization (ROMP)	40
	Section B: Modification of BINAP	50
	Section C: Synthesis of a ROMP-active BINAP ligand	54
	Results and Discussion	63
	Section A: Synthesis of [RhCl((<i>R</i>)-5,5'-dinorimido-BINAP)] ₂ (38) MCM	63
	Section B: Synthesis of [Rh(NBD)((<i>R</i>)-5,5'-dinorimido-BINAP)](SbF ₆) (40) MCM	66
	Section C: Polymerization of MCMs 38 and 40 via Alternating ROMP Assembly (altROMP)	72
	Section D: Deposition of Frameworks 41 and 42 on Insoluble Supports	88
	Section E: Activation of Catalyst-Organic Frameworks 41 and 42	90

Conclusion	93
Experimental	94
References	105
3 The Asymmetric Intramolecular Cycloisomerization of 1,6-Enynes	
Introduction	115
Results and Discussion	126
Section A: Synthesis of 1,6-Enyne Substrates	126
Section B: Reusability of the Polymer-Supported Rhodium Catalyst-Organic Framework 41 for the Cycloisomerization of 1,6-Enynes	128
Section C: Batch Reactivity of the Polymer-Supported Rhodium Catalyst-Organic Framework 41 for the Cycloisomerization of 1,6-Enynes	138
Section D: Comparison of the Polymer-Supported Rhodium Catalyst-Organic Framework 41 to the Homogeneous Catalyst Analogue	143
Section E: Production of a (+)-Pilocarpine Precursor	146

Conclusion	149
Experimental	150
References	163
4 The Solvent-Free Isomerization of Allylic Alcohols	
Introduction	166
Results and Discussion	176
Section A: Isomerization of Primary Allylic Alcohols	176
Section B: The Effect of Silver Salts on the Catalytic Activity of the Polymer-Supported Rhodium Catalyst-Organic Framework 41	180
Section C: Isomerization of Secondary Allylic Alcohols	182
Section D: Comparison of the Polymer-Supported Rhodium Catalyst-Organic Framework 41 to the Homogeneous Catalyst Analogue	188
Section E: Kinetic Resolution of 3-Buten-2-ol	190
Conclusion	194

Experimental	196
References	200

5 The Continuous-Flow, Asymmetric Hydrogenation of Olefins

Introduction	204
Section A: Rhodium-BINAP Catalyzed Asymmetric Hydrogenation Reactions	204
Section B: Continuous-Flow Hydrogenation Reactions	214
Results and Discussion	227
Section A: Activation of the Poly-[Rh(NBD)(N-BINAP)](SbF ₆)/BaSO ₄ Catalyst-Organic Framework 42 via Hydrogenation of 3-Buten-2-ol	227
Section B: Secondary Allylic Alcohol Size Effects	232
Section C: Hydrogenation of Dehydro Amino Acid Derivatives	234
Section D: Hydrogenation of Itaconic Acid	239
Section E: Hydrogenation of Dimethyl Itaconate	244

Section F: Kinetic Resolution/Hydrogenation of α -Vinylbenzyl Alcohol	246
Section G: Overall Summary of the Poly-[Rh(NBD)((<i>R</i>)-5,5'-dinorimido-BINAP)](SbF ₆)/BaSO ₄ Catalyst-Organic Framework 42 Activity	251
Section H: CatCart® Removal from the H-Cube®	253
Section I: Solid State NMR Analysis	254
Section J: Neutron Activation Analysis	259
Section K: CatCart® Lifetime Assessment	262
Section L: Utilization of the Poly-[RhCl((<i>R</i>)-5,5'-dinorimido-BINAP)] ₂ /Ba-L-tartrate 41 Catalyst-Organic Framework in the H-Cube®	263
Conclusion	270
Experimental	272
References	281
6 Concluding Remarks	
General summary	287

Section A: Synthesis of Polymer-Supported Rhodium Catalyst- Organic Frameworks via AltROMP Assembly	288
Section B: Intramolecular 1,6-Enyne Cycloisomerizations	289
Section C: Solvent-Free Allylic Alcohol Isomerizations	291
Section D: Continuous-Flow Hydrogenations	292
Section E: Future Directions	294
References	296

List of Tables

Chapter		Page
1	No Tables	
2	Table 2-1. Rh(I)-catalyzed asymmetric hydrogenation of functionalized olefins using substituted BINAP-phosphinite ligands.	53
3	Table 3-1. Reuse results for the cycloisomerization of the cyclohexyl1,6-enyne substrate 53 catalyzed by the polymer-supported rhodium catalyst-organic framework 41 .	130
	Table 3-2. Reuse results for the cycloisomerization of the phenyl 1,6-enyne substrate 46 catalyzed by the polymer-supported rhodium catalyst-organic framework 41 .	136
	Table 3-3. Batch reactivity results for the cycloisomerization of the cyclohexyl1,6-enyne substrate 53 catalyzed by the polymer-supported rhodium catalyst-organic framework 41	140

	Table 3-4. Batch reactivity results for the cycloisomerization of the phenyl 1,6-enyne substrate 46 catalyzed by the polymer-supported rhodium catalyst-organic framework 41 .	142
	Table 3-5. Synthesis of lactone 52 ; a precursor to the pharmaceutical (+)-pilocarpine.	147
4	Table 4-1. Solvent-free isomerization of 3-buten-2-ol 71 using different silver salts.	180
	Table 4-2. Solvent-free batch isomerization reactions of secondary allylic alcohols catalyzed by rhodium catalyst-organic framework 41 .	184
	Table 4-3. Comparison of the rhodium catalyst-organic framework 41 and the homogeneous $[\text{RhCl}((R)\text{-BINAP})_2]$ catalyst in the solvent-free isomerization of 3-buten-2-ol 71 .	189
5	Table 5-1. Catalyst activation with 3-buten-2-ol.	229
	Table 5-2. Continuous-flow hydrogenation/isomerization of allylic alcohol substrates catalyzed by rhodium catalyst-organic framework 42 .	233

Table 5-3. Continuous-flow hydrogenation of α -acetamidocinnamic acid 100 catalyzed by rhodium catalyst-organic framework 42 .	235
Table 5-4. Continuous-flow hydrogenation of MAA catalyzed by rhodium catalyst-organic framework 42 .	236
Table 5-5. Continuous-flow hydrogenation of itaconic acid 102 catalyzed by rhodium catalyst-organic framework 42 .	240
Table 5-6. Continuous-flow hydrogenation of dimethyl itaconate 88 catalyzed by rhodium catalyst-organic framework 42 .	244
Table 5-7. Continuous-flow hydrogenation of α -vinylbenzyl alcohol 77 catalyzed by rhodium catalyst-organic framework 42 .	248
Table 5-8. Summary of the longevity and total TONs obtained from the CatCarts® loaded with the rhodium catalyst-organic framework 42 .	251
Table 5-9. Neutron activation analysis of the rhodium catalyst-organic framework 42 before and after use in the H-Cube®.	260

Table 5-10. Continuous-flow hydrogenation of 3-buten-2-ol (71) catalyzed by rhodium catalyst-organic framework 41. 265

Table 5-11. Continuous-flow hydrogenation of itaconic acid 102 catalyzed by rhodium catalyst-organic framework 41. 267

6 No Tables

List of Figures

Chapter		Page
1	Figure 1-1. Enantiomers of thalidomide.	1
	Figure 1-2. Non-covalent methods of immobilization.	6
	Figure 1-3. Covalent methods of immobilization.	6
	Figure 1-4. Various (<i>R</i>)-BINAP derivatives and (<i>R,R</i>)-diamines used in Noyori's <i>trans</i> -[RuCl ₂ (diphosphine)(diamine)] catalyst.	17
2	Figure 2-1. Commercially available olefin metathesis catalysts.	43
	Figure 2-2. Chiral environment of an (<i>R</i>)-BINAP-transition metal complex.	50
	Figure 2-3. Diastereomeric atropisomers of 36 .	58
	Figure 2-4. ³¹ P-NMR spectrum of the atropisomers of 36 .	59
	Figure 2-5. ³¹ P-NMR spectrum of rotamerically pure 36 .	61
	Figure 2-6. ¹ H-NMR spectrum of MCM 38 .	64

Figure 2-7. ^{31}P -NMR spectrum of MCM 38 .	65
Figure 2-8. ^1H -NMR spectrum of MCM 40 .	68
Figure 2-9. ^{31}P -NMR spectrum of MCM 40 .	69
Figure 2-10. ^{31}P -NMR spectrum of MCM 40 taken at a higher field.	70
Figure 2-11. ^{31}P -NMR spectrum of framework 41 .	76
Figure 2-12. ^1H -NMR spectra of (a) 38 with COE and 23 after initial mixing and (b) the catalyst-organic framework 41 after 24 hours.	77
Figure 2-13. ^{31}P -NMR spectra of the altROMP assembly of 40 with COE after (a) 24 hours, (b) 48 hours and (c) 72 hours.	83
Figure 2-14. ^1H -NMR spectra of the altROMP assembly of 40 with COE after (a) 24 hours, (b) 48 hours and (c) 72 hours.	85
Figure 2-15. $[\text{Rh}(\text{BINAP})_2]^{2+}$ (45) catalyst resting state.	91

3	Figure 3-1. 1,6-Enyne substrates chosen for the evaluation of the polymer-supported rhodium catalyst-organic framework 41 .	126
	Figure 3-2. ¹ H-NMR spectrum of cycloisomerized product 59 .	131
	Figure 3-3. ¹ H-NMR spectra of the effects of the addition of Eu(hfc) ₃ to a racemic sample of cycloisomerized product 59 .	133
	Figure 3-4. ¹ H-NMR spectrum of the addition of Eu(hfc) ₃ to the cycloisomerized product 59 , prepared using the rhodium catalyst-organic framework 41 .	134
4	Figure 4-1. ¹ H-NMR spectrum of the reaction mixture from the solvent-free isomerization of 2-propen-1-ol 68 .	177
	Figure 4-2. Secondary allylic alcohol substrates chosen for the rhodium catalyst-organic framework 41 catalyzed solvent-free isomerization reactions.	183
	Figure 4-3. ¹ H-NMR spectrum of the kinetic resolution reaction mixture mixed with Mosher's acid chloride 78 .	199

5	Figure 5-1. Pharmaceuticals synthesized utilizing rhodium-catalyzed hydrogenation reactions.	205
	Figure 5-2. Keay's 3,3'-disubstituted BINAP ligands.	207
	Figure 5-3. Vizza's silica supported [Rh(NBD)((S)-BINAP)](OTf) catalyst.	209
	Figure 5-4. Recent examples of catalysts used in continuous-flow processes.	217
	Figure 5-5. Schematic representation of the H-Cube®.	218
	Figure 5-6. Ding's rhodium-MonoPhos metal-organic framework 92 .	221
	Figure 5-7. Possible catalyst resting states.	227
	Figure 5-8. Proposed mechanism for the isomerization and hydrogenation of olefins via metal hydride intermediates.	231
	Figure 5-9. Reaction profile for H-Cube® hydrogenations.	238
	Figure 5-10. Catalyst deactivation through formation of a rhodium(III)-alkyl complex.	242
	Figure 5-11. ³¹ P-NMR spectra of used and unused samples of the rhodium catalyst-organic framework 42 .	255

Figure 5-12. ^{31}P -NMR spectral comparison of the (*R*)-5,5'- 257
dinorimido-BINAP-dioxide ligand with the used and unused
poly-[Rh(NBD)((*R*)-5,5'-dinorimido-BINAP)](SbF₆)/BaSO₄
catalyst-organic framework.

6 No Figures

List of Schemes

Chapter		Page
1	Scheme 1-1. Isomerization to produce enantiopure (<i>R</i>)-citronellal and Takasago (-)-menthol synthesis.	3
	Scheme 1-2. Synthesis of (<i>S</i>)-naproxen by asymmetric hydrogenation.	4
	Scheme 1-3. Synthesis of polymer-supported Wilkinson's catalyst.	8
	Scheme 1-4. Polymer-supported DIOP ligand.	9
	Scheme 1-5. Bayston's polymer-supported BINAP ligand.	12
	Scheme 1-6. A key step in the synthesis of carbapenem antibiotics.	13
	Scheme 1-7. Asymmetric hydrogenation using Bayston's polymer-supported Ru-BINAP catalyst.	14
	Scheme 1-8. Synthesis of polystyrene-supported catalyst 11.	18
	Scheme 1-9. Asymmetric hydrogenation of 1'-acetonephthone using polystyrene-supported catalyst 11.	19

	Scheme 1-10. Lemaire's copolymerization of BINAP with diisocyanates.	21
	Scheme 1-11. Synthesis of Chan's soluble, polymer-supported BINAP ligand.	24
	Scheme 1-12. Pu's rigid and sterically regular BINAP containing polymer ligand.	26
	Scheme 1-13. Asymmetric hydrogenation of dehydroamino acids.	27
	Scheme 1-14. Synthesis of catalyst-organic framework 23 by ROMP.	29
	Scheme 1-15. Synthesis of BINAP-based, catalyst-organic framework 26 .	31
2	Scheme 2-1. Mechanism of ROMP.	45
	Scheme 2-2. Buchmeiser's polymer/monolith-supported Pd catalyst prepared by ROMP.	48
	Scheme 2-3. Weck's poly(norbornene)-supported Pd-NHC catalysts prepared by ROMP.	49

	Scheme 2-4. Synthesis of (<i>R</i>)-5,5'-diamino-BINAP 18 .	54
	Scheme 2-5. Ralph's improved nitration of (<i>R</i>)-BINAP.	55
	Scheme 2-6. Synthesis of the ROMP active BINAP ligand 36 .	57
	Scheme 2-7. Synthesis of ROMP active rhodium MCM 38 .	63
	Scheme 2-8. Synthesis of ROMP active rhodium MCM 40 .	67
	Scheme 2-9. Synthesis of polymer-supported catalyst-organic framework 41 from altROMP assembly.	75
	Scheme 2-10. Synthesis of polymer-supported catalyst-organic framework 42 from altROMP assembly.	82
3	Scheme 3-1. The thermal cycloisomerization of 6-octen-1-yne.	116
	Scheme 3-2. Zhang's asymmetric cycloisomerization of 1,6-enyne 46 .	117
	Scheme 3-3. Examples of the rhodium-BINAP catalyzed intramolecular cycloisomerization of 1,6-enynes to produce chiral (a) tetrahydrofurans, (b) lactams, (c) lactones, (d)	119

cyclopentanes and (e) cyclopentanones.

Scheme 3-4. Zhang's proposed mechanism for the intramolecular cycloisomerization of 1,6-enynes catalyzed by $[\text{Rh}(\text{BINAP})]^+$. 121

Scheme 3-5. Synthesis of (+)-blastmycinone. 123

Scheme 3-6. The formation of a spirocycle intermediate for the synthesis of (-)-platensimycin. 124

Scheme 3-7. Zhang's synthesis of a key intermediate in the production of (+)-pilocarpine. 124

Scheme 3-8. Literature procedure for the synthesis of 1,6-enyne **46**. 127

Scheme 3-9. Modified procedure for the synthesis of 1,6-enyne **46**. 128

4 **Scheme 4-1.** Isomerization to produce enantiopure (*R*)-citronellal. 167

Scheme 4-2. Proposed mechanism for the isomerization of allylic alcohols. 168

Scheme 4-3. The isomerization of allylic alcohols catalyzed by Fu's rhodium-phosphaferrocene catalyst.	169
Scheme 4-4. The isomerization of 1-octen-3-ol 64 by Gimeno's ruthenium(II)-(η^6 - <i>p</i> -cymene) complexes 61 , 62 and 63 .	170
Scheme 4-5. Polshettiwar's immobilized RAPTA catalyst 66 .	172
Scheme 4-6. Synthesis of Cadierno's RAPTA complex 67 .	174
Scheme 4-7. The attempted isomerization of 2-propen-1-ol 68 catalyzed by rhodium catalyst-organic framework 41 .	176
Scheme 4-8. Solvent-free isomerization of 3-buten-2-ol 71 catalyzed by rhodium catalyst-organic framework 41 .	179
Scheme 4-9. Noyori's kinetic resolution of 4-hydroxy-2-cyclopentenone 76 .	191
Scheme 4-10. Gimeno's kinetic resolution of α -vinylbenzyl alcohol 77 .	191
Scheme 4-11. The kinetic resolution of 3-buten-2-ol catalyzed by rhodium catalyst-organic framework 41 .	192

5	Scheme 5-1.	The $[\text{Rh}((R,R)\text{-DIPAMP})(\text{sol})_2]^+$ catalyzed synthesis of L-Dopa.	205
	Scheme 5-2.	Noyori's $[\text{Rh}((R)\text{-BINAP})(\text{sol})_2]^+$ catalyzed asymmetric hydrogenation of (<i>Z</i>)- α -benzamidocinnamic acid 80 .	206
	Scheme 5-3.	Asymmetric hydrogenation of 86 using 3,3'-disubstituted BINAP ligands 82-85 .	208
	Scheme 5-4.	Hydrogenation of dimethyl itaconate 88 catalyzed by silica supported $[\text{Rh}(\text{NBD})((S)\text{-BINAP})](\text{OTf})$.	210
	Scheme 5-5.	van Koten's synthesis of a silica supported BINAP ligand 90 .	211
	Scheme 5-6.	Hydrogenation of <i>trans</i> - α -(acetamido)-cinnamic acid 91 catalyzed by silica supported $[\text{Rh}(\text{COD})((R)\text{-BINAP})](\text{BF}_4)$.	212
	Scheme 5-7.	Examples of transition metal catalyzed hydrogenation/reduction reactions performed in the H-Cube®.	220
	Scheme 5-8.	Asymmetric hydrogenation of (<i>Z</i>)-methyl-2-acetamidobut-2-enoate 93 in continuous-flow.	222

Scheme 5-9. Bakos' synthesis of phosphine-phosphoramidite ligand **96**. 224

Scheme 5-10. The asymmetric hydrogenation of (*Z*)- α -acetamidocinnamic acid methyl ester **97** in the H-Cube®. 224

6 No Schemes

List of Equations

Chapter		Page
1	No Equations	
2	No Equations	
3	Equation 3-1. Product isomerization side reaction.	117
4	Equation 4-1. Isomerization of primary and secondary allylic alcohols into aldehydes and ketones.	166
	Equation 4-2. The kinetic resolution of secondary allylic alcohols.	190
5	Equation 5-1. Olefin isomerization and hydrogenation of 3-buten-2-ol 71.	228
	Equation 5-2. Rhodium-carboxylate equilibrium.	243

Equation 5-3. The kinetic resolution of α -vinylbenzyl alcohol 247

77.

6 No Equations

List of Abbreviations

AcOH	acetic acid
altROMP	alternating ring-opening metathesis polymerization
atm	atmospheres
BINAP	(<i>R</i>)- or (<i>S</i>)-2,2'-bis(diphenylphosphino)-1,1'-binaphthyl
BINOL	(<i>R</i>)- or (<i>S</i>)-1,1'-binaphthalene-2,2'-diol
BuLi	butyllithium
CD	cinchonidine
COD	1,5-cyclooctadiene
COE	<i>cis</i> -cyclooctene
COF	catalyst-organic framework
CPME	cyclopentylmethyl ether
dba	dibenzylideneacetone
DCE	1,2-dichloroethane
<i>de</i>	diastereomeric excess
diapen	(<i>R</i>)- or (<i>S</i>)-1,2,-di-4-anisyl-2-isopropyl-1,2-ethylenediamine
DIC	diisopropylcarbodiimide
DIOP	2,3-O-isopropylidene-2,3-dihydroxy-1,4-bis(diphenylphosphino)-butane
DIPAMP	1,2-ethanediylbis[(2-methoxyphenyl)phenylphosphine]
DLS	Dynamic Light Scattering
DMA	<i>N,N</i> -dimethylacetamide

DME	1,2-dimethoxyethane
DMF	<i>N,N</i> -dimethylformamide
dpen	(<i>R,R</i>)- or (<i>S,S</i>)-1,2-diphenylethylenediamine
dppe	1,2-bis(diphenylphosphino)ethane
dppf	1,1'-bis(diphenylphosphino)ferrocene
ee	enantiomeric excess
equiv	equivalents
ESI-MS	electrospray ionization mass spectrometry
Et	ethyl
EtOAc	ethyl acetate
EtOH	ethanol
FDA	United States Food and Drug Administration
g	grams
GC	gas chromatography
GPC	Gel Permeation Chromatography
h	hours
hfc	3-(heptafluoropropylhydroxymethylene)-(+)-camphorate
HOBt	hydroxybenzotriazole
HPLC	high-performance liquid chromatography
ICP	inductively coupled plasma
ICP-AES	inductively coupled plasma atomic emission spectroscopy
ICP-MS	inductively coupled plasma mass spectrometry
<i>i</i> Pr	isopropyl

L-Dopa	L-3,4-dihydroxyphenylalanine
M	molar
MAA	methyl α -acetamido acrylate
MALDI-TOF	matrix-assisted laser desorption/ionization time-of-flight
MAS	magic angle spinning
MCM	metal-containing monomer
Me	methyl
Me-DuPhos	(-)-1,2-bis[(2 <i>R</i> ,5 <i>R</i>)-2,5-dimethylphospholano]
MeOH	methanol
Mes	mesityl
2-MeTHF	2-methyltetrahydrofuran
MHz	megahertz
min	minutes
MonoPhos	(3,5-dioxa-4-phosphacyclohepta[2,1- <i>a</i> :3,4- <i>a'</i>]dinaphthalen-4-yl)dimethylamine
NAA	neutron activation analysis
NBD	norbornadiene
NHC	<i>N</i> -heterocyclic carbene
NMR	nuclear magnetic resonance
Norphos	(2 <i>R</i> ,3 <i>R</i>)-2,3-bis(diphenylphosphino)bicycle[2.2.1]hept-5-ene
NTf ₂	bis(trifluoromethanesulfonyl)amide
OTf	triflate or trifluoromethanesulfonate
PCy ₃	tricyclohexylphosphine

Ph	phenyl
ppb	parts per billion
ppm	parts per million
PS	polystyrene
PS-NH ₂	aminomethylated polystyrene
psi	pounds per square inch
psig	pounds per square inch gauge pressure
PTA	phosphotungstic acid
Py	pyridine
<i>rac</i>	racemic
ROMP	ring-opening metathesis polymerization
rt	room temperature
s	seconds
S/C	substrate to catalyst ratio
SEM	Scanning Electron Microscopy
Sub	substrate
^t Bu	tert-butyl
<i>t</i> -BuOK	potassium <i>tert</i> -butoxide
TEM	Transmission Electron Microscopy
Temp	temperature
THF	tetrahydrofuran
TO	turnover
TOF	turnover frequency

TON turnover number

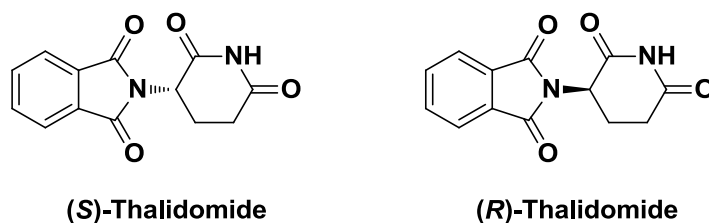
wt% weight percent

Chapter 1

Introduction

The synthesis of enantiopure compounds is an important and rapidly expanding area of chemistry with applications in the agrochemical,¹ flavouring and fragrance,² and pharmaceutical³ industries. For example, in 2006, 80% of small-molecule pharmaceuticals approved by the United States Food and Drug Administration (FDA) were chiral, 75% of which were composed of a single enantiomer.⁴ The demand for enantiopure pharmaceuticals results from strict regulations imposed by the FDA⁵ regarding the use of racemates as drugs. Racemic pharmaceuticals pose a potentially hazardous problem to public health in that one enantiomer often exhibits the desired bioactivity while the other enantiomer exhibits decreased bioactivity, complete inactivity, or some degree of toxicity. An infamous example is thalidomide (Figure 1-1) where (*R*)-thalidomide relieves nausea and acts as a sedative while (*S*)-thalidomide is a teratogen.⁶

Figure 1-1. Enantiomers of thalidomide.



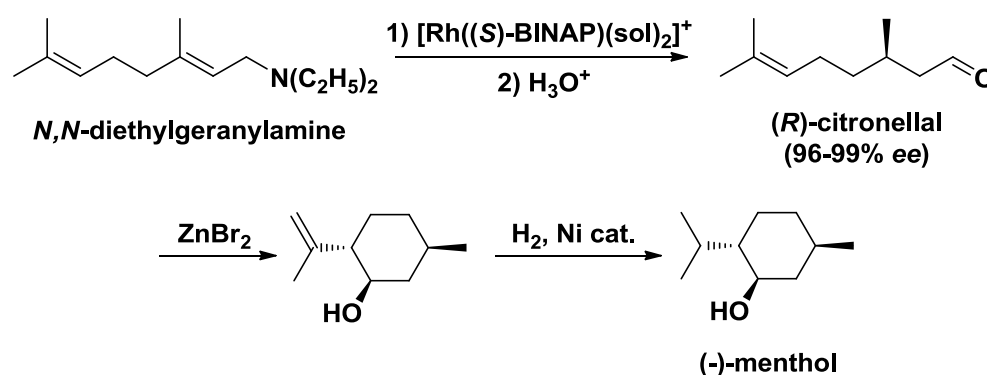
Racemic thalidomide was prescribed to pregnant women in the late 1950s and early 1960s for treatment of morning sickness and tragically caused numerous cases of deformities and birth defects in newborns. To prevent further tragedies, both enantiomers of any prospective racemic pharmaceutical must undergo complete toxicological testing, resulting in an increase in time and cost of development. Thus, the synthesis of enantiopure compounds, for pharmaceutical use in particular, is a very attractive alternative.

Enantiopure compounds can be prepared from a wide variety of methods including resolution of racemates, transformation of pre-existing chiral compounds, chirality transfer reactions, and chirality multiplication via asymmetric catalysis.⁷ Asymmetric catalysis is the enantioselective conversion of a prochiral substrate to a chiral product through the use of a chiral catalyst and is arguably the most efficient method to produce enantiopure compounds as only a small amount of chiral catalyst is required to produce large quantities of enantiopure product. Asymmetric catalysis also has the most potential for general asymmetric synthesis as chiral catalysts can be easily tailored/modified for desired reactions. As well, catalysis in general is more environmentally friendly than large-scale, stoichiometric reactions in that less waste and byproduct material is generated.

Asymmetric catalysis is currently utilized in the industrial synthesis of a variety of natural products. One such example is the rhodium-(S)-

BINAP ((*S*)-BINAP = (*S*)-2,2'-bis(diphenylphosphino)-1,1'-binaphthyl)) catalyzed isomerization of *N,N*-diethylgeranylamine to give, after hydrolysis, enantio-enriched (*R*)-citronellal⁸ (Scheme 1-1) developed by Ryoji Noyori, recipient of the 2001 Nobel Prize in Chemistry. This reaction is a key step in the industrial synthesis of (-)-menthol, a common anesthetic, which is produced on the scale of 3000 tons per year by the Takasago International Corporation.⁹

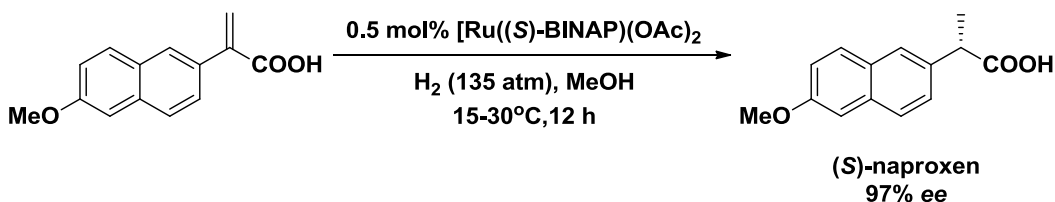
Scheme 1-1. Isomerization to produce enantiopure (*R*)-citronellal and Takasago (-)-menthol synthesis.



Another example illustrating the importance of asymmetric catalysis in industry is the ruthenium-(*S*)-BINAP-catalyzed hydrogenation of unsaturated carboxylic acids in the synthesis of (*S*)-naproxen,¹⁰ a common non-steroidal anti-inflammatory medication (Scheme 1-2). The enantioselectivity of this reaction is of particular importance as (*S*)-naproxen is approximately 30 times more effective than (*R*)-naproxen.¹¹

Thus, a lower dosage of enantiopure (*S*)-naproxen will provide the desired bioactivity while reducing potentially harmful side-effects.

Scheme 1-2. Synthesis of (*S*)-naproxen by asymmetric hydrogenation.



Despite the obvious advantages in using asymmetric catalysis to obtain enantiopure compounds, there are some inherent challenges that are ultimately affecting the utility and applicability of the catalysts. In particular, the catalysts are usually quite toxic due to the presence of the transition metal center.¹² Thus, there is the requirement for potentially costly and time consuming clean-up steps to separate catalyst residues from the product(s). To further complicate matters, the transition metal catalysts typically decompose during the clean-up process, preventing catalyst reuse. In addition, the catalysts are often air sensitive, requiring specialized handling techniques, and, finally, the catalyst itself is often quite expensive. In fact, the chiral ligands can be more costly than the transition metal precursors required for catalyst synthesis.¹³ Due to the high cost of these catalysts, combined with the requirement for low product toxicity, a significant amount of research in the field of asymmetric catalysis has been directed towards the development of immobilized chiral

catalysts in an effort to reduce costs and provide more sustainable and environmentally friendly industrial processes for the production of enantiopure compounds.¹⁴

The goal of immobilizing homogeneous catalysts is to combine the advantages of homogeneous catalysis with those of heterogeneous catalysis. Specifically, heterogeneous catalysts can be easily separated from the desired product(s) and have the potential to be reused. However, the catalytic efficiencies of heterogeneous catalysts are often lower than homogeneous catalysts due to mass transport and diffusion effects. On the other hand, homogeneous catalysts are difficult to reuse and separate from product(s) but they are usually well-defined at the molecular level. This provides a higher degree of mechanistic insight, which is integral for catalyst fine-tuning. In addition, immobilizing homogeneous catalysts would allow for continuous-flow processes, which would increase the production of chiral compounds significantly (refer to Chapter 5 for an indepth discussion).¹⁵ Therefore, the ideal immobilized catalyst should be easily recovered from the reaction mixture, reused with constant selectivities and activities that are comparable to or better than the homogeneous analogue, and that limit the amount of metal leached into the reaction mixture.

In recent years, various approaches have been developed for the immobilization of homogeneous catalysts with differing degrees of success. The two most general methods of immobilization involve non-

covalent¹⁶ or covalent interactions¹⁷ between the metal center and the support or between a chiral ligand and the support. Non-covalent methods of immobilization include electrostatic interactions between ionic catalysts and supports, adsorption of a catalyst onto a support and entrapment of a catalyst within a support¹⁶ (Figure 1-2). Covalent methods of immobilization include the formation of a direct metal-support bond and the formation of a bond between a modified ligand and a support¹⁷ (Figure 1-3).

Figure 1-2. Non-covalent methods of immobilization.

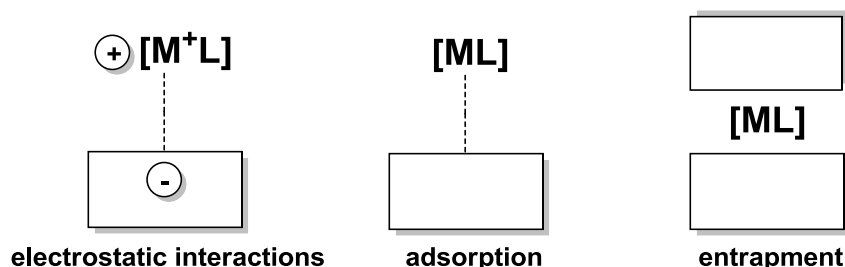
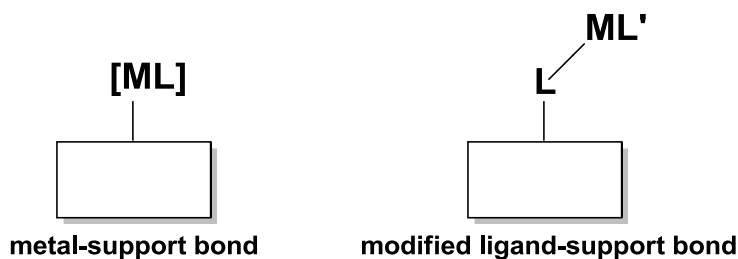


Figure 1-3. Covalent methods of immobilization.



In addition to non-covalent and covalent immobilization techniques, the emergence of biphasic systems in catalysis is another promising method of immobilization. In biphasic systems, the catalyst is immobilized in one

phase (i.e. aqueous/organic,¹⁸ supercritical CO₂,¹⁹ fluoruous solvents²⁰ and ionic liquids²¹), the substrate(s)/product(s) are retained in the other phase and the reaction itself takes place at the interface between the two phases. This is a very attractive technique due to the ease of separating and isolating the catalyst and products and the interested reader is directed to the following reviews on the subject.¹⁸⁻²¹

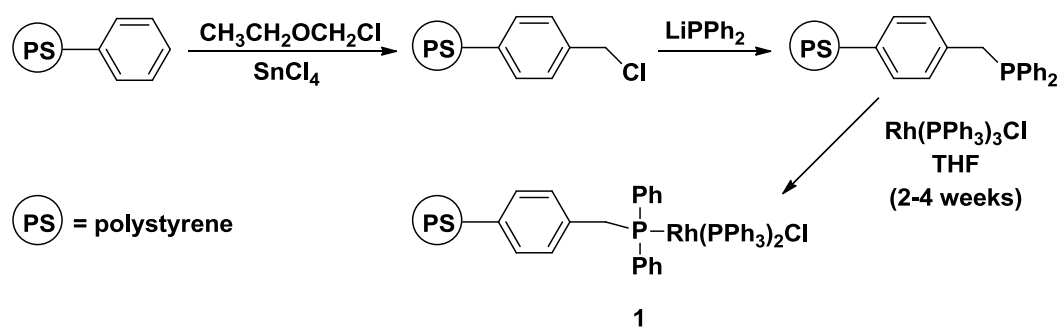
Despite the recent advances, non-covalently immobilized catalysts remain plagued by poor activity compared to their homogenous analogues and attempts at catalyst reuse are not very promising. It is probable that significant metal leaching occurs over the catalyst lifetime, due to the relatively weak interaction between the catalyst and the support, resulting in this poor activity and reusability. Covalent immobilization has become a more attractive technique as the interaction between the catalyst and the support is quite strong, which would prevent significant metal leaching, hence resulting in improved reusability. However, covalently immobilized catalysts often have unpredictable activities and selectivities due to changes in the electronic environment of the metal center upon formation of direct metal-support or ligand-support bonds. As a more comprehensive discussion is outside the scope of this project, the interested reader is directed to the following reviews and the references therein.^{16,17}

A significant amount of research has been focused on synthesizing polymer-supported asymmetric catalysts by either copolymerization of modified catalyst ligands or grafting modified ligands onto polymeric

supports. Polymerization as a means to immobilize homogeneous catalysts provides a strong interaction between the catalyst and the support, limiting metal leaching and increasing reusability potential. As well, polymerized units and/or polymerizable functional groups can be incorporated into chiral ligands easily and with a large degree of synthetic control, limiting potential support effects on the electronic environment of the metal center resulting in more predictable catalytic activity and selectivity.

Early approaches for synthesizing polymer-supported catalysts were inspired by Merrifield's solid-phase peptide synthesis, where polystyrene was chosen as the support.²² In 1971, Grubbs reported the first example of a polymer-supported rhodium-phosphine catalyst for olefin hydrogenation reactions (Scheme 1-3).²³

Scheme 1-3. Synthesis of polymer-supported Wilkinson's catalyst.

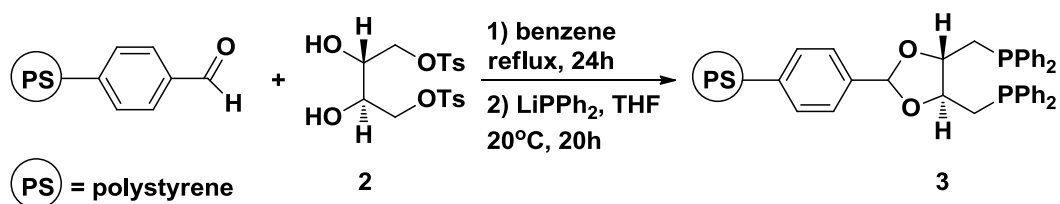


In this report, the polystyrene support was first functionalized by electrophilic chloromethylation²⁴ and then reacted with lithium diphenylphosphide to incorporate diphenylphosphinomethyl groups into

the support. The polymer-supported ligand was then treated with a two-fold excess of tris(triphenylphosphine)rhodium(I) chloride for a period of 2-4 weeks in THF to give the immobilized version of Wilkinson's catalyst (**1**). The synthesis of **1** was quite sluggish and elemental analysis indicated that only 17% of the available phosphine groups had been successfully metallated, making this methodology impractical. However, the immobilized catalyst was reused 10 times for the hydrogenation of cyclohexene in benzene and had comparable activities to unsupported Wilkinson's catalyst for the hydrogenation of a variety of olefins, thus demonstrating that polymerization to covalently immobilize homogeneous catalysts was a viable immobilization technique that required further investigation and optimization.

As a direct extension of Grubbs' polymer-supported Wilkinson's catalyst, the first polymer-supported chiral enantioselective catalyst was reported by Kagan in 1973 where their chiral diphosphine ligand DIOP, (2,3-O-isopropylidene-2,3-dihydroxy-1,4-bis(diphenylphosphino)-butane), was supported on polystyrene (Scheme 1-4) and used in the hydrogenation of olefins.²⁵

Scheme 1-4. Polymer-supported DIOP ligand.

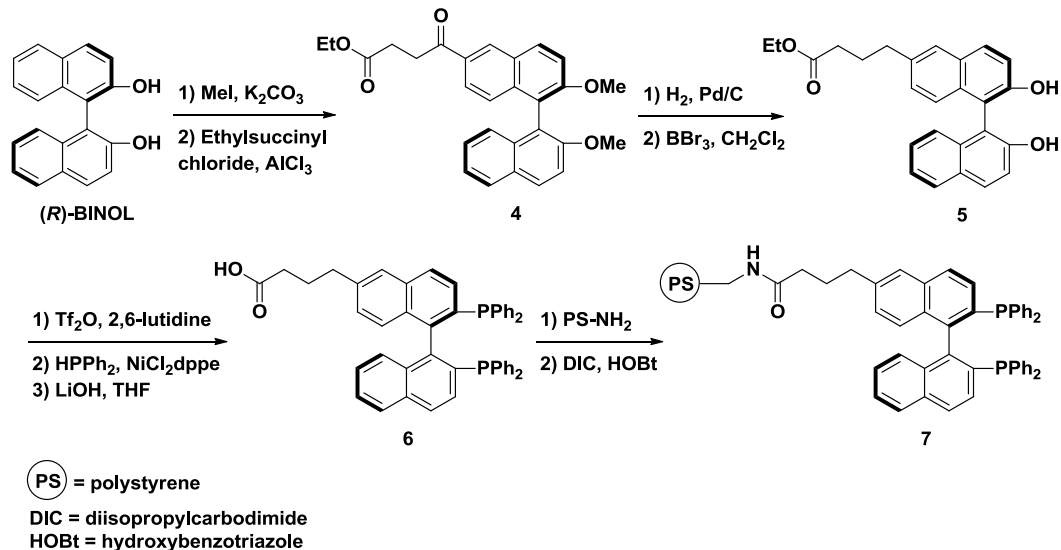


Here, the chiral diol **2** was reacted with polystyrene-supported benzaldehyde and then treated with lithium diphenylphosphide to give polymer-supported DIOP. **3** was then reacted with Cramer's compound, $[\text{RhCl}(\text{C}_2\text{H}_4)_2]_2$, in benzene at room temperature for 21 hours to generate the polymer-supported chiral rhodium-DIOP catalyst. The immobilized catalyst was used for the asymmetric hydrogenation of simple olefins but the activity and enantioselectivity was much poorer than the homogeneous rhodium-DIOP analogue. For example, the polymer-supported catalyst quantitatively hydrogenated α -ethylstyrene to 2-phenylbutane in 12 hours at room temperature with an ee of only 1.5%. However, the homogeneous rhodium-DIOP catalyst performed the same hydrogenation quantitatively in 5 hours with an ee of 15%. As well, the polymer-supported catalyst was unable to hydrogenate α -acetamidocinnamic acid at all. Kagan attributed the poor enantioselectivity to some unknown support effect and the low activity to poor solvent compatibility. In particular, the polystyrene resin was observed to contract strongly in ethanol, which is the solvent of choice for the hydrogenation of dehydroamino acids, thus preventing substrate from accessing the catalytic active sites. In fact, the polymer-supported catalyst was unable to hydrogenate even simple olefins when a more polar solvent was chosen. To this day, solvent dependence, mass transport to the catalytic active sites and unknown support effects remain characteristic features of immobilized asymmetric catalysts and continue to pose challenges.

These early examples of polymer-supported catalysts provide little in terms of practical application. However, they do illustrate the common challenges and the viability of polymerization as a method of immobilizing homogeneous catalysts. More recently, significant developments have been made in bridging the gap between polymer-supported catalysts and their homogeneous counterparts. The strategies that are currently employed typically involve the immobilization of BINAP on polymeric supports.²⁶ BINAP is one of the most common and successful ligands in asymmetric catalysis and has been used in a variety of industrially relevant asymmetric transformations, such as the synthesis of (-)-menthol⁸ and (S)-naproxen¹⁰ which were mentioned previously (Schemes 1-1 and 1-2). Specifically, Ru- and Rh-BINAP catalysts have been very well studied and developed for asymmetric isomerization of olefins, C-C bond forming reactions, such as cycloisomerization, and for the asymmetric hydrogenation of a variety of prochiral substrates, such as ketones, olefins and imines.²⁷ As such, the remaining examples that are presented will deal with techniques used to prepare polymer-supported BINAP containing catalysts.

One of the most successful polymer-supported BINAP ligands was reported in 1998 by Bayston where a modified BINAP monomer was grafted onto aminomethylated polystyrene resin (Scheme 1-5).²⁸ In this example, the functionalized BINAP monomer **6** was prepared in three synthetic steps from (*R*)-BINOL. In the first step, the (*R*)-BINOL, protected

Scheme 1-5. Bayston's polymer-supported BINAP ligand.

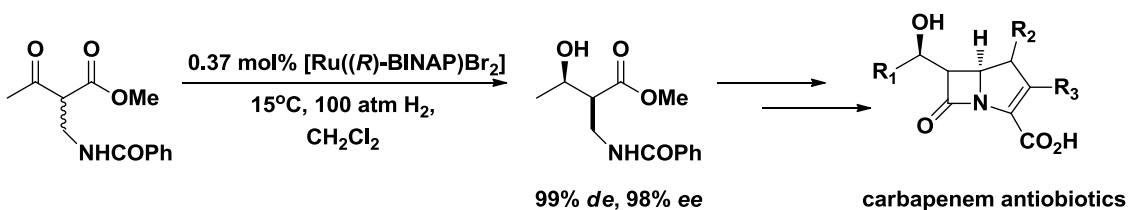


by ether groups, underwent a Friedel-Crafts acylation to form **4**. Next, the ketone group was selectively reduced and the methyl ethers were removed by using BBr₃ to produce **5**. Lastly, after conversion to the ditriflate compound, the two phosphine groups were introduced through routine synthesis of BINAP, which involves a nickel mediated double phosphination with HPPH₂,²⁹ to give the mono-substituted BINAP containing monomer **6**. **6** was then coupled to the commercially available aminomethylated polystyrene by a condensation reaction between the carboxylic acid group on **6** and the amino group on the polystyrene polymer to give the polymer-supported BINAP ligand **7**. In this report it was noted that not all of the available amino groups on the polystyrene were actually ligated with the BINAP containing monomer. Of the available 0.21 mmol of NH₂/g of polystyrene, 0.18 mmol/g were successfully

coupled with **6**. Despite the incomplete incorporation of BINAP onto the polystyrene resin, Bayston postulated that this could potentially provide the bulky ligands with greater degrees of freedom, which would make the resulting polymer-supported catalyst behave more like a solution phase homogeneous catalyst.

As part of the same report, Bayston prepared a Ru-based hydrogenation catalyst by reacting $[(\text{COD})\text{Ru}(\text{methylallyl})_2]$ with the polymer-supported BINAP ligand **7** and HBr in acetone for a period of one hour. The active catalyst that is believed to have been generated is $[\text{Ru}(\mathbf{7})\text{Br}_2]$,³⁰ however there is no reported characterization of the metallated BINAP polymer to substantiate this claim and the number of ligand sites that were actually metallated was not reported. Homogeneous catalysts of the form $[\text{Ru}(\text{BINAP})\text{X}_2]$ ($\text{X} = \text{Cl}, \text{Br}$) were first developed by Noyori for the asymmetric hydrogenation of functionalized ketones.³¹ Today, these types of catalysts are applied in the synthesis of a wide variety of enantiopure pharmaceuticals.³² For example, this catalyst system has been utilized by the Takasago International Corporation for a key step in the synthesis of carbapenem antibiotics (Scheme 1-6).³³

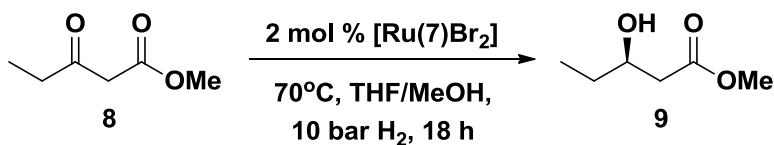
Scheme 1-6. A key step in the synthesis of carbapenem antibiotics.



Therefore, Bayston's immobilization of this catalyst system has the potential to have an immediate impact on an already well established industrial process.

Bayston's polymer-supported Ru-BINAP catalyst was tested in the asymmetric hydrogenation of methyl acetoacetate **8** (Scheme 1-7).²⁸

Scheme 1-7. Asymmetric hydrogenation using Bayston's polymer-supported Ru-BINAP catalyst.



Substrate **8** was hydrogenated using the polymer-supported catalyst in a yield of 99% and in 97% *ee* under the following conditions: S/C = 50, 10 bar H₂, 70°C, THF/MeOH, 18 hours. These results are comparable to the homogeneous Ru-BINAP catalyst, which hydrogenated the same substrate in 100% yield and 99% *ee* under very similar conditions: S/C = 50, 20 bar H₂, 40°C, CH₂Cl₂, 16 hours. The polymer-supported catalyst was easily recovered by filtration, washed with THF and reused by subjecting that catalyst to the same hydrogenation conditions. After the first reuse, there was no drop in yield (99%) and very little decrease in *ee* (91%), however the reaction time did increase to 24 hours. After the second reuse, the yield dropped to 82% and the reaction time was doubled to 36 hours; however, the *ee* remained constant at 90%. In

addition to these results, the reaction products from the immobilized hydrogenations were analyzed for ruthenium content by ICP-AES (inductively coupled plasma atomic emission spectroscopy) and it was determined that less than 1 mol % of the total amount of ruthenium used was leached into the reaction products. The comparable activity of the polymer-supported Ru-BINAP catalyst to the homogeneous analogue coupled with the promising reusability results and minimal ruthenium leaching garnered a lot of attention for Bayston's polymer-supported BINAP ligand. In fact, the commercial availability of **7** has resulted in its use in a variety of heterogeneous, asymmetric catalysts, making it one of the most successful polymer-supported BINAP ligands.

As a direct extension of the work done by Bayston, Chapuis and coworkers at Firmenich reacted the polystyrene-supported BINAP ligand **7** with $[\text{Rh}(\text{COD})_2]\text{CF}_3\text{SO}_3$ to generate the immobilized catalyst $[\text{Rh}(\mathbf{7})(\text{COD})]^+$ (**10**).³⁴ The homogeneous analogue of the supported catalyst, $[\text{Rh}(\text{BINAP})]^+$, was first discovered by Noyori in 1982 and is currently utilized by the Takasago International Corporation for the industrial synthesis of (-)-menthol, which was mentioned earlier in this review (see Scheme 1-1).^{8,9} Specifically, this catalyst is used in the isomerization of *N,N*-diethylgeranylamine to (*R*)-citronellal and represents the first industrial application of BINAP. Interestingly, in the industrial synthesis of (-)-menthol, the homogeneous catalyst $[\text{Rh}(\text{S-BINAP})]^+$ is actually able to be reused, which is a key reason as to why this catalyst is

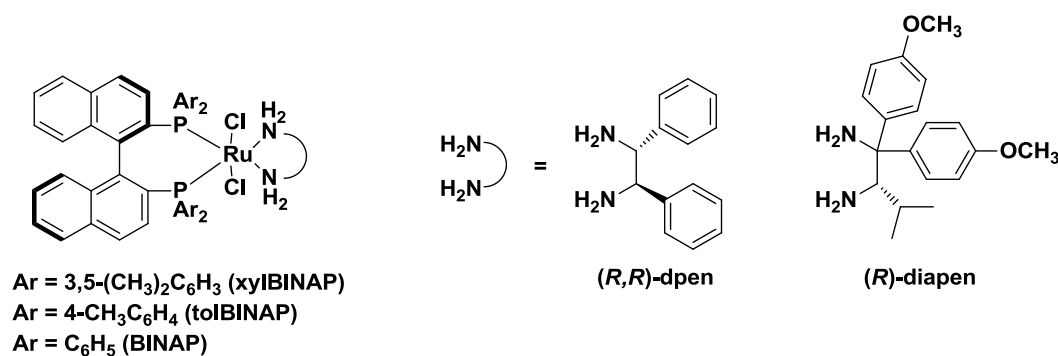
commercially viable. In this case, the catalyst is recovered by distilling off the product. Distillation as a method of catalyst recovery can only be used if the product is volatile as most homogeneous catalysts are thermally sensitive and decompose at elevated temperatures.³⁵ An immobilized catalyst would eliminate the need for the extra distillation step, which would decrease the overall time required between catalyst runs and increase productivity.

Chapuis tested the immobilized catalyst **10** in the asymmetric isomerization of *N,N*-diethylgeranylamine, giving (*R*)-citronellal after hydrolysis (Scheme 1-1), under the following conditions: S/C = 400, refluxing THF, 20 hours. For this reaction, (*R*)-citronellal was obtained in 100% yield and 98% ee. As well, **10** was recovered by filtration and reused 37 times, resulting in a total TON of approximately 14,000. Despite the remarkable reusability and selectivity of the polymer-supported catalyst **10**, the homogeneous catalyst is still far superior in terms of overall activity. In fact, in the industrial process, the homogeneous catalyst converts 8000 equivalents of *N,N*-diethylgeranylamine to (*R*)-citronellal per run (80-100°C, THF) in 99% ee and the catalyst can be reused for more than 50 runs, resulting in a total TON greater than 400,000.

Another prominent BINAP-based catalyst system in the literature is Noyori's *trans*-[RuCl₂(BINAP)(diamine)] catalyst.³⁶ In the presence of base and alcohol solvents, this catalyst system provides very high TONs, TOFs and enantioselectivities for the asymmetric hydrogenation of simple

ketones to alcohols. By altering the chiral diphosphine and diamine portions of this catalyst, one can affectively tune the sterics and electronics of the catalyst to optimize both reactivity and selectivity. An example of common diphosphine and diamine ligands that have been used in the preparation of this catalyst system are illustrated in Figure 1-4.

Figure 1-4. Various (*R*)-BINAP derivatives and (*R,R*)-diamines used in Noyori's *trans*-[RuCl₂(diphosphine)(diamine)] catalyst.

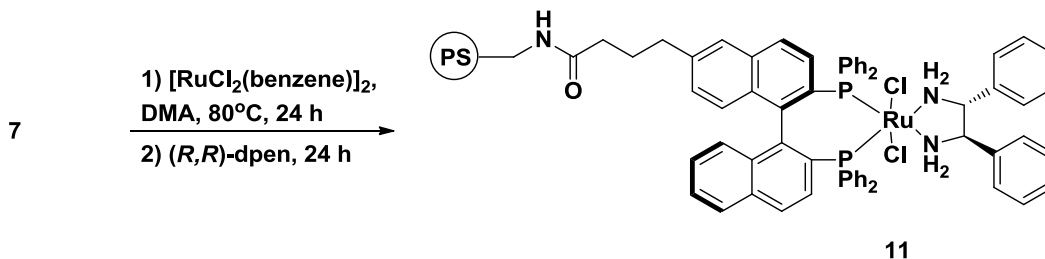


Due to the easily tunable nature of this catalytic system, this technology has been utilized in the synthesis of a variety of chiral pharmaceuticals.³⁷ The industrial applications of this catalytic system make it an ideal candidate for immobilization.

In a particular example, Noyori reacted the complex [RuCl₂(η⁶-benzene)]₂ first with Bayston's polystyrene-supported BINAP ligand **7** (Ru:diphosphine = 3:1) in *N,N*-dimethylacetamide (DMA) at 80°C for 24 hours and then with (*R,R*)-dpen (Ru:diamine = 1:5) for an additional 24 hours to produce the polystyrene-supported catalyst [RuCl₂(**7**)(*R,R*)-

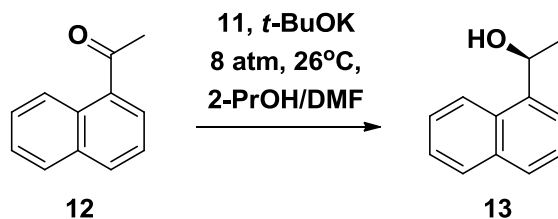
dpen)] (**11**, Scheme 1-8).³⁸ The ³¹P-NMR analysis of the solid product showed that **11** was formed as mixture of the *trans*- and *cis*-dichloro isomers in a 7:1 ratio, both of which are known to catalyze the hydrogenation of ketones. As well, the metallation step was not clean as the polystyrene resin consisted of 81% of the desired Ru-diphosphine/diamine complex contaminated with unreacted polystyrene-supported BINAP ligand **7** and some unknown compounds. Despite the mixture of products, **11** was tested for the asymmetric hydrogenation of various aromatic ketones.

Scheme 1-8. Synthesis of polystyrene-supported catalyst **11**.



When 1'-acetonaphthone (**12**), polystyrene-supported catalyst **11** (S/C = 2470/1) and 2 mol % of *t*-BuOK were added to a 1:1 2-propanol:DMF mixture under 8 atm of H₂ at 26°C for a period of 26 hours, the chiral alcohol **13** was obtained in 99% conversion with an ee of 98% (Scheme 1-9). The ee was identical to the ee obtained with the homogeneous catalyst, *trans*-[RuCl₂((*R*)-BINAP)(*R,R*-dpen)], under the same conditions in 2-propanol solvent.

Scheme 1-9. Asymmetric hydrogenation of 1'-acetonaphthone using polystyrene-supported catalyst **11**.



In addition to the remarkable conversion and *ee*, the catalyst was easily separated from the product solution by filtration and reused in 14 further hydrogenation experiments. The total TON achieved in the 14 experiments was 33,000 and the product enantioselectivity remained consistently high (97-98% *ee*) throughout the reuses. However, the catalyst activity did decrease quite rapidly after the ninth run, where the reaction time was extended from 30 hours to 84 hours for 100% conversion. Noyori also investigated the batch reactivity of this catalyst by performing a 20 gram scale hydrogenation of **12** (S/C = 12,300/1). **13** was obtained in 96% conversion with an *ee* of 97%; however, attempts at reuse under such a high loading of substrate were unsuccessful.

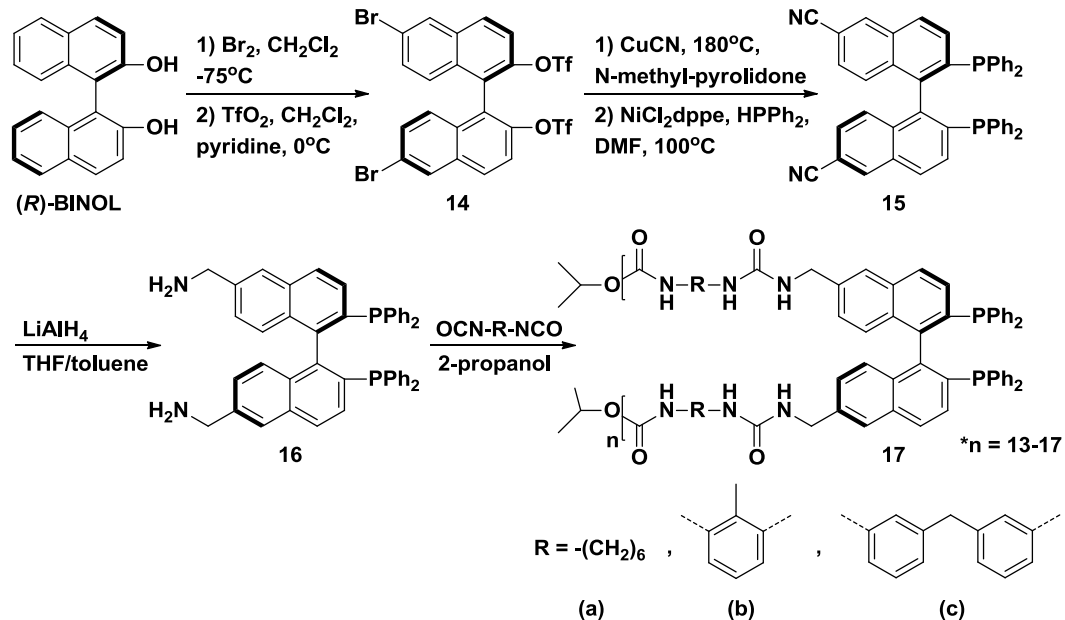
Despite these promising results, the incompatibility of the polystyrene resin with 2-propanol, the optimal solvent for these hydrogenations, remains a significant drawback. DMF was required as a swelling co-solvent to provide better access to the catalytic active sites within the polymer framework in order to maintain a reasonable TOF. Due

to the toxic nature of DMF, this catalyst system would not be suitable for large scale, industrial operations.

The previous examples all involve grafting a modified BINAP ligand onto a polystyrene resin as a way to prepare polymer-supported asymmetric catalysts. However, copolymerization of modified BINAP ligands has also been successful in the preparation of similar polymer-supported catalysts. In fact, copolymerization provides certain advantages that grafting on polymeric supports does not. For example, the copolymerization method allows for fine-tuning of the polymer backbone itself and catalytic active sites can be incorporated along the polymer chain rather than being limited to the terminals of the polymer support. As a result, the remaining examples that are presented will focus on the copolymerization of modified BINAP.

Well known for their research in chiral ligand immobilization, Lemaire and coworkers developed a method to incorporate BINAP into the backbone of a variety of polymers by copolymerization of a 6,6'-substituted BINAP monomer with various diisocyanates (Scheme 1-10).³⁹ In this synthesis, optically pure BINOL was first brominated at the 6,6'-positions, followed by triflation of the alcohol groups to give the protected dibromo-BINOL compound **14**. Next, the two bromo groups were substituted with cyano groups and two phosphine groups were introduced through a nickel mediated double phosphination with HPPH_2 ²⁹ to give 6,6'-dicyano-BINAP **15**. Finally, the cyano groups were reduced using lithium aluminum

Scheme 1-10. Lemaire's copolymerization of BINAP with diisocyanates.



hydride to form the 6,6'-diaminomethyl-BINAP monomer **16**. The monomer underwent poly-condensation with a variety of diisocyanates to generate the BINAP-containing polyureas **17a-c**. The incorporation of the polyurea moiety into the backbone of the polymers was entirely strategic as that functionality is responsible for obtaining the correct solubility/swellability properties in methanol, the solvent of choice for β -keto ester hydrogenations.

The BINAP-containing polyureas **17a-c** were reacted with $[(\text{COD})\text{Ru}(\text{methylallyl})_2]$ and HBr in acetone to generate active hydrogenation catalysts *in situ*. It should be noted that no characterization data were reported for any of the metallated polymers. These catalysts were then tested in the hydrogenation of methyl acetoacetate **8** under the

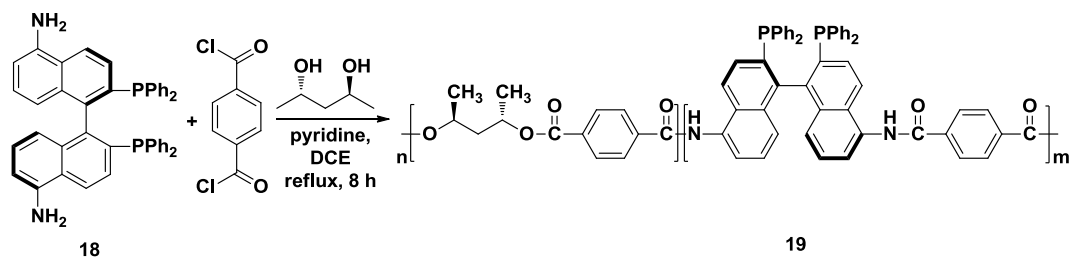
following conditions: S/C = 1000, 40 atm of H₂, 50°C, MeOH, 14 hours. The results showed that the catalyst system containing **17b** was the most effective for the hydrogenation, giving 100% yield and 99% ee. This result is identical to the result obtained from the homogeneous [Ru((*R*)-BINAP)Br₂] catalyst. As well, **17b** was recovered by filtration and reused in two additional runs, under the same conditions, without any drop in activity or selectivity. When **17c** was tested, comparable results were obtained for the first run (97% yield and 99% ee); however, a significant drop in activity, from 97% to 53% yield, occurred upon reuse. The least successful catalyst system contained the flexible ligand **17a**. In the first run, 52% yield and 88% ee were obtained for the hydrogenation; however, reuse of this catalyst was completely unsuccessful. Lemaire attributed these differences in catalytic activity to the rigidity of the polymer-catalyst system. The evidence suggests that the rigidity of the polymer plays an important role in the catalyst activity and selectivity as the more rigid polymer provided better results and was able to be reused (**17b**). Therefore, it is likely that a more rigid polymer is able to maintain a more stable catalyst conformation in the polymer, which is why better activity, selectivity and reusability are obtained. However, too much rigidity can actually restrict access to the catalytic active sites, thereby decreasing yield and enantioselectivity. As an example, Lemaire cross-linked **17b** with 30% tri-isocyanatotoluene to increase the rigidity. As a result of this increase, a large decrease in activity and selectivity (35% yield and 9%

ee) for the hydrogenation of **8** was obtained. This illustrates the importance of the degree of rigidity in the polymer backbone and the necessity of maintaining a balance between stable catalyst conformations and accessibility of the catalytic active sites.

In an attempt to address the inaccessibility of the catalytic active sites in many insoluble, polymer-supported catalysts, Chan reported the first soluble, polymer-supported BINAP catalyst.⁴⁰ This polymer-supported chiral catalyst was designed and developed by using the concept of “one-phase catalysis, two-phase separation”. Essentially what this means is that catalysis will take place in the homogeneous phase, which limits the restriction of the polymer matrix resulting in an increase in overall catalyst activity, and the recovery of the catalyst will be achieved through precipitation, followed by filtration.

The actual synthesis of the soluble, polymer-supported BINAP ligand was achieved through co-polymerization. In particular, (*R*)-5,5'-diamino-BINAP **18** underwent a polycondensation with terephthaloyl chloride and (2*S*,4*S*)-pentanediol in the presence of pyridine in 1,2-dichloroethane (DCE) solvent to give the soluble polymer-supported BINAP ligand **19** (Scheme 1-11). The synthesis of the (*R*)-5,5'-diamino-BINAP component is not covered here but will be discussed in detail in Chapter 2 of this dissertation. The active catalyst was generated *in situ* from **19** and [Ru(cymene)Cl₂]₂ in a methanol-toluene mixed solvent system (2:3, v/v) to give a completely homogeneous solution.

Scheme 1-11. Synthesis of Chan's soluble, polymer-supported BINAP ligand.

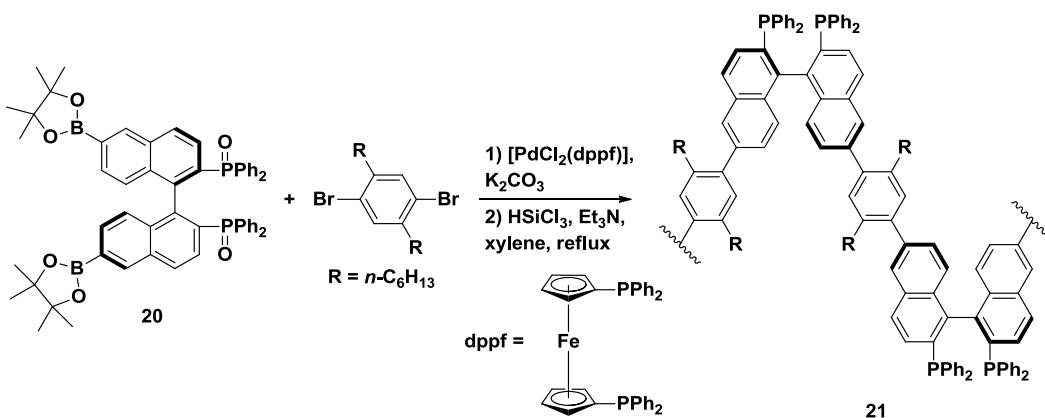


The soluble, polymer-supported catalyst was then tested in the hydrogenation of 2-(6'-methoxy-2'-naphthyl)acrylic acid to naproxen (see Scheme 1-2) under the following conditions: S/C = 200, 1000 psi of H₂, room temperature. After 4 hours, naproxen was obtained in 87.7% ee and 95.5% conversion. Under identical conditions, the homogeneous BINAP-containing ruthenium catalyst gave naproxen in comparable ee (88.7%) but with a much lower conversion of only 56.5%. In addition to the higher activity, the polymer-supported catalyst was quantitatively precipitated from solution, by addition of a large excess (7x) of methanol, filtered and then reused for a further 10 runs with no significant drop in activity or selectivity. The filtrates containing the hydrogenation product were analyzed for metal leaching from the polymer and the level of ruthenium in the samples was found to be less than 16 ppb, indicating that 99.9% of the catalyst was recovered and successfully reused. Although these results are significant and have the potential to directly influence an industry established process, the main limitation is the large excess of solvent

required for the precipitation of the catalyst from solution. The scale-up of this reaction has the potential to generate a significant amount of waste, therefore further research into more compatible solvent systems would need to be pursued.

Another example of a soluble, polymer-supported BINAP-containing catalyst was reported by Pu and coworkers in 2000.⁴¹ In this study, Pu synthesized a rigid and sterically regular BINAP containing polymer, reasoning that the incorporation of rigidity and regularity into the polymer backbone would help to preserve the electronic and steric environment of the monomer catalyst. In particular, the synthesis involved the Suzuki coupling of a chiral BINAP-boronic ester **20** with 1,4-dibromo-2,5-dialkylbenzene, followed by a reduction of the phosphinoxy groups with trichlorosilane to give the polymer-supported BINAP ligand **21** (Scheme 1-12). The BINAP monomer **20** was synthesized in eight steps from optically pure (*R*)-BINOL, which, due to the length and breadth of the synthetic procedure, will not be covered in this dissertation.⁴²

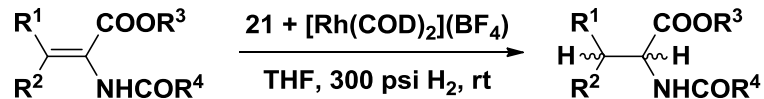
Scheme 1-12. Pu's rigid and sterically regular BINAP containing polymer ligand.



The ^{31}P -NMR analysis of the polymer ligand **21** was dominated by a sharp singlet at -14.8 ppm, identical to the phosphine signal of (*R*)-BINAP, suggesting that the electronic environment of the ligand remained unchanged after polymerization. The ^1H -NMR spectrum was also quite well resolved, indicating that the structure of the polymer is regular and well-defined.

The polymer-supported BINAP ligand **21** is soluble in common organic solvents, including dichloromethane, toluene, THF and chloroform, but is insoluble in methanol. Therefore, the subsequent catalyst was recovered by the precipitation/filtration method outlined by Chan in the previous example. The active catalyst was generated *in situ* by reacting **21** with $[\text{Rh}(\text{COD})_2](\text{BF}_4)$ in a 1.1:1 ratio in THF and tested for the asymmetric hydrogenation of dehydroamino acid derivatives (Scheme 1-13).

Scheme 1-13. Asymmetric hydrogenation of dehydroamino acids.



$\text{R}^1, \text{R}^2, \text{R}^3, \text{R}^4 = \text{H, alkyl or aryl}$

In the hydrogenation of (*Z*)-methyl α -(benzamido) cinnamate (*S/C* = 50), the hydrogenated product was obtained in 99% yield with an *ee* of 75%, which is almost identical to the result obtained from the (*R*)-BINAP-containing homogeneous catalyst (99% yield, 76% *ee*). Despite this promising result, the polymer-supported catalyst was only recovered and reused once before a significant drop in activity and selectivity was observed. The poor reusability of this catalyst could perhaps be due to metal leaching from the polymer; however, no such data were included in this report.

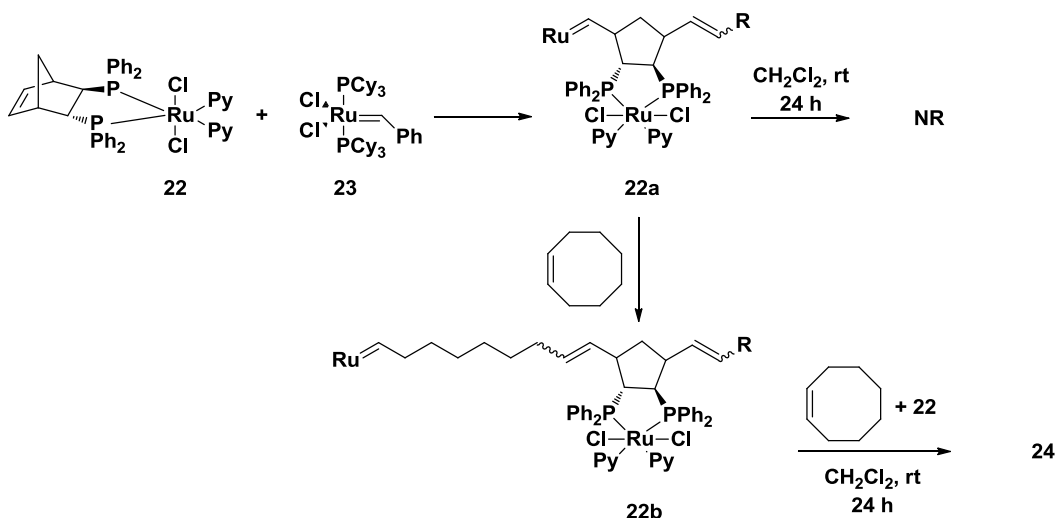
This review provides a good illustration of the common challenges and problems associated with polymer-supported catalysts. In order for these catalysts to be suitable for industrial use, these drawbacks must be addressed. For example, the syntheses of these polymer-supported ligands can be quite complicated and lengthy, involving multiple synthetic steps, resulting in relatively poor overall yield and poor ligand loading. As well, the final immobilized catalyst often suffers from incomplete metallation of the ligand sites and poor mass transport to the catalytic active sites, leading to low catalyst activity and poor reusability. Although

some of the examples did discuss polymer-supported catalysts that exhibited an increase in activity and selectivity compared to the homogeneous analogue, most polymer-supported catalysts still exhibit lower activities. In these cases, the benefits of the recovery and reuse of the catalysts are negated by the decrease in activity compared to the homogeneous catalyst. Therefore, there is a need for more efficient polymer-supported catalysts that have well-defined and accessible catalytic active sites and that maintain constant activity and selectivity, that are as good as or better than the homogeneous version, with high levels of reusability.

In an attempt to address the limitations of polymer-supported catalysts mentioned above, the Bergens group recently developed a method where a metal-containing monomer (MCM) was directly polymerized, via ring-opening metathesis polymerization (ROMP), resulting in a polymer-supported, catalyst-organic framework.^{43,44} This differs from traditional methods in that the MCM itself, rather than just the ligand, is polymerized.⁴⁵ Therefore, the problem of incomplete metallation of ligand sites is no longer an issue and the often low ligand loading on the polymer support has been addressed with the MCM being directly incorporated into the polymer itself. Specifically, *trans*-[RuCl₂(Py)₂((*R,R*)-Norphos)] **22** underwent ROMP with Grubbs' first generation catalyst **23**, in the presence of the spacer monomer COE, to give the polymer-supported catalyst **24** (Scheme 1-14).⁴³ It was discovered that ROMP of

22 did not readily occur in the absence of COE due to steric crowding. In more detail, it was postulated that ROMP with COE proceeded by a reaction between the norbornene ring in **22** and **23** to form the complex **22a**. The newly formed ruthenium-alkylidene in **22a** is too crowded to further react with another molecule of **22**. Instead, it reacts with COE to insert an eight-carbon long spacer as shown in **22b**. This less crowded ruthenium-alkylidene can now react with another molecule of **22**, followed by COE, etc. to form the polymer-supported, catalyst-organic framework **24**. This alternating ROMP assembly is possible as COE is intrinsically less reactive to ROMP than Norphos because of smaller ring strain. This concept will be discussed in more detail in Chapter 2.

Scheme 1-14. Synthesis of catalyst-organic framework **24** by ROMP.

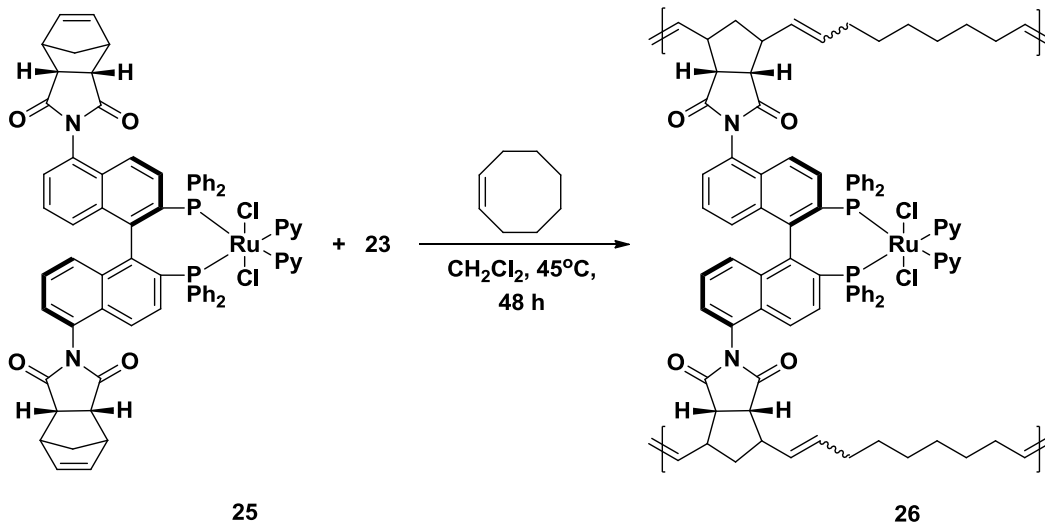


The pyridine groups coordinated to the ruthenium catalytic center were then replaced with (*R,R*)-dpen to generate the active Noyori-type

hydrogenation catalyst. This was followed by deposition of the polymer-supported, catalyst-organic framework on BaSO₄. The catalyst was then used in the hydrogenation of 1-acetonaphthone (see Scheme 1-9) under the following conditions: S/C = 500, 4 atm of H₂, 4 equiv *t*-BuOK, 22°C for 15 hours in 2-propanol. The hydrogenated product was obtained in ~95% yield with an *ee* of 83%, compared to the homogeneous hydrogenation where the product was obtained in 48% *ee*. In addition, the catalyst was easily recovered by filtration and reused in another ten runs with no appreciable drop in % yield or % *ee*. When this report was published, this was the highest number of reuses obtained for a polymer-supported asymmetric hydrogenation catalyst that was not soluble in the reaction medium and that did not require a swelling co-solvent.

In a second study, the Bergens group extended this alternating ROMP methodology to a BINAP-based system.⁴⁴ Here, *trans*-[RuCl₂(Py)₂((*R*)-5,5'-dinorimido-BINAP)] **25** underwent ROMP with **23**, in the presence of the spacer monomer COE, to give the polymer-supported catalyst **26** (Scheme 1-15). The actual synthesis of this ROMP-active, BINAP-based ligand will be discussed in detail in Chapter 2.

Scheme 1-15. Synthesis of BINAP-based, catalyst-organic framework **26**.



Similar to the previous example, COE was required in order for the ROMP to proceed. As well, the pyridine groups on the ruthenium catalytic center were replaced with (*R,R*)-dpen and the polymer-supported, catalyst-organic framework was then deposited on BaSO₄. The catalyst was then tested in the hydrogenation of 1'-acetonaphthone (see Scheme 1-9) under the following conditions: S/C = 1000, 10 atm of H₂, 20 equiv *t*-BuOK, 40°C for 21 hours in 2-propanol. The hydrogenated product was obtained in 100% yield with an *ee* of 96%, which is directly comparable to the homogeneous catalyst analogue. This catalyst was easily recovered by filtration and reused in 35 consecutive runs with no significant drop in activity or selectivity. In addition, the amount of rhodium leaching was below the detectable limit for ICP-MS (≤ 4 ppb). To date, this is the highest number of reuses ever reported for a polymer-supported asymmetric hydrogenation catalyst.

Due to the success of these systems, the primary goal of the research presented in this dissertation was to extend the alternating ROMP methodology, developed by the Bergens group, to rhodium-BINAP containing catalysts. These polymer-supported, rhodium-BINAP containing catalyst-organic frameworks were used in the cycloisomerization of 1,6-enynes and the isomerization of allylic alcohols. The catalysts themselves exhibited not only remarkable reusability, but were highly successful in large TON batch reactions as well. In addition, the polymer-supported catalysts were found to be more active and more selective than the homogeneous catalyst analogues. To show the industrial viability of these catalyst systems, a method was developed to adapt these polymer-supported catalysts for use in an H-Cube® continuous-flow hydrogenation reactor. In the hydrogenation of olefins under continuous-flow conditions, these catalysts exhibited remarkable activity, diversity and longevity. In addition, detailed solid state NMR and neutron activation analysis studies were performed on the catalysts, both before and after use, to better understand why deactivation occurs over time. The work presented in this dissertation is thus a major step forward in the development of sustainable, industrially viable, asymmetric catalyzed processes.

References

- (1) (a) *Pesticide Chemistry and Bioscience*; Brooks, G. T., Roberts, T. R., Eds.; Royal Society of Chemistry, **1999**. (b) *Pesticide Chemistry: Crop Protection, Public Health, Environmental Safety*; Ohkawa, H., Miyagawa, H., Lee, P. W., Eds.; Wiley-VCH: Weinheim, Germany, **2007**.
- (2) (a) *Common Fragrance and Flavor Materials*; Surburg, H., Panten J., Eds.; Wiley-VCH: Weinheim, Germany, **2006**. (b) Saudan, L. A. *Acc. Chem. Res.* **2007**, *40*, 1309.
- (3) (a) Farina, V.; Reeves, J. T.; Senanayake, C. H.; Song, J. J. *Chem. Rev.* **2006**, *106*, 2734. (b) Klingler, F. D. *Acc. Chem. Res.* **2007**, *40*, 1367. (c) Chhabra, N.; Aseri, M. L.; Padmanabhan, D. *Int. J. Appl. Basic Med. Res.* **2013**, *3*, 16.
- (4) Thayer, A. M. *Chem. Eng. News* **2007**, *85*(32), 11.
- (5) Tomaszewski, J.; Rumore, M. M. *Drug Dev. Ind. Pharm.* **1994**, *20*, 119.
- (6) (a) Smith, S. W. *Toxicol. Sci.* **2009**, *110*, 4. (b) Kim, J. H.; Scialli, A. R. *Toxicol. Sci.* **2011**, *122*, 1.
- (7) (a) *Fundamentals of Asymmetric Catalysis*; Walsh, P. J., Kozlowski, M. C., Eds.; University Science Books: Sausalito, California, **2009**. (b) Noyori, R. *Asymmetric Catalysis in Organic Synthesis*; Wiley and Sons, Inc.: New York, **1994**. (c) Noyori, R. *Angew. Chem. Int.*

- Ed.* **2002**, *41*, 2008. (d) Arróniz, C.; Escolano, C.; Strategies for the Synthesis of Enantiopure Compounds Focused on Organocatalysis. In *Recent Advances in Pharmaceutical Sciences II*; Munoz-Torrero, D., Haro, D., Valles, J., Eds.; Transworld Research Network, **2012**.
- (8) (a) Tani, K.; Yamagata, T.; Otsuka, S.; Akutagawa, S.; Kumobayashi, H.; Taketomi, T.; Takaya, H.; Miyashita, A.; Noyori, R. *J. Am. Chem. Soc., Chem. Commun.* **1982**, 600. (b) Tani, K.; Yamagata, T.; Akutagawa, S.; Kumobayashi, H.; Taketomi, T.; Takaya, H.; Miyashita, A.; Noyori, R.; Otsuka, S. *J. Am. Chem. Soc.* **1984**, *106*, 5208. (c) Inoue, S.-I.; Takaya, H.; Tani, K.; Otsuka, S.; Sato, T.; Noyori, R. *J. Am. Chem. Soc.* **1990**, *112*, 4897.
- (9) <http://www.flex-news-food.com/console/PageViewer.aspx?page=13467>.
- (10) Ohta, T.; Takaya, H.; Kitamura, M.; Nagai, K.; Noyori, R. *J. Org. Chem.* **1987**, *52*, 3174.
- (11) Koul, S.; Parshad, R.; Taneja, S. C.; Qazi, G. N. *Tetrahedron: Asymmetry* **2003**, *14*, 2459.
- (12) Garrett, C. E.; Prasad, K. *Adv. Synth. Catal.* **2004**, *346*, 889.
- (13) Hawkins, J. M.; Watson, T. J. N. *Angew. Chem. Int. Ed.* **2004**, *43*, 3224.
- (14) (a) *Asymmetric Catalysis on Industrial Scale*; Blaser, H. U., Schmidt, E., Eds.; Wiley-VHC: Weinheim, Germany, **2003**. (b) *Chiral Catalyst Immobilization and Recycling*; De Vos, D. E.,

- Vankelecom, I. F. J., Jacobs, P. A., Eds.; Wiley-VHC: Weinheim, Germany, **2008**. (c) *Enantioselective Homogeneous Supported Catalysis*; Pericàs, M. A., Ed.; Wiley-VHC: Weinheim, Germany, **2012**.
- (15) (a) Kirschning, A.; Jas, G. *Immobilized Catalysts Topic in Current Chemistry* **2004**, 242, 209. (b) Nagy, K. D. (**2012**). *Catalyst Immobilization Techniques for Continuous Flow Synthesis*. Ph. D. Thesis. Massachusetts Institute of Technology: Cambridge. (c) Chen, B.; Dingerdissen, U.; Krauter, J. G. E.; Rotgerink, H.; Mobus, K.; Ostgard, D. J.; Panster, P.; Riermeier, T. H.; Seebald, S.; Tacke, T.; Trauthwein, H. *Appl. Catal. A: General* **2005**, 280, 17.
- (16) (a) Fraile, J. M.; García, J. I.; Mayoral, J. A. *Chem. Rev.* **2009**, 109, 360. (b) Heitbaum, M.; Glorius, F.; Escher, I. *Angew. Chem. Int. Ed.* **2006**, 45, 4732. (c) McMorn, P.; Hutchings, G.; *Chem. Soc. Rev.* **2004**, 33, 108. (d) Zhao, X. S.; Bao, X. Y.; Guo, W.; Lee, F. Y. *Mater. Today* **2006**, 9, 32. (e) Barbaro, P.; Liguori, F. *Chem. Rev.* **2009**, 109, 515.
- (17) (a) Dooos, B. M. L.; Vankelecom, I. F. J.; Jacobs, P. A. *Adv. Synth. Catal.* **2006**, 348, 1413. (b) Leadbeater, N. E.; Marco, M. *Chem. Rev.* **2002**, 102, 3217. (c) Fan, Q.-H.; Li, Y.-M.; Chan, A. S. C. *Chem. Rev.* **2002**, 102, 3385. (d) Wang, Z.; Chen, G.; Ding, K. *Chem. Rev.* **2009**, 109, 322. (e) Valvekens, P.; Vermoortele, F.; De Vos, D. *Catal. Sci. Technol.* **2013**, 3, 1435.

- (18) (a) Dwars, T.; Oehme, G. *Adv. Synth. Catal.* **2002**, *344*, 239. (b) Joó, F. *Acc. Chem. Res.* **2002**, *35*, 738. (c) Pinault, N.; Bruce, D. W. *Coord. Chem. Rev.* **2003**, *241*, 1.
- (19) (a) Gordon, C. M.; Leitner, W. Homogeneous Catalysis in Supercritical Solvents as a Special Unit Operation. In *Multiphase Homogeneous Catalysis*; Cornils, B., Herrmann, W. A., Vogt, D., Horváth, I., Olivier-Bourbignon, H., Leitner, W., Mecking, S., Eds.; Wiley-VHC: Weinheim, Germany, **2005**. (b) Heldebrant, D. J.; Witt, H. N.; Walsh, S. M.; Ellis, T.; Rauscher, J.; Jessop, P. G. *Green Chem.* **2006**, *8*, 807.
- (20) (a) *Handbook of Fluorous Chemistry*; Gladysz, J. A., Curran, D. P., Horváth, I., Eds.; Wiley-VHC: Weinheim, Germany, **2004**. (b) de Wolfe, E.; van Koten, G.; Deelman, B.-J. *Chem. Soc. Rev.* **1999**, *28*, 37. (c) Horváth, I. T. *Acc. Chem. Res.* **1998**, *31*, 641.
- (21) (a) Welton, T. *Coord. Chem. Rev.* **2004**, *248*, 2459. (b) Sheldon, R. *Chem. Commun.* **2001**, 2399. (c) Wasserscheid, P.; Keim, W. *Angew. Chem. Int. Ed.* **2000**, *39*, 3772.
- (22) (a) Merrifield, R. B. *J. Am. Chem. Soc.* **1963**, *85*, 2149. (b) Merrifield, R. B. *Science* **1986**, *232*, 341.
- (23) Grubbs, R. H.; Kroll, L. C. *J. Am. Chem. Soc.* **1971**, *93*, 3062.
- (24) Pepper, K. W.; Paisley, H. M.; Young, M. A. *J. Chem. Soc.* **1953**, 4097.

- (25) Dumont, W.; Poulin, J.-C.; Dang, T.-P.; Kagan, H. B. *J. Am. Chem. Soc.* **1973**, *95*, 8295.
- (26) (a) Framery, E.; Andrioletti, B.; Lemaire, M. *Tetrahedron: Asymmetry* **2010**, *21*, 1110. (b) Hu, A.; Ngo, H. L.; Lin, W. B. *J. Am. Chem. Soc.* **2003**, *125*, 11490. (c) Wang, P.; Liu, X.; Yang, J.; Yang, Y.; Zhang, L.; Yang, Q.; Li, C. *J. Mater. Chem.* **2009**, *19*, 8009. (d) Guerreiro, P.; Ratovelomanana-Vidal, V.; Genêt, J.-P.; Dellis, P. *Tetrahedron Lett.* **2001**, *42*, 3423.
- (27) (a) *Modern Rhodium-Catalyzed Organic Reactions*; Evans, P. A., Ed.; Wiley-VHC: Weinheim, Germany, **2005**. (b) Bergens, S. H.; Bosnich, B. *J. Am. Chem. Soc.* **1991**, *113*, 958. (c) Miyashita, A.; Yasuda, A.; Takaya, H.; Toriumi, K.; Ito, T.; Souchi, T.; Noyori, R. *J. Am. Chem. Soc.* **1980**, *102*, 7932. (d) Ping, C.; Zhang, X. *Angew. Chem. Int. Ed.* **2000**, *39*, 4104. (e) Akutagawa, S. *Appl. Catal. A: General* **1995**, *128*, 171. (f) Ohkuma, T.; Kurono, N. BINAP. in *Privileged Chiral Ligands and Catalysts*; Zhou, Q.-L., Ed.; Wiley-VHC: Weinheim, Germany, **2011**.
- (28) Bayston, D. J.; Fraser, J. L.; Ashton, M. R.; Baxter, A. D.; Polywka, M. E. C.; Moses, E. J. *J. Org. Chem.* **1998**, *63*, 3137.
- (29) Cai, D. W.; Payack, J. F.; Bender, D. R.; Hughes, D. L.; Verhoeven, T. R.; Reider, P. J. *J. Org. Chem.* **1994**, *59*, 7180.
- (30) (a) Genet, J. P.; Pinel, C.; Ratovelomanana-Vidal, V.; Mallart, S.; Pfister, X.; Cano De Andrade, M. C.; Laffitte, J. A. *Tetrahedron:*

- Asymmetry* **1994**, *5*, 665. (b) Genet, J. P.; Ratovelomanana-Vidal, V.; Cano De Andrade, M. C. *Tetrahedron Lett.* **1995**, *36*, 2063.
- (31) (a) Kitamura, M.; Ohkuma, T.; Inoue, S.; Sayo, N.; Kumobayashi, H.; Akutagawa, S.; Ohta, T.; Takaya, H.; Noyori, R. *J. Am. Chem. Soc.* **1988**, *110*, 629. (b) Mashima, K.; Kusano, K. H.; Sato, N.; Matsumura, Y.; Nozaki, K.; Kumobayashi, H.; Sayo, N.; Hori, Y.; Ishizaki, Y.; Akutagawa, S.; Takaya, H. *J. Org. Chem.* **1994**, *59*, 3064.
- (32) (a) Kitamura, M.; Ohkuma, T.; Takaya, H.; Noyori, R. *Tetrahedron Lett.* **1988**, *29*, 1555. (b) Kitamura, M.; Tokunaga, M.; Noyori, R. *J. Am. Chem. Soc.* **1995**, *117*, 2931. (c) Kitamura, M.; Tokunaga, M.; Ohkuma, T.; Noyori, R. *Tetrahedron Lett.* **1991**, *32*, 4163. (d) Nishi, T.; Kitamura, M.; Ohkuma, T.; Noyori, R. *Tetrahedron Lett.* **1988**, *29*, 6327. (e) Noyori, R.; Ohkuma, T.; Kitamura, M.; Takaya, H.; Sayo, N.; Kumobayashi, H.; Akutagawa, S. *J. Am. Chem. Soc.* **1987**, *109*, 5856.
- (33) Noyori, R.; Ikeda, T.; Ohkuma, T.; Widhalm, M.; Kitamura, M.; Takaya, H.; Akutagawa, S.; Sayo, N.; Saito, T.; Taketomi, T.; Kumobayashi, H. *J. Am. Chem. Soc.* **1989**, *111*, 9134.
- (34) Chapuis, C.; Barthe, M.; Laumer, J. Y. D. *Helv. Chim. Acta.* **2001**, *84*, 230.
- (35) Cole-Hamilton, D. J. *Science* **2003**, *299*, 1702.
- (36) Noyori, R.; Ohkuma, T. *Angew. Chem. Int. Ed.* **2001**, *40*, 40.

- (37) (a) Kumobayashi, H.; Miura, T.; Sayo, N.; Saito, T.; Zhang, X. Y. *Synlett*. **2001**, 1055. (b) Ohkuma, T.; Koizumi, M.; Doucet, H.; Pham, T.; Kozawa, M.; Murata, K.; Katayama, E.; Yokozawa, T.; Ikariya, T.; Noyori, R. *J. Am. Chem. Soc.* **1998**, *120*, 13529. (c) O'Shea, P. D.; Chen, C. Y.; Chen, W. R.; Dagneau, P.; Frey, L. F.; Grabowski, E. J. J.; Marcantonio, K. M.; Reamer, R. A.; Tan, L. S.; Tilyer, R. D.; Roy, A.; Wang, X.; Zhao, D. L. *J. Org. Chem.* **2005**, *70*, 3021.
- (38) Ohkuma, T.; Takeno, H.; Honda, Y.; Noyori, R. *Adv. Synth. Catal.* **2001**, *343*, 369.
- (39) (a) ter Halle, R.; Colasson, B.; Schulz, E.; Spagnol, M.; Lemaire, M. *Tetrahedron Lett.* **2000**, *41*, 643. (b) Saluzzo, C.; Lamouille, T.; Le Guyader, F.; Lemaire, M. *Tetrahedron: Asymmetry* **2002**, *13*, 1141. (c) Saluzzo, C.; Lemaire, M. *Adv. Synth. Catal.* **2002**, *344*, 915.
- (40) Fan, Q.; Ren, C.; Yeung, C.; Hu, W.; Chan, A. S. C. *J. Am. Chem. Soc.* **1999**, *121*, 7407.
- (41) Pu, L. *Chem. Eur. J.* **1999**, *5*, 2227. (b) Yu, H. B.; Hu, Q. S.; Pu, L. *Tetrahedron Lett.* **2000**, *41*, 1681.
- (42) Yu, H. B.; Hu, Q. S.; Pu, L. *J. Am. Chem. Soc.* **2000**, *122*, 6500.
- (43) Ralph, C. K.; Akotsi, O. M.; Bergens, S. H. *Organometallics* **2004**, *23*, 1484.
- (44) Ralph, C. K.; Bergens, S. H. *Organometallics* **2007**, *26*, 1571.
- (45) Mastrorilli, P.; Nobile, C. F. *Coord. Chem. Rev.* **2004**, *248*, 377.

Chapter 2

Polymer-Supported Rhodium-BINAP Catalyst-Organic Frameworks Synthesized by Ring-Opening Metathesis Polymerization¹

Introduction

Section A: Ring-Opening Metathesis Polymerization (ROMP)

As discussed in Chapter 1, the immobilization of homogeneous catalysts has become a significant area of interest in the field of asymmetric catalysis due to the increased demand for more environmentally sustainable industrial processes.¹ In general, the goal is to combine the advantages of homogeneous catalysis, such as high definition, excellent selectivities and activities, with the advantages of heterogeneous catalysis, such as easy separation, recycling and improved handling.² Although numerous strategies have been employed to

¹ A version of this chapter has been published with the exception of the synthesis of the poly-[Rh((*R*)-5,5'-dinorimido-BINAP)NBD](SbF₆) catalyst. Elizabeth G. Corkum, Michael J. Hass, Andrew D. Sullivan, Steven H. Bergens. "A Highly Reusable Rhodium Catalyst-Organic Framework for the Intramolecular Cycloisomerization of 1,6-Enynes." *Org. Lett.* **2011**, *13*, 3522. With the exception of the analysis of the alternating ROMP of poly-[RhCl((*R*)-5,5'-dinorimido-BINAP)]₂ with COE, all work presented in this chapter is that of Elizabeth G. Corkum.

immobilize homogeneous asymmetric catalysts, it still remains a challenge to develop heterogeneous systems that demonstrate catalytic efficiencies as good as or better than their corresponding homogeneous analogues. Despite some success, the majority of immobilized catalysts display no or limited reusability (< 3 x) before a significant decrease in activity and/or selectivity is observed.³ Thus, new strategies are required for the development of practical immobilized asymmetric catalysts that sustain a large number of reuses and maintain the same, or better, activities and selectivities than the homogeneous analogues without metal leaching.

The majority of the published research on immobilization of homogeneous catalysts has been directed towards the development of hydrogenation catalysts (refer to Chapter 1). Nevertheless, by drawing on the successes and failures of these previously reported polymeric catalysts, key insights towards the development of more efficient and reusable systems can be made. For example, most polymer-supported immobilized catalysts are synthesized via grafting onto polymeric resins,⁴ radical copolymerization of vinyl derivatives of arenes and phosphines,⁵ condensation reactions between acid derivatives and amines or alcohols,⁶ condensation polymerizations between amines and isocyanates⁷ and Suzuki-type couplings.⁸ As the presence of a metal center can interfere with these reactions, they are often used to polymerize a chiral phosphine ligand, or to graft it to a polymeric support. The critical step then becomes metallating the resulting polymeric ligand, through reaction with a common

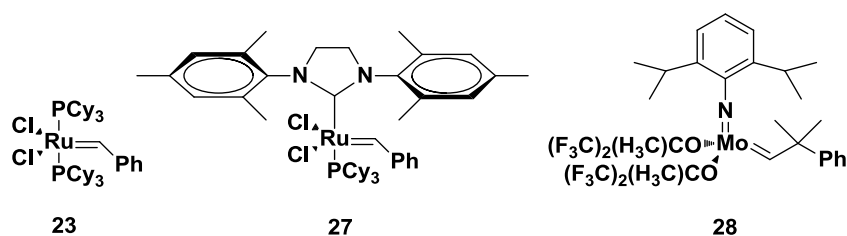
metal precursor, to produce the catalytic active sites.⁹ This procedure has several disadvantages. For example, the metallation step may not be quantitative due to restricted access to some of the chelating ligand sites in the polymer matrix, resulting in low catalyst loadings and wasted ligand.¹⁰ Unfortunately this point is often not addressed in the literature. In order to overcome the matrix diffusion problems and to ensure high catalyst loadings, the polymeric ligands are typically treated with an excess of the metal precursor in a swelling solvent. Not only does this increase the amount of waste generated, the extra step often results in oxidation of the phosphines, which further prevents complete metallation and can lead to catalyst poisoning.³ An alternative approach would be the direct incorporation of the active catalyst through polymerization of a suitable metal-containing monomer (MCM).¹¹ This would result in a higher density of catalytic sites in the polymer matrix and, since the MCM can be studied as a homogeneous catalyst before polymerization, a more accurate comparison between the homogeneous and heterogeneous systems can be made. Despite the obvious advantages associated with MCMs, there are relatively few examples of using a metal-phosphine complex directly as a monomer in the synthesis of a polymeric catalyst.¹²

Another disadvantage of the previous methods used to prepare polymeric catalysts is the lack of control over the polymerization process, which results in ill-defined polymeric systems. Random distribution and limited access to the active sites and unfavorable interactions with the

supports are often the consequence. These factors lead to poor catalyst performance for the heterogenized systems compared to the homogeneous analogues. As a result, the Bergens group postulated that a regular, rigid, polymeric system with a high density of well-defined active centers would provide a highly efficient and reusable polymeric catalyst. With these goals in mind, they focused on using ring-opening metathesis polymerization (ROMP) to prepare such a well-defined polymeric system.¹³

ROMP, a variant of olefin metathesis, has become one of the most powerful methods for the preparation of advanced functionalized polymers.^{14,15} The significant growth of ROMP-type polymers is due in part to the development and commercial availability of the well-defined olefin metathesis catalysts **23**, **27** and **28** (Figure 2-1), which promote controlled, living polymerizations.

Figure 2-1. Commercially available olefin metathesis catalysts.



The molybdenum-based catalysts related to **28**, developed by Schrock, are known for their high activity and are often employed for the polymerization of sterically hindered and electron deficient monomers.¹⁶

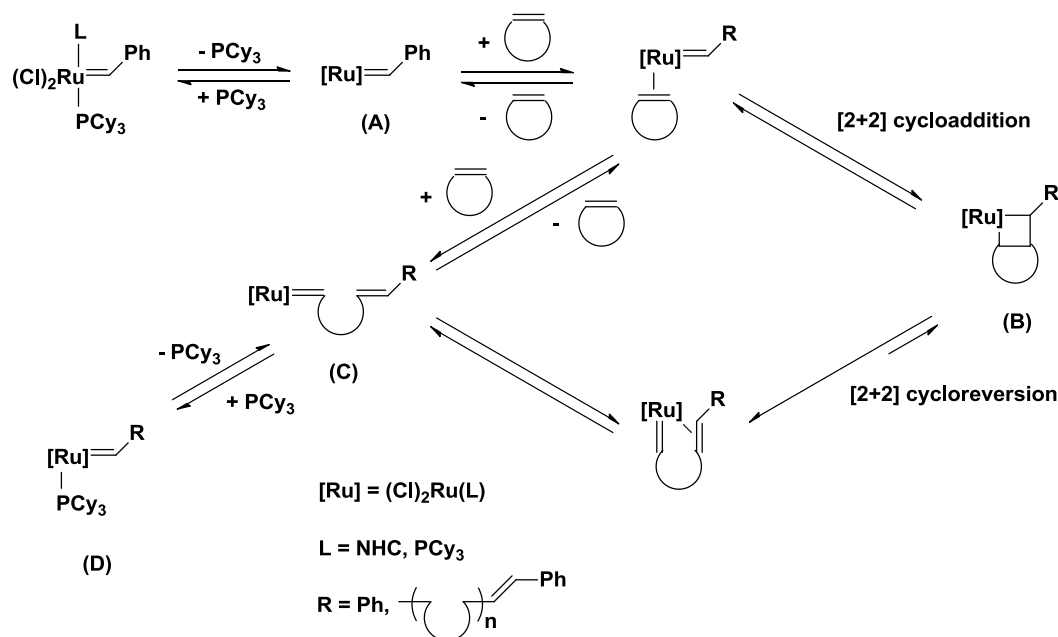
However, the “Schrock catalysts” are limited by restricted functional group tolerance and sensitivity towards oxygen and moisture. The development of the ruthenium-based catalyst **23** by Grubbs, known as the “1st generation Grubbs catalyst”, addressed the limitations of the “Schrock catalysts”.¹⁷ However, despite tolerating a wider range of protic and polar functional groups, **23** is less active than **28**. Replacing one of the phosphine ligands in **23** with an *N*-heterocyclic carbene (NHC) ligand resulted in the “2nd generation Grubbs catalyst” **27**, which exhibits activity comparable to **28** and remains tolerant of many functional groups.¹⁸ Thus, the ruthenium-based catalysts are more convenient as they allow for the direct incorporation of high degrees of functionality to afford novel polymers with well-defined structures.

The mechanism of olefin metathesis, known as the “Chauvin mechanism”, involves the interconversion of olefins and metal alkylidenes via metallacyclobutane intermediates generated by a sequence of [2+2] cycloadditions and cycloreversions to form new olefins and alkylidenes.¹⁹ ROMP reactions adopt the same mechanism except, since the reaction involves a cyclic olefin, the newly generated olefin remains attached to the active metal alkylidene as part of a growing polymer chain and the driving force for the reaction is the release of ring strain from the cyclic olefin. As a result, most monomers employed for ROMP contain norbornene units as they possess sufficient ring strain to make the process irreversible.¹⁴ Moreover, a wide range of norbornene-containing

monomers are commercially available or they can be easily synthesized by Diels-Alder reactions with cyclopentadiene.²⁰

The “Chauvin mechanism”, as it pertains to ROMP, is shown with a generic cyclic olefin in Scheme 2-1.²¹

Scheme 2-1. Mechanism of ROMP.



The initiation step with Grubbs catalyst involves dissociation of one of the phosphines to generate the 14-electron reactive intermediate **A**. The rate of phosphine versus olefin coordination to **A** dictates the net activity of the catalyst. In fact, this observation accounts for the activity difference between catalysts **23** and **27**. Once in the catalytic cycle, **A** rapidly undergoes a [2+2] cycloaddition to form the metallacyclobutane intermediate **B**, followed by a [2+2] cycloreversion and olefin dissociation

to generate the propagating metal alkylidene species **C**. **C** can then react with another monomer unit thus continuing the catalytic cycle and promoting polymer growth. **C** can also rebind with free phosphine to generate the dormant species **D**. It should be noted that, typically, the propagating species (i.e. **C**) contains a bulky polymer chain that prevents phosphine coordination, resulting in high rates of propagation.²² As well, ROMP is considered a living process and thus the catalytic cycle shown in Scheme 2-1 continues until all monomer units are consumed.²³

The living nature of ROMP is an important feature as it allows for the synthesis of reproducible well-defined polymers.²⁴ For example, molecular weights can be controlled by adjusting the monomer/catalyst ratio and narrow molecular weight polydispersities can be achieved by controlling the rates of initiation and propagation. Specifically, low polydispersities are obtained in cases where the initiation is faster than the propagation.²⁴ In fact, Grubbs developed a procedure where, by simply adding excess phosphine, the rate of propagation is decreased without influencing the rate of initiation.²² Grubbs suggested that the excess phosphine competes with monomer units for the propagating species **C**, thereby lowering the number of turnovers (TOs) that occur before **C** is trapped to give the dormant species **D**.

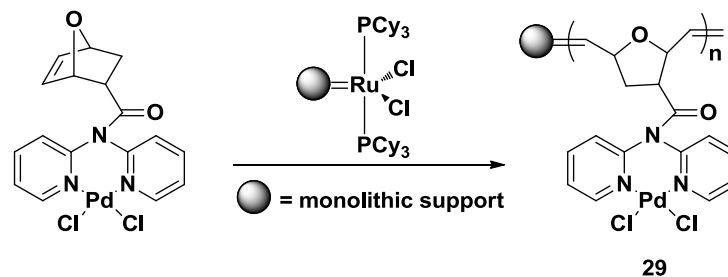
That being said, a related problem that is encountered with ROMP reactions is secondary metathesis or “backbiting”. Here, the active catalyst reacts with olefin bonds in the growing polymer chain, reducing the

molecular weight and increasing the polydispersity of the polymers. However, recent studies have shown that backbiting is minimized for the ROMP of norbornene monomers due to steric hindrance around the olefins in the polymer chain.²⁵ As a result, norbornene-containing monomers are ideal for controlled living polymerizations. In fact, combined with the benefits of high ring strain and availability, functionalized norbornene derivatives are the most preferred monomers for advanced functional polymer preparation.¹⁴ Applications of these types of polymers include block copolymers,²⁶ bioactive,²⁷ electroactive,²⁸ liquid crystalline,²⁹ and nonlinear optic polymers.³⁰

In addition to the applications mentioned above, ROMP has also been used to prepare a small number of metal-based polymeric catalysts.³¹ These include supported Pd-based systems for Heck and related reactions,³²⁻³⁴ a supported Co-salen system for kinetic resolution,³⁵ and reusable Ru and Mo-based metathesis catalysts grafted onto polymer supports,³⁶ and onto monolithic supports.³⁷⁻³⁹ As previously discussed and similar to other metal-based polymer catalysts, the critical step in the synthesis of these catalysts is metallation of the polymeric ligand. However, there are a few cases where ROMP of certain MCMs was reported.^{31,40,41} As an example, Buchmeiser prepared a Pd-based polymer/monolith-supported catalyst from a MCM as shown in Scheme 2-2.⁴² Here, a norbornene-based dipyritylamide-PdCl₂ complex was grafted

to a monolith-supported version of Grubbs catalyst **23** by ROMP to give immobilized catalyst **29**.

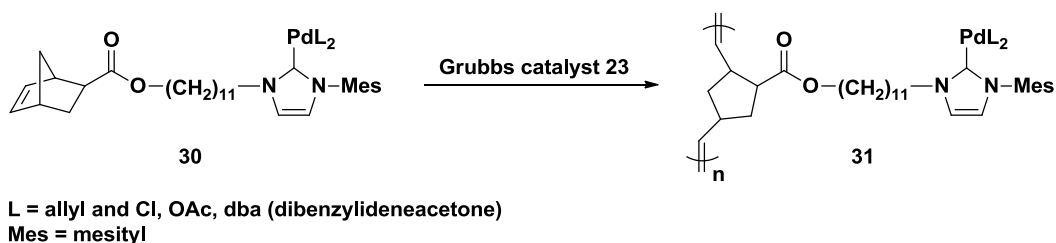
Scheme 2-2. Buchmeiser's polymer/monolith-supported Pd catalyst prepared by ROMP.



Immobilized catalyst **29** was then used in the Heck carbon-carbon coupling reaction of styrene and iodobenzene and gave higher turnover numbers (TONs) than a similar supported system that was prepared by ROMP of the free ligand followed by metallation.

In another example, Weck reported the synthesis of poly(norbornene)-supported Pd-NHC catalysts (Scheme 2-3) for use in Suzuki-Miyaura, Sonogashira and Heck carbon-carbon coupling reactions.⁴³ Here, the norbornene-containing Pd-NHC MCMs **30** underwent ROMP with Grubbs catalyst **23** to give polymeric catalysts **31**. For the carbon-carbon coupling reactions mentioned above, all of the polymer-immobilized catalysts demonstrated similar activity to their small molecule analogues.

Scheme 2-3. Weck's poly(norbornene)-supported Pd-NHC catalysts prepared by ROMP.

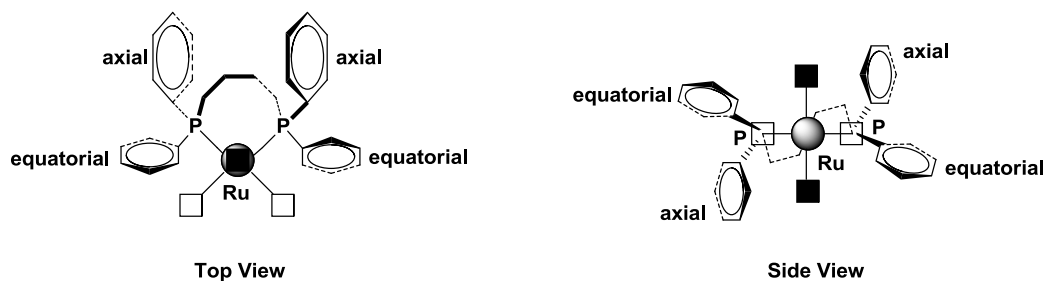


These examples show that ROMP can be used to prepare a wide range of functionalized polymers. Therefore, it is surprising that such a well-controlled, versatile technique has not been applied in the preparation of asymmetric polymer catalysts. In fact, to the best of our knowledge, the Bergens group is the only research group to have utilized ROMP in the preparation of polymeric catalysts for asymmetric hydrogenations (refer to Chapter 1).¹³ Specifically, Bergens and coworkers synthesized a Ru-BINAP (BINAP = 2,2'-bis(diphenylphosphino)-1,1'-binaphthyl) MCM (**25**), where the BINAP ligand had been modified to incorporate norbornene units, that underwent alternating ROMP with *cis*-cyclooctene (COE) in the presence of Grubbs catalyst **23**, to produce the polymeric catalyst-organic framework (COF) **26** (Scheme 1-15).^{13b} As the primary goal of the research presented in this dissertation was to extend this methodology to Rh-BINAP containing catalysts, the next section of this introduction will focus on BINAP and its modification.

Section B: Modification of BINAP

BINAP is one of the most extensively utilized chiral phosphine ligands in enantioselective catalysis as it is not easily oxidized, it is conformationally rigid and often affords high enantioselectivities.^{44,45} This high enantioselectivity is a result of the C_2 -dissymmetry of BINAP and the large projection of the phosphine phenyl rings into the spatial domain of the coordinated metal center, forming sterically congested quadrants.⁴⁶ Figure 2-2 illustrates the chiral template created by the (*R*)-BINAP ligand and a transition metal, M.⁴⁷

Figure 2-2. Chiral environment of an (*R*)-BINAP-transition metal complex.



□ = coordination site in the P-M-P plane

■ = coordination site out of the P-M-P plane

*The binaphthyl skeleton is omitted for clarity

The chirality of the binaphthyl skeleton is transmitted spatially via the phosphine phenyl rings to the in-plane and out-of-plane coordination sites. The in-plane coordination sites are sterically affected by the equatorial phenyl rings while the out-of-plane sites are influenced by the axial phenyl

substituents. Reactions that occur in such a dissymmetric environment display excellent chiral discrimination (i.e. high enantioselectivity). These features make BINAP one of the most utilized chiral ligands in catalysis. Further discussion on the use and properties of BINAP and related ligands are beyond the scope of this dissertation and the interested reader is directed to the following review articles.⁴⁸

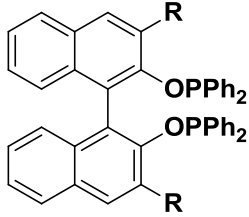
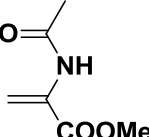
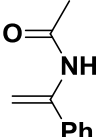
As discussed in Chapter 1, most recent methodologies aimed at immobilizing homogeneous catalysts are developed with BINAP and require that it be functionalized to allow for immobilization of the catalysts. Moreover, to adapt the Bergens alternating ROMP methodology to BINAP, the key step was to functionalize BINAP with a cyclic olefin (i.e. norbornene) susceptible to ROMP. Prior to COF **26**, there were no known examples whereby BINAP had been modified with a cyclic olefin, however, the large literature precedent documenting numerous methods to functionalize BINAP suggested that such functionalization was attainable.⁴⁹

Previously, BINAP was functionalized either to increase the catalyst efficiency and selectivity, or to facilitate separation of the catalyst from the bulk of the reaction. BINAP has been functionalized at the phosphine-phenyl groups and the 3, 4, 5 and 6 positions of the binaphthyl rings. Typically, changes in the catalyst performance are observed for modifications made to the phenyl rings since they are directly bonded to the phosphorus atom. Modifying the phenyl substituents influences the

electron density of the phosphorus atoms and the steric hindrance around these coordinating sites.⁵⁰ Two well-known examples are the TolBINAP and XylBINAP derivatives, whereby the phenyl groups are substituted for *p*-CH₃C₆H₄ and 3,5-(CH₃)₂C₆H₃, respectively. The increased steric bulk of the modified phenyl substituents can result in a significant increase in enantioselectivity. For example, Noyori's *trans*-RuCl₂(diphosphine)(diamine) catalyst systems for the hydrogenation of aromatic ketones displayed > 20% ee enhancements with XylBINAP.⁵¹

For catalyst recycling purposes, modifications of the binaphthyl skeleton are more common because of their accessibility. In addition, modifications to the naphthyl rings are less likely to interfere with the catalyst selectivity since they are distal from the catalytic active sites. However, this is dependent on which position is functionalized on the naphthyl ring. For example, functionalization at the 3,3'-positions can result in hindered rotation about the phenyl-phosphorus bond thereby influencing the ee. Zhang and coworkers prepared BINAP-phosphinite derivatives that were substituted at the 3,3'-positions and used these new ligands to prepare rhodium-based catalysts by reaction with [Rh(COD)₂](PF₆). An increase in selectivity occurred for the asymmetric hydrogenation of dehydroamino acid derivatives and enamides as shown in Table 2-1.⁵²

Table 2-1. Rh(I)-catalyzed asymmetric hydrogenation of functionalized olefins using substituted BINAP-phosphinite ligands.^a

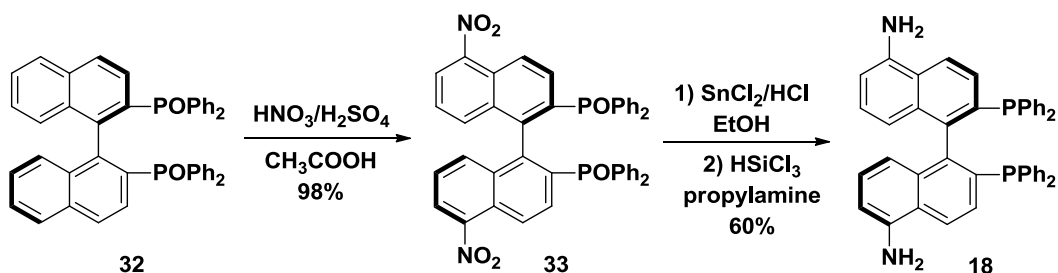
		
Me	95% ee	97% ee
Ph	99% ee	94% ee
H	73% ee	28% ee

^a Reactions were done at 22°C under 3 atm H₂ for 12 hours in THF (S/C = 100/1).

More commonly, BINAP is functionalized at the 5,5'-positions, largely because electrophilic aromatic substitution reactions with BINAP dioxide are directed towards these positions and optically pure BINAP can be used directly as a starting material as the stereochemistry is preserved throughout the synthetic sequence. As well, these positions on the naphthyl rings are among the farthest from the active sites and are least likely to influence the ligand properties. Therefore, modification at the 5,5'-positions on the binaphthyl skeleton are frequently made when heterogenizing BINAP (see Scheme 1-11 and Scheme 5-5).⁴⁹

BINAP is most commonly functionalized at the 5,5'-positions by halogenation⁵³ and nitration.⁵⁴ Nitration of BINAP dioxide was first carried out by Kumobayashi and coworkers in 1986 to give (*R*)-5,5'-diamino-BINAP (**18**) according to Scheme 2-4.⁵⁴

Scheme 2-4. Synthesis of (*R*)-5,5'-diamino-BINAP **18**.

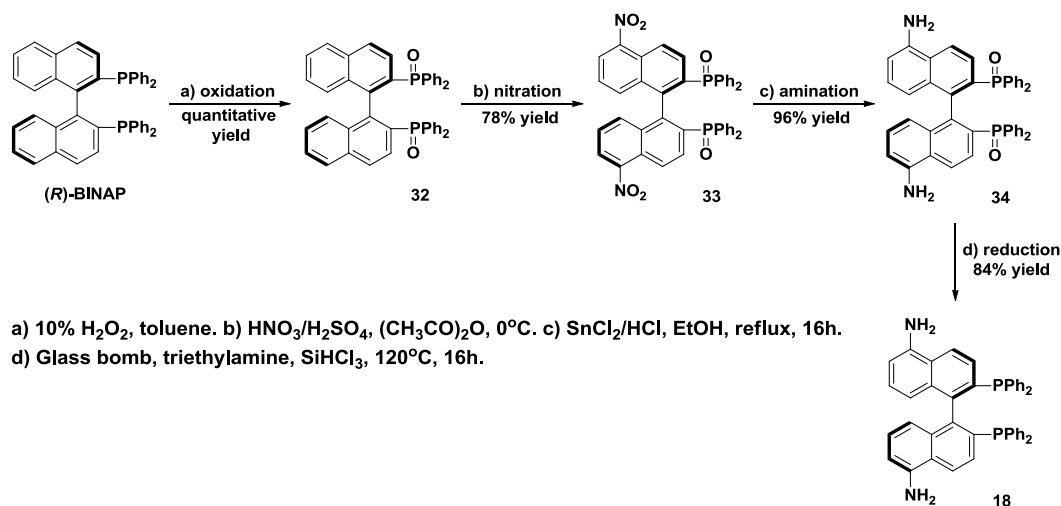


Since then, **18** has been utilized to prepare soluble polymer⁵⁵ or dendrimer⁵⁶ supported catalysts (see Scheme 1-11 in Chapter 1). As a result, Bergens and coworkers decided to use **18** as a building block for the synthesis of the ROMP active BINAP ligand.^{13b,57} The remainder of this introduction will discuss the synthetic procedures developed by past coworkers for synthesizing this ligand.

Section C: Synthesis of a ROMP active BINAP ligand

The original literature procedure for the synthesis of (*R*)-5,5'-diamino-BINAP **18** is shown in Scheme 2-4.⁵⁴ Previous coworker Corbin Ralph found that this method gave low yields and several of the procedures, particularly involving product isolation, could not be duplicated in our laboratories. As a result, Ralph developed an improved and reproducible synthesis of (*R*)-5,5'-diamino-BINAP **18** that is shown in Scheme 2-5.⁵⁷

Scheme 2-5. Ralph's improved nitration of (*R*)-BINAP.



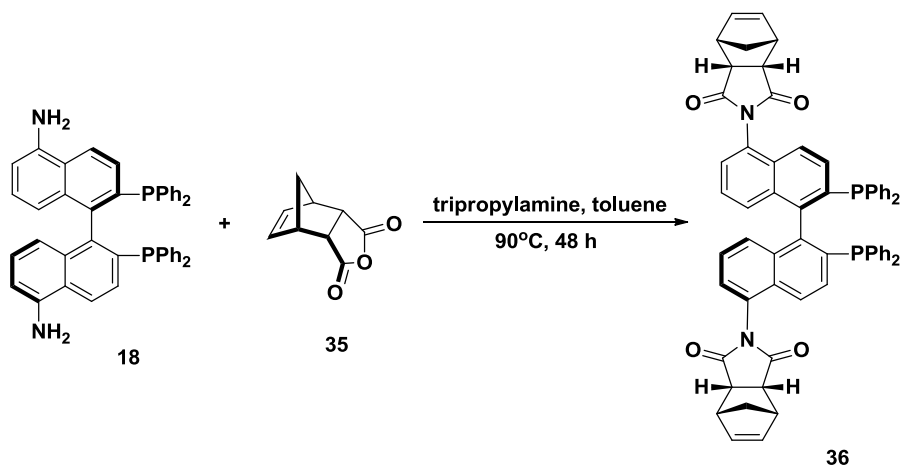
Commercially available (*R*)-BINAP was oxidized with 10% hydrogen peroxide to produce BINAP dioxide (**32**) in quantitative yield. The nitration of **32** was carried out using nitric acid and acetic anhydride as a nitrating agent in the presence of a small amount of sulfuric acid as a catalyst to produce (*R*)-5,5'-dinitro-BINAP dioxide (**33**). The procedure described in the patent⁵⁴ for the isolation of clean **33** was attempted by Ralph several times but failed to give pure product. Unlike the patent method which used a hot THF/water mixture for purification, Ralph's method gave **33** as a crystalline solid in 78% yield by recrystallization from a CH₂Cl₂/hexanes solution. The nitro groups in **33** were selectively reduced using stannous chloride in concentrated hydrochloric acid as a reducing agent to form (*R*)-5,5'-diamino-BINAP dioxide (**34**). Again, the method for product isolation described in the patent could not be duplicated. Ralph's method afforded **34** as a crystalline solid in 96% yield by recrystallization from THF. Finally,

(*R*)-5,5'-diamino-BINAP (**18**) was obtained in 84% yield by reducing **34** with trichlorosilane as the reducing agent in the presence of triethylamine at 120°C for 16 hours in a sealed pressure reactor.

Although Ralph's procedure for the synthesis of **18** was successful, former coworkers Andrew Sullivan and Michael Hass found that hydrogenation of **33** over 5 wt% Pd/C was vastly superior to the stannous chloride reduction in the formation of **34**, due to its shorter reaction time and simplified post-reaction workup.^{58,59} Specifically, the hydrogenation proceeds under 45 psig (psig = pounds per square inch gauge pressure) H₂ at 50°C in 6 hours to provide **34** in near quantitative crude yield. Purification by flash chromatography (neutral alumina) gives pure **34** in 87% yield and the Pd/C catalyst can be recovered and reused. **18** was then obtained by reduction of **34** as outlined above (Scheme 2-5). With a reproducible synthesis of **18** established, the next step was to prepare the desired ROMP active BINAP ligand through reaction of **18** with a suitable norbornene monomer.

Ralph prepared a ROMP active version of BINAP in one step by condensation between **18** and *cis*-5-norbornene-*endo*-2,3-dicarboxylic anhydride (**35**) to give (*R*)-5,5'-di(*cis*-5-norbornene-2,3-*endo*-dicarboximido)-2,2'-bis(diphenylphosphine)-1,1'-BINAP, henceforth referred to as (*R*)-5,5'-dinorimido-BINAP (**36**) (Scheme 2-6).^{13b, 57}

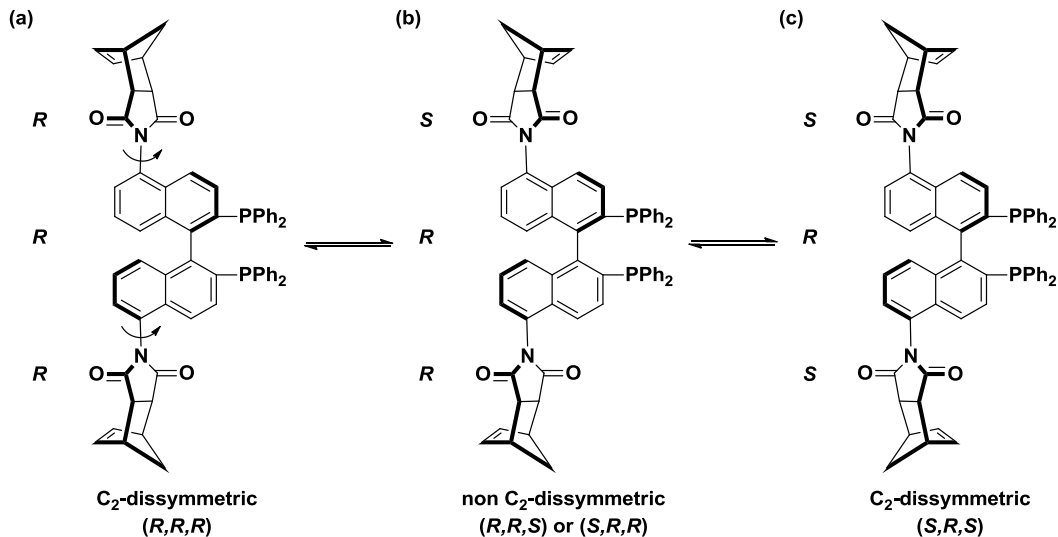
Scheme 2-6. Synthesis of the ROMP active BINAP ligand **36**.



Here, the condensation reaction between **18** and **35** went to completion after 48 hours at 90°C in toluene and in the presence of tripropylamine and a large excess (12 equiv.) of the anhydride **35**. Washing the crude reaction mixture in toluene with aqueous base (1M NaOH) hydrolyzed the unreacted anhydride to give the corresponding diacid, which was soluble in water. The organic product **36** was then easily recovered from the organic phase in 81% yield.

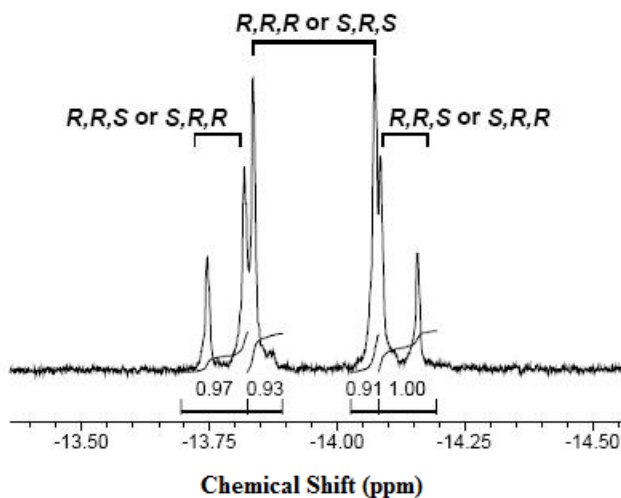
From the ³¹P-NMR spectrum (Figure 2-4), it was discovered that **36** exists as a mixture of distinct diastereomeric atropisomers,^{13b} which are illustrated in Figure 2-3.

Figure 2-3. Diastereomeric atropisomers of **36**.



Atropisomers are stereoisomers that result from hindered rotation about single bonds where the steric strain barrier to rotation is sufficiently high that individual conformers can be isolated.⁶⁰ Analysis of molecular models of **36** showed two new chiral axes along the naphthyl-N bonds and hindered rotation of the norimido groups about these axes give rise to the atropisomers shown above. The rate of rotation is slow, relative to the NMR timescale, and as a result the atropisomers can be differentiated by NMR spectroscopy (see Figure 2-4). The origin of the slow rate of rotation will be discussed at a later time.

Figure 2-4. ^{31}P -NMR spectrum of the atropisomers of **36**.^a



^[a] 202 MHz, CD_2Cl_2 , 27°C.

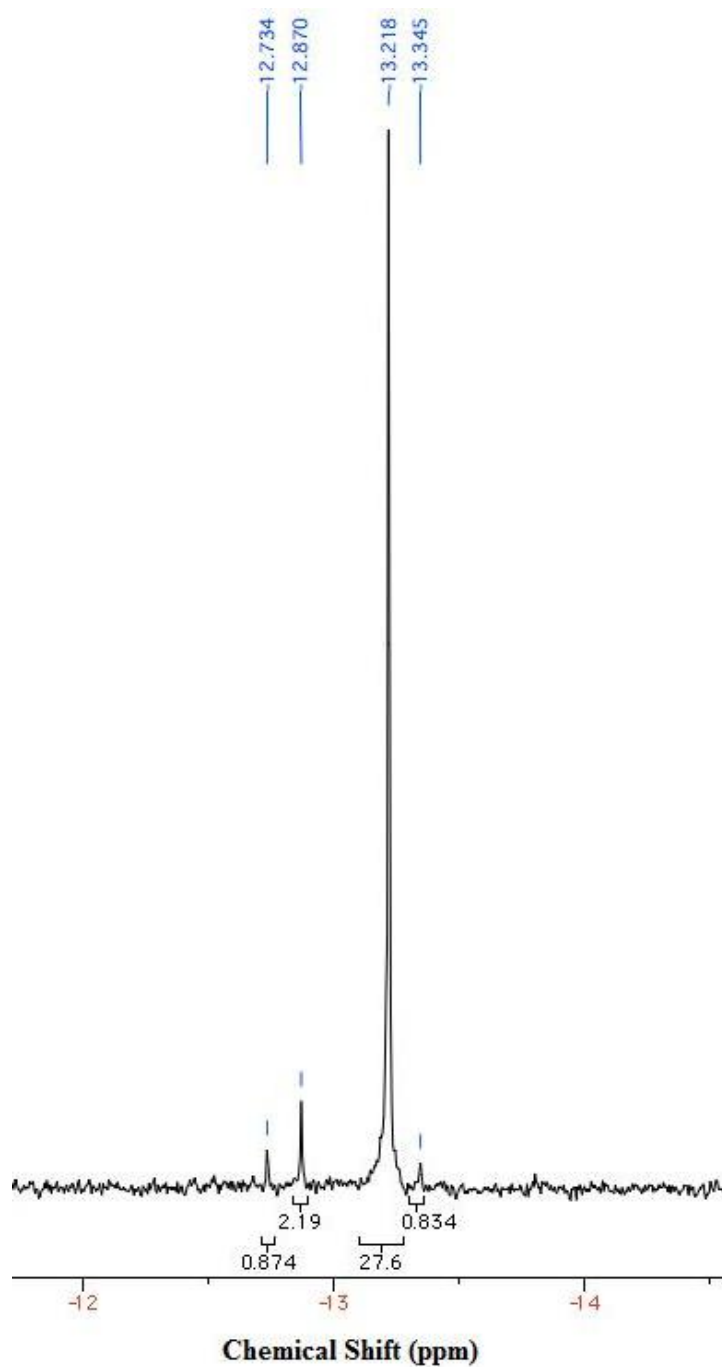
As illustrated in Figure 2-3, two atropisomers of **36** are C_2 -dissymmetric (R,R,R and S,R,S) and one atropisomer is non C_2 -dissymmetric (S,R,R and the equivalent R,R,S). In the C_2 -dissymmetric atropisomers, both of the norimido groups have the same spatial orientation and, as a result, the C_2 -axis that renders the ^{31}P nuclei chemically equivalent is maintained. Therefore, two singlets, one for both of the (R,R,R) and (S,R,S) atropisomers, are observed in the ^{31}P -NMR spectrum (-13.88 and -14.12 ppm, Figure 2-4). In the non C_2 -dissymmetric atropisomer, which consists of an NMR equivalent pair (i.e. R,R,S and S,R,R), the norimido groups have the opposite spatial orientation. As a result, the C_2 -axis is lost and the ^{31}P nuclei are rendered chemically inequivalent. Therefore, two doublets, arising from P-P coupling, are observed in the ^{31}P -NMR spectrum: -13.83 ppm (d, $J_{\text{PP}} = 14.6$ Hz, 1P) and -14.17 ppm (d, $J_{\text{PP}} = 14.6$ Hz, 1P) (Figure 2-4). The roughly equal

integration of the C₂-dissymmetric and non C₂-dissymmetric atropisomers suggests that at room temperature **36** exists as an equal mixture of all three atropisomers and that there is a high barrier to rotation that prevents rapid interconversion of the atropisomers.

The hindered rotation about the aryl-N bond in **36** results from both steric and electronic effects. Specifically, the lone pair on the N can donate into the π^* orbitals of the naphthalene ring, resulting in partial double bond character and a significant barrier to rotation around the sp²-sp² aryl-N bond. Additionally, steric interactions between the imide carbonyl groups and the naphthalene ring will disfavor a coplanar arrangement of the two moieties. In fact, X-ray crystallography has shown that aryl-N imides twist $\sim 90^\circ$ relative to the arene ring, when prepared from 2,5-di-*tert*-butylaniline, in order to reduce the steric interactions.⁶¹

Interestingly, one C₂-dissymmetric atropisomer of **36** can be easily obtained by prolonged heating in toluene at 90°C, due to the different solubilities of the atropisomers.⁵⁷ In the ³¹P-NMR spectrum (Figure 2-5) there is a large singlet at -13.22 ppm that corresponds to one atropisomer of **36**. However, within the preparation time and acquisition of the NMR spectrum (~ 10 -15 minutes), minimal amounts of the other atropisomers were visible. To avoid this interconversion, solutions of rotamerically pure **36** must be kept at low temperatures.

Figure 2-5. ^{31}P -NMR spectrum of rotamerically pure **36**.^a



^[a] 162.1 MHz, CD_2Cl_2 , 27°C.

The isolation of a single C_2 -dissymmetric atropisomer can be explained by the fact that as the temperature increases, there is sufficient energy to

overcome the barrier of rotation about the naphthyl-N bonds and the atropisomers are able to freely interconvert. The solubilities of the atropisomers are different as one precipitates from toluene upon heating and remains insoluble in toluene at lower temperatures. Ralph postulated that upon heating, the population of the atropisomers changes whereby one of the C₂-dissymmetric atropisomers becomes more favored and precipitates from solution as it is less soluble in toluene. This drives the interconversion process forward in order to maintain equilibrium. With prolonged heating, Ralph obtained one atropisomer of **36** in 87% yield.

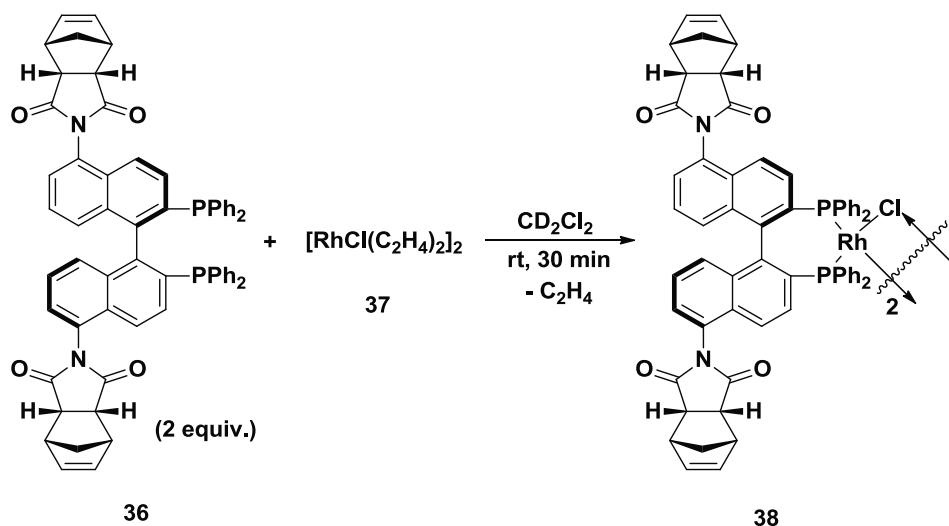
With a reliable and reproducible synthetic procedure for synthesizing a ROMP active BINAP ligand, **36** can be metallated with a desired rhodium precursor and polymerized via ROMP to generate a polymer-supported Rh-BINAP catalyst. The remainder of this chapter will discuss the synthesis of two novel rhodium catalyst-organic frameworks; specifically, the preparation of rhodium MCMs and their subsequent polymerization will be presented. This will be followed by a brief discussion on catalyst activation.

Results and Discussion

Section A: Synthesis of $[\text{RhCl}((R)\text{-}5,5'\text{-dinorimido-BINAP})]_2$ (**38**) MCM

With the (R) -5,5'-dinorimido-BINAP ligand (**36**) in hand, the next step was to prepare rhodium MCMs that can then be polymerized to give the corresponding polymer-supported catalysts. To this end, reaction between $[\text{RhCl}(\text{C}_2\text{H}_4)_2]_2$ (**37**) and rotamerically pure **36** afforded the rhodium MCM **38** as outlined in Scheme 2-7.

Scheme 2-7. Synthesis of ROMP active rhodium MCM **38**.

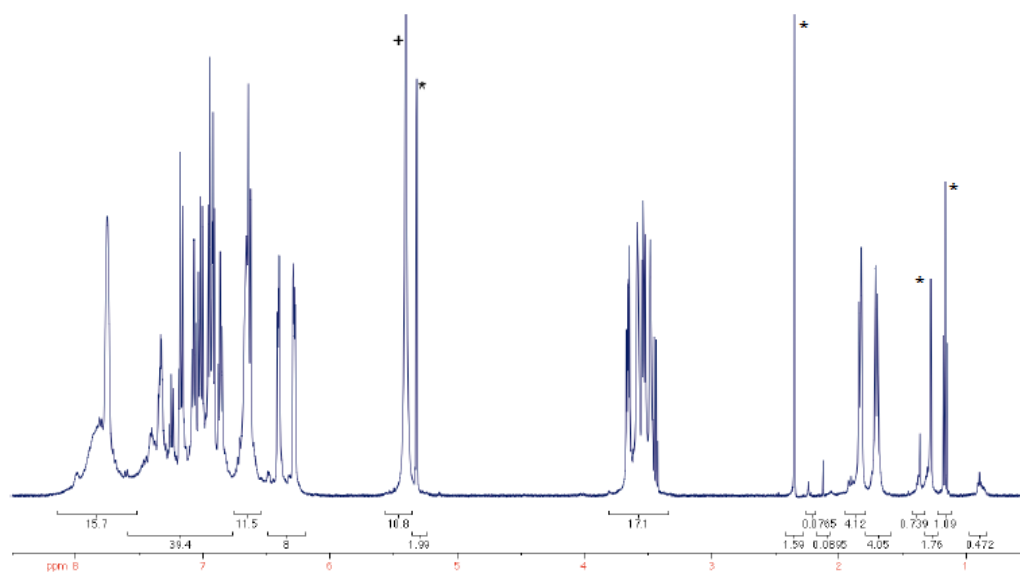


Here, the rhodium chloro-bridged dimer MCM **38** was generated *in situ* from reaction between two equiv. of **36** and one equiv. of **37** in CD_2Cl_2 for 30 minutes at room temperature. It is important to recognize that loss of the labile ethylene ligands in **37** results in the formation of **38** and a

marked color change from orange to dark red accompanies the reaction. Characterization of **38** by NMR spectroscopy ($^1\text{H-NMR}$ and $^{31}\text{P-NMR}$) was carried out *in situ* as attempts to isolate **38** resulted in decomposition through an uninvestigated mechanism. As a result, **38** was used directly in the ROMP assembly.

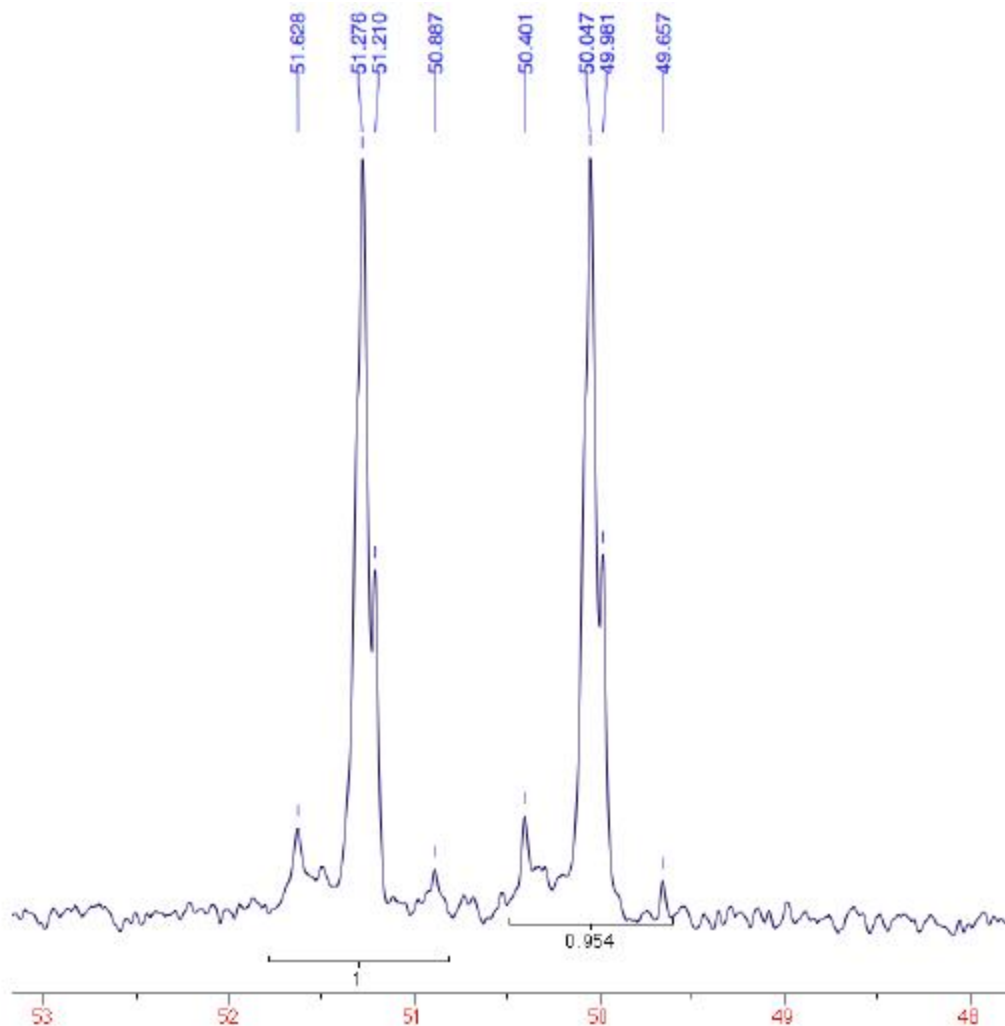
The $^1\text{H-NMR}$ and the $^{31}\text{P-NMR}$ spectra for MCM **38** are shown in Figures 2-6 and 2-7, respectively. Of particular note, the $^1\text{H-NMR}$ spectrum shows signals for residual ethylene ($\delta = 5.4$ ppm) from either the displaced ethylene ligands or excess **37**. Any excess **37** was removed before ROMP polymerization by carefully decanting the solution of **38**. However, residual ethylene still remained in the flask during polymerization, which will be discussed in more detail later in this chapter.

Figure 2-6. $^1\text{H-NMR}$ spectrum of MCM **38**.^a



[a] 399.8 MHz, CD_2Cl_2 , 27°C. + = residual C_2H_4 , * = residual solvent signals.

Figure 2-7. ^{31}P -NMR spectrum of MCM **38**.^a



[a] 162.1 MHz, CD_2Cl_2 , 27°C.

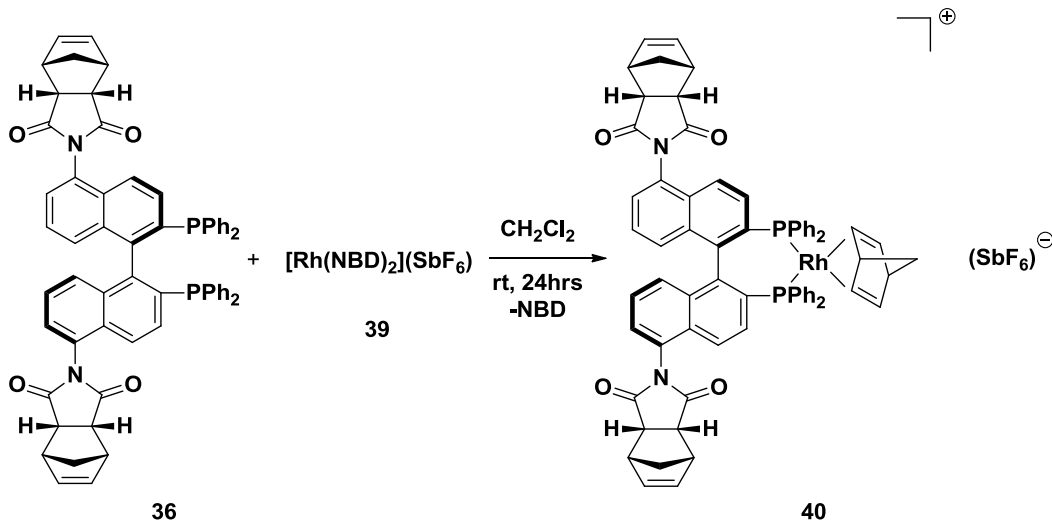
The ^{31}P -NMR spectrum of **38** consists of a doublet of multiplets due to coupling between the Rh and P nuclei ($^1J_{\text{Rh-P}} = 199$ Hz) and the presence of atropisomers of **36**. Further, the main diastereomeric atropisomer of **38** was formed from the addition of one of the C_2 -dissymmetric atropisomers of **36** to **37**. It should be noted that the ^{31}P -NMR spectrum did not contain a signal for free **36**, indicating that all of the ligand had been consumed in the formation of **38**.

It was also discovered that the presence of the rhodium metal center influenced the atropisomerism of ligand **36**. For example, after 90 minutes in solution, signals from all three atropisomers were clearly observed in the ^{31}P -NMR spectrum of **38** whereas these signals were observed immediately for the free ligand. This indicates that rotation about the aryl-N bond is faster in **36** than in **38**. The decreased rate of rotation is most likely due to less electron density in the naphthyl system of **38**, from coordination to the rhodium metal center, than **36**. This would result in more donation from the imide-N to the π^* orbitals on the naphthalene ring, resulting in more C-N double bond character and more hindered, slower rotation.

Section B: Synthesis of $[\text{Rh}(\text{NBD})((R)\text{-}5,5'\text{-dinorimido-BINAP})](\text{SbF}_6)$ (40) MCM

In addition to the rhodium chloro-bridged MCM **38**, we also synthesized a ROMP active rhodium-NBD MCM (**40**) through reaction between $[\text{Rh}(\text{NBD})_2](\text{SbF}_6)$ (**39**) and rotamerically pure **36** as outlined by Scheme 2-8. Here, reaction between one equiv. of **36** and one equiv. of **39** in CH_2Cl_2 for 24 hours at room temperature afforded MCM **40** in 86% yield.

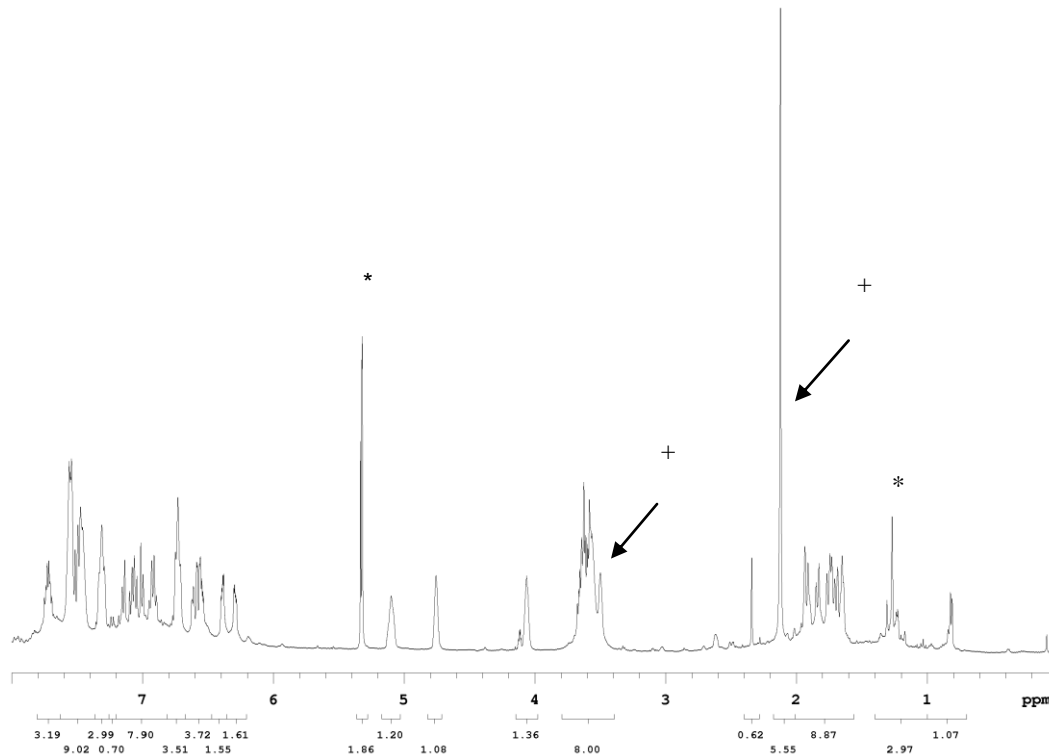
Scheme 2-8. Synthesis of ROMP active rhodium MCM **40**.



Unlike **38**, **40** did not undergo decomposition upon isolation and could be stored as a solid for a significant amount of time (~ 3 years) without decomposing or oxidizing.

The ¹H-NMR and ³¹P-NMR spectra for MCM **40** are shown in Figures 2-8 and 2-9, respectively. In particular, the ¹H-NMR spectrum shows signals for free NBD displaced by **36** ($\delta = 2.10, 3.45$ Hz). It should be noted that the olefinic protons in the free NBD are most likely hidden underneath the binaphthyl aryl protons located at ~ 6.5-7.8 ppm. A portion of the free NBD was removed from **40** by washing with hexanes and decanting off the solution. However, the polymerization of **40** suggested that a portion of the free NBD remained in the flask and became polymerized. Nevertheless, the excess NBD did not appear to prevent the polymerization and the poly-NBD was removed with methanol washes subsequent to the polymerization (refer to section D of this chapter).

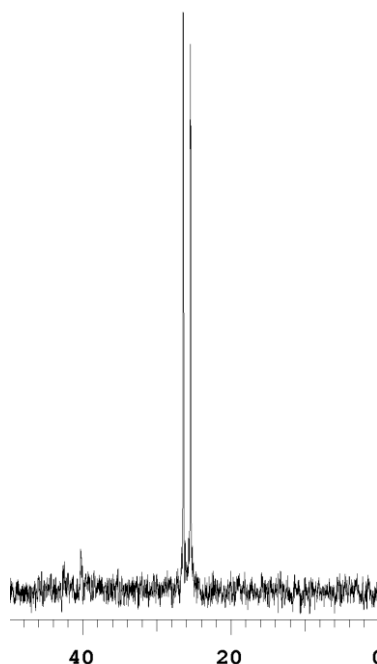
Figure 2-8. $^1\text{H-NMR}$ spectrum of MCM **40**.^a



[a] 399.8 MHz, CD_2Cl_2 , 27°C. * = residual solvent signals, + = signals from free NBD.

The $^{31}\text{P-NMR}$ spectrum of **40** consists of what appears to be a doublet (26.02 ppm, $^1J_{\text{Rh-P}} = 155$ Hz) rather than a doublet of multiplets. Previous coworker Corbin Ralph suggested that this corresponds to **40** being C_2 -dissymmetric and implies that exchange between the ligand atropisomers is occurring faster than the relaxation time so that on the NMR time scale all three of the atropisomers become equivalent.⁵⁷

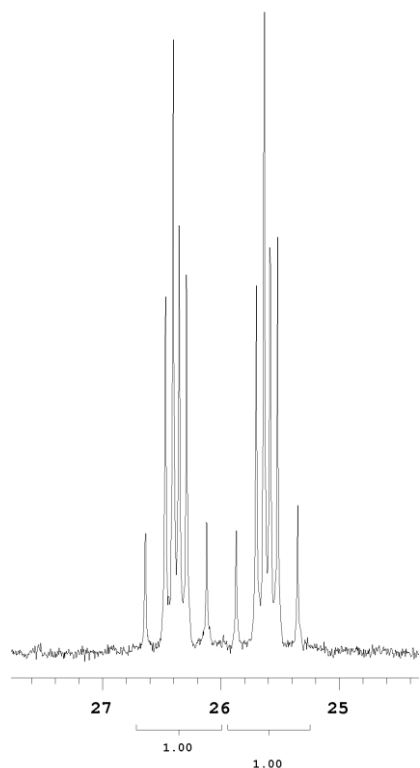
Figure 2-9. ^{31}P -NMR spectrum of MCM **40**.^a



[a] 161.8 MHz, CD_2Cl_2 , 27°C.

However, recording the ^{31}P -NMR of **40** at a higher field gave resonances for all three atropisomers (Figure 2-10) indicating that the rate of rotation is slow relative to the NMR timescale. In fact, the peak pattern for **40** closely resembles the pattern for **36** taken at a higher field at room temperature (see Figure 2-4 for a comparison). This suggests that the rotation about the aryl-N bond in MCM **40** occurs at a similar rate as the free ligand **36**.

Figure 2-10. ^{31}P -NMR spectrum of MCM **40** taken at a higher field.



[a] 202.3 MHz, CD_2Cl_2 , 27°C.

Comparison of the ^{31}P -NMR spectra for MCMs **38** and **40** (Figures 2-7 and 2-10) suggests that the electron density of the rhodium metal center has an effect on the atropisomerism of the ligand. For example, after 90 minutes in solution, signals from all three atropisomers were clearly observed in the ^{31}P -NMR spectrum of **38** whereas these signals were observed immediately for MCM **40**. Therefore, we can conclude that rotation about the aryl-N bond is faster in **40** than in **38**. This phenomenon can be explained by considering the electronic changes that occur upon coordination of **36** to a metal center and the influence that the metal center

may have on the π -conjugation between the norimido groups and the binaphthyl framework. Specifically, a phosphine ligand coordinates to a metal center through σ -donation from the ligand to the metal and π -backbonding from the metal to the ligand.⁶² The rate of rotation about the aryl-N bond will depend, in part, on the amount of π -donation from the norimido groups to the naphthylene units. As a result of π -conjugation in the binaphthyl framework, it is thought that the amount of π -donation from the metal to the ligand is influenced by the amount of π -donation from the norimido groups to the binaphthyl framework and vice versa. Our results show that the [Rh(I)Cl] moiety of **38** is a poorer π -donor than the [Rh(I)(NBD)]⁺ moiety of **40**. The binaphthyl aromatic π -conjugated system in **38** thereby has less electron density than **40** and, as a result, the aryl-N bond in **38** has more double bond character than **40**. As such, the increase in double bond character along the aryl-N bond restricts that rotation of the norimido groups, and thus a decrease in the rate of interconversion between the atropisomers of **38** is observed. Conversely, the interconversion process is faster in **40** as the norimido groups are able to rotate more freely about the aryl-N bond.

At this point it is unknown what effect the mixture of atropisomers may have on the polymerization of these MCMs and on the structure of the polymer-supported catalysts. As well, it may be possible that the rotational behavior of the norimido groups may have an effect on the catalytic properties of the catalysts. Therefore, the ability to dictate the

rotational behavior by changing the electron density of the metal center should be studied in more detail.

Section C: Polymerization of MCMs 38 and 40 via Alternating ROMP

Assembly (altROMP)

As discussed in Chapter 1, Bergens and coworkers found that direct ROMP of MCMs *trans*-[RuCl₂(Py)₂((*R,R*)-Norphos)] (**22**) and *trans*-[RuCl₂(Py)₂((*R*)-5,5'-dinorimido-BINAP)] (**25**) did not readily occur with Grubbs' metathesis catalysts **23** and **27** due to the steric crowding around the norbornene moiety in the ligands.¹³ As detailed in Scheme 1-14, reaction between the MCM and **23** resulted in one event of ring-opening metathesis rather than catalytic ROMP (formation of **22a**). The newly formed ruthenium-alkylidene is too crowded to react with another molecule of the MCM. To successfully assemble the catalyst-organic frameworks, *cis*-cyclooctene (COE) was introduced as a spacer monomer as it is intrinsically less reactive, or strained, than the norbornene units in **22** and **25** and less crowded. In particular, the ring strain energy in COE and norbornene is 7.4 kcal/mol⁶³ and 18.8 kcal/mol⁶⁴, respectively. Therefore, the norbornene units react first with the metathesis catalyst to generate the crowded ruthenium-alkylidene and then this reacts with the COE to insert an eight-carbon long spacer capped with a less crowded ruthenium-alkylidene (formation of **22b**). This can then react with another molecule of

the MCM to form a new, crowded ruthenium-alkylidene, followed by reaction with COE, etc. This alternating cycle will continue until all the norbornene units are consumed generating a three-dimensional, cross-linked, polymer-supported catalyst-organic framework. Due to the alternating nature of this polymerization, Bergens and coworkers termed this process alternating ROMP assembly (altROMP). This methodology was utilized in the synthesis of the rhodium catalyst-organic frameworks from MCMs **38** and **40**, which will be discussed shortly.

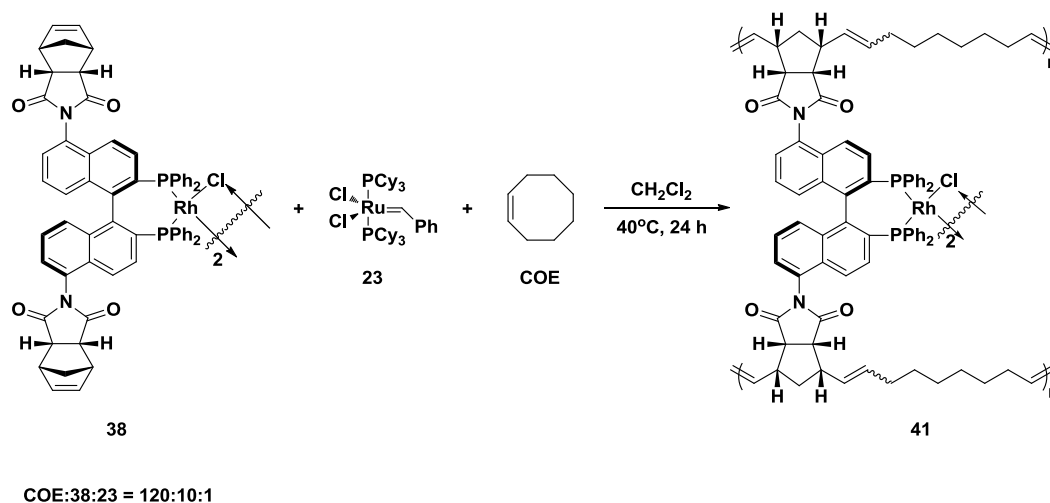
In addition, previous coworker Corbin Ralph found that better control over the altROMP was achieved using the less active 1st generation Grubbs catalyst **23**, than using the more active 2nd generation Grubbs catalyst **27**.⁵⁷ He illustrated this better control in separate experiments involving the altROMP of **22**:COE:**23** or **27** in 20:80:1 ratio. During the reaction with **23**, a peak in the ³¹P-NMR spectrum representing free PCy₃ (tricyclohexylphosphine) was present in equal intensity as **23**, whereas with **27**, only a trace amount of free PCy₃ was present. The difference in intensity of the signals for free PCy₃ suggests that the initiation is faster for catalyst **23** than for **27**. Thus, the rate of propagation is slower than the rate of initiation for **23** and the reverse is true for **27**; only traces of **27** are active during altROMP. It is known that faster initiation catalysts result in narrow molecular weight distributions of ROMP products,⁶⁵ therefore, Ralph postulated that use of **23** would produce an alternating polymer with a narrow molecular weight distribution.

As well, Ralph observed that altROMP went to completion when **23** was used while a considerable amount of unreacted **22** was left in solution after all of the COE was consumed when **27** was employed. This suggested that the consumption of COE was more favored than the MCM **22** and, as a result, the addition of extra COE during the polymerization was required for consumption of **22**. Ralph speculated that the steric bulk of the mesityl groups in **27** decreased its reactivity towards **22** and it was probable that not all of **27** had formed to generate the propagating catalyst as only a trace of free PCy₃ was observed in the ³¹P-NMR spectrum. As a result of this study, 1st generation Grubbs catalyst **23** was the catalyst of choice for the altROMP of MCMs **38** and **40** with COE.

The altROMP assembly of the MCM **38** was performed using a 120:10:1 ratio of COE:**38**:**23** as shown in Scheme 2-9.⁶⁶ This corresponds to three COEs for every norimido group present. Specifically, 10 equiv. of **38** were reacted with 1 equiv. of **23** and 120 equiv. of COE in CH₂Cl₂ at 40°C for 24 hours to give the polymer-supported catalyst-organic framework **41**. We expected **41** to be quite different from the ruthenium frameworks **24** and **26** synthesized by Ralph (see Chapter 1) as the chloro-bridging ligands in MCM **38** bridge the two catalyst centers and act as an additional crosslinking agent. This additional crosslinking likely alters the rigidity and the solubility of the framework. In fact, we found that **41** precipitates from solution at concentrations greater than 6.5 x 10⁻³ M in CH₂Cl₂ while **24** and **26** remain in solution at concentrations as high as 1.0

$\times 10^{-2}$ M, indicating that **41** is significantly less soluble than the other, less rigid/crosslinked frameworks.

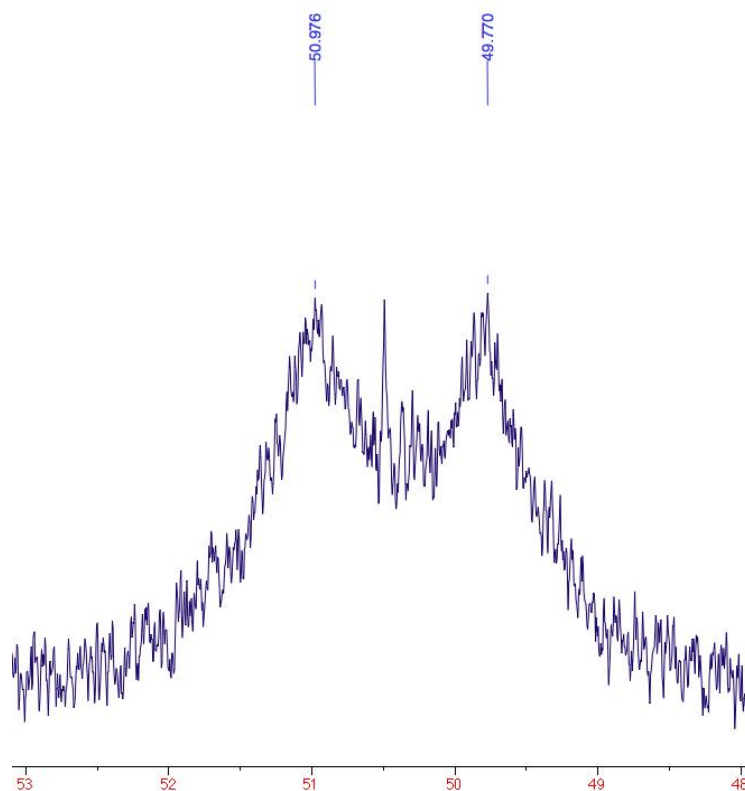
Scheme 2-9. Synthesis of polymer-supported catalyst-organic framework **41** from altROMP assembly.



The ^{31}P -NMR spectrum of framework **41** is given in Figure 2-11 and contains a broad doublet at 50.4 ppm ($^1J_{\text{Rh-P}} = 195$ Hz). By comparison, the ^{31}P -NMR spectrum of MCM **38** contained a doublet of multiplets (50.6 ppm, $^1J_{\text{Rh-P}} = 199$ Hz) (refer to Figure 2-7). As the chemical shift and the Rh-P coupling constant are nearly identical for both the framework and the MCM, we concluded that the electronic environment of the rhodium metal center was not significantly altered during polymerization. This is a desirable benefit of both the design of the MCM and the altROMP immobilization methodology since, as discussed in Chapter 1, changes in

the electronic environment of a metal center can result in unpredictable activities and selectivities.⁴⁴

Figure 2-11. ³¹P-NMR spectrum of framework **41**.^a



[a] 161.2 MHz, CD₂Cl₂, 27°C.

The ¹H-NMR spectra of **38** with COE and **23** after initial mixing and the framework **41** after 24 hours are shown in Figure 2-12.

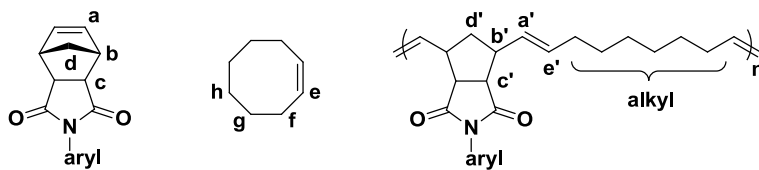
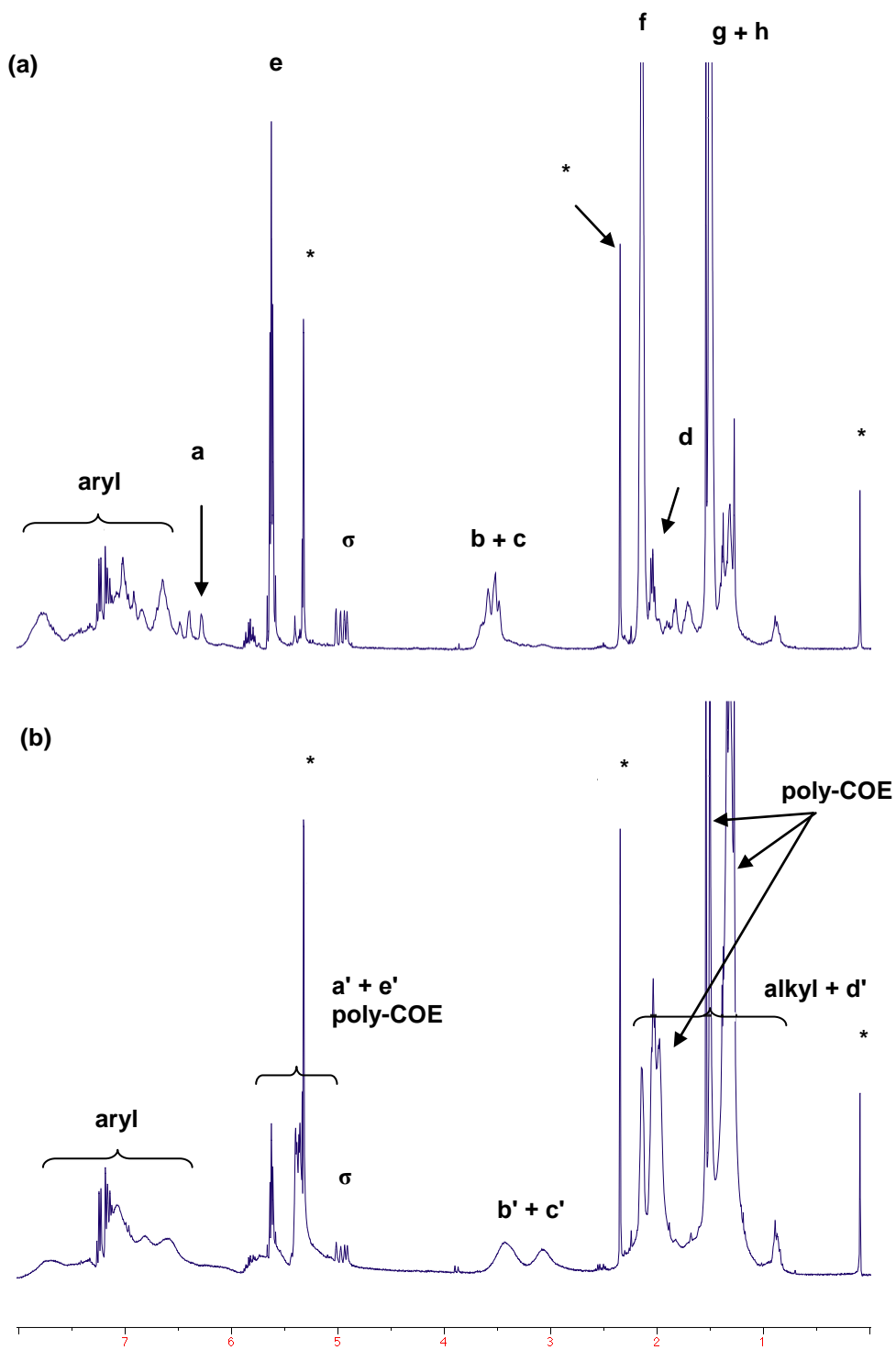


Figure 2-12. $^1\text{H-NMR}$ spectra of (a) **38** with COE and **23** after initial mixing and (b) the catalyst-organic framework **41** after 24 hours.



[a] 399.8 MHz, CD_2Cl_2 , 27°C . * = residual CH_2Cl_2 , toluene and TMS, σ = product between COE and residual C_2H_4 .

Analysis of the $^1\text{H-NMR}$ spectra reveals some key characteristic features of the polymerization as the sharp proton peaks of both monomers **38** and COE decrease and broad polymer peaks increase during the polymerization. The olefinic signals for **38** and COE are labeled **a** and **e** respectively and the polymer olefin signals are labeled **a'** and **e'**. As the polymerization proceeds, the olefin protons **a** in **38** are converted into the polymer olefin region between 5.2-5.9 ppm when **38** is consumed. The olefin protons **e** in COE overlap with the polymer olefin region and these are also converted into this region when COE is consumed. As well, the norbornene protons, labeled **b** and **c**, are buried under the broad polymer norbornene signals (**b'** and **c'**) between 2.8-3.6 ppm and the alkyl protons of both monomers overlap with the polymer alkyl protons, labeled **alkyl** and **d'**, between 0.9-2.3 ppm. As a result of the large degree of overlap between the monomer signals and the polymer signals, the consumption of **38** was extremely difficult to monitor. Nevertheless, from *in situ* peak-height comparison of olefin signals, a general rate of reaction was determined by previous coworker Michael Hass.⁶⁷

The $^1\text{H-NMR}$ spectrum recorded minutes after mixing the metathesis catalyst **23** and the solution of **38** and COE (Figure 2-12a) showed that polymerization had already begun. Specifically, the broadening of the norbornene proton signals (**b** and **c**), aryl signals and norimido olefin signal **a** was an indication that polymerization was occurring (for a comparison to MCM **38** refer to Figure 2-6). After 3 hours

of reaction time, 53% of the norimido units in **38** and 29% of the COE had been consumed. Although less COE was consumed, there was initially three times the amount of COE present in comparison to one norimido moiety. When normalized, the ratio of COE to norimido consumed is ~ 1.7:1. This indicates that the polymerization is not truly alternating as approximately 5 COEs are consumed for every 3 norimido units; not 1:1 as was observed by Ralph in the polymerization of **25**.^{13b} After 7 hours of reaction time, 80% of the norimido units and 56% of the COE were consumed, again corresponding to a normalized ratio of ~ 1.7:1 COE to norimido units. Within 24 hours all of the norimido units and only 80% of the COE units had been consumed, corresponding to a ratio of COE to norimido consumed of ~ 2.4:1.

During polymerization, peaks at ~ 5.4, 2.0, 1.5 and 1.2 ppm were observed in the ¹H-NMR spectrum and were consistent with poly-COE made by ROMP.⁶⁸ These signals may arise from two or more COEs joined during altROMP or by ROMP of COE alone and the intensity of these peaks increased as the altROMP assembly proceeded. After 7 hours, most of the norimido units had been consumed (80%) and the rate of COE consumption increased, resulting in an increase in the growth of the poly-COE signals. This suggests that while norimido units are present in the reaction mixture, the majority of **23** is involved in the altROMP assembly of **38** with COE. However, as the norimido units are consumed, more COE becomes polymerized until eventually when all the norimido units have

reacted, the polymerization of COE to poly-COE takes over completely. Therefore, we postulated that the ratio of COE to norimido groups within the framework the ratio of COE to norimido group is ~ 1.7:1 and that some portion of the remaining COE was grafted to the outside of the framework as poly-COE or involved in the production of pure poly-COE. The poly-COE was subsequently removed by methanol washes after catalyst deposition.

As mentioned previously, framework **41** differs from the ruthenium-BINAP framework (**26**) synthesized by Ralph as it is not truly alternating (i.e. 1:1 ratio of COE to norimido group). We attributed this difference to the dimeric nature of **38** and the resulting steric hindrance between the opposite ends of the dimer (refer to Scheme 2-7). More specifically, the crystal structure of the iridium analogue $[\text{IrCl}((S)\text{-BINAP})]_2$ shows that this complex is not planar; rather a “butterfly” shape is adopted with the angle between the coordination planes of the iridium centers is 126° .⁶⁹ It is likely that the rhodium dimer **38** adopts a similar structure. This “butterfly” shape imparts a greater degree of steric hindrance about the norimido groups in **38** that is not present in the ruthenium MCM **25** and, as a result, decreases the net reactivity of the norimido groups to ROMP relative to COE, resulting in more incorporation of COE into the framework.

There was also a signal at ~ 5.0 ppm (multiplet) present in all of the spectra recorded. Previous coworker Michael Hass confirmed that this peak was due to metathesis reactions between COE and the residual

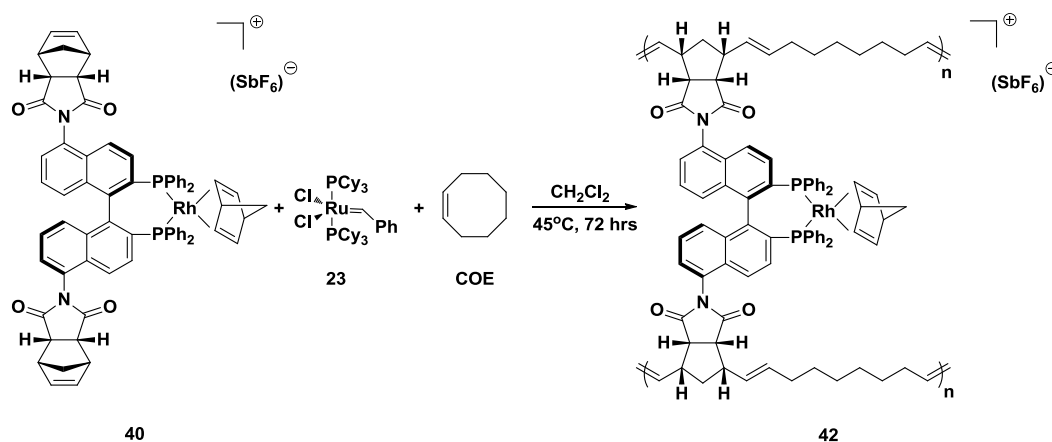
ethylene found in solution during the preparation of **38** (refer to Figure 2-6 for the $^1\text{H-NMR}$ spectrum of **38**) from an experiment wherein COE was polymerized with **23** in a 120:1 ratio and then spiked with ethylene.⁶⁷ It should be noted that this side product was removed in methanol washes after catalyst deposition.

Previous coworker Michael Hass also attempted to characterize both the MCM **38** and the framework **41** by mass spectrometry and elemental analysis.⁶⁷ He found that both ESI-MS (electrospray ionization mass spectrometry) and MALDI-TOF (matrix-assisted laser desorption/ionization time-of-flight) mass spectrometry were unsuccessful. Specifically, it was found that **38** would not ionize through positive mode electrospray ionization; the only m/z (mass-to-charge ratio) detected was attributed to THF. Ionization of **38** did occur with MALDI-TOF mass spectrometry; however, the highest m/z species detected corresponded to a dimer with one phosphorus of one of the **36** ligands oxidized and one bridging chloride abstracted (i.e. $[\text{Rh}_2\text{Cl}((R)\text{-}5,5'\text{-dinorimido-BINAP})((R)\text{-}5,5'\text{-dinorimido-BINAP-oxide})]$). Attempts to carry out mass spectrometry on framework **41** were also unsuccessful as the only m/z detected was attributed to THF. Elemental analysis indicated that framework **41** consisted of 70.31% carbon, 1.92% nitrogen and 7.23% hydrogen, which is consistent with NMR evidence that ~1.7 to 2.4 COEs per norimido group were incorporated into the framework. These results are by no means

conclusive and more extensive characterization of the polymer framework should be done (see Chapter 6 for a discussion).

In addition to framework **41**, we also synthesized a catalyst-organic framework from the altROMP assembly of the rhodium MCM **40** as outlined in Scheme 2-10.

Scheme 2-10. Synthesis of polymer-supported catalyst-organic framework **42** from altROMP assembly.



COE:40:23 = 120:20:1

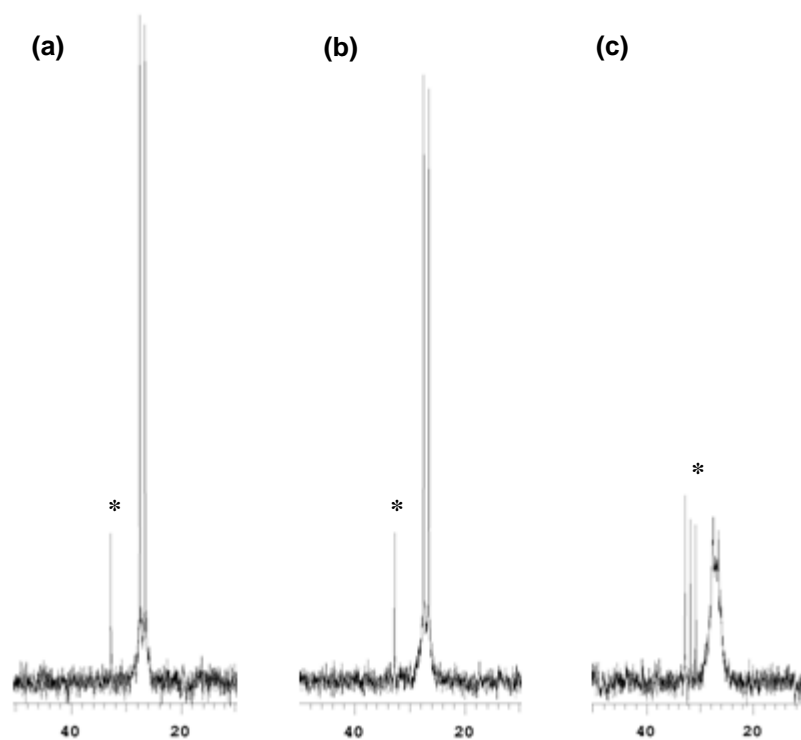
** An additional equivalent of 23 was added after 48 hours to speed up the polymerization

Here, COE, the MCM **40** and the metathesis catalyst **23** were reacted in a 120:20:1 ratio, respectively, in CH_2Cl_2 at 45°C for 48 hours, after which an additional equivalent of **23** was added to speed up the polymerization. The polymer-supported catalyst-organic framework **42** was produced after 72 hours of total reaction time. Similar to the synthesis of **41**, this corresponds to three COEs for every norimido group present. Unlike **41**, framework **42** does not have additional crosslinking at the rhodium metal

centers. As well, the altROMP of **40** may differ from that of **38** as **40** is a charged complex and **38** is neutral. For example, more COE units may be incorporated into framework **42** to minimize repulsions between the charged metal centers.

The polymerization of **40** with COE in the presence of metathesis catalyst **23** was followed by ^{31}P -NMR spectroscopy, the spectra of which are given in Figure 2-13.

Figure 2-13. ^{31}P -NMR spectra of the altROMP assembly of **40** with COE after (a) 24 hours, (b) 48 hours and (c) 72 hours.^a

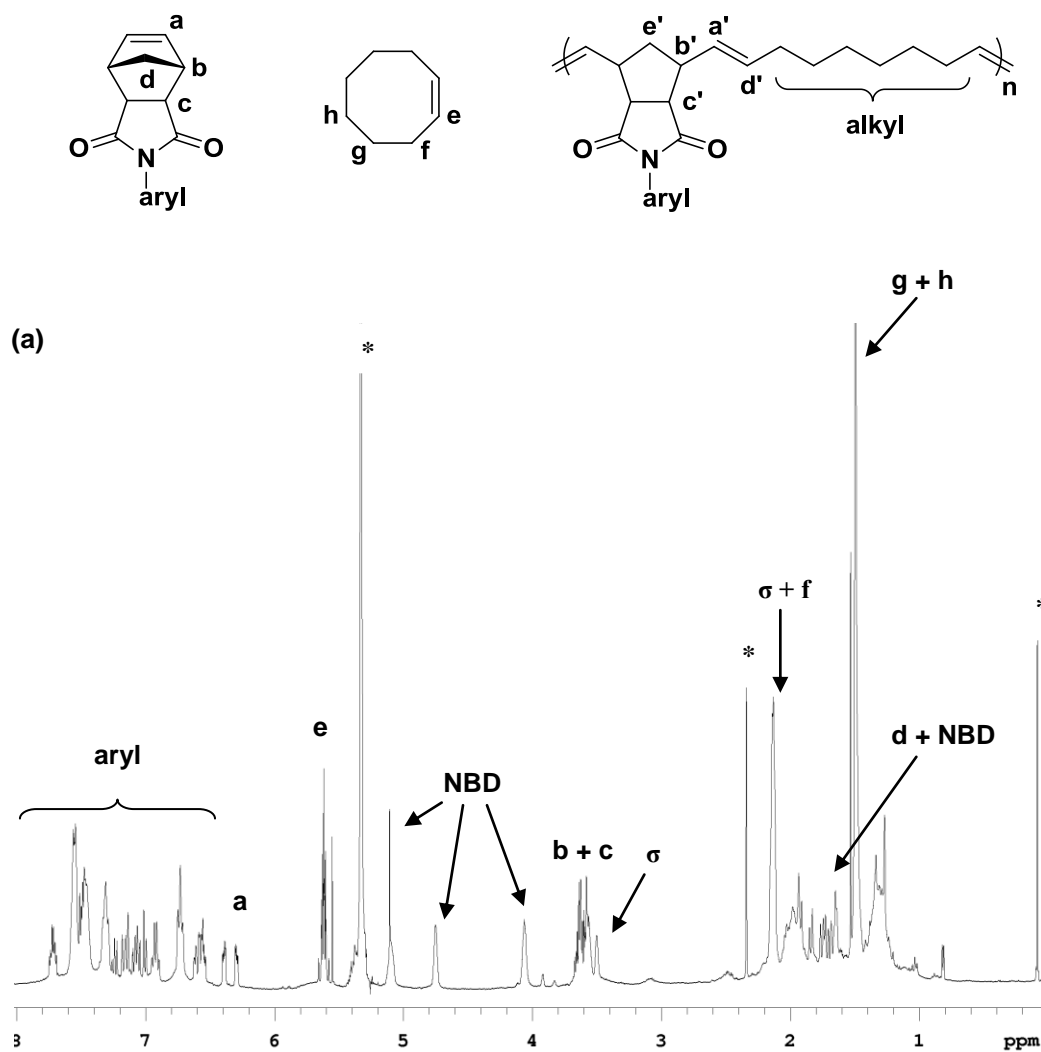


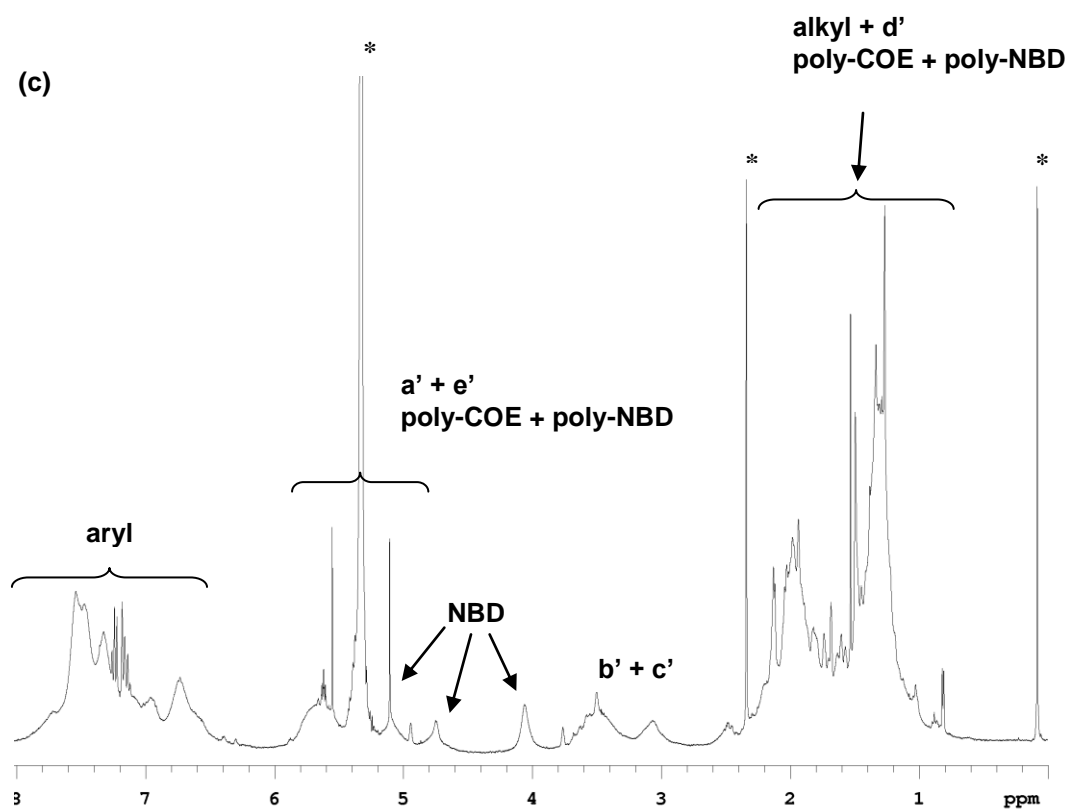
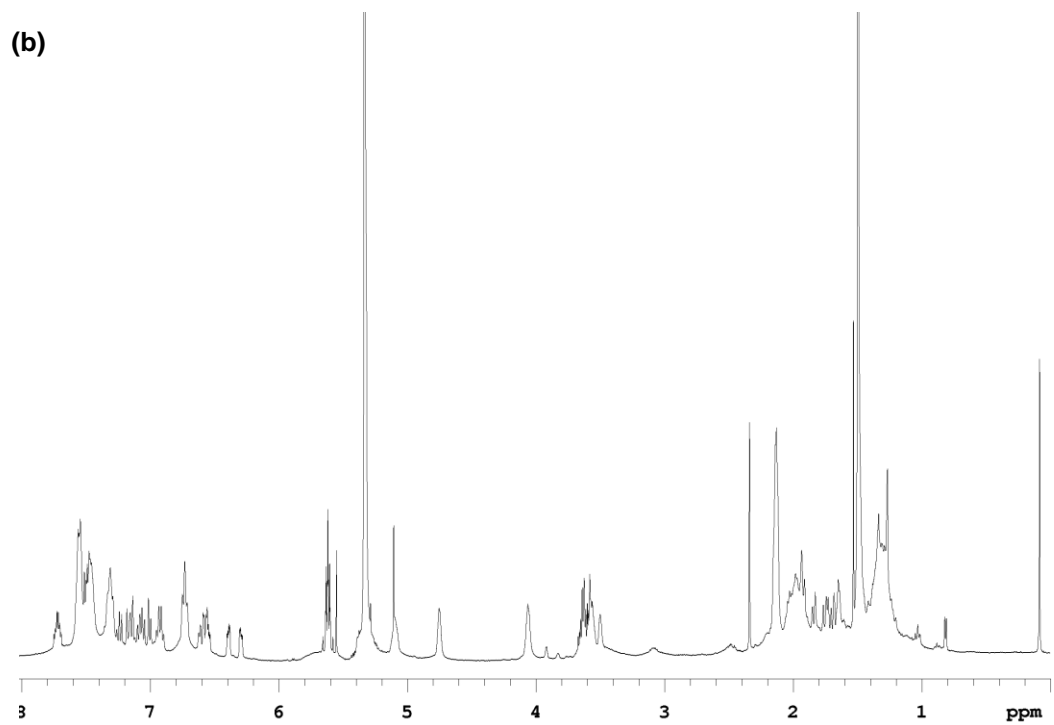
^[a] 161.8 MHz, CD_2Cl_2 , 27°C. * = residues of metathesis catalyst **23**.

The ^{31}P -NMR spectra were recorded 24 hours (Figure 2-13a), 48 hours (Figure 2-13b) and 72 hours (Figure 2-13c) after mixing **40** with COE and **23** and show a gradual broadening of the sharp apparent doublet, indicative of polymerization (refer to Figures 2-9 and 2-10 for the ^{31}P -NMR spectra of MCM **40**). The broad doublet for framework **42** at ~ 27.0 ppm ($^1J_{\text{Rh-P}} = 155$ Hz) has nearly the same chemical shift and Rh-P coupling as the MCM **40** (26.0 ppm, $^1J_{\text{Rh-P}} = 155$ Hz), thereby indicating that the electronic environment of the rhodium metal center was not significantly altered during polymerization. As well, the peak for framework **42** has the same shape as the MCM. This finding is consistent with the results obtained from the synthesis of framework **41** discussed previously in this section.

The altROMP assembly of **40** with COE was also monitored by ^1H -NMR spectroscopy 24 hours, 48 hours and 72 hours after mixing as shown in Figure 2-14. Similar to the ^1H -NMR spectra recorded for the altROMP assembly of **38** (Figure 2-12), there is a large degree of overlap between the monomer signals and the polymer signals. This makes it difficult to monitor the consumption of **40** and, as this was only a preliminary study, *in situ* NMR studies still need to be done in order to determine the amount of COE incorporated into the framework. Nevertheless, some conclusions can be made about the polymerization and comparison can be made to the polymerization of **38**, discussed at length previously in this chapter.

Figure 2-14. $^1\text{H-NMR}$ spectra of the altROMP assembly of **40** with COE after (a) 24 hours, (b) 48 hours and (c) 72 hours.^a





[a] 399.8 MHz, CD_2Cl_2 , 27°C. * = residual CH_2Cl_2 , toluene and TMS. σ = residual free NBD.

The $^1\text{H-NMR}$ spectrum recorded 24 hours after mixing the metathesis catalyst **23** and the solution of **40** and COE (Figure 2-14a) showed that the polymerization, although quite sluggish, had begun. Specifically, the appearance of a peak at ~ 3.1 ppm, due to one of the bridgehead protons **b'** and **c'**, and the slight broadening of norbornene proton signals **b** and **c**, suggests that the norimido olefin in the ligand has started to undergo ROMP. After 48 hours (Figure 2-14b), the aryl signals began to show signs of broadening and signals attributed to poly-COE (or poly-NBD) began to appear indicating that the polymerization, although not anywhere near complete, was progressing. Therefore, we decided to add an additional equivalent of **23** to the reaction mixture to speed up the polymerization. After an additional 24 hours, 72 hours of total reaction time (Figure 2-14c), the norimido olefin peaks labeled **a** (6.2-6.4 ppm) had largely disappeared and the presence of signals **b'** and **c'** suggest that the polymerization had gone to completion.

In the synthesis of framework **41**, the polymerization had been complete after 24 hours, while the polymerization of **40** with COE took 72 hours to complete and required an extra equivalent of **23**. The reason for this slower rate of polymerization is currently unknown and more research is required. In particular, *in situ* NMR studies of the altROMP and more extensive characterization of the polymer framework should be done (refer to Chapter 6).

Section D: Deposition of Frameworks **41** and **42** on Insoluble Supports

A common problem often encountered with polymer-supported catalysts is lower catalytic activity and selectivity due to restrictions of the polymer matrix that prevent substrate from reaching the catalytic active sites (refer to Chapter 1). Particularly, the surface areas of such catalysts are typically quite low and, as a result, only the catalytic active sites on the surface are involved in the catalytic process. Common approaches to overcome this problem include the use of co-solvents that swell the polymer matrix thereby opening paths to and from the active sites.⁷⁰ Crosslinking agents are often used to impart rigidity to the polymer matrix thus preventing the matrix from collapsing on the active sites. High surface area monolithic^{39,71} or silica systems^{37,72} and nanoparticles³² have also been used to support either thin films of polymeric catalysts or bonded monomeric catalysts. We decided to utilize economic, inert and high surface area supports that do not require additional functionalization of the polymeric catalyst to attach it to the support. This was accomplished by depositing frameworks **41** and **42** as thin films over BaSO₄ and, in the case of **41**, Ba-L-tartrate in a one-pot procedure. These supports act as filtration aids and impart mechanical stability towards rapidly stirred batch reactions in which the catalysts are reused. To the best of our knowledge,

barium salt supports have not been used to support polymeric catalysts outside of the Bergens group.

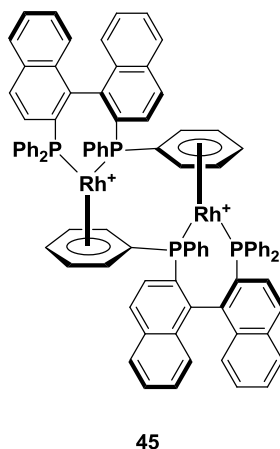
After altROMP assembly, the polymer-supported catalyst-organic frameworks **41** and **42** were supported as thin films over BaSO₄ or Ba-L-tartrate by slow evaporation of a dilute solution of the desired polymer in CH₂Cl₂ with rapid stirring. A concern encountered with polymeric catalysts is metal leaching caused by the presence of un-polymerized or soluble low molecular weight oligomers of the catalyst monomer, which renders the reaction mechanism homogeneous rather than heterogeneous.⁷³ In order to remove any low molecular weight oligomers present from the altROMP assembly, the BaSO₄ and Ba-L-tartrate-supported catalysts were washed with methanol before use. ³¹P-NMR and ¹H-NMR spectra of the washings showed only the presence of poly-COE in the case of **41** and poly-COE and poly-NBD in the case of **42** indicating that all of **38** and **40** were consumed and incorporated into catalyst-organic frameworks **41** and **42**, respectively. Once supported, frameworks **41** and **42** were tested as heterogeneous catalysts in 1,6-enyne cycloisomerizations (Chapter 3), allylic alcohol isomerizations (Chapter 4) and continuous-flow hydrogenation reactions (Chapter 5).

Section E: Activation of Catalyst-Organic Frameworks 41 and 42

Both frameworks **41** and **42** have the same catalytic active species “[Rh((*R*)-5,5'-dinorimido-BINAP)]⁺” (**43**). **43** is generated by abstracting the bridging chloride ligands in **41** with silver salts (e.g. AgBF₄, AgSbF₆, etc.) and hydrogenating the NBD ligand in **42** to norbornane. Once generated, **43** most likely exists as a disolvento complex in the presence of coordinating solvents. In fact upon hydrogenation of [Rh(BINAP)(diolefin)]X (diolefin = COD or NBD, X = weakly coordinating counter ion) in coordinating solvents such as MeOH, THF and acetone, Heller and coworkers isolated the disolvento species [Rh(BINAP)(sol)₂]⁺ (**44**) (sol = solvent).^{74a} **44** is capable of undergoing oxidative additions resulting in loss of the solvent ligands and is generally believed to be an active catalyst in a variety of reactions.

In the absence of coordinating solvents, **43** most likely forms bonds to the support or the framework until substrate is present in the reaction mixture. For example, Heller and Miyashita both reported the preparation of [Rh(BINAP)₂]²⁺ (**45**),⁷⁴ as shown in Figure 2-15.

Figure 2-15. $[\text{Rh}(\text{BINAP})_2]^{2+}$ (**45**) catalyst resting state.



Here, the phenyl rings on the BINAP ligand bridge two rhodium centers by coordinating to another rhodium center in an η^6 fashion. Although this bonding interaction yields two 18-electron rhodium centers, Miyashita showed that in the presence of coordinating substrates or solvents this bonding interaction is disfavored.^{74b} Moreover, this weak bonding interaction is believed to stabilize the catalytic active centers prior to addition of substrate.

After abstraction of the chloride bridges in **41** with a silver salt, it is possible that the rhodium centers exist as close proximity pairs within the framework. As a result, there may be Rh-Rh interactions or cooperativity in **41** and, in the absence of coordinating solvents or substrate, the interaction illustrated in Figure 2-15 would be possible within the framework. On the other hand, it is unlikely that framework **42** contains close proximity rhodium pairs (refer to Scheme 2-10) and, as a result, the rhodium-arene bridged species is unlikely to form within the framework.

Rather, it is possible that the active species in **42**, in the absence of coordinating solvents or substrate, forms bonds to olefin groups in the backbone of the polymer or interacts with the BaSO₄ support. Characterization of the active catalysts in **41** and **42** could potentially confirm these speculations but was not within the scope of this project (refer to Chapter 6 for a discussion on future work).

Conclusion

The work presented in this chapter illustrates the versatility of the altROMP methodology developed by Bergens and coworkers. Here, the ROMP active BINAP ligand **36** prepared previously in our laboratories was used to prepare the rhodium MCMs **38** and **40**. Detailed NMR studies provided a greater understanding of the rotational behavior of the norimido groups in the MCMs and insight into ways to control the interconversion process between the atropisomers. Using Grubbs metathesis catalyst **23**, polymer-supported catalyst-organic frameworks **41** and **42** were prepared by the altROMP assembly of **38** and **40** with COE, respectively. Although more characterization of these frameworks is required, NMR studies suggest that the electronic environment of the rhodium metal center was not significantly altered during polymerization. Frameworks **41** and **42** were deposited as thin films onto insoluble, chemically inert barium salts to improve mass transport to the active sites and impart mechanical stability to the frameworks. The remaining chapters in this dissertation discuss the use of **41** and **42** as heterogeneous catalysts for 1,6-enyne cycloisomerizations (Chapter 3), allylic alcohol isomerizations (Chapter 4) and continuous-flow hydrogenation reactions (Chapter 5).

Experimental

General procedures and methods. ^1H -NMR and ^{31}P -NMR spectra were recorded using Varian Inova (300, 400, 500 MHz) or Varian Unity (500 MHz) spectrometers. ^1H -NMR chemical shifts are reported in parts per million (δ) relative to TMS with the solvent as the internal reference. ^{31}P -NMR chemical shifts are reported in parts per million (δ) relative to an external reference of 85% $\text{H}_3\text{PO}_{4(\text{aq})}$.

Unless otherwise stated, all experiments were performed under an inert atmosphere using standard Schlenk and glove-box techniques. Argon and nitrogen gas (Praxair, 99.998%) were passed through a drying train containing 3Å molecular sieves and indicating DrieriteTM before use. All solvents were dried and distilled under a nitrogen atmosphere using standard drying agents, unless otherwise noted. All common reagents and solvents were obtained from Sigma Aldrich Co. and used without further purification, unless otherwise stated. The ROMP catalyst bis(tricyclohexylphosphine)benzylidene ruthenium(IV) dichloride (**23**) and (*R*)-BINAP were obtained from Strem Chemicals, Inc. and used without further purification. $[\text{RhCl}(\text{C}_2\text{H}_4)_2]_2$ ⁷⁵ and $[\text{Rh}(\text{NBD})_2](\text{SbF}_6)$ ⁷⁶ were synthesized according to literature procedures. BaSO_4 (white reflectance) and Ba-L-tartrate were obtained from Eastman Chemical Co., Inc. and washed thoroughly with CH_2Cl_2 and MeOH and dried under vacuum prior to use.

Synthesis of (*R*)-BINAP dioxide (32). Commercially available (*R*)-BINAP (1.08 g, 1.73 mmol) was dissolved in toluene (200 mL, undistilled) and oxidized by adding a solution of 10% H₂O₂ (90 mL). The reaction mixture was stirred overnight at room temperature and then washed with a solution of saturated Na₂S₂O₃ (3 x 50 mL) until the excess H₂O₂ was neutralized. This was followed by washing with H₂O (3 x 50 mL) and saturated NaCl solution (3 x 50 mL). The organic layer was dried over Na₂SO₄, filtered, and concentrated under reduced pressure to afford a white powder of **32** in 99% yield (1.125 g, 1.72 mmol). Further purification was unnecessary. The spectroscopic data were in accordance with the literature.^{13b}

Synthesis of (*R*)-5,5'-dinitro-BINAP dioxide (33). Under a N₂ atmosphere, a 100 mL side-arm round-bottom flask was charged with 10 mL of freshly distilled acetic anhydride. The flask was chilled in a salt (NaCl) ice bath and 3 mL of concentrated nitric acid was added dropwise with stirring over a period of 1 hour. A small amount of concentrated sulfuric acid (0.3 mL) was added dropwise to the reaction mixture. **32** (1.125 g, 1.72 mmol) was added to the colorless reaction mixture followed by stirring at 0°C for 2 hours. The resulting yellow reaction mixture was quenched by slow addition into 200 mL of a 10% NaOH_(aq) solution. A yellow precipitate immediately crashed out of solution and the mixture was left in the ice-water bath for 1 hour. The yellow precipitate was collected by

filtration, washed with cold H₂O (3 x 10 mL) and dried under reduced pressure. The yellow solid was dissolved in a minimum amount of CH₂Cl₂ and precipitated by the slow addition of hexanes to afford orange crystals of **33** in 93% yield (1.19 g, 1.60 mmol). The spectroscopic data were in accordance with the literature.^{13b}

Synthesis of (R)-5,5'-diamino-BINAP dioxide (34). A glass autoclave equipped with a ½" stir bar was charged with 0.912 g (1.22 mmol) of **33** along with 0.1368 g of 5 wt% Pd/C (0.0643 mmol of Pd). The autoclave was purged with hydrogen gas for 20 minutes and then charged with 15 mL of degassed EtOH. The vessel was sealed, pressurized to 45 psig and lowered into a 50°C oil bath for 6 hours. The reaction mixture was filtered to remove the Pd/C, which was washed with EtOH and CH₂Cl₂ in succession until the washings ran colorless. The filtrate was concentrated under reduced pressure and purified with flash chromatography (neutral alumina, 93:7 CH₂Cl₂:EtOH, R_f = 0.75). Fractions collected were monitored by thin layer chromatography. The volatile solvents were removed under reduced pressure, giving **34** as a black solid in 87% yield (0.730 g, 1.07 mmol). The spectroscopic data were in accordance with the literature.^{13b}

Synthesis of (R)-5,5'-diamino BINAP (18). A high pressure reactor flask was charged with a solution of **34** (1.05 g, 1.53 mmol) in

distilled toluene (18 mL). The reactor was then placed in an ice-water bath. Distilled triethylamine (4.27 mL, 30.6 mmol) and trichlorosilane (3.09 mL, 30.6 mmol) were added and the reactor was sealed. The reaction mixture was warmed to room temperature and then heated to 120°C for 16 hours. The reactor was cooled to room temperature and the reaction mixture was treated with 10% deoxygenated NaOH_(aq) (150 mL). The reaction mixture was stirred at room temperature under a nitrogen atmosphere for 30 minutes. The layers were separated and the aqueous layer was back-extracted with deoxygenated toluene (3 x 75 mL). The combined organic layers were washed with deoxygenated water (3 x 50 mL), dried over Na₂SO₄, filtered and concentrated under reduced pressure to give **18** as a brown solid in 84% yield (0.88 g, 1.4 mmol). The spectroscopic data were in accordance with the literature.^{13b}

Synthesis of ((R)-5,5'-N-di(cis-5-norbornene-2,3-dicarboximido)-2,2'-bis(diphenylphosphino)-1,1'-binaphthyl), (R)-5,5'-dinorimido-BINAP (36). A heavy walled Schlenk flask was charged with **18** (0.144 g, 0.221 mmol). The flask was evacuated and back-filled (3 x) with nitrogen gas and then sealed with a rubber septum. 5 mL of deoxygenated toluene were added to the flask using a gas-tight syringe to from an orange mixture, with the ligand only partially dissolved. A large excess (12 equiv.) of cis-5-norbornene-*endo*-2,3-dicarboxylic anhydride (**35**) (0.4355 g, 2.65 mmol) was quickly weighed in air and transferred to a

25 mL round-bottom flask equipped with a side-arm. The flask was evacuated and back-filled (3 x) with nitrogen gas and 5 mL of deoxygenated toluene were added to the flask using a gas-tight syringe to form a clear colorless solution. The solution was transferred by cannula to the high-pressure reactor flask using 5 mL of toluene wash. Next, freshly distilled triethylamine (0.268 g, 2.65 mmol) was transferred to the high-pressure reaction flask using a gas-tight syringe. The flask was then sealed with a Teflon valve and the reaction mixture was heated at 90°C with stirring for 48 hours. The reactor was cooled to room temperature and the reaction mixture was transferred via cannula to a nitrogen-purged round-bottom flask (200 mL) with a side-arm using toluene wash (3 x 5 mL). The combined toluene fractions were then treated with 1 M deoxygenated NaOH_(aq) (100 mL) to hydrolyze the excess unreacted anhydride. The flask was gently swirled for 20 minutes to ensure complete mixing and then left to settle. The layers were separated and the aqueous layer was back-extracted with deoxygenated toluene (4 x 20 mL). The combined organic layers were washed with deoxygenated water (3 x 20 mL), dried over anhydrous Na₂SO₄ and cannula filtered using toluene wash (3 x 10 mL) into a round-bottom flask (250 mL). The volatiles were removed under reduced pressure to give **36** as a brown solid in 81% yield (0.169 g, 0.179 mmol). The spectroscopic data were in accordance with the literature.^{13b}

Isolation of a C₂-dissymmetric diastereomer of 36. A nitrogen purged high-pressure flask was charged with **36** (0.514 g) and 15 mL of deoxygenated toluene. The flask was sealed with a Teflon valve and the brown solution was warmed to 90°C. Within 10 minutes, a white precipitate was observed in the solution. After continued heating for 3 days, the sides of the flask were covered with the white precipitate and the flask was cooled to room temperature. The remaining solid was isolated by cannula filtration, washed with cold toluene (2 x 5 mL), hexanes (2 x 5 mL) and dried under high-vacuum overnight to yield a white powder in 87% yield (0.445 g). The spectroscopic data were in accordance with the literature.^{13b}

Synthesis of [RhCl((*R*)-5,5'-dinorimido-BINAP)]₂ (38). Under a nitrogen atmosphere, a solution of 32.2 mg (0.0340 mmol) of rotamerically pure (*R*)-5,5'-dinorimido-BINAP (**36**) in 0.5 mL of CD₂Cl₂ was added to a slurry of 7.0 mg (0.0182 mmol) [RhCl(C₂H₄)₂]₂ in 0.1 mL of CD₂Cl₂ in an NMR tube. The NMR tube was shaken, and occasionally purged with nitrogen gas for 30 minutes, before ¹H-NMR and ³¹P-NMR spectra were obtained. Upon addition of the ligand solution to the [RhCl(C₂H₄)₂]₂ slurry, there was a rapid color change from yellow-orange to brick red, with accompanying evolution of ethylene gas. After identification of **38** by NMR, the compound was used immediately and without isolation as attempts at isolation resulted in decomposition of the product. The spectroscopic data

were in accordance with the literature spectrum of $[\text{RhCl}(\text{BINAP})]_2$.⁷⁷ ^1H -NMR (400 MHz, CD_2Cl_2) δ ppm 1.67 (d, $J=8.4\text{Hz}$, 2H), 1.81 (d, $J=8.4\text{Hz}$, 2H), 3.48-3.53 (m, 4H), 3.56-3.60 (m, 4H), 6.28 (dd, $J=2.0\text{Hz}$, 2H), 6.38 (dd, $J=2.0\text{Hz}$, 2H), 6.47 (d, $J=4.8\text{Hz}$, 2H), 6.57 (d, $J=4.8\text{Hz}$, 2H), 6.60-6.76 (m, 4H), 6.81-6.90 (m, 2H), 6.92 (d, $J=7.2\text{Hz}$, 2H), 7.05 (m, 2H), 7.22 (t, $J=8.6\text{Hz}$, 2H), 7.41 (m, 6H), 7.73 (br s, 4H), 7.98 (br s, 4H); ^{31}P -NMR (161 MHz, CD_2Cl_2) δ ppm 50.77 (d, $J=195\text{Hz}$, 2P).⁶⁶

Preparation of polymer-supported rhodium catalyst-organic framework 41. In a typical experiment, 36.9 mg (0.0170 mmol) of **38** was prepared in 0.6 mL of CD_2Cl_2 in an NMR tube as described above. Under a nitrogen atmosphere 26.6 μL of COE (0.204 mmol) was added to the solution and the tube was shaken. The color of the solution remained brick red. This solution was then cannulated, under a nitrogen atmosphere, into a Schlenk tube equipped with a stir bar and rinsed in with 1.0 mL of CH_2Cl_2 . Next, 1.5 mg (0.00182 mmol) of *trans*- $\text{RuCl}_2(\text{PCy}_3)_2(=\text{CHPh})$ (**23**) was dissolved in 1.1 mL of CH_2Cl_2 , yielding a purple solution. This solution was then cannulated, under a nitrogen atmosphere into the Schlenk tube. The vessel was then sealed and placed, with moderate stirring, into an oil bath at 40°C for 24 hours. This mixture was then diluted with 10 mL of CH_2Cl_2 . The ^{31}P -NMR and ^1H -NMR spectra are given in Figure 2-11 and 2-12.⁶⁶

Deposition of 41 onto BaSO₄ or Ba-L-tartrate. 10 g of BaSO₄ or Ba-L-tartrate was washed consecutively with 4 x 50 mL of CH₂Cl₂ followed by 3 x 50 mL of MeOH, and then dried under vacuum at room temperature overnight.

1.633 g (6.99 mmol) of the washed and dried Ba salt in a 250 mL round-bottom flask equipped with a stir bar was back-filled with nitrogen gas. To this flask was added 20 mL of CH₂Cl₂, which was stirred slowly to create a slurry. The reaction mixture that contained **41** prepared above was cannulated onto the Ba salt/CH₂Cl₂ slurry, creating a tan-coloured mixture. The polymer reaction vessel was rinsed with 3 x 5 mL of CH₂Cl₂ that were added to the slurry and this was stirred for 20 minutes to achieve an even distribution of the catalyst-organic framework on the Ba salt. The solvent was then removed slowly under reduced pressure (1 hour) with rapid stirring at room temperature. After the removal of the solvent to dryness, the flask was dried further under vacuum for 1 hour. After the initial drying, the supported catalyst was rinsed with 3 x 50 mL of MeOH to remove any polymerized COE and low molecular weight oligomers. The MeOH portions were decanted off the support with a cannula under a nitrogen atmosphere. Filtration was avoided to prevent plugging of the filter. After the final rinse, the catalyst was dried for 1 hour under vacuum, then immediately transferred to the glove-box, where it was stored in the freezer. NMR spectra recorded in CD₂Cl₂ of the pumped down MeOH

residue showed only poly-COE present. There was also no observable signal in the ^{31}P -NMR spectrum.⁶⁶

Synthesis of [Rh(NBD)((*R*)-5,5'-dinorimido-BINAP)](SbF₆) (40**).**

Under a nitrogen atmosphere, a solution of 79.0 mg (0.0836 mmol) of rotamerically pure (*R*)-5,5'-dinorimido-BINAP (**36**) in 0.7 mL of CD₂Cl₂ was added to a flask containing 43.9 mg (0.0836 mmol) of [Rh(NBD)₂](SbF₆). **36** was rinsed into the flask with an additional 0.3 mL of CD₂Cl₂ after which the flask was sealed and stirred at room temperature for 24 hours. After identification of **40** by NMR, the brown solution was cooled to room temperature and cannula filtered into a new flask where the solvent was removed under reduced pressure. The brown solid was then rinsed with hexane and dried under reduced pressure to give **40** in 86% yield (98.5 mg). The spectroscopic data was in accordance with the literature spectrum of [Rh((*S*)-BINAP)(NBD)](BF₄).⁷⁸ ^1H -NMR (400 MHz, CD₂Cl₂) δ ppm 1.68 (d, *J* = 8.8Hz, 2H), 1.81 (d, *J*=8.8Hz, 2H), 1.93 (t, *J* = 1.6Hz, 2H), 3.51-3.66 (m, 8H), 4.06 (br s, 2H), 4.75 (br s, 2H), 5.10 (br s, 2H), 6.26 (dd, *J* = 5.7, 2.78Hz, 2H), 6.36 (dd, *J* = 5.6, 2.86Hz, 2H), 6.85 (d, *J* = 8.0Hz, 2H), 6.99-7.07 (m, 12H), 7.24-7.33 (m, 12H), 7.46 (d, *J* = 9.2Hz, 2H), 7.64-7.73 (m, 2H); ^{31}P -NMR (202.3 MHz, CD₂Cl₂) δ ppm 26.03 (doublet of multiplets, *J* = 155Hz, 2P).

Preparation of polymer-supported rhodium catalyst-organic framework 42. In a typical experiment, 24.6 mg (0.0179 mmol) of **40** was dissolved in 0.5 mL of CH₂Cl₂ and transferred via cannula to a purged Schlenk flask. Under a nitrogen gas atmosphere, 14 μL (0.1074 mmol) of COE was added to the Schlenk flask and rinsed in with 1.25 mL of CH₂Cl₂. Next, 0.7 mg (0.000895 mmol) of *trans*-RuCl₂(PCy₃)₂(=CHPh) (**23**) was dissolved in 0.5 mL of CH₂Cl₂, yielding a purple solution. This solution was then transferred via cannula, under a nitrogen gas atmosphere, into the Schlenk flask. The vessel was then sealed and placed, with moderate stirring, into an oil bath at 45°C for 48 hours. After analysis by ¹H-NMR and ³¹P-NMR, an additional equivalent of **23** (0.7 mg, 0.000895 mmol) dissolved in 0.5 mL of CH₂Cl₂ was added to the flask and the reaction mixture was stirred at 45°C for an additional 24 hours. After 72 hours of total reaction time, an aliquot of the mixture was taken and the recorded NMR spectra confirmed that polymerization was complete. This mixture was then diluted with 10 mL of CH₂Cl₂. The ³¹P-NMR and ¹H-NMR spectra are given in Figure 2-13 and 2-14.

Deposition of 42 onto BaSO₄. 10 g of BaSO₄ was washed consecutively with 4 x 50 mL of CH₂Cl₂ followed by 3 x 50 mL of MeOH and then dried under vacuum at room temperature overnight.

2.592 g of the washed and dried BaSO₄ was weighed into a 250 mL round-bottom flask equipped with a side-arm and a stir bar and was

evacuated and back-filled with nitrogen gas (3 x). 15 mL of CH₂Cl₂ was added to the flask and was stirred slowly to create a BaSO₄ slurry. The reaction mixture that contained **42** prepared above was transferred via cannula, under a nitrogen gas atmosphere, into the flask containing the BaSO₄/CH₂Cl₂ slurry, creating a light-brown colored mixture. This was followed by 3 x 5 mL rinses of CH₂Cl₂ and the final slurry was stirred for 1 hour at room temperature to ensure an even distribution of **42** on the BaSO₄. The solvent was then slowly removed under reduced pressure. After removal of the solvent to dryness, the solid product was dried further under high-vacuum for 1 hour. After the initial drying, the BaSO₄ supported **42** was rinsed with 3 x 20 mL of distilled MeOH to remove any poly-COE, poly-NBD and low molecular weight oligomers. The pale yellow MeOH portions were cannula filtered under a nitrogen gas atmosphere into a round-bottom flask. After the final MeOH rinse, the catalyst was dried under high-vacuum for ~ 2 hours then immediately transferred to the glove-box where it was stored until needed. NMR spectra recorded in CD₂Cl₂ of the MeOH residue showed only poly-COE and poly-NBD. There was no observable signal in the ³¹P-NMR spectrum.

References

- (1) *Asymmetric Catalysis on Industrial Scale*; Blaser, H. U., Schmidt, E., Eds.; Wiley-VHC: Weinheim, Germany, **2003**.
- (2) (a) Benaglia, M.; Puglisi, A.; Cozzi, F. *Chem. Rev.* **2003**, *103*, 3401. (b) Clapham, B.; Reger, T. S.; Janda, K. D. *Tetrahedron* **2001**, *57*, 4637. (c) Fan, Q. H.; Li, Y. M.; Chan, A. S. C. *Chem. Rev.* **2002**, *102*, 3385. (d) Leadbeater, N. E.; Marco, M. *Chem. Rev.* **2002**, *102*, 3217. (e) Saluzzo, C.; Lemaire, M. *Adv. Synth. Catal.* **2002**, *344*, 915.
- (3) *Chiral Catalyst Immobilization and Recycling*; De Vos, D. E., Vankelecom, I. F. J., Jacobs, P. A., Eds.; Wiley-VHC: Weinheim, Germany, **2008**.
- (4) (a) Bayston, D. J.; Fraser, J. L.; Ashton, M. R.; Baxter, A. D.; Polywka, M. E. C.; Moses, E. *J. Org. Chem.* **1998**, *63*, 3137. (b) Chapuis, C.; Barthe, M.; de Saint Laumer, J.-Y.; *Helv. Chim. Acta* **2001**, *84*, 230. (c) Song, C. E.; Yang, J. W.; Roh, E. J.; Lee, S.-G.; Ahn, J. H.; Han, H. *Angew. Chem. Int. Ed.* **2002**, *41*, 3852.
- (5) (a) Bianchini, C.; Frediani, M.; Mantovani, G.; Vizza, F. *Organometallics* **2001**, *20*, 2660. (b) Bianchini, C.; Frediani, M.; Vizza, F. *Chem. Commun.* **2001**, 479. (c) Deschenaux, R.; Stille, J. K. *J. Org. Chem.* **1985**, *50*, 2299.

- (6) (a) Deng, G. J.; Fan, Q. H.; Chen, X. M.; Liu, D. S.; Chan, A. S. C. *Chem. Commun.* **2002**, 1570. (b) Fan, Q. H.; Ren, C. Y.; Yeung, C. H.; Hu, W. H.; Chan, A. S. C. *J. Am. Chem. Soc.* **1999**, *121*, 7407.
- (7) (a) Saluzzo, C.; Lamouille, T.; Herault, D.; Lemaire, M. *Bioorg. Med. Chem. Lett.* **2002**, *12*, 1841. (b) Saluzzo, C.; ter Halle, R.; Touchard, F.; Fache, F.; Schulz, E.; Leamire, M. *J. Organomet. Chem.* **2000**, *603*, 30. (c) ter Halle, R.; Colasson, B.; Schulz, E.; Spagnol, M.; Lemaire, M. *Tetrahedron Lett.* **2000**, *41*, 643. (d) ter Halle, R.; Schulz, E.; Spagnol, M.; Lemaire, M. *Synlett* **2000**, 680.
- (8) (a) Pu, L. *Chem. Rev.* **1998**, *98*, 2405. (b) Pu, L. *Chem. Eur. J.* **1999**, *5*, 2227. (c) Yu, H. B.; Hu, Q. S.; Pu, L. *J. Am. Chem. Soc.* **2000**, *122*, 6500.
- (9) Buchmeiser, M. R.; Kroll, R.; Wurst, K.; Schareina, T.; Kempe, R.; Eschbaumer, C.; Schubert, U. S. *Macromol. Symp.* **2001**, *164* (Reactive Polymers), 187.
- (10) Pugin, B.; Blaser, H.-U. *Top. Catal.* **2010**, *53*, 953.
- (11) Mastroilli, P.; Nobile, C. F. *Coord. Chem. Rev.* **2004**, *248*, 377.
- (12) Fan, Q. H.; Deng, G. J.; Lin, C. C.; Chan, A. S. C. *Tetrahedron: Asymmetry* **2001**, *12*, 1241.
- (13) (a) Ralph, C. K.; Akotsi, O. M.; Bergens, S. H. *Organometallics* **2004**, *23*, 1484. (b) Ralph, C. K.; Bergens, S. H. *Organometallics* **2007**, *26*, 1571.

- (14) (a) Dragutan, V.; Dragutan, I.; Fischer, H. *J. Inorg. Organomet. Polym.* **2008**, *18*, 311. (b) Esteruelas, M. A.; González, F.; Herrero, J.; Lucio, P.; Oliván, M.; Ruiz-Labrador, B. *Polymer Bulletin* **2007**, *58*, 923.
- (15) (a) Casey, C. P. *J. Chem. Educ.* **2006**, *83*, 192. (b) Furstner, A. *Angew. Chem. Int. Ed.* **2000**, *39*, 3013. (c) Grubbs, R. H. *Tetrahedron* **2004**, *60*, 7117. (d) Trnka, T. M.; Grubbs, R. H. *Acc. Chem. Res.* **2001**, *34*, 18.
- (16) (a) Schrock, R. R.; Hoveyda, A. H. *Angew. Chem. Int. Ed.* **2003**, *42*, 4592. (b) Schrock, R. R. *Acc. Chem. Res.* **1990**, *23*, 158. (c) Schrock, R. R.; Merdzek, J. S.; Bazan, G. C.; Robbins, J.; Dimare, M.; Oregan, M. *J. Am. Chem. Soc.* **1990**, *112*, 3875.
- (17) Schwab, P.; Grubbs, R. H.; Ziller, J. W. *J. Am. Chem. Soc.* **1996**, *118*, 100.
- (18) (a) Bielawski, C. W.; Grubbs, R. H. *Angew. Chem. Int. Ed.* **2000**, *39*, 2903. (b) Frenzel, U.; Weskamp, T.; Kohl, F. J.; Schattenman, W. C.; Nuyken, O.; Herrmann, W. A. *J. Organomet. Chem.* **1999**, *586*, 263. (c) Scholl, M.; Ding, S.; Lee, C. W.; Grubbs, R. H. *Org. Lett.* **1999**, *1*, 953.
- (19) Herisson, J. L.; Chauvin, Y. *Makromol. Chem.* **1971**, *141*, 161.
- (20) (a) Slugovc, C. *Macromol. Rapid Commun.* **2004**, *25*, 1283. (b) Leitgeb, A.; Wappel, J.; Slugovc, C. *Polymer* **2010**, *51*, 2927.

- (21) (a) Love, J. A.; Sanford, M. S.; Day, M. W.; Grubbs, R. H. *J. Am. Chem. Soc.* **2003**, *125*, 10103. (b) Sanford, M. S.; Love, J. A.; Grubbs, R. H. *J. Am. Chem. Soc.* **2001**, *123*, 6543. (c) Sanford, M. S.; Ulman, M.; Grubbs, R. H. *J. Am. Chem. Soc.* **2001**, *123*, 749.
- (22) Bielawski, C. W.; Grubbs, R. H. *Macromolecules* **2001**, *3*, 8838.
- (23) Szwarc, M. *Nature* **1956**, 1168.
- (24) Bielawski, C. W.; Grubbs, R. H. *Prog. Polym. Sci.* **2007**, *32*, 1.
- (25) Choi, T. L. Rutenberg, I. M.; Grubbs, R. H. *Angew. Chem. Int. Ed.* **2002**, *41*, 3839.
- (26) (a) Jung, H.; ten Brummelhuis, N.; Yang, S. K.; Weck, M. *Polym. Chem.* **2013**, *4*, 2837. (b) Slugovc, C.; Riegler, S.; Hayn, G.; Saf, R. Stelzer, F. *Macromol. Rapid Commun.* **2003**, *24*, 435.
- (27) (a) Leeuwenburgh, M. A.; van der Marel, G. A.; Overjleeft, H. S. *Curr. Opin. Chem. Biol.* **2003**, *7*, 757. (b) Iyer, S.; Rele, S.; Grasa, G.; Nolan, S.; Chaikof, E. L. *Chem. Commun.* **2003**, 1518.
- (28) (a) Izuhara, D.; Swager, T. M. *Macromolecules* **2009**, *42*, 5416. (b) Lian, W.-R.; Huang, Y.-C.; Liao, Y.-A.; Wang, K.-L.; Li, L.-J.; Su, C.-Y.; Liaw, D.-J.; Lee, K.-R.; Lai, J.-Y. *Macromolecules* **2011**, *44*, 9550.
- (29) (a) Yang, H.; Zhang, F.; Lin, B.-P.; Keller, P.; Zhang, X.-Q.; Sun, Y.; Guo, L.-X. *J. Mater. Chem. C.* **2013**, *1*, 1482. (b) Maghon, B. R.; Weck, M.; Mohr, B.; Grubbs, R. H. *Macromolecules* **1997**, *30*, 257.

- (30) (a) Sattigeri, J. A.; Shiau, C.-W.; Hsu, C.-C.; Yeh, F.-F.; Liu, S.; Jin, B.-Y.; Luh, T.-H. *J. Am. Chem. Soc.* **1999**, 1607. (b) Hsu, C.-C.; Huang, T.-H.; Liu, S.; Yeh, F.-F.; Jin, B.-Y.; Sattigeri, J. A.; Shiau, C.-W.; Luh, T.-H. *Chem. Phys. Lett.* **1999**, 311, 355.
- (31) Buchmeiser, M. R. *Chem. Rev.* **2000**, 100, 1565.
- (32) (a) Buchmeiser, M. R. *Bioorganic & Medicinal Chemistry Letters* **2002**, 12, 1837. (b) Buchmeiser, M. R.; Kroll, R.; Wurst, K.; Schareina, T.; Kempe, R.; Eschbaumer, C.; Schubert, U. S. *Macromolecular Symposia* **2001**, 164, 187. (c) Buchmeiser, M. R.; Sinner, F.; Mupa, M. *Macromolecular Symposia* **2001**, 163, 25.
- (33) Buchmeiser, M. R.; Wurst, K. *J. Am. Chem. Soc.* **1999**, 121, 11101.
- (34) Pollino, J. M.; Weck, M. *Org. Lett.* **2002**, 4, 753.
- (35) Liu, Y.; Piñón, V.; Weck, M. *Polym. Chem.* **2011**, 2, 1964.
- (36) (a) Ahmed, M.; Barrett, A. G. M.; Braddock, D. C.; Cramp, S. M.; Procopiou, P. A. *Tetrahedron Lett.* **1999**, 8657. (b) Hultsch, K. C.; Jernelius, J. A.; Hoveyda, A. H.; Schrock, R. R. *Angew. Chem. Int. Ed.* **2002**, 41, 589. (d) Nguyen, S. T.; Grubbs, R. H. *J. Organomet. Chem.* **1995**, 497, 195.
- (37) Krause, J. O.; Lubbad, S.; Nuyken, O.; Buchmeiser, M. R. *Adv. Synth. Catal.* **2003**, 345, 996.
- (38) (a) Krause, J. O.; Lubbad, S. H.; Nuyken, O.; Buchmeiser, M. R. *Macromol. Rapid Commun.* **2003**, 24, 875. (b) Kroll, R. N.; Schuler, N.; Lubbad, S.; Buchmeiser, M. R. *Chem. Commun.* **2003**, 2742.

- (39) Mayr, M.; Mayr, B.; Buchmeiser, M. R. *Angew. Chem. Int. Ed.* **2001**, *40*, 3839.
- (40) (a) Abd-El-Aziz, A.; Todd, E. K.; Okasha, R. M.; Afifi, T. H. *Macromol. Symp.* **2003**, *196*, 89. (b) Abd-El-Aziz, A. S.; Okasha, R. M.; Afifi, T. H.; Todd, E. K. *Macromol. Chem. Phys.* **2003**, *204*, 555.
- (41) Kroll, R.; Eschbaumer, C.; Schubert, U. S.; Buchmeiser, M. R.; Wurst, K. *Macromol. Chem. Phys.* **2001**, *202*, 645.
- (42) Buchmeiser, M. R.; Lubbad, S.; Mayr, M.; Wurst, K. *Inorg. Chim. Acta.* **2003**, *345*, 145.
- (43) Sommer, W. J.; Weck, M. *Adv. Synth. Catal.* **2006**, *348*, 2101.
- (44) Berthod, M.; Mignani, G.; Woodward, G.; Lemaire, M. *Chem. Rev.* **2005**, *105*, 1801.
- (45) (a) Akutagawa, S. *Appl. Catal. A: General* **1995**, *128*, 171. (b) Noyori, R. *Angew. Chem. Int. Ed.* **2002**, *41*, 2008.
- (46) (a) Noyori, R. *Acta Chem. Scand.* **1996**, *50*, 380. (b) Kitamura, M.; Tsukamoto, M.; Bessho, Y.; Yoshimura, M.; Kobs, U.; Widhalm, M.; Noyori, R. *J. Am. Chem. Soc.* **2002**, *124*, 6649.
- (47) (a) Toriumi, K.; Ito, T.; Takaya, H.; Souchi, T.; Noyori, R. *Acta Crystallogr., Sect. B38* **1982**, 807. (b) Ohta, T.; Takaya, H.; Noyori, R. *Inorg. Chem.* **1988**, *27*, 566.
- (48) (a) Noyori, R. Takaya, H. *Acc. Chem. Res.* **1990**, *23*, 345. (b) Akutagawa, S. *Appl. Catal. A.* **1995**, *128*, 171. (c) Noyori, R. *Angew. Chem. Int. Ed.* **2013**, *52*, 79.

- (49) Berthod, M.; Mignani, G.; Woodward, G.; Lemaire, M. *Chem. Rev.* **2005**, *105*, 1801.
- (50) Mashima, K. M.; Kusano, K. H.; Kumobayashi, H.; Sayo, N.; Hori, Y.; Ishizaki, T.; Akutagawa, S.; Takaya, H. *Chem. Commun.* **1991**, 609.
- (51) (a) Doucet, H.; Ohkuma, T.; Murata, K.; Yokozawa, T.; Kozawa, M.; Katayama, E.; England, A. F.; Ikariya, T.; Noyori, R. *Angew. Chem. Int. Ed.* **1998**, *37*, 1703. (b) Noyori, R.; Koizumi, M.; Ishii, D.; Ohkuma, T. *Pure Appl. Chem.* **2001**, *73*, 227. (c) Ohkuma, T.; Koizumi, M.; Doucet, H.; Pham, T.; Kozawa, M.; Murata, K.; Katayama, E.; Yokozawa, T.; Ikariya, T.; Noyori, R. *J. Am. Chem. Soc.* **1998**, *120*, 13529.
- (52) Zhang, X. Patent WO 02/4091 (**2002**).
- (53) Berthod, M.; Saluzzo, C.; Mignami, G.; Lemaire, M. *Tetrahedron: Asymmetry* **2004**, *15*, 639.
- (54) Okano, T.; Kumobayashi, H.; Akutagawa, S.; Kiji, J.; Konishi, H.; Fukuyama, K.; Shimano, Y. US Patent 4 705 895 (**1987**).
- (55) (a) Fan, Q. H.; Deng, G. J.; Chen, X. M.; Xie, W. C.; Jiang, D. Z.; Liu, D. S.; Chan, A. S. C. *J. Mol. Catal. A* **2000**, *159*, 37. (b) Fan, Q. H.; Ren, C. Y.; Yeung, C. H.; Hu, W. H.; Chan, A. S. C. *J. Am. Chem. Soc.* **1999**, *121*, 7407.
- (56) Fan, Q. H.; Chen, Y. M.; Chen, X. M.; Jiang, D. Z.; Xi, F.; Chan, A. S. C. *Chem. Commun.* **2000**, 789.

- (57) Ralph, C. K. (2007). *Immobilization of Homogeneous Asymmetric Hydrogenation Catalysts by Alternating ROMP Assembly*. Ph.D. Thesis. University of Alberta: Edmonton, Canada.
- (58) Huang, Y.-Y.; Deng, G.-J.; Wang, X.-Y.; He, Y.-M.; Fan, Q.-H.; *Chin. J. Chem.* **2004**, *22*, 3.
- (59) Corkum, E. G.; Hass, M. J.; Sullivan, A. D.; Bergens, S. H. *Org. Lett.* **2011**, *13*, 3522.
- (60) Bringmann, G.; Mortimer, A. J. P.; Keller, P. A.; Gresser, M. J.; Garner, J.; Breuning, M. *Angew. Chem. Int. Ed.* **2005**, *44*, 5384.
- (61) Curran, D. P.; Qi, H.; Geib, S. J.; DeMello, N. C. *J. Am. Chem. Soc.* **1994**, *116*, 3131.
- (62) Jeulin, S.; de Paule, S. D.; Ratovelomanana-Vidal, V.; Genet, J. P.; Champion, N.; Dellis, P. *Proc. Natl. Acad. Sci. U. S. A.* **2004**, *101*, 5799.
- (63) Walker, R.; Conrad, R. M.; Grubbs, R. H. *Macromolecules* **2009**, *42*, 599.
- (64) Howell, J.; Goddard, J. D.; Tam, W. *Tetrahedron Lett.* **2009**, *65*, 4562.
- (65) Schwab, P. G.; Grubbs, R. H.; Ziller, J. W. *J. Am. Chem. Soc.* **1996**, *118*, 100.
- (66) Corkum, E. G.; Hass, M. J.; Sullivan, A. D.; Bergens, S. H. *Org. Lett.* **2011**, *13*, 3522.

- (67) Hass, M. J. (2011). *Reusable Ru and Rh Catalyst-Organic Frameworks for Ester Hydrogenations and Enyne Cycloisomerizations*. M.Sc. Thesis. University of Alberta: Edmonton, Canada.
- (68) Simon, Y. C.; Coughlin, E. B. *J. Polym. Sci., Part A: Polym. Chem.* **2010**, *48*, 2557.
- (69) Dorta, R.; Egli, P.; Zuercher, F.; Togni, A. *J. Am. Chem. Soc.* **1997**, *119*, 10857.
- (70) (a) Ohkuma, T.; Takeno, H.; Honda, Y.; Noyori, R. *Adv. Synth. Catal.* **2001**, *343*, 369. (b) Rana, S.; White, P.; Bradley, M. *J. Comb. Chem.* **2001**, *3*, 9.
- (71) Buchmeiser, M. R. *Macromol. Rapid Commun.* **2001**, *22*, 1082.
- (72) Mayr, M.; Buchmeiser, M. R.; Wurst, K. *Adv. Synth. Catal.* **2002**, *344*, 712.
- (73) Köhler, K.; Heidenreich, R. G.; Krauter, J. G. E.; Pietsch, J. *Chem. Eur. J.* **2002**, *8*, 622.
- (74) (a) Preetz, A.; Fischer, C.; Kohrt, C.; Drexler, H.-J.; Baumann, W.; Heller, D. *Organometallics* **2011**, *30*, 5155. (b) Miyashita, A.; Yasuda, A.; Takaya, H.; Toriumi, K.; Ito, T.; Souchi, T.; Noyori, R. *J. Am. Chem. Soc.* **1980**, *102*, 7932.
- (75) Cramer, R. *Inorg. Synth.* **1990**, *28* (Reagents Transition Met. Complex Organomet. Synth.), 86.
- (76) Osborn, J. A.; Schrock, R. R. *J. Am. Chem. Soc.* **1971**, *93*, 2397.

- (77) Tokunaga, N.; Yoshida, K.; Hayashi, T. *Proceedings of the National Academy of Sciences of the United States of America* **2004**, *101*, 5445.
- (78) Preetz, A.; Drexler, H.-J.; Schulz, S.; Heller, D. *Organometallics* **2010**, *21*, 1226.

Chapter 3

The Asymmetric Intramolecular Cycloisomerization of 1,6-Enynes²

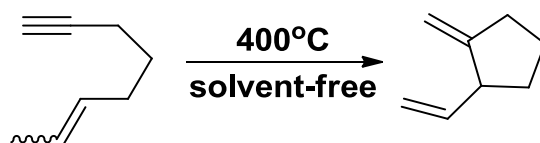
Introduction

The intramolecular cycloisomerization of 1,6-enynes, a specific type of the more general ene or Alder-ene reaction, is a carbon-carbon bond-forming reaction that has many potential pharmaceutical applications. First discovered in the 1940s by Alder¹, the ene reaction involves the addition of an olefin containing an allylic proton to an unsaturated carbon-carbon bond. The reaction is compatible with a wide variety of functional groups, however high temperatures are typically required to induce the transformation. To this end, the thermal cycloisomerization of 1,6-enynes was first discovered in 1962 by Huntsman.² Here, under solvent-free conditions, 6-octen-1-yne was heated to 400°C to produce a cyclic 1,4-diene (Scheme 3-1). Thermal cycloisomerizations of enyne substrates were quite prevalent in the literature until the 1980s,³ however the elevated temperatures required to overcome the high activation energy

² A version of this chapter has been published. Elizabeth G. Corkum, Michael J. Hass, Andrew D. Sullivan, Steven H. Bergens. "A Highly Reusable Rhodium Catalyst-Organic Framework for the Intramolecular Cycloisomerization of 1,6-Enynes." *Org. Lett.* **2011**, 13, 3522. With the exception of the chiral NMR shift reagent study, all work presented in this chapter is that of Elizabeth G. Corkum.

barriers and the surprisingly limited number of substrates compatible with this reaction⁴ resulted in little attention being given to the field.

Scheme 3-1. The thermal cycloisomerization of 6-octen-1-yne.

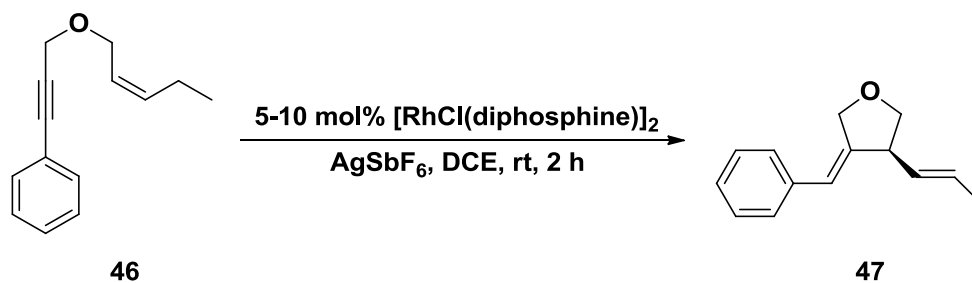


The 1984 discovery by Trost of a palladium-catalyzed intramolecular ene reaction brought new interest to the field.⁵ Since then, the field has expanded rapidly and the range of metals that catalyze the cycloisomerization of 1,*n*-enynes now includes platinum,⁶ nickel,⁷ gold,⁸ silver,⁹ ruthenium¹⁰ and iridium.¹¹ Despite the newfound interest, the asymmetric intramolecular cycloisomerization of 1,6-enynes has not been reported until relatively recently. Of the numerous chiral catalytic systems reported in the literature, the rhodium-catalyzed cycloisomerization of 1,6-enynes is of particular interest as these catalysts typically afford excellent enantioselectivities, are tolerant to a wide variety of 1,6-enyne substrates and have been successfully utilized in the synthesis of natural products and pharmaceuticals.¹² As a result, the remaining discussion will be focused on rhodium-catalyzed cycloisomerization reactions.

The rhodium-catalyzed asymmetric cycloisomerization of 1,6-enyne substrates was initially reported in 2000 by Xumu Zhang.¹³ In this initial study, the active catalysts, believed to be of the general form

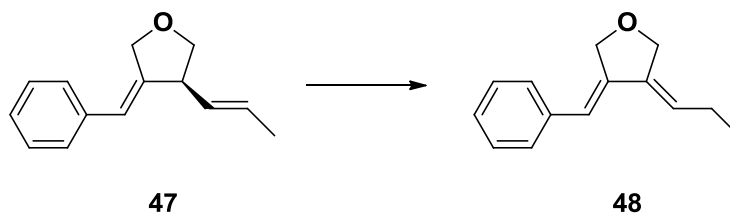
$[\text{Rh}(\text{diphosphine})]^+$, were generated *in situ* from reaction between $[\text{RhCl}(\text{diphosphine})]_2$ and two equivalents of AgSbF_6 in 1,2-dichloroethane (DCE) solvent. They were then tested in the asymmetric cycloisomerization of 1,6-enyne **46** (Scheme 3-2).

Scheme 3-2. Zhang's asymmetric cycloisomerization of 1,6-enyne **46**.



The diphosphine ligand that gave the best results for this transformation was (*R,R*)-Me-DuPhos, where **47** was obtained in 62% yield with an ee of 96%. It was also found that at higher catalyst loadings (>20 mol%) and increased reaction time the 1,4-diene product **47** became isomerized to the more stable, conjugated 1,3-diene **48** (Equation 3-1).

Equation 3-1. Product isomerization side reaction.



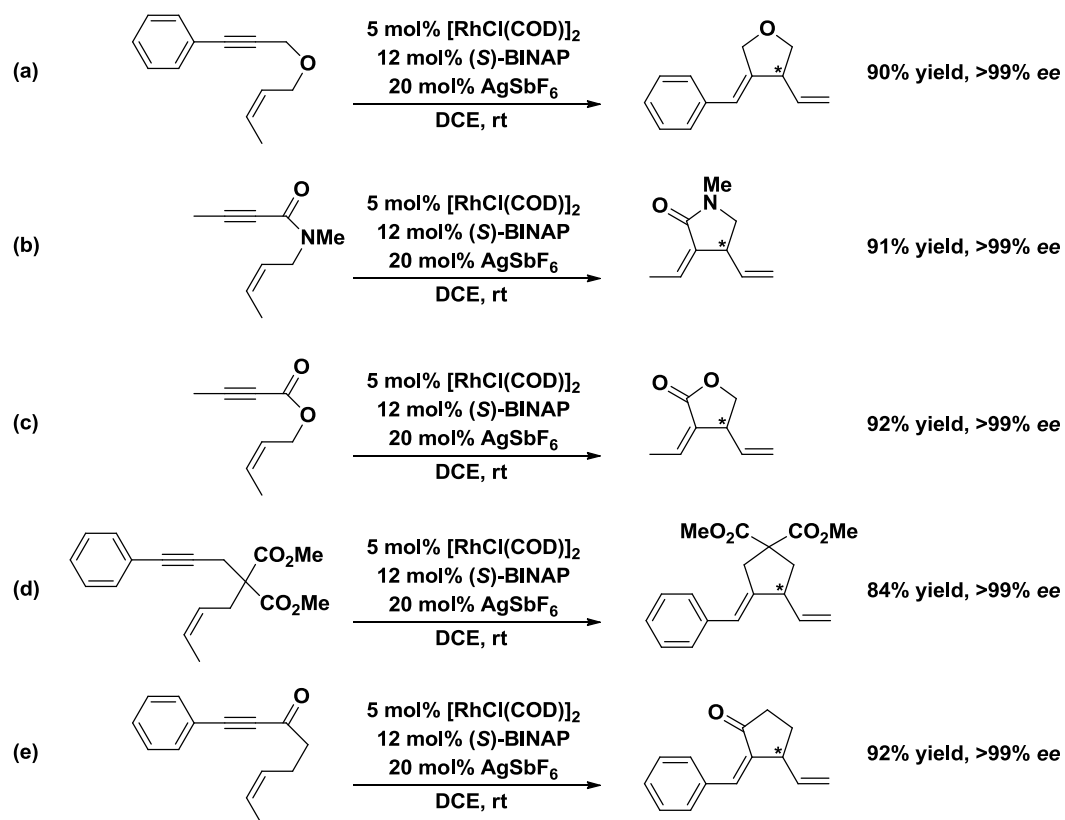
Therefore, the catalytic cycloisomerization reactions had to be carefully monitored and quenched as soon as the substrate was consumed to avoid this unwanted product isomerization.

Surprisingly, in this initial report Zhang found that the catalyst $[\text{RhCl}(\text{BINAP})]_2$ was completely inactive in the cycloisomerization of 1,6-enyne **46**. However, later studies done by Zhang completely contradict this finding.¹⁴ Interestingly, it was discovered that the method used to prepare these catalysts often dictated the catalysts' activity in the cycloisomerization reactions.¹⁴ For example, when the $[\text{RhCl}(\text{BINAP})]_2$ catalyst was prepared *in situ* by simply mixing *rac*-BINAP together with $[\text{RhCl}(\text{COD})]_2$ (COD = 1,5-cyclooctadiene), the catalyst (10 mol%), in the presence of AgSbF_6 (20 mol%) and DCE solvent, afforded 100% conversion (10 TOs) of the test 1,6-enyne substrate to the corresponding 1,4-diene product. Also, when optically pure (*S*)-BINAP was used, the catalyst afforded the desired cycloisomerized products in >82% yield and >99% ee.¹⁴ In fact, when prepared in this way, the $[\text{Rh}(\text{BINAP})]^+$ catalyst system is the most selective homogeneous rhodium-based catalytic system for the cycloisomerization of 1,6-enynes to date. However, the relatively low TONs and large amounts of catalyst (10 mol%) and silver salt (20 mol%) limits the industrial application of this system.

Following these pioneering studies by Zhang, the $[\text{Rh}(\text{BINAP})]^+$ catalyst system was utilized in the production of a variety of chiral carbo- and heterocycles, including tetrahydrofurans^{14,15} (Scheme 3-3a), lactams¹⁶

(Scheme 3-3b), lactones¹⁷ (Scheme 3-3c), cyclopentanes¹⁸ (Scheme 3-3d), and cyclopentanones^{18a} (Scheme 3-3e). The products were all obtained in >99% ee, illustrating the remarkable versatility of this catalyst system.

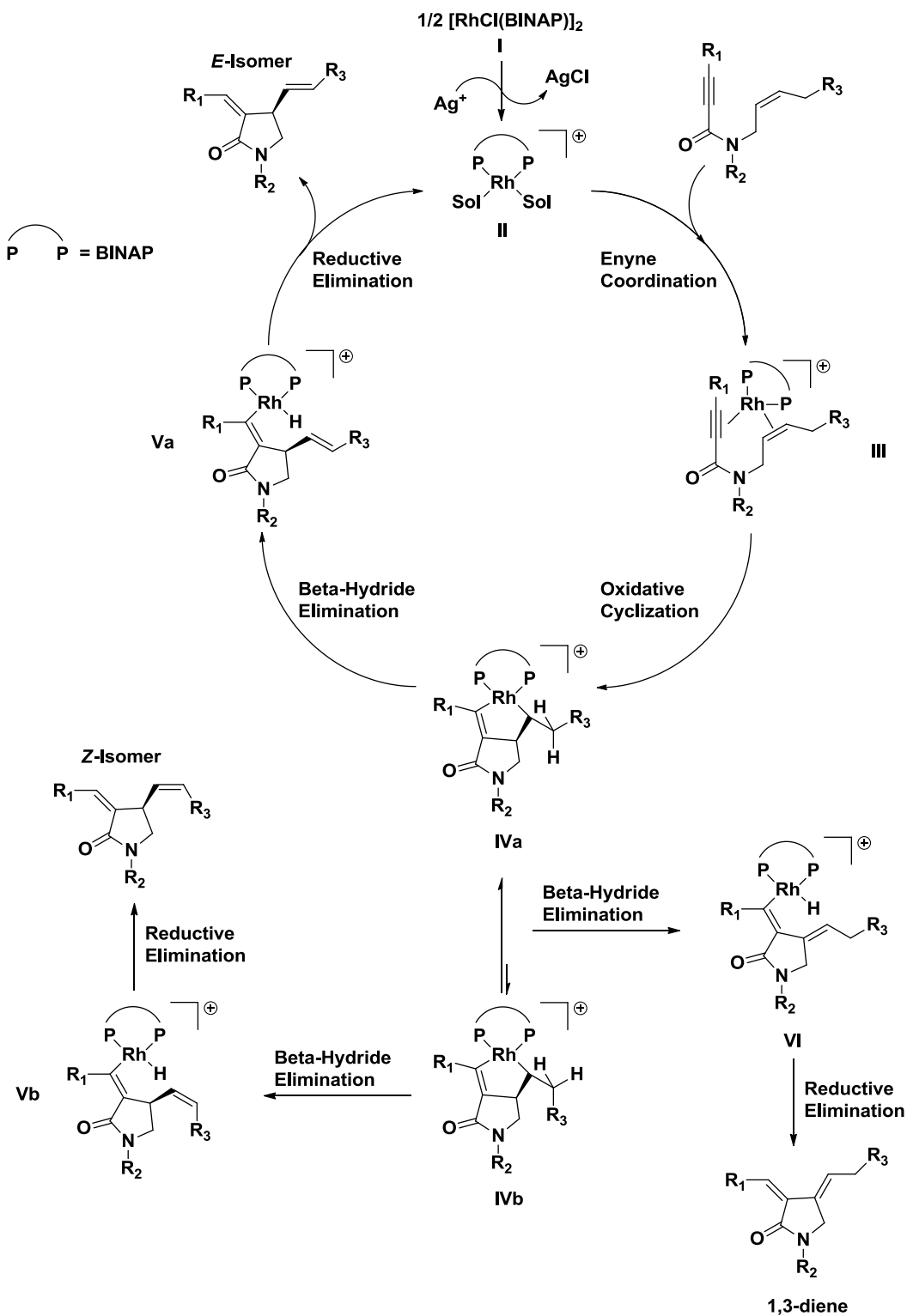
Scheme 3-3. Examples of the rhodium-BINAP catalyzed intramolecular cycloisomerization of 1,6-enynes to produce chiral (a) tetrahydrofurans,^{14,15} (b) lactams,¹⁶ (c) lactones,¹⁷ (d) cyclopentanes¹⁸ and (e) cyclopentanones.^{18a}



In addition to the substrate scope studies, Zhang also investigated the mechanism of the [Rh(BINAP)]⁺ catalyst system for the

cycloisomerization of 1,6-enynes in an attempt to understand the origin of the unprecedented, high selectivity exhibited by this catalyst. The mechanism that was postulated by Zhang is shown in Scheme 3-4.^{16a,19} In the first step, the inactive chloro-bridged rhodium-dimer **I** is converted *in situ* to the active cationic disolvento species **II** by abstraction of the bridging chlorides with a silver source that contains a weakly-coordinating anion, such as SbF_6^- . It is important that the anion does not coordinate strongly to the rhodium metal centers, otherwise the number of catalytic active sites would be greatly diminished. The next step in the catalytic cycle involves the coordination of the enyne substrate to the active catalyst **II** to form the intermediate **III**. It is then thought that this intermediate undergoes an oxidative cyclization to form a metallacyclopentane (**IVa**) in one concerted step. This metallacyclopentane intermediate can exist as two different conformers, labeled **IVa** and **IVb** for clarity, with the less sterically crowded conformer **IVa** being more favored. Subsequent β -hydride elimination results in the formation of the rhodium-hydride intermediate **Va** and reductive elimination generates the *E*-isomer of the 1,4-diene product and regenerates the active catalyst **II**. The *Z*-isomer of the 1,4-diene product would be produced if **IVb** underwent β -hydride elimination followed by reductive elimination.

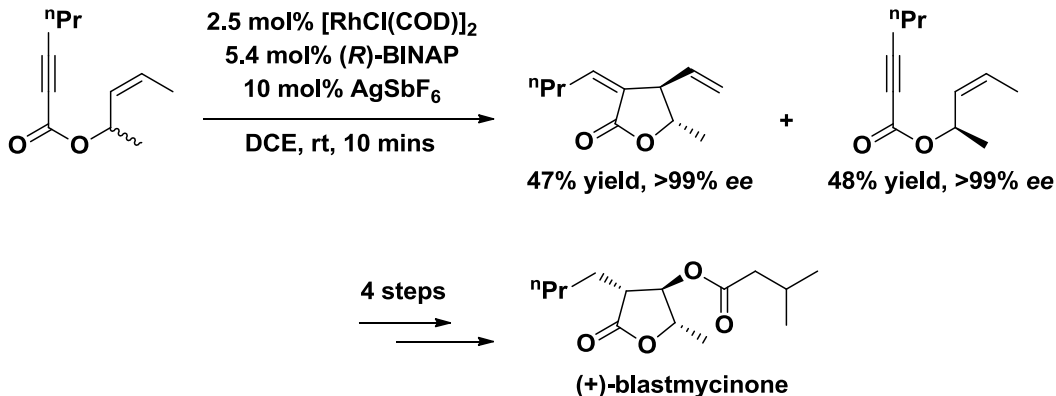
Scheme 3-4. Zhang's proposed mechanism for the intramolecular cycloisomerization of 1,6-enynes catalyzed by $[\text{Rh}(\text{BINAP})]^+$.



Zhang also postulated that **IVa** and **IVb** could undergo β -hydride elimination at the other β -carbon center to generate intermediate **VI**. Subsequent reductive elimination would result in the production of the undesired 1,3-diene product. However, it remains unclear whether 1,4-diene product isomerization (see Scheme 3-1) or alternate β -hydride elimination is responsible for the production of the 1,3-diene.

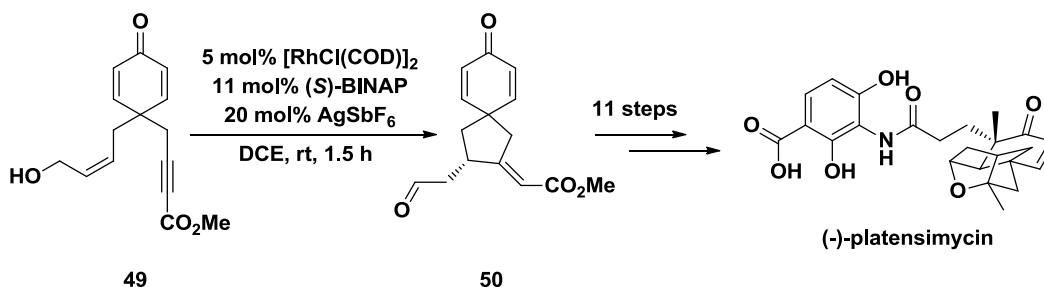
The $[\text{Rh}(\text{BINAP})]^+$ catalyzed intramolecular cycloisomerization of 1,6-enynes has also been utilized in the synthesis of pharmaceuticals and natural products. For example, Zhang recently reported the formal synthesis of (+)-blastmycinone, a degradation product and potential synthetic precursor of (+)-antimycin, a common antifungal medication isolated from the family *Streptomycetaceae*.^{17b,20} In this report, Zhang utilized the $[\text{Rh}((R)\text{-BINAP})]^+$ catalyst in the intramolecular cycloisomerization of 1,6-enyne esters, followed by a 1,3-hydrogen shift (Scheme 3-5). Kinetic resolution of the starting 1,6-enyne ester was also observed for this reaction. The product lactone was produced in 99% ee and 47% yield and the (*R*)-enriched starting 1,6-enyne ester was obtained in 99% ee and 48% yield. These yields are particularly remarkable considering that 50% is the highest theoretical yield that can be obtained for both species. Afterward, the product lactone was converted to (+)-blastmycinone in four subsequent synthetic steps.

Scheme 3-5. Synthesis of (+)-blastmycinone.



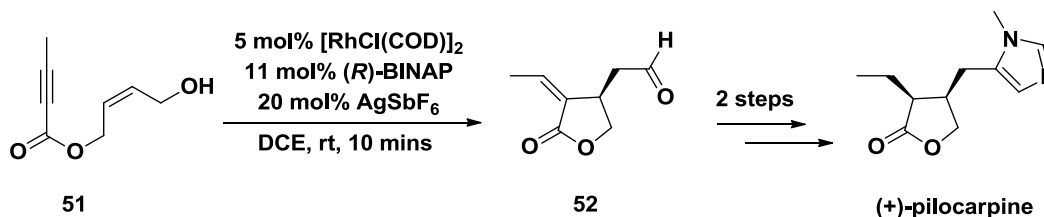
Using Zhang's cycloisomerization methodology, Nicolaou and coworkers developed a synthetic strategy for the production of (-)-platensimycin (Scheme 3-6), a promising antibiotic for the treatment of drug-resistant bacteria.²¹ The synthetic strategy involved the intramolecular cycloisomerization of **49**, which formed the desired spirocycle **50** in 91% yield with an ee of 95%. In this example, the enyne substrate contains an allylic alcohol, which undergoes a 1,3-hydrogen shift to form the aldehyde functional group in the spirocycle product. Such isomerizations have been reported previously with $[\text{Rh}(\text{BINAP})]^+$ catalyst systems²² and is discussed in detail in Chapter 4 of this dissertation. Once obtained, the spirocycle **50** was then converted to (-)-platensimycin in eleven synthetic steps.²³

Scheme 3-6. The formation of a spirocycle intermediate for the synthesis of (-)-platensimycin.



Zhang has also utilized the $[\text{Rh}(\text{BINAP})]^+$ catalyzed intramolecular cycloisomerization of 1,6-enynes in the synthesis of (+)-pilocarpine (Scheme 3-7),^{17a} a pharmaceutical used in the treatment of narrow- or wide-angle glaucoma. In this report, the lactone product **52** was obtained from the cycloisomerization of the 1,6-enyne ester substrate **51** in 10 minutes with a yield of 99% and an ee greater than 99%. Similar to the last example, here the 1,6-enyne ester substrate contains an allylic alcohol that is subsequently isomerized to give the aldehyde functionality in the product lactone. From the product lactone **52**, (+)-pilocarpine was synthesized in two further steps.

Scheme 3-7. Zhang's synthesis of a key intermediate in the production of (+)-pilocarpine.



Zhang's synthesis of the lactone intermediate **52** in one synthetic step with high yield and ee is particularly remarkable considering that the previously best known synthesis for this intermediate took five synthetic steps with an overall yield of 20% and an ee of 92%.²⁴

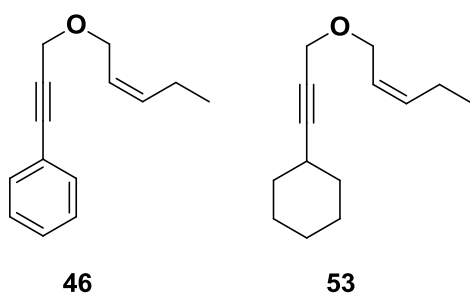
The examples presented in this review all highlight the versatility of the $[\text{Rh}(\text{BINAP})]^+$ catalyst system in the intramolecular cycloisomerization of 1,6-enynes. The high selectivity exhibited by this catalyst for a variety of different 1,6-enyne substrates is unprecedented and the potential for pharmaceutical synthesis makes this system very promising. However, the relatively low TONs and large amounts of catalyst (5-10 mol%) and silver salt (20 mol%) required to avoid product inhibition and the formation of undesired side products narrows the industrial applications of this system. We reasoned that use of an immobilized catalyst would provide higher TONs by allowing catalyst reuse, which would in turn prevent product inhibition and isomerization that may occur during high TON homogeneous reactions. The remainder of this chapter discusses the reuse and batch reactivity achieved with the immobilized, polymer-supported rhodium catalyst-organic framework (COF) **41** and its subsequent use in the production of the (+)-pilocarpine lactone intermediate **52**.

Results and Discussion

Section A: Synthesis of 1,6-Enyne Substrates

The 1,6-enyne substrates that were chosen for cycloisomerization are shown in Figure 3-1. The phenyl substrate **46** had previously been used in homogeneously catalyzed 1,6-enyne cycloisomerization reactions^{13,25}, thus its use would allow for the direct comparison of our polymer-supported rhodium catalyst-organic framework **41** with the homogenous $[\text{Rh}(\text{BINAP})]^+$ catalyst. Conversely, to the best of our knowledge, the cyclohexyl substrate **53** has not been reported for the cycloisomerization. Its absence from the literature was quite intriguing and thus it was chosen as a substrate for this study.

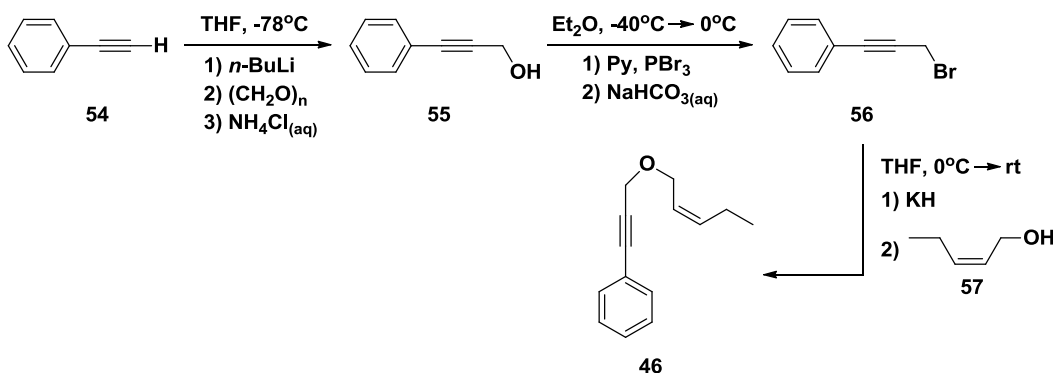
Figure 3-1. 1,6-Enyne substrates chosen for the evaluation of the polymer-supported rhodium catalyst-organic framework **41**.



The synthesis of the phenyl substrate **46** has been reported in the literature (Scheme 3-8).²⁵ Here, the phenyl acetylene **54** is converted to

the corresponding propargyl bromide (**56**) in two steps, and then reacted with *cis*-2-penten-1-ol **57** to form the 1,6-enyne **46**. Although this procedure is functional, it suffers from difficult purification of nearly all the intermediates and required a large number of transformations on the more expensive phenyl acetylene **54**, while leaving the cheaper *cis*-2-penten-1-ol **57** unaltered.

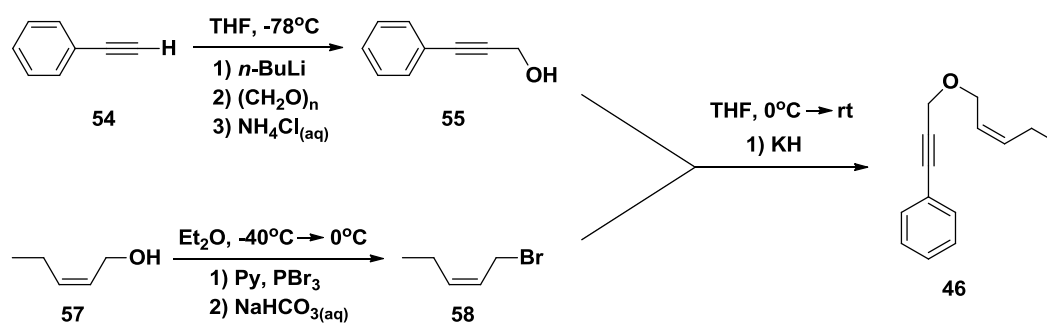
Scheme 3-8. Literature procedure for the synthesis of 1,6-enyne **46**.



A modification of this procedure was developed by former co-worker Michael Hass in an effort to simplify the purification of the intermediates and minimize the number of transformations required for the given alkyne (Scheme 3-9). In this new procedure, the *cis*-2-penten-1-ol **57** is brominated to form **58**. The brominated alkene can be synthesized and stored in gram quantities and can be reacted with a number of different propargyl alcohols to prepare any number of 1,6-enyne substrates, making this procedure more practical than the literature procedure. In addition, purification became far simpler as the brominated

alkene **58** is quite volatile and any excess present in the final product mixture can be removed by evaporation under reduced pressure.

Scheme 3-9. Modified procedure for the synthesis of 1,6-enyne **46**.



In summary, a new procedure was developed for synthesizing 1,6-enyne substrates that is more practical and convenient than the literature procedure. This new procedure was designed to be more compatible with a varying array of propargyl alcohols, allowing for the relatively easy synthesis of the desired 1,6-enyne substrate.

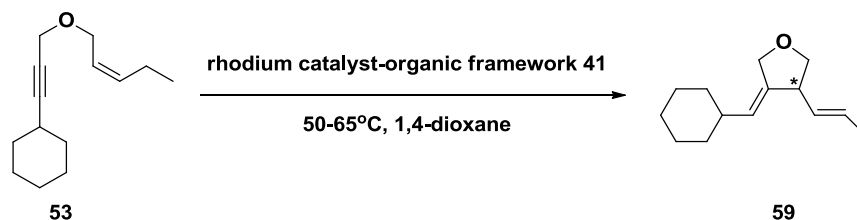
Section B: Reusability of the Polymer-Supported Rhodium Catalyst-Organic Framework **41** for the Cycloisomerization of 1,6-Enynes

Initial studies using the polymer-supported rhodium COF involved the use of DCE as solvent as this is the solvent of choice for the homogeneous cycloisomerization reactions. However, the DCE actually dissolved the polymer catalyst, causing a rapid decrease in catalyst activity and notable rhodium leaching. As a result, 1,4-dioxane was

chosen as COF **41** is insoluble in this solvent and 1,4-dioxane has a relatively low toxicity, making it a suitable solvent for potential industrial and pharmaceutical applications. In fact, the maximum concentrations of 1,4-dioxane and DCE allowed in pharmaceuticals are 380 and 5 ppm, respectively.²⁶

The reuse results for the cyclohexyl 1,6-enyne substrate **53** are summarized in Table 3-1. The initial run in the reuse of COF **41** was a semi-sacrificial run consisting of 20 equivalents (per rhodium) of the cyclohexyl 1,6-enyne substrate **53** added to the catalyst (5 mol% rhodium) as a 0.1M solution in 1,4-dioxane. This loading of 20 equivalents of substrate per rhodium is already twice the substrate loading of the common literature reactions discussed previously. In addition to the 20 equivalents of substrate, two equivalents (per rhodium) of AgSbF₆ were added to the catalyst as a slurry in 1,4-dioxane. The AgSbF₆ is necessary to abstract the bridging chlorides, facilitating the formation of the active [Rh((*R*)-BINAP)(sol)₂]⁺ catalyst. The purpose of this semi-sacrificial run was to prepare the catalyst for subsequent, silver-free runs, as well as to swell the polymer for maximum catalytic efficiency. In fact, after this initial run, no additional AgSbF₆ was required during the lifetime of the polymer-supported rhodium catalyst-organic framework and the catalyst was able to cycloisomerize 100 equivalents (per rhodium) of substrate.

Table 3-1. Reuse results for the cycloisomerization of the cyclohexyl1,6-enyne substrate **53** catalyzed by the polymer-supported rhodium catalyst-organic framework **41**.^a

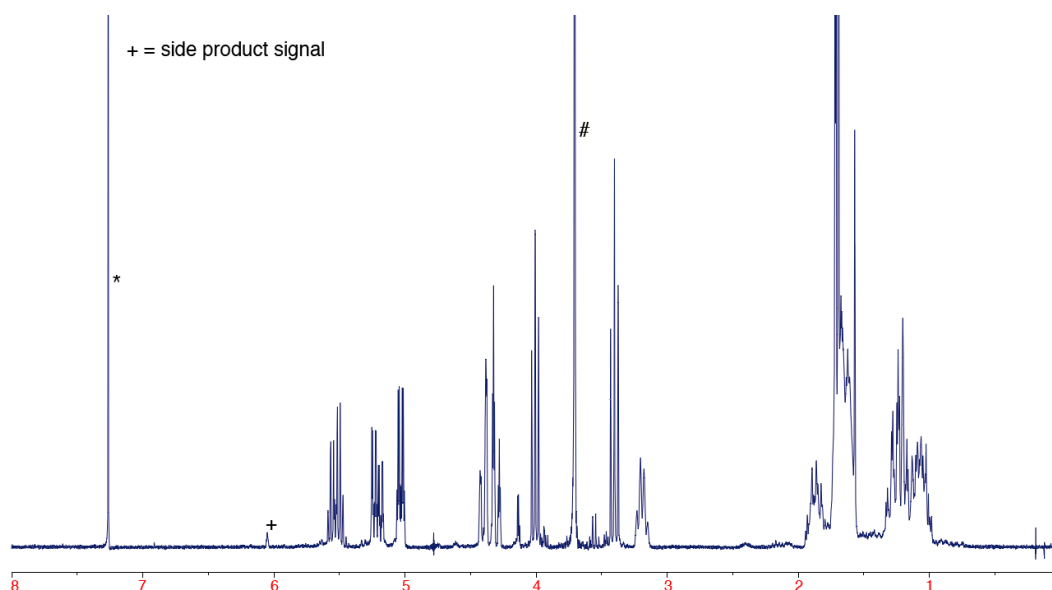


Run #	Temp (°C)	Time (h)	Conversion ^b (%)	ee ^c (%)
1	60	3	100	>95
2	50	18	100	>95
3	50	22.5	100	>95
4 ^d	50	22	<99	
	65	4	100	>95
5	65	19.5	100	>95
6	65	24	100	>95
7	65	24	100	>95

^[a] The reaction was carried out in a 0.1M solution of substrate **53** in 1,4-dioxane under the following conditions: Sub/Ag/Rh = 20/2/1, 60°C. All subsequent runs were carried out in 0.2M solutions of substrate **53** without any additional AgSbF₆ added under the following conditions: Sub/Rh = 100/1. ^[b] Conversion was determined by ¹H-NMR. ^[c] ee was determined by chiral NMR shift reagent. ^[d] The reaction was incomplete after 22 hours at 50°C, therefore the reaction mixture was warmed to 65°C for 4 hours to ensure its completion.

For these reactions a procedure was devised to isolate the immobilized COF **41** without loss in activity. After a particular run, the catalyst was washed several times with 1,4-dioxane without letting the catalyst dry. After rinsing, another 100 equivalents of substrate as a 0.2M solution in 1,4-dioxane was added to the catalyst. As summarized in Table 3-1, this reuse procedure proved very effective allowing the catalyst to be reused six times, with a total TON of 620 and without any drop in enantioselectivity, in the cycloisomerization of the cyclohexyl 1,6-enyne substrate **53**. This is the first reported instance where the cyclohexyl 1,6-enyne substrate **53** was successfully cycloisomerized with minimal side-product formation (as shown in Figure 3-2).

Figure 3-2. $^1\text{H-NMR}$ spectrum of cycloisomerized product **59**.^a

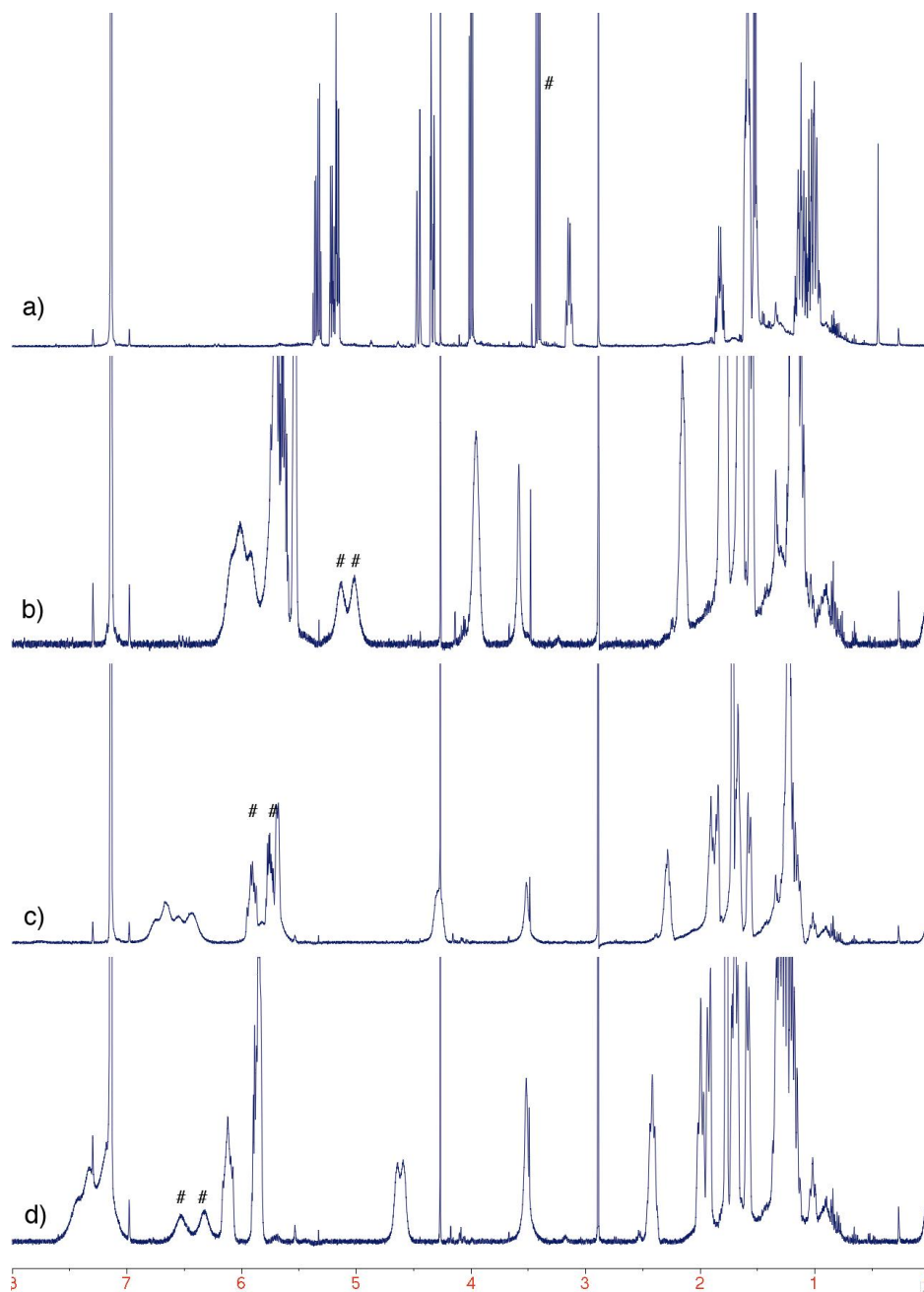


[^a] 399.8 MHz, CDCl_3 , 27°C, * = residual CHCl_3 , # = residual 1,4-dioxane.

Despite these remarkable results, the activity did decrease slightly over time. However, this slight drop in activity was countered by increasing the reaction temperature from 50°C to 65°C. In fact, the reuse of COF **41** was stopped not because the catalyst became deactivated but because the substrate stock had been entirely depleted. Therefore, it is highly likely that the catalyst could have sustained further reuse if more substrate would have been available.

It was discovered that the ee of the cycloisomerized product **59** could not be determined using chiral HPLC or GC. Thus a procedure was developed that utilized the chiral NMR shift reagent $\text{Eu}(\text{hfc})_3$ (where $\text{hfc} = 3\text{-(heptafluoropropylhydroxymethylene)-(+)-camphorate}$). Here, $\text{Eu}(\text{hfc})_3$ was repeatedly added to a sample of racemic cycloisomerized product **59** in benzene- d_6 , the results of which are shown in Figure 3-3. Upon addition of $\text{Eu}(\text{hfc})_3$, the triplet located at approximately $\delta = 3.4$ ppm, as shown in Figure 3-3a (indicated with a #), shifted downfield and initially broadened to form an apparent singlet. Upon further additions of $\text{Eu}(\text{hfc})_3$, this broad singlet shifted to approximately $\delta = 4.5$ ppm and began to split into an apparent doublet, as shown in Figure 3-3b, due to the separation of the different enantiomers of the cycloisomerized product **59**. Further additions of $\text{Eu}(\text{hfc})_3$ shifted this doublet more downfield to approximately $\delta = 6.3$ and 6.4 ppm, as shown in Figure 3-3d, where the two signals were completely separated with an integration ratio of 1:1.

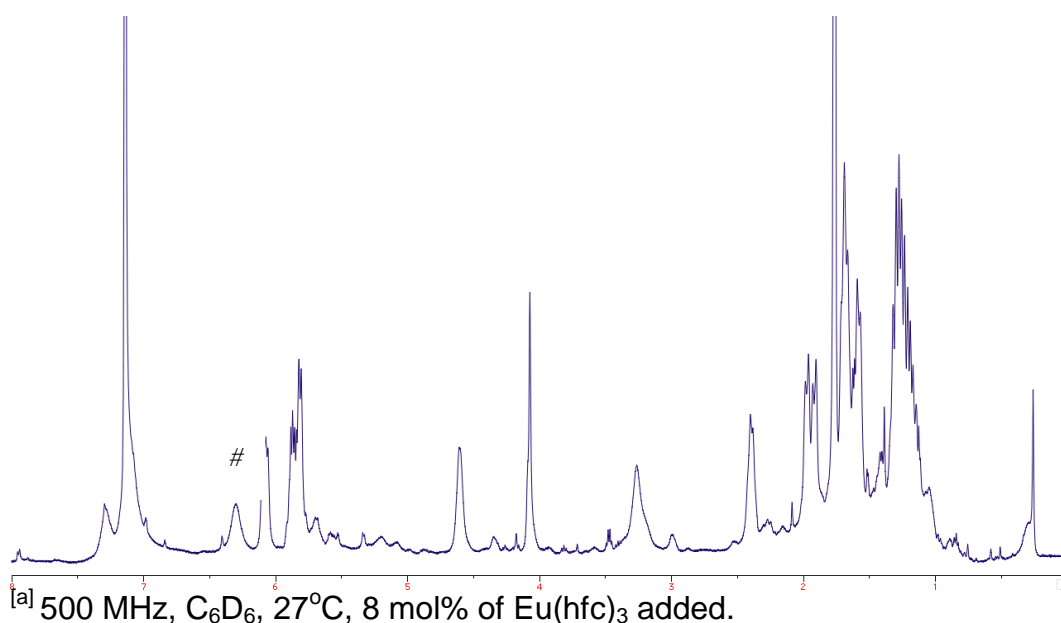
Figure 3-3. $^1\text{H-NMR}$ spectra of the effects of the addition of $\text{Eu}(\text{hfc})_3$ to a racemic sample of cycloisomerized product **59**.^a



^[a] 500 MHz, C_6D_6 , 27°C . Amount of $\text{Eu}(\text{hfc})_3$ added: a) 0 mol%, b) 4 mol%, c) 6 mol%, d) 8 mol%.

Once it was determined that the enantiomers of product **59** could in fact be separated using chiral NMR shift reagents, $\text{Eu}(\text{hfc})_3$ was added to a sample of the cycloisomerized product **59**, that was prepared using COF **41**. The results of this addition are shown in Figure 3-4.

Figure 3-4. ^1H -NMR spectrum of the addition of $\text{Eu}(\text{hfc})_3$ to the cycloisomerized product **59**, prepared using the rhodium catalyst-organic framework **41**.^a



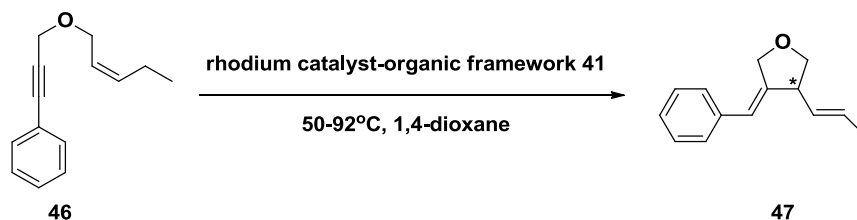
Upon addition of $\text{Eu}(\text{hfc})_3$ to the sample of cycloisomerized product **59**, only a broad singlet is observed at approximately $\delta = 6.3$ ppm. This differs from the racemic sample of the cycloisomerized product **59** as the second peak located at $\delta = 6.4$ ppm is not observed. This experiment suggested that only one enantiomer of the product was formed from the COF catalyzed intramolecular cycloisomerization of 1,6-enyne **53**. The ee was

reported as >95% rather than >99% as this value is limited by the relatively low signal-to-noise ratio of the NMR spectra.

The COF **41** was also highly active and selective for the phenyl 1,6-enyne substrate **46**, as shown by the reuse results displayed in Table 3-2. These reuse experiments were performed in the same manner as the experiments for the cyclohexyl 1,6-enyne **53**, mentioned previously in this chapter. The COF was reused a total of four times with an overall TON of 360 and produced the cycloisomerized product **47** in >99.9% *ee*.

Contrasting with the previous cyclohexyl 1,6-enyne **53**, chiral GC was used to determine the enantioselectivity of the cycloisomerized product **47**. Here, racemic samples of the cycloisomerized product **47** were analyzed by chiral GC and compared to the samples of the cycloisomerized product **47** that were prepared using the polymer-supported rhodium catalyst-organic framework **41**. The peak representing the minor enantiomer was not detectable within the rejection limits of the GC (0.025% of major peak integration), meaning that the *ee* of the cycloisomerized product **47** formed from the COF was >99.9%. This enantioselectivity is identical to that which is reported in the literature for the homogeneous catalyst $[\text{Rh}((R)\text{-BINAP})]^+$.²⁵

Table 3-2. Reuse results for the cycloisomerization of the phenyl1,6-enyne substrate **46** catalyzed by the polymer-supported rhodium catalyst-organic framework **41**.^a



Run #	Temp (°C)	Time (h)	Conversion ^b (%)	ee ^c (%)
1	60	3	100	>99.9
2	50	18.5	18	
	70 ^d	42	96	>99.9
3	70	24	47	
	70	45	88	
	70	48	91	>99.9
4	80	22.5	48	
	80	45.5	81	
	80	51	85	
	80	69.5	97	>99.9
5	92	46	53	>99.9

^[a] The reaction was carried out in a 0.1M solution of substrate **46** in 1,4-dioxane under the following conditions: Sub/Ag/Rh = 20/2/1, 60°C. All subsequent runs were carried out in 0.2M solutions of substrate **46** without any additional AgSbF₆ added under the following conditions: Sub/Rh = 100/1. ^[b] Conversion was determined by ¹H-NMR and by comparison to authentic samples. ^[c] ee was determined by chiral GC analysis. ^[d] After the decrease to 50°C, the temperature was increased as needed for the completion of the reaction.

Despite the remarkable results and similar to the previous study, the activity did decrease over time, but in this case the drop in activity was more pronounced. For example, the reaction time increased from 42 hours in the second run to 69.5 hours in the fourth run and was accompanied by a 10°C increase in temperature to achieve similar conversions of 96% and 97%, respectively. In addition, the overall TON afforded in the cycloisomerization of the phenyl 1,6-enyne **46** was approximately half the value obtained in the cycloisomerization of the cyclohexyl 1,6-enyne **53** (TON of 360 and 620, respectively). We postulated that the slower rate of reaction and lower overall TON for the phenyl 1,6-enyne **46** may be due to competitive η^6 -binding of the aromatic ring on the substrate or cycloisomerized product to the rhodium metal center. This substrate and/or product inhibition would essentially block available rhodium catalytic sites preventing additional substrate from accessing these catalytic centers, which would decrease the overall rate of reaction and lower the TON. As well, there would be the requirement for higher temperatures to overcome this unfavorable interaction and push the reaction along. It should be noted that this η^6 -coordination is not possible with the cyclohexyl 1,6-enyne **53**, explaining the faster reaction rates and higher TONs.

In summary, the COF **41** was reused a total of six times (TON of 620) and four times (TON of 360) in the cycloisomerization of 1,6-enynes **53** and **46**, respectively, performing the reactions with near perfect

enantioselectivities. As well, this is the first reported example of the successful cycloisomerization of the cyclohexyl 1,6-enyne **53**. Having established the high reusability of the polymer-supported catalyst, the batch reactivity of this catalyst was next investigated, the results of which will be discussed in the following section.

Section C: Batch Reactivity of the Polymer-Supported Rhodium Catalyst-Organic Framework **41 for the Cycloisomerization of 1,6-Enynes**

Before performing batch reactivity studies with COF **41**, former co-worker Michael Hass investigated the use of various solvents that exhibit lower toxicities than 1,4-dioxane. The solvents that were chosen for this study were cyclopentylmethyl ether (CPME), 2-methyltetrahydrofuran (2-MeTHF), 1,2-dimethoxyethane (DME) and methanol. Without going into significant detail, with 1 mol% rhodium, 2 mol% AgSbF₆ in 2-MeTHF solvent at 50°C, the cyclohexyl substrate **53** was successfully cycloisomerized to the product **59** in 100% yield by the polymer-supported rhodium catalyst-organic framework, which is an improvement on the results obtained when 1,4-dioxane was used as the solvent. Under the same conditions, the use of CPME, DME or methanol only resulted in conversions ranging from 50 to 64%. Thus, 2-MeTHF, along with 1,4-

dioxane, were chosen as solvents for the batch reactivity studies of the COF **41**.

Interestingly, attempts at catalyst reuse in 2-MeTHF were completely unsuccessful. As a result, it was postulated that perhaps 1,4-dioxane is capable of stabilizing the rhodium centers through coordination in the absence of substrate or product and even during catalysis itself. In fact, the coordination of 1,4-dioxane to metal centers is known,²⁷ which lends support to this claim. In addition, the coordinating ability of 2-MeTHF is thought to be quite a bit lower than 1,4-dioxane due to steric interactions arising from the presence of a methyl group on the alpha carbon. Therefore, the use of 2-MeTHF should theoretically provide a higher rate of reaction and overall TON than 1,4-dioxane in batch reactions of the cycloisomerization of 1,6-enynes as it cannot competitively coordinate to the rhodium catalytic centers. On the other hand, 1,4-dioxane would be a better choice for catalyst reuse studies as it is capable of coordinating and stabilizing the rhodium centers not only during catalysis but also between catalytic runs.

Once the solvents were chosen, the batch reactivity of COF **41** was investigated in the cycloisomerization of the cyclohexyl 1,6-enyne **53**. The results of this study are given in Table 3-3.

Table 3-3. Batch reactivity results for the cycloisomerization of the cyclohexyl 1,6-enyne substrate **53** catalyzed by the polymer-supported rhodium catalyst-organic framework **41**.^a

Loading (Sub/Ag/Rh)	Solvent	Time (h)	TON ^b	ee ^c (%)
1000/5/1	1,4-dioxane	2	200	>95
		45	800	>95
1000/5/1	2-MeTHF	2	500	>95
		4	630	>95
500/5/1	2-MeTHF	2	500	>95

^[a] The reactions were carried out in 2.0M solutions of substrate **53** in 1,4-dioxanes or 2-MeTHF at 70°C. ^[b] TONs were determined by ¹H-NMR. ^[c] ee was determined by chiral NMR shift reagent.

As theoretically predicted, the cycloisomerization of the cyclohexyl 1,6-enyne **53** went much faster in 2-MeTHF than 1,4-dioxane. For example, with a S/C ratio of 1000:1, after two hours the reaction was 50% complete (TON of 500) in 2-MeTHF. However, under the same conditions, the reaction was only 20% complete (TON of 200) when 1,4-dioxane was used. As well, it was observed that the rate of reaction decreased significantly when 1,4-dioxane was chosen as 45 hours were required to achieve a total TON of 800. These results support the proposition that perhaps 1,4-dioxane is competitively coordinating to the rhodium catalytic centers during catalysis, which is not the case for 2-MeTHF. It can therefore be concluded that 2-MeTHF is in fact a better solvent for batch 1,6-enyne cycloisomerization reactions. It should also be noted that the

enantioselectivity of the cycloisomerized product **59** was not affected by choice of solvent.

The results presented in Table 3-2 also suggest that in 2-MeTHF solvent a S/C ratio of 500 is optimal for the cycloisomerization of the cyclohexyl 1,6-enyne **53**. After two hours at this substrate loading, 100% conversion (TON of 500) was achieved with no drop in catalytic activity over the course of those two hours. This corresponds to a TOF of 250 hour⁻¹, where TOF is a direct representation of the rate of reaction. This result is particularly remarkable considering that the cycloisomerization of ten equivalents of 1,6-enyne substrate in ten minutes, a TOF of 60 hour⁻¹, is the precedent in the literature. It should also be noted that attempts at catalyst reuse were unsuccessful under these conditions, which again is in accordance with the theoretical predictions mentioned earlier.

The batch reactivity of the COF **41** was also investigated for the cycloisomerization of the phenyl 1,6-enyne substrate **46**. The results of this study are presented in Table 3-4. Here, with a S/C ratio of 500:1, a total TON of 480 was obtained after 23 hours of reaction time in 1,4-dioxane. Under a higher S/C loading of 1600:1, 890 TOs were obtained in 20 hours in 2-MeTHF. This result confirms the finding of the previous study that 2-MeTHF is in fact a better solvent choice for batch reactivity than 1,4-dioxane. As well, the enantioselectivity of the cycloisomerized product **47** was not affected by the choice of solvent.

Table 3-4. Batch reactivity results for the cycloisomerization of the phenyl 1,6-enyne substrate **46** catalyzed by the polymer-supported rhodium catalyst-organic framework **41**.^a

Loading (Sub/Ag/Rh)	Solvent	Time (h)	TON ^b	ee ^c (%)
500/5/1	1,4-dioxane	23	480	>99.9
1600/5/1	2-MeTHF	20	890	>99.9

^[a] The reactions were carried out in 2.0M solutions of substrate **46** in 1,4-dioxanes or 2-MeTHF at 70°C. ^[b] TONs were determined by ¹H-NMR and by comparison to authentic samples. ^[c] ee was determined by chiral GC.

Similar to the results obtained from the reuse studies, it was found that COF **41** was more active for the cycloisomerization of the cyclohexyl 1,6-enyne substrate **53** than the phenyl substrate **46**. For example, a TOF of 250 hour⁻¹ was obtained in the cycloisomerization of cyclohexyl 1,6-enyne **53** in 2-MeTHF solvent while a TOF of 44 hour⁻¹ was obtained in the cycloisomerization of phenyl 1,6-enyne **46** in 2-MeTHF solvent. As discussed previously, this difference in activity was attributed to the competitive η^6 -binding of the aromatic ring in the phenyl 1,6-enyne substrate **46**, which is not present for the cyclohexyl 1,6-enyne substrate **53**.

In summary, the polymer-supported rhodium catalyst-organic framework **41** provided overall TONs as high as 800 and 890 in the intramolecular cycloisomerization of 1,6-enynes **53** and **46**, respectively. To the best of our knowledge, these are the highest TONs reported for any cycloisomerization reaction. It was also discovered that the coordinating

ability of the solvent has a significant effect on the reusability and batch reactivity of the catalyst, however choice of solvent has no effect on the overall enantioselectivity. Thus, the catalyst-organic framework can be tailored for reuse or batch reactions simply by selecting an appropriate solvent.

Having investigated both the reusability and batch reactivity of the immobilized catalyst, a comparison of the rhodium catalyst-organic framework to the homogeneous $[\text{Rh}((R)\text{-BINAP})]^+$ catalyst for the cycloisomerization of the 1,6-enyne substrates **53** and **46** was studied next. The results of this comparison will be discussed in the following section.

Section D: Comparison of the Polymer-Supported Rhodium Catalyst-Organic Framework **41 to the Homogeneous Catalyst Analogue**

As mentioned previously, the intramolecular cycloisomerization of the cyclohexyl 1,6-enyne **53** was never reported in the literature prior to this study. With such a large substrate scope already reported, the omission of the cyclohexyl 1,6-enyne substrate **53** was quite intriguing. Therefore, as a means of comparison, the homogenous catalyst analogue $[\text{RhCl}((R)\text{-BINAP})]$ was synthesized and studied for the cycloisomerization of the cyclohexyl 1,6-enyne substrate **53**. In addition, Zhang's *in situ* synthesis of the highly active $[\text{RhCl}((R)\text{-BINAP})]$ homogeneous catalyst

was also utilized, with the catalyst being used in the cycloisomerization of the cyclohexyl 1,6-enyne **53** as well.

In the first study, the intramolecular cycloisomerization of cyclohexyl 1,6-enyne **53** was performed under the following conditions: 2.5 mol% of [RhCl((*R*)-BINAP)], 10 mol% of AgSbF₆ and a 0.1M solution of substrate **53** in 1,4-dioxane at 40°C. After two hours of reaction time, 100% conversion had been achieved (TON = 20), however a complex mixture of products was obtained. It was postulated that isomerization of the desired product was responsible for the mixture of products that was generated.

In the second study, the [RhCl((*R*)-BINAP)] homogeneous catalyst was generated *in situ* from reaction between 5 mol% of [RhCl(COD)]₂ and 10 mol% (*R*)-BINAP in DCE solvent. Once the catalyst was generated, 20 mol% of AgSbF₆ was added followed by the cyclohexyl 1,6-enyne substrate **53**. It should be noted that these conditions are the most common in the literature for the cycloisomerization of 1,6-enynes. After five minutes of reaction time at room temperature all of the substrate had been consumed (TON = 10 and 100% conversion). However, as in the previous study, a complex mixture of products, likely arising from the isomerization of the desired product, was obtained. The poor selectivity of the homogeneous catalyst in the cycloisomerization of the cyclohexyl 1,6-enyne substrate **53** explains why this substrate was never reported in the literature prior to this study.

Based on these results, it was determined that the COF **41** was more selective than the homogeneous catalyst analogue [RhCl(*R*-BINAP)] in the cycloisomerization of 1,6-enyne **53**. To the best of our knowledge, this is the first enantioselective catalytic reaction where the immobilized catalyst is more selective than the homogeneous catalyst.

As mentioned, the cycloisomerization of the phenyl 1,6-enyne substrate **46** has previously been reported in the literature.^{13,25} The best reported homogeneous catalyst for the cycloisomerization of this substrate was developed by Hashmi. Here, 10 mol% of [Rh(COD)₂](BF₄) and 10 mol% of (*R*)-BINAP were reacted in DCE at 50°C to give the cycloisomerized product **47** in 93% yield with an ee of 99%.²⁵ Despite the remarkable enantioselectivity exhibited by this catalyst, the total TON obtained was only 9.3. On the other hand, the polymer-supported rhodium catalyst-organic framework **41** provided 890 TOs of the cycloisomerized product **47** in twenty hours of reaction time and was successful with catalyst loadings as low as 0.06 mol%. This catalyst loading is 160 times lower than the 10 mol% of homogeneous catalyst reported in the literature for the cycloisomerization of this substrate. As well, the polymer-supported catalyst provided the cycloisomerized product in >99.9% ee, which is identical to the ee obtained with the homogeneous catalyst. To the best of our knowledge, this is the first immobilized catalyst that provided higher TONs than the homogeneous catalyst analogue while still exhibiting remarkable enantioselectivity.

There are many possible factors that contribute to the high activity/selectivity of the supported catalyst. These include catalyst/framework-support interactions (i.e. the BaSO₄ interaction with catalytic active sites and/or the framework, swellability, etc.) and framework-catalyst interactions (i.e. cross-linking, size exclusion, etc.). Future research in the Bergens group is in part focused on understanding/determining the origins of this high activity and, as a result, a more in depth discussion will be presented in the conclusions and future work chapter of this dissertation (Chapter 6).

In summary, the COF **41** is the first immobilized catalyst that is both more selective and more active than the homogeneous catalyst analogue for the intramolecular cycloisomerization of 1,6-enynes.

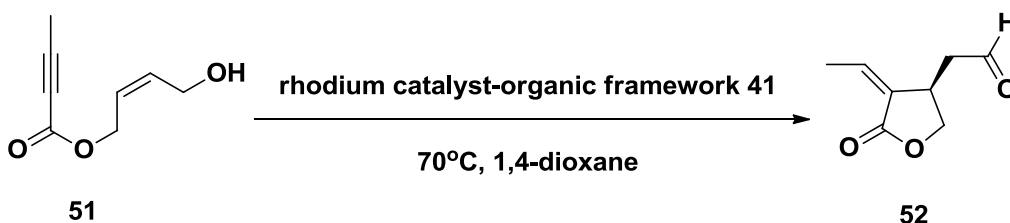
Section E: Production of a (+)-Pilocarpine Precursor

As discussed earlier in this chapter, Zhang reported the synthesis of the lactone **52**, which can be converted into the pharmaceutical (+)-pilocarpine in two subsequent synthetic steps. This lactone was obtained from the [Rh((*R*)-BINAP)]⁺ catalyzed cycloisomerization of the 1,6-enyne ester **51**, followed by a 1,3-hydrogen shift to generate the aldehyde functionality in the product (see Scheme 3-7).^{17a} In particular, the lactone **52** was produced in 99% yield and 99% ee after 10 minutes of reaction time from the following conditions: 5 mol% [RhCl((*R*)-BINAP)] and 20 mol% AgSbF₆ in DCE at room temperature. Despite the high

enantioselectivity, this only corresponds to a total TON of 10. Therefore, the COF **41** was utilized in an attempt to increase the overall TON of this industrially relevant reaction.

The results obtained from the use of the polymer-supported catalyst are summarized in Table 3-5.

Table 3-5. Synthesis of lactone **52**; a precursor to the pharmaceutical (+)-pilocarpine.^a



Loading (Sub/Ag/Rh)	Time (h)	TON ^b	ee ^c (%)
100/5/1	2.5	100	>99.9
300/5/1	48	285	>99.9

^[a] The reactions were carried out at 70°C in 0.9 mL of 1,4-dioxane. ^[b] TONs were determined by ¹H-NMR and by comparison to authentic samples. ^[c] ee was determined by chiral GC.

With a S/C ratio of 100:1 (1 mol% rhodium), the product lactone **52** was produced in 100% yield and >99.9% ee. This corresponds to a total TON of 100, which is already ten times the TON obtained with Zhang's homogeneous catalyst. At the higher S/C ratio of 300:1 (0.33 mol% rhodium), the above reaction was 90% complete after 24 hours and 100% complete after 48 hours, with 5% of the product identified as isomerization

by-products. Thus, the total TON of the desired lactone **52** was 285, which is 28.5 times more TOs than that obtained by Zhang. These are the highest reported TONs for the synthesis of the product lactone **52**. As well, these results lend additional support to the claim that the COF **41** provides higher TONs than the homogeneous catalyst analogue for the cycloisomerization of 1,6-enynes. It should also be noted that the above reaction was attempted in 2-MeTHF solvent, however, a mixture of products was obtained, which was attributed to isomerization. This was an interesting development as this was the only reaction performed where the product obtained was solely solvent dependent. Further study is required to explain the nature of this solvent dependence.

Conclusion

In summary, this is the first report of a polymer-supported catalyst that is both more active and more selective than the parent, homogeneous catalyst. In the intramolecular cycloisomerization of 1,6-enynes **53** and **46**, the polymer-supported rhodium catalyst **41** was reused up to six times and provided the highest TONs to date (up to 890) with no drop in enantioselectivity (95-99.9% *ee*) and with catalyst loadings ranging from 0.2 to 0.06 mol%. As well, a key intermediate in the production of the pharmaceutical (+)-pilocarpine was synthesized in >99.9% *ee*, illustrating the industrial potential of the polymer-supported rhodium catalyst-organic framework.

In addition to these remarkable results, some other notable discoveries and developments were made along the way. For example, a more practical procedure for synthesizing 1,6-enyne substrates was developed and successfully utilized. As well, it was discovered that the catalyst can be tailored for reuse or batch reactions simply by selecting an appropriate solvent. These developments are major contributors to the practicality of not only the catalyst system but to the catalytic reaction as well.

Experimental

General procedures and methods. $^1\text{H-NMR}$ and $^{13}\text{C-NMR}$ spectra were recorded using Varian Inova (300, 400, 500 MHz) or Varian Unity (500 MHz) spectrometers. $^1\text{H-NMR}$ and $^{13}\text{C-NMR}$ chemical shifts are reported in parts per million (δ) relative to TMS with the solvent as the internal reference. Selected NMR spectra have been vertically and horizontally enhanced to better show characteristic chemical shifts. Gas chromatography analyses were carried out using a Hewlett-Packard 5890 chromatograph equipped with a flame ionization detector, a 3392A integrator, and a Supelco Beta DexTM 120 fused silica capillary column (30m x 0.25mm x 0.25 μm). Polarimetry data was recorded using a Perkin Elmer 241 Polarimeter and using the sodium D line (589nm) with a cell length of 10.002 cm.

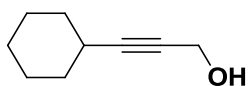
Unless otherwise stated, all experiments were performed under an inert atmosphere using standard Schlenk and glove-box techniques. Argon and nitrogen gas (Praxair, 99.998%) were passed through a drying train containing 3Å molecular sieves and indicating DrieriteTM before use. All solvents were dried and distilled under a nitrogen atmosphere using standard drying agents, unless otherwise noted. All common reagents and solvents were obtained from Sigma-Aldrich Co. and used without further purification, unless otherwise stated. (*R*)-BINAP was obtained from Strem

Chemicals, Inc. and used without further purification. $[\text{Rh}(\text{NBD})_2](\text{SbF}_6)^{28}$ and $[\text{RhCl}(\text{C}_2\text{H}_4)_2]_2^{29}$ were synthesized according to literature procedures.

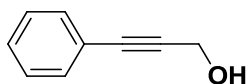
Synthesis of *cis*-2-penten-1-bromide (58). In 60 mL of diethyl ether, 5.2 mL of *cis*-2-penten-1-ol **57** (4.643g, 53.4 mmol) and 0.5 mL of pyridine were cooled to -40°C . To this mixture, 2.03 mL of phosphorous (III) bromide (5.784g, 21.3 mmol) was added via syringe. This mixture was allowed to stir and warm to room temperature slowly over 2 hours, and then maintained at room temperature for an additional hour. The reaction was then quenched by addition of 100 mL of saturated NaHCO_3 in distilled water. The aqueous layer was extracted with 3 x 50 mL diethyl ether; the organic layer was then dried over MgSO_4 and filtered. The product was isolated as a colorless liquid and then purified by silica gel flash chromatography using 50:1 petroleum ether : diethyl ether as eluent, $R_f = 0.4$. Yield = 5.973 g (39.8mmol, 75%). $^1\text{H-NMR}$ (300 MHz, CDCl_3) δ ppm 1.03 (t, $J=7.6\text{Hz}$, 3H), 2.17 (quintet, $J=7.3\text{Hz}$, 2H), 4.01 (d, $J=8.1\text{Hz}$, 2H), 5.56-5.72 (m, 2H).

Synthesis of propargyl alcohols (e.g. 55). Under an inert atmosphere, 38.8 mmol of the desired acetylene in 30 mL of THF was cooled to -78°C . To this, 39 mmol of 1.6M *n*-butyllithium in hexanes was added dropwise over 30 minutes. The solution was then warmed to 0°C . 62 mmol of paraformaldehyde was then added as a solid while flushing

with N₂, and the solution warmed to room temperature over 1 hour, after which it was heated to 45°C for 90 minutes. This solution was then cooled to room temperature and quenched with 125 mL of 10% NH₄Cl in distilled water. After separation of phases, the aqueous layer was extracted with 3 x 50 mL diethyl ether; the organic layer was then dried over MgSO₄ and filtered. The product was isolated as a yellow oil and was purified by silica gel flash chromatography using 60:40 CH₂Cl₂ : hexanes as eluent.



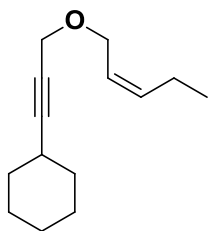
Yield = 4.962 g (35.9mmol, 93%). ¹H-NMR (300 MHz, CDCl₃) δ ppm 1.26-1.66 (m, 7H), 1.69-1.81 (m, 2H), 1.81-1.93 (m, 2H), 2.38-2.52 (m, 1H), 4.33 (d, J=1.8Hz, 2H).



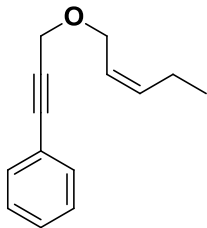
Yield = 4.611 g (34.9mmol, 90%). ¹H-NMR (300 MHz, CDCl₃) δ ppm 4.53 (s, 2H), 7.27-7.36 (m, 3H), 7.40-7.43 (m, 2H).

Synthesis of 1,6-enyne substrates (53 and 46). In a typical experiment, a 200 mL round-bottom flask equipped with a stir bar was charged with 1.301 g of a 30 wt% dispersion of KH in mineral oil (0.390g, 9.7 mmol). The flask was then evacuated and backfilled 3 times with nitrogen gas. The KH was then rinsed with 4 x 5 mL THF to quantitatively remove the mineral oil. To the KH, another 20 mL of THF was added, and the mixture cooled to 0°C. Next, 1.002 g (6.7 mmol) of *cis*-2-penten-1-

bromide **58** was added by cannula under an inert atmosphere, followed by 2 x 5 mL THF rinses. This was followed by addition of 6.1 mmol of the propargyl alcohol via cannulation under an inert atmosphere, followed by 2 x 5 mL THF rinses. Upon addition of the alcohol, H₂ gas evolves, and the reaction mixture goes to a bright orange color. The reaction was allowed to warm up to room temperature, and then stirred for 3 hours, after which the reaction was quenched with 50 mL distilled water. The aqueous phase was then extracted with 3 x 50 mL of diethyl ether; the organic layer was then dried over MgSO₄ and filtered. The product was isolated as a yellow oil and was purified by silica gel flash chromatography using 50:1 petroleum ether : diethyl ether as eluent.



Yield = 0.852 g (4.1mmol, 68%), R_f = 0.3. ¹H-NMR (400 MHz, CDCl₃) δ ppm 0.91 (t, J=7.6Hz, 3H), 1.15-1.29 (m, 3H), 1.29-1.48 (m, 3H), 1.57-1.66 (m, 2H), 1.67-1.76 (m, 2H), 2.03 (qd, J=1.2, 7.4Hz, 2H), 2.28-2.37 (m, 1H), 4.00-4.03 (m, 2H), 4.03 (d, J=2.2Hz, 2H), 5.35-5.57 (m, 2H); ¹³C-NMR (101 MHz, CDCl₃) δ ppm 14.05, 20.76, 24.70, 25.80, 28.99, 32.52, 57.19, 64.28, 75.82, 90.60, 124.80, 135.74; anal. calcd. for C₁₄H₂₂O (206.32): C 81.50, H 10.75; found C 81.51, H 10.68.



Yield = 0.610 g (3.0mmol, 49%), $R_f = 0.2$. $^1\text{H-NMR}$ (400 MHz, CDCl_3) δ ppm 1.07 (t, $J=7.5\text{Hz}$, 3H), 2.14-2.28 (m, 2H), 4.25 (d, $J=6.6\text{Hz}$, 2H), 4.43 (s, 2H), 5.56-5.64 (m, 1H), 5.68-5.76 (m, 1H), 7.30-7.42 (m, 3H), 7.47-7.56 (m, 2H); anal. calcd. for $\text{C}_{14}\text{H}_{16}\text{O}$ (200.28): C 83.96, H 7.99; found: C 83.60, H 8.36.

Synthesis of the 1,6-enyne ester substrate (51). A 200mL round-bottom flask, equipped with a stir bar, was charged with 16 mmol (1.35 g) of 2-butyric acid and 0.16 mmol (19.6 mg) of 4-dimethylaminopyridine (DMAP). The flask was then evacuated and backfilled 3 times with nitrogen gas. These were then dissolved in 32 mL of dry CH_2Cl_2 resulting in the formation of a yellow solution. Next, 16 mmol (1.41 g, 1.31 mL) of (Z)-2-buten-1,4-diol was added to the flask and the solution was then cooled to 0°C . Finally, 17.6 mmol (3.64 g) of 1,3-dicyclohexylcarbodiimide (DCC) dissolved in 16mL of CH_2Cl_2 was added dropwise to the flask at 0°C over a period of 2 hours. Upon addition of DCC, solid 1,3-dicyclohexylurea (DCU) is produced. After 2 hours, the product solution was filtered and the product concentrated via rotary evaporation to give a yellow oil. The crude product was a 50:50 mixture of the desired mono-ester compound and the undesired di-ester compound. The product was

further purified by silica gel flash chromatography using 100% CH₂Cl₂ as eluent, R_f = 0.1. Yield = 1.157g (7.5mmol, 47%). ¹H-NMR (300 MHz, CDCl₃) δ ppm 1.98 (s, 3H), 4.26 (t, J=4.5Hz, 2H), 4.75 (d, J=5.1Hz, 2H), 5.68-5.61 (m, 1H), 5.91-5.85 (m, 1H).

Representative procedures for the intramolecular cycloisomerization of 1,6-enynes catalyzed by the polymer-supported rhodium catalyst-organic framework 41. All substrates and solvents were bubbled for 30 minutes under argon or nitrogen gas prior to use.

Low-loading cycloisomerizations of 1,6-enynes with reuse. In a typical experiment, a Schlenk flask equipped with a TeflonTM valve was charged with 0.4736 g of the polymer-supported rhodium catalyst on BaSO₄ (**41**/BaSO₄) (5.66 mg of “[RhCl((*R*)-5,5'-dinorimido-BINAP)]₂”, 2.61 x 10⁻³ mmol) under an inert atmosphere. An NMR tube was charged with 1.05 x 10⁻² mmol of AgSbF₆ under N₂ in the dark and sealed using a rubber septum. 0.105 mmol of substrate was then added into the flask containing the catalyst, rinsed in with 0.5 mL of 1,4-dioxanes and stirred for 1 minute. Next, 0.1 mL of 1,4-dioxanes was added to the AgSbF₆, which was then cannulated onto the substrate/catalyst mixture, along with 5 x 0.1 mL rinses of 1,4-dioxanes. The Schlenk flask was then sealed with the TeflonTM valve and then placed into an oil bath set at 60°C. After 3 hours, an aliquot was taken via inverse filtration under an inert atmosphere, and

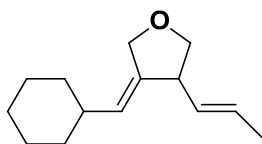
analyzed by $^1\text{H-NMR}$. Upon confirmation that the initial batch reaction was complete, the Schlenk flask was charged with 5 mL of 1,4-dioxanes and stirred for 5 minutes. The solvent and cycloisomerized product was then removed by inverse filtration, and the catalyst was again treated with another 5 mL of 1,4-dioxanes. As soon as the 2 x 5 mL rinses of 1,4-dioxanes were collected, the Schlenk flask containing the catalyst was charged with 0.525 mmol of substrate and 2.61 mL of 1,4-dioxanes. The flask was then sealed and again immersed in an oil bath. The temperature of the oil bath was modified depending on the amount of conversion obtained. All further reuses were carried out in this manner.

High-loading cycloisomerizations of 1,6-enynes. For these experiments, the polymer-supported rhodium catalyst-organic framework (**41**/ BaSO_4) and the AgSbF_6 were weighed into the same flask.

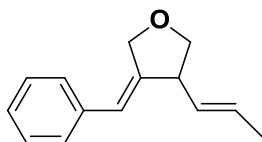
In a typical experiment, under nitrogen or argon atmosphere, a Schlenk flask equipped with a TeflonTM valve was charged with 0.1011 g of the polymer-supported rhodium catalyst (**41**/ BaSO_4) (1.24 mg of “[$\text{RhCl}((R)\text{-}5,5'\text{-dinorimido-BINAP})_2$ ”, 5.74×10^{-4} mmol) and 5.74×10^{-3} mmol of AgSbF_6 . Next, 0.575 mmol of substrate in 0.6 mL of 2-MeTHF was cannulated onto the catalyst/silver mixture and the Schlenk flask was sealed with the TeflonTM valve. The Schlenk flask was then placed in an oil bath set at 70°C . After 2 hours, an aliquot was taken via inverse filtration and the extent of reaction determined by $^1\text{H-NMR}$.

Optimized cycloisomerizations of 1,6-enyne ester substrate 51. In these optimized experiments it was found that swelling the polymer-supported rhodium catalyst-organic framework **41** in the presence of AgSbF_6 for 30 minutes at 40°C maximized the initial rate and yields obtained from the catalyst.

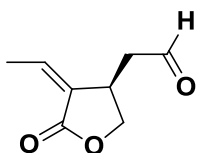
A Schlenk flask equipped with a Teflon™ valve was charged with 0.1090 g of the polymer-supported rhodium catalyst (**41**/ BaSO_4) (1.33 mg of “[$\text{RhCl}((R)\text{-}5,5'\text{-dinoimidobinap}$)]₂”, 6.16×10^{-4} mmol) and 6.16×10^{-3} mmol of AgSbF_6 . The Schlenk flask was then removed from the glove box and covered in tinfoil. Next, 0.4 mL of 1,4-dioxanes was added to the Schlenk flask and stirred at 40°C for 30 minutes. 0.123 mmol of the 1,6-enyne ester substrate **51** in 0.2 mL of 1,4-dioxanes was cannulated onto the catalyst/silver mixture followed by a 0.3 mL rinse of 1,4-dioxanes. The Schlenk flask was then sealed with the Teflon™ valve and placed in an oil bath set at 70°C . Conversion was monitored by $^1\text{H-NMR}$ of aliquots.



$^1\text{H-NMR}$ (300 MHz, CDCl_3) δ ppm 1.00-1.30 (m, 6H), 1.54-1.59 (br m, 3H), 1.67-1.74 (br m, 1H), 1.71 (dd, $J=1.6, 6.6\text{Hz}$, 3H), 1.88 (m, 1H), 3.19 (q, $J=6\text{Hz}$, 1H), 3.40 (t, $J=6.4\text{Hz}$, 1H), 4.00 (t, $J=6\text{Hz}$, 1H), 4.30 (dt, $J=1.7, 10\text{Hz}$, 1H), 4.40 (d, $J=9.6\text{Hz}$, 1H), 5.01-5.06 (m, 1H), 5.17-5.25 (m, 1H), 5.45-5.58 (m, 1H); MS (EI) m/z : [M^+] 206; >95% ee.



$^1\text{H-NMR}$ (300 MHz, CDCl_3) δ ppm 1.76 (dd, $J=1.5, 6.9\text{Hz}$, 3H), 3.38-3.50 (m, 2H), 4.06-4.12 (m, 1H), 4.60 (dt, $J=2.2, 14.1\text{Hz}$, 1H), 4.74 (dd, $J=2.1, 14.1\text{Hz}$, 1H), 5.29-5.40 (m, 1H), 5.60-5.71 (m, 1H), 6.25 (q, $J=2.3\text{Hz}$, 1H), 7.12-7.17 (m, 2H), 7.18-7.24 (m, 1H), 7.29-7.37 (m, 2H); MS (EI) m/z : $[\text{M}^+]$ 200; >99% ee.



$^1\text{H-NMR}$ (300 MHz, CDCl_3) δ ppm 2.21 (dd, $J=1.8, 7.2\text{Hz}$, 3H), 2.72 (dd, $J=8.5, 18.8\text{Hz}$, 1H), 2.88 (dd, $J=5.1, 18.9\text{Hz}$, 1H), 3.43-3.57 (br m, 1H), 3.84 (dd, $J=5.4, 9.3\text{Hz}$, 1H), 4.55 (t, 8.7Hz , 1H), 6.29 (dq, $J=1.9, 7.5\text{Hz}$, 1H), 9.82 (s, 1H); MS (EI) m/z : $[\text{M}^+]$ 154; >99% ee.

Homogeneous cycloisomerization of 1,6-enyne **53** in dioxane.

6.3 mg of $[\text{RhCl}(\text{BINAP})]_2$ (3.99×10^{-3} mmol) and 5.5 mg of AgSbF_6 (1.59×10^{-2} mmol) were weighed out in a glove box into separate NMR tubes and sealed with rubber septa. The catalyst was then dissolved in 0.6mL of 1,4-dioxane and transferred to a Schlenk flask equipped with a TeflonTM valve, followed by 2 x 0.2mL rinses of 1,4-dioxane. Next, the AgSbF_6 was rinsed into the Schlenk flask with 0.2mL of 1,4-dioxane, followed by a further 2 x 0.2mL of 1,4-dioxane. Lastly, 32.9 mg of cyclohexyl 1,6-enyne substrate **53** (0.159 mmol) was added to the Schlenk flask. The flask was then

sealed and stirred in an oil bath set at 40°C. After 2 hours, an aliquot was taken and ¹H-NMR showed that 100% conversion had been achieved and a mixture of cycloisomerization products had been obtained, probably due to olefin isomerization in the product.

Homogeneous cycloisomerization of 1,6-enyne **53 using Zhang's *in situ* [Rh(*R*-BINAP)]⁺ catalyst.** 3.7 mg of [RhCl(COD)]₂ (7.5 x 10⁻³ mmol), 10.3 mg of AgSbF₆ (3.0 x 10⁻² mmol) and 9.4 mg of (*R*)-BINAP (1.5 x 10⁻² mmol) were weighed in a glove box into separate NMR tubes and sealed with rubber septa. The (*R*)-BINAP was dissolved in 0.5 mL of DCE and cannulated onto the [RhCl(COD)]₂ followed by a 0.1 mL rinse of DCE. This was followed by addition of 31 mg of cyclohexyl 1,6-enyne substrate **53** (0.150 mmol) to the catalyst/ligand solution. Next, the AgSbF₆ was dissolved in 0.4 mL of DCE and this was cannulated into the NMR tube containing the substrate, ligand and catalyst. The solution turned from a dark red color to an orange/brown color immediately and a solid (AgCl) was visible in the NMR tube. The NMR tube was then shaken for 5 minutes at room temperature and then run immediately through a FluorosilTM plug to remove any metal residues. ¹H-NMR showed 100% conversion and that a complex mixture of products was obtained.

Determination of enantiomeric excess. For these experiments, a racemic sample of the desired product was synthesized, analyzed and then compared to the spectrum/chromatogram obtained for the product

synthesized from the polymer-supported rhodium catalyst-organic framework **41**.

Synthesis of racemic products. 6.8 mg of $[\text{Rh}(\text{NBD})_2](\text{SbF}_6)$ (1.3×10^{-2} mmol) dissolved in 1 mL of DCE and 1.3×10^{-1} mmol of substrate in 0.3 mL of DCE were both cannulated into a Schlenk flask, followed by 2 x 0.4 mL rinses of DCE. The Schlenk tube was then placed in an oil bath at 65°C. Within 5 minutes the reaction solution went from red to brown in color. After 1.5 hours, 100% conversion to the racemic product was achieved.

Determination of the ee for the cyclohexyl 1,6-enyne product **59.** 12.6 mg of racemic cyclohexyl product **59** (6.11×10^{-2} mmol) was dissolved in 0.6 mL of benzene- d^6 in an NMR tube. A solution of 22.1 mg of europium-tris[3-(heptafluoropropylhydroxymethylene)-(+)-camphorate] (1.85×10^{-2} mmol) in benzene- d^6 was also prepared. The europium solution was added in 10 μL increments until the signal originally at 3.4 ppm had shifted to ~6.5 ppm, where the peak was cleanly resolved into two signals in a 1:1 ratio (Figure 3-3). Only one signal, that at $\delta=6.3$ ppm, was observed when the experiment was repeated with cyclohexyl product **59** obtained from the polymer-supported rhodium catalyst-organic framework catalyzed cycloisomerization (Figure 3-4). From the spectra obtained, it was determined that the ee was >95%. Absolute configuration was not determined.

Determination of the ee for the phenyl 1,6-enyne product 47. The ee of the phenyl cycloisomerized product **47** was determined with chiral gas chromatography and confirmed with the racemic product. The cycloisomerization product **47** was passed through a Fluorosil™ plug using CH₂Cl₂ as eluent. The eluted compound was concentrated under reduced pressure, and a solution was prepared in CH₂Cl₂ at a concentration of 2 mg per 1 mL. Next, 1 μL was injected into the GC under the following conditions: helium carrier gas (20 psig); initial temperature of 100°C, rate of 0.4°C/min up to 220°C; injector temperature of 220°C; detector temperature of 220°C. Retention time for the racemic product: 122.6 minutes for enantiomer 1 and 123.4 minutes for enantiomer 2. From the chromatograms, it was determined that the ee was >99.9%. Absolute configuration was not determined.

Determination of the ee for the lactone product 52. $[\alpha] = +51.79$, $c=0.2$, CH₂Cl₂; From Zhang *et al.*,^{17a} for the (*R*) enantiomer, $[\alpha] = +92.400$, $c=1$, CH₃Cl.

The ee of lactone **52** was determined with chiral gas chromatography followed by comparison to the racemic product. Sample preparation was the same as mentioned above. 1 μL of the solution was injected into the GC under the following conditions: helium carrier gas (20 psig; temperature of 140°C; injector temperature of 220°C; detector temperature of 220°C. Retention time for the racemic product: 37.057 minutes for

enantiomer 1 and 38.840 minutes for enantiomer 2. From the chromatograms it was determined that the ee was >99.9%.

References

- (1) Alder, K., In *Diene Synthesis and Related Reaction Types*. (Nobel Lecture, 1950). In *Nobel Lectures, Chemistry 1942-1962*, Elsevier: Amsterdam, **1964**, pg. 267-303.
- (2) Huntsman, W. D.; Hall, R. P. *J. Org. Chem.* **1962**, *27*, 1988.
- (3) (a) Hoffmann, H. M. R. *Angew. Chem. Int. Ed.* **1969**, *8*, 556. (b) Snieckus, W. O. V. *Angew. Chem. Int. Ed.* **1978**, *17*, 476.
- (4) Mikami, K.; Shimizu, M. *Chem. Rev.* **1992**, *92*, 1021.
- (5) Trost, P. M.; Lautens, M.; Hung, M. H.; Carmichael, C. S. *J. Am. Chem. Soc.* **1984**, *106*, 7641.
- (6) (a) Zhang, L.; Sun, J.; Kozmin, S. A. *Adv. Synth. Catal.* **2006**, *348*, 2271. (b) Pardo, P.; Fernández, A.; Fañanás, F. J.; Rodríguez, F. *Adv. Synth. Catal.* **2012**, *354*, 2141.
- (7) Ikeda, S.-I.; Daimon, N.; Sanuki, R.; Odashima, K. *Chem. Eur. J.* **2006**, *12*, 1797.
- (8) (a) Fürstner, A.; Davies, P. W. *Angew. Chem. Int. Ed.* **2007**, *119*, 3410. (b) Cui, J.; Chai, D. I.; Miller, C.; Hao, J.; Thomas, C.; Wang, J.; Scheidt, K. A.; Kozmin, S. A. *J. Org. Chem.* **2012**, *77*, 7435.
- (9) Harrison, T. J.; Dake, G. R. *Org. Lett.* **2004**, *6*, 5023.
- (10) (a) Trost, B. M.; Frederiksen, M. U.; Rudd, M. T. *Angew. Chem. Int. Ed.* **2005**, *44*, 6630. (b) Fürstner, A.; Schlecker, A.; Lehmann, C. W. *Chem. Commun.* **2007**, 4277.

- (11) (a) Chatani, N.; Inoue, H.; Morimoto, T.; Muto, T.; Murai, S. *J. Org. Chem.* **2001**, *66*, 4433. (b) Barbazanges, M.; Augé, M.; Moussa, J.; Amouri, H.; Aubert, C.; Desmarets, C.; Fensterbank, L.; Gandon, V.; Malacria, M.; Ollivier, C. *Chem. Eur. J.* **2011**, *17*, 13789.
- (12) (a) Michelet, V.; Toullec, P. Y.; Genêt, J.-P. *Angew. Chem. Int. Ed.* **2008**, *47*, 4268. (b) Zhang, Z.; Zhu, G.; Tong, X.; Wang, F.; Xie, X.; Wang, J.; Jiang, L. *Curr. Org. Chem.* **2006**, *10*, 1457. (c) *Modern Rhodium-Catalyzed Organic Reactions*; Evans, P. A., Ed.; Wiley-VHC: Weinheim, Germany, **2005**. (d) Watson, I. D. G.; Toste, F. D. *Chem. Sci.* **2012**, *3*, 2899. (e) Marinetti, A.; Jullien, H.; Voituriez, A. *Chem. Soc. Rev.* **2012**, *41*, 4884.
- (13) Cao, P.; Zhang, X. *Angew. Chem. Int. Ed.* **2000**, *39*, 4104.
- (14) Lei, A.; He, M.; Wu, S.; Zhang, X. *Angew. Chem. Int. Ed.* **2002**, *41*, 3457.
- (15) Lei, A.; He, M.; Zhang, X. *J. Am. Chem. Soc.* **2003**, *125*, 11472.
- (16) Lei, A.; Waldkirch, J. P.; He, M.; Zhang, X. *Angew. Chem. Int. Ed.* **2002**, *41*, 4526.
- (17) (a) Lei, A.; He, M.; Zhang, X. *J. Am. Chem. Soc.* **2002**, *124*, 8198. (b) He, M.; Lei, A.; Zhang, X. *Tetrahedron Lett.* **2005**, *46*, 1823.
- (18) (a) Lui, F.; Liu, Q.; He, M.; Zhang, X.; Lei, A. *Org. Biomol. Chem.* **2007**, *5*, 3531. (b) Kinder, R. E.; Widenhoefer, R. A. *Org. Lett.* **2006**, *8*, 1967.

- (19) (a) Tong, X.; Li, D.; Zhang, Z.; Zhang, X. *J. Am. Chem. Soc.* **2004**, *126*, 7601. (b) Tong, X.; Zhang, Z.; Zhang, X. *J. Am. Chem. Soc.* **2003**, *125*, 6370.
- (20) (a) Tener, G. M.; van Tamelen, E. E.; Strong, F. M. *J. Am. Chem. Soc.* **1953**, *75*, 3623. (b) de Azevedo, M. B. M.; Greene, A. E. *J. Org. Chem.* **1995**, *60*, 4940.
- (21) Sayah, R.; Framery, E.; Dufaud, V. *Green Chem.* **2009**, *11*, 1694.
- (22) Bergens, S. H.; Bosnich, B. *J. Am. Chem. Soc.* **1991**, *113*, 958.
- (23) (a) Nicolaou, K. C.; Edmonds, D. J.; Li, A.; Tria, G. S. *Angew. Chem. Int. Ed.* **2007**, *46*, 3942. (b) Nicolaou, K. C.; Li, A.; Ellery, S. P.; Edmonds, D. J. *Angew. Chem. Int. Ed.* **2009**, *48*, 6293.
- (24) Horne, D. A.; Fugmann, B.; Yakushijin, K.; Buchi, G. *J. Org. Chem.* **1993**, *58*, 62.
- (25) Hashmi, A. S. K.; Haufe, P.; Nass, A. R. *Adv. Synth. Catal.* **2003**, *345*, 1237.
- (26) Dwivedi, A. M. *Int. J. Pharm Excipients* **2003**, (April – June), 33.
- (27) Langer, J.; Krieck, S.; Fischer, R.; Goerls, H.; Walther, D.; Westerhausen, M. *Organometallics* **2009**, *28*, 5814.
- (28) Osborn, J. A.; Schrock, R. R. *J. Am. Chem. Soc.* **1971**, *93*, 2397.
- (29) Cramer, R. *Inorg. Synth.* **1990**, *28* (Reagents Transition Met. Complex Organomet. Synth.), 86.

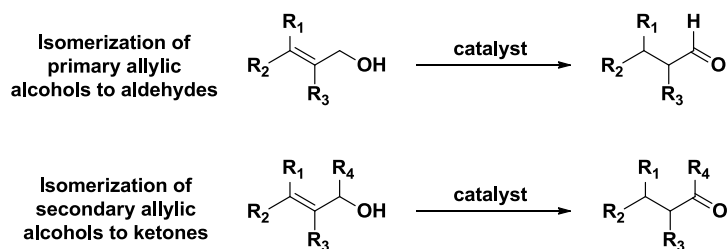
Chapter 4

The Solvent-Free Isomerization of Allylic Alcohols³

Introduction

A prominent strategy to minimize the cost and environmental impact of chemical synthesis is to develop atom-economical reactions that occur over reusable catalysts in inexpensive, non-toxic solvents.¹ The catalytic isomerization of primary and secondary allylic alcohols into the corresponding aldehydes or ketones (Equation 4-1) is an ideal candidate for such a transformation because it occurs with 100% atom economy and produces useful, versatile products.²

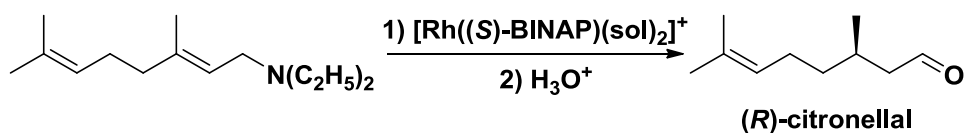
Equation 4-1. Isomerization of primary and secondary allylic alcohols into aldehydes and ketones.



³ A version of this chapter has been published. Elizabeth G. Corkum, Suneth Kalapugama, Michael J. Hass, Steven H. Bergens. "Solvent-Free Isomerization of Allylic Alcohols Catalyzed by a Rhodium Catalyst-Organic Framework." *RSC Advances*. **2012**, 2, 3473. All work presented in this chapter is that of Elizabeth G. Corkum.

Perhaps the most prominent example of the industrial application of this type of catalytic transformation is the $[\text{Rh}((S)\text{-BINAP})(\text{sol})_2]^+$ (sol = solvent) catalyzed asymmetric isomerization of *N,N*-diethylgeranylamine to give, after hydrolysis, enantiopure (*R*)-citronellal (Scheme 4-1).³ This reaction is a key step in the industrial synthesis of (-)-menthol (see Chapter 1 for a more in depth discussion of this reaction).

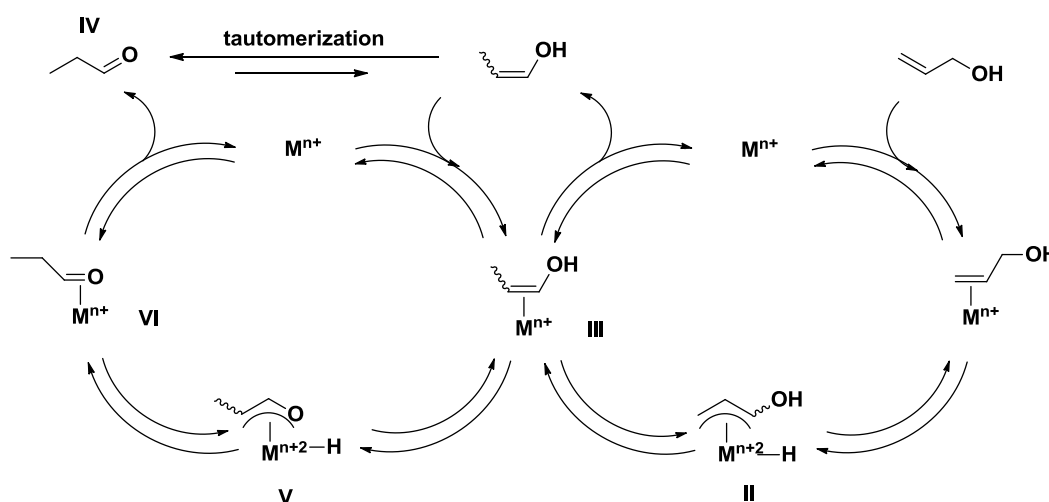
Scheme 4-1. Isomerization to produce enantiopure (*R*)-citronellal.



The mechanism of the isomerization of allylic alcohols has been extensively studied and the most accepted conclusion is that these reactions proceed via an intramolecular net 1,3-hydride shift (Scheme 4-2).² Specifically, the reaction begins with η^2 -complexation of the allylic alcohol on the transition metal catalyst **(I)**. Next, there is a migration of the hydrogen linked to the carbinol center onto the metal (i.e. allylic C-H oxidation addition), resulting in the formation of a π -allyl metal hydride intermediate **II**. Elimination of this hydride to the other side of the π -allylic system leads to the η^2 - π -complexed enol (**III**). Dissociation regenerates the catalytic species **M** and gives the enol, which can tautomerize to the carbonyl product **IV** in the presence of acid or base. Alternatively, it is possible that complex **III** can undergo another 1,3-hydride shift, where the

alcohol hydrogen migrates first to the transition metal M (V) (i.e. allylic C-H oxidation addition) and then to the carbon vicinal to the carbonyl to give the π -C=O complex VI. Dissociation regenerates the catalyst M and gives the carbonyl product IV.

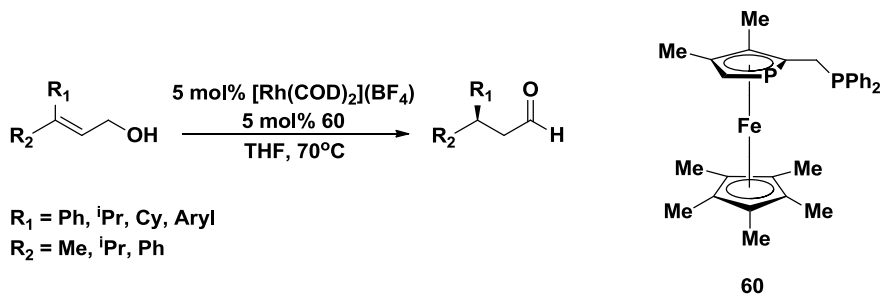
Scheme 4-2. Proposed mechanism for the isomerization of allylic alcohols.



The majority of the reports on the isomerization of allylic alcohols are performed in organic media and are catalyzed by homogeneous, precious metal containing catalysts.⁴⁻⁶ Although there are obvious disadvantages in using such homogeneous catalytic systems, which has been discussed in detail in Chapter 1, the relatively high enantioselectivities obtained with the rhodium⁴ and iridium-containing catalysts⁵ justifies their continued study. As an example, Fu and coworkers reported the *in situ* synthesis of a rhodium-phosphaferrocene

(**60**) complex, which was subsequently utilized in the isomerization of various allylic alcohol substrates (Scheme 4-3).^{4a,7}

Scheme 4-3. The isomerization of allylic alcohols catalyzed by Fu's rhodium-phosphaferrocene catalyst.



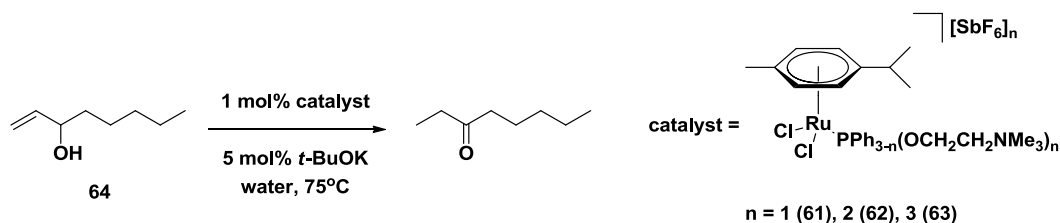
Enantioselectivities and yields as high as 86% and 91%, respectively, were obtained under the following conditions: S/C = 20, 70°C in THF. Prior to this report, the highest enantioselectivity reported for these reactions was 53%, obtained with the $[\text{Rh}((S)\text{-BINAP})(\text{sol})_2]^+$ catalyst system.⁸ Fu's rhodium-phosphaferrocene catalyst is the most selective, rhodium asymmetric catalyst for the isomerization of allylic alcohols to date. Despite the promising results obtained by Fu, the high catalyst loadings and the inability for reuse limits the industrial applicability of this catalyst system.

In an effort to design more sustainable, environmentally friendly and industrially applicable catalytic systems for the isomerization of allylic alcohols, current research is focused on utilizing "greener" solvent systems, such as water,⁹ and developing methods to separate and reuse

the catalyst. The most common strategy is to synthesize water-soluble catalysts that can be separated from the organic isomerized products by an aqueous-biphasic solvent system or liquid-liquid extraction.¹⁰ The majority of these reports utilize ruthenium-containing catalysts as they are the most active catalysts to date for the isomerization of allylic alcohols.⁶

In general, the ruthenium-based water-soluble catalysts have exhibited relatively high activity, with catalyst loadings typically ranging from 0.2 – 1.6 mol%.¹¹ The aqueous-biphasic solvent system typically allows up to four catalyst reuse runs.¹² The most successful reusable, ruthenium-based water-soluble catalysts to date were reported by Gimeno and coworkers. In this study, ruthenium(II)-(η^6 -*p*-cymene) complexes (**61**, **62**, and **63**) were evaluated in the isomerization of 1-octen-3-ol (**64**, Scheme 4-4).¹³

Scheme 4-4. The isomerization of 1-octen-3-ol **64** by Gimeno's ruthenium(II)-(η^6 -*p*-cymene) complexes **61**, **62** and **63**.



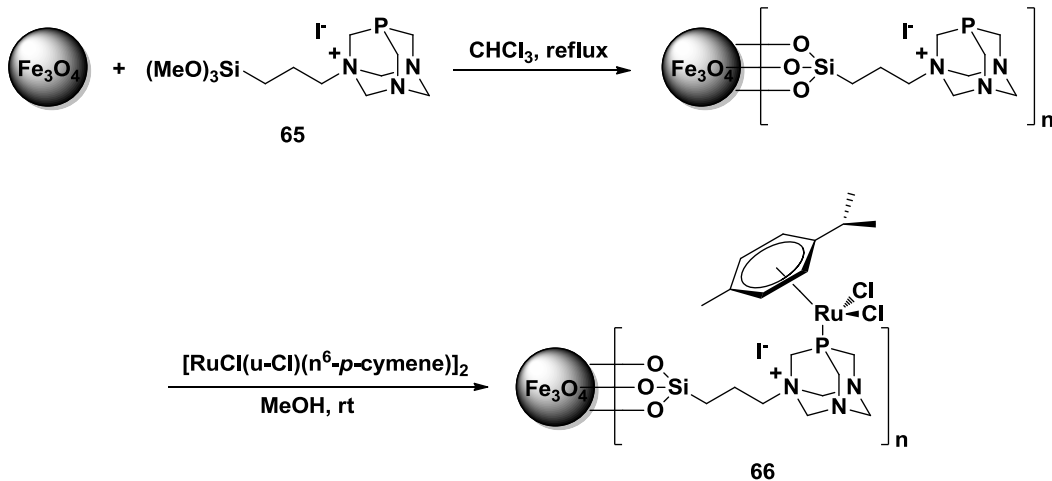
Through liquid-liquid extraction, the catalysts were successfully separated and reused in the isomerization of 1-octen-3-ol. Catalyst **63** proved to be the most successful, sustaining up to nine reuses and providing a total of

990 TOs. However, catalyst deactivation was observed over time as the final run required 215 minutes, compared to 35 minutes in the first run, to achieve 99% yield of the isomerized product. Deactivation was attributed to catalyst leaching into the organic phase during extraction. As well, the overall TONs obtained with these catalysts were relatively low, despite the extensive catalyst reuse. Nevertheless, taken altogether these results are promising and optimization of these water-soluble ruthenium-based catalysts is currently underway.

Due to the success of Gimeno's catalysts, the immobilization of similar catalyst systems has recently been reported.^{14,15} Immobilization not only allows for easy catalyst separation and reuse, but it introduces the possibility for solvent-free catalysis, an unavailable option for homogeneous, biphasic catalyst systems. Thus, the environmental impact of immobilized catalyst systems should theoretically be lower than the biphasic systems. There are few reports of the use of immobilized catalysts in the isomerization of allylic alcohols. The majority of immobilized catalysts that have been reported to date are based on Gimeno's water-soluble ruthenium catalysts.

In a recent study, Polshettiwar and coworkers reported the immobilization of a ruthenium(II)-arene-1,3,5-triaza-7-phosphatricyclo[3.3.1.1]decane (RAPTA) catalyst on silica-coated ferrite nanoparticles (**66**, Scheme 4-5).¹⁴

Scheme 4-5. Polshettiwar's immobilized RAPTA catalyst **66**.



Preparation of the immobilized RAPTA catalyst **66** involved the initial dispersion of preformed silica-coated Fe_3O_4 nanoparticles in chloroform and subsequent treatment with the alkylated ligand **65**. The phosphorus loading of the resulting ligand-functionalized nanoparticles was 10 wt% as measured by ICP-AES (inductively coupled plasma atomic emission spectroscopy). Further reaction with $[\text{RuCl}(\mu\text{-Cl})(\eta^6\text{-}p\text{-cymene})]_2$ in methanol at room temperature for 24 hours afforded the Fe_3O_4 -RAPTA nanoparticles **66**. ICP-AES analysis showed that only 40% of the available ligand sites were metallated by the ruthenium precursor. Despite the incomplete metallation, which could potentially affect the catalytic activity (refer to Chapter 1 and Chapter 2), the Fe_3O_4 supported RAPTA catalyst **66** was utilized in the isomerization of 1-octen-3-ol **64**. Using 1.6 mol% of the catalyst in water at 150°C , the isomerized product (3-octanone) was obtained in 99% yield after 15 minutes. Magnetic separation allowed for

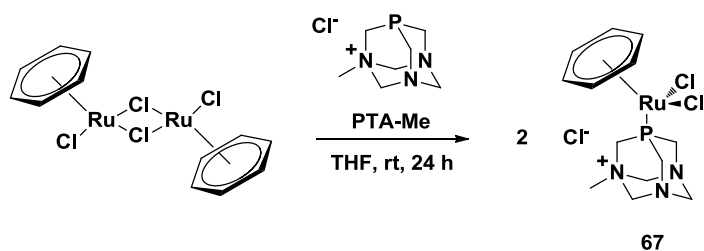
easy catalyst reuse and, in fact, the immobilized catalyst sustained an additional three reuses before significant loss in catalytic activity was observed. The authors did not speculate on the origins of catalyst deactivation however it is probable that significant metal leaching from the Fe_3O_4 support was responsible for the gradual loss in activity.

Although the Fe_3O_4 supported RAPTA catalyst was not as successful as Gimeno's water-soluble ruthenium catalyst **63**, comparable initial activity was obtained with the homogeneous and immobilized RAPTA catalysts (TOFs of 253 h^{-1} and 283 h^{-1} , respectively). In addition, the immobilized catalyst sustained more reuses (four vs three) and exhibited slightly better overall activity (total TONs of 283 vs 210) than the homogeneous catalyst. The authors attributed this difference to the method of catalyst separation employed during reuse for the different catalysts. For example, the homogeneous catalyst could only be separated by liquid-liquid extraction, which resulted in a gradual loss of catalyst into the organic phase. Conversely, magnetic separation was employed for the immobilized catalyst due to the magnetic nature of the Fe_3O_4 nanoparticles, which proved to be more successful in retaining the catalyst for reuse.

Cadierno and coworkers attempted to improve the reusability and activity by utilizing a different support.¹⁵ In this case, the mononuclear RAPTA complex **67** was synthesized by the reaction of dimeric $[\text{RuCl}(\mu\text{-Cl})(\eta^6\text{-C}_6\text{H}_6)]_2$ with excess 1-methyl-3,5-diaza-1-azonia-7-

phosphaadamantane chloride (PTA-Me) ligand in THF at room temperature for a period of 24 hours (Scheme 4-6).

Scheme 4-6. Synthesis of Cadierno's RAPTA complex **67**.



Once synthesized, the RAPTA complex **67** was then immobilized on the commercially available clay Montmorillonite K-10 via solvent-impregnation. In particular, a solution containing 0.4 mmol of **67** in 15 mL of CH₂Cl₂ was treated with 1 gram of the clay until complete discoloration of the solutions was observed. The resulting solid was then washed with CH₂Cl₂ and dried under vacuum. ICP-MS analysis showed that only 73% of the total ruthenium was incorporated into the clay (2.5 wt%), indicating that some of the RAPTA complex **67** was either not adsorbed by the clay initially or was leached from the clay during the CH₂Cl₂ washings.

In the isomerization of 1-octen-3-ol (**64**), the immobilized RAPTA complex **67** was recycled by filtration and reused 10 times with no significant loss in catalytic activity and provided a total of 872 TOs under the following conditions: S/C ratio of 80:1, 3.12 mol% of K₂CO₃ in THF at 75°C for 1-4 hours of reaction time. Cadierno and coworkers attributed the high activity and extensive reusability of this catalyst system to the lack of ruthenium leaching from the clay support. In fact, ICP-MS of the product

solutions showed a ruthenium content of only 28 ppm. This study illustrates that the nature of the support can greatly affect the overall catalytic activity and reusability and, in fact, the Montmorillonite K-10 supported RAPTA catalyst **67** is the most successful immobilized catalyst to date for the isomerization of allylic alcohols.

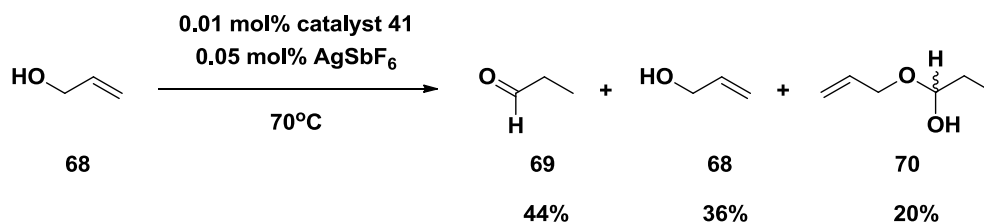
Despite these advances there are still significant improvements that have yet to be made. For example, although the existing immobilized and homogeneous, water-soluble catalysts exhibit reusability, the overall TONs obtained from these systems are relatively low. As well, in most cases, organic solvents are still an integral part of the reaction mixture and/or the catalyst separation step(s) despite their toxicity and the need to minimize waste. In fact, to the best of our knowledge, there are no reports of solvent-free isomerization reactions catalyzed by an immobilized catalyst. Therefore, our goal was to utilize the rhodium catalyst-organic framework **41**, which had previously exhibited remarkable reusability and batch reactivity (refer to Chapter 3), in high substrate loading, solvent-free isomerization reactions of allylic alcohols. If successful, these will be among the first solvent-free, 100% atom economical catalyzed reactions; a prominent step forward in the development of sustainable, environmentally-friendly catalytic systems.

Results and Discussion

Section A: Isomerization of Primary Allylic Alcohols

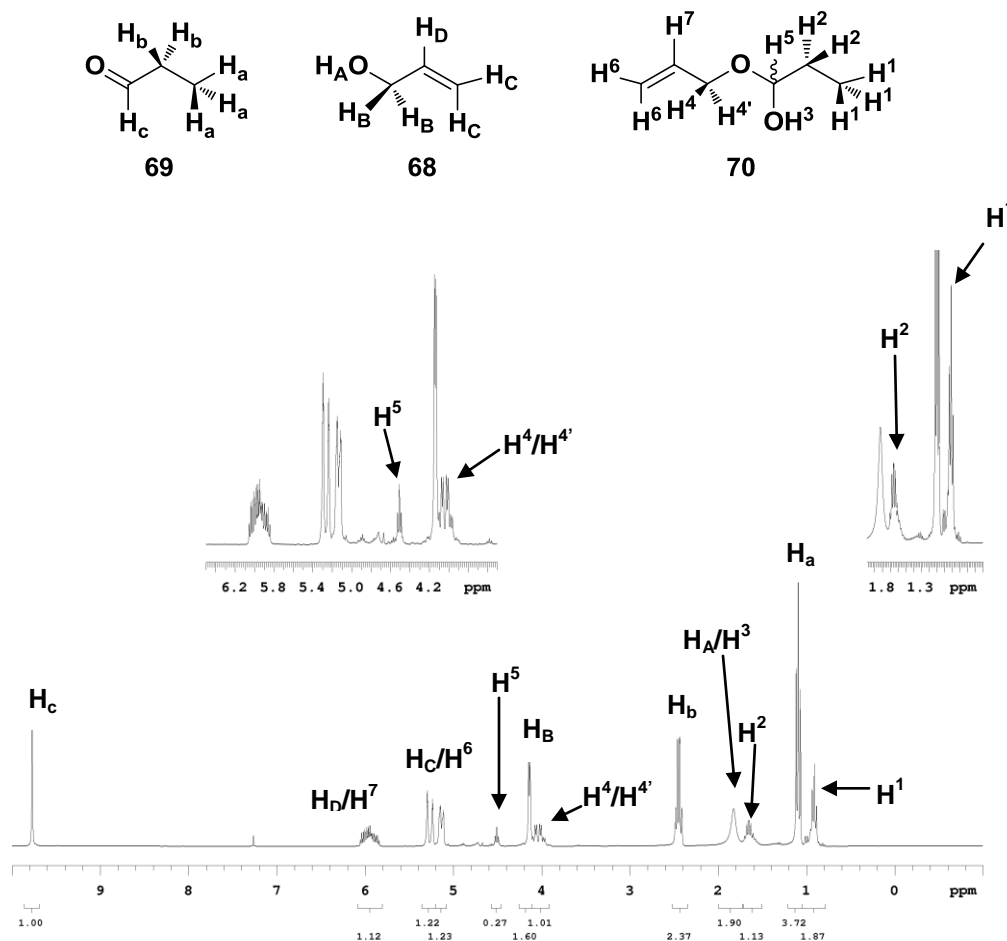
The primary allylic alcohol 2-propen-1-ol (**68**) was initially chosen in the evaluation of the polymer-supported rhodium catalyst-organic framework (COF) **41** as this substrate is the smallest primary allylic alcohol. With 0.01 mol% of rhodium and 0.05 mol% of AgSbF_6 at 70°C in the absence of solvent, 6400 TOs were obtained after 45 minutes (Scheme 4-7).

Scheme 4-7. The attempted isomerization of 2-propen-1-ol **68** catalyzed by rhodium catalyst-organic framework **41**.



The reaction mixture contained 36% of unreacted starting material **68** and 44% of the desired aldehyde product **69**. The remaining 20% was comprised of an unknown side product. The $^1\text{H-NMR}$ of the reaction mixture is shown in Figure 4-1.

Figure 4-1. ^1H -NMR spectrum of the reaction mixture from the solvent-free isomerization of 2-propen-1-ol **68**.^a



[a] 300 MHz, CDCl_3 , 27°C .

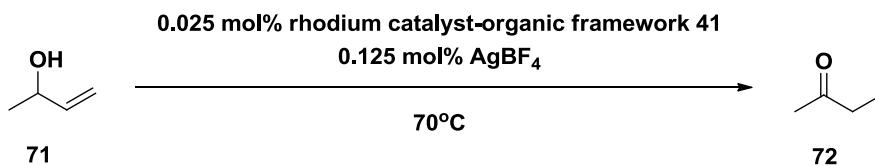
As shown in the NMR spectrum, the isomerized product **69** has peaks for the aldehyde proton at 9.7 ppm (H_c), the methylene protons at 2.4 ppm (H_b) and the methyl protons at 1.1 ppm (H_a). Unreacted starting material **68** was also present in the reaction mixture as the peak at 4.15 ppm (H_B) is diagnostic for 2-propen-1-ol **68**. When evaluating the integration values for the starting material peaks (H_A , H_C , H_D), we realized that protons from the unknown product were under these signals, implying that this side

product contains a 2-propen-1-ol fragment. As well, new methylene and methyl proton signals were present at 1.65 ppm (H^2) and 0.91 ppm (H^1), respectively, along with two signals at 4.1 ppm (H^4) and 4.5 ppm (H^5) (refer to the insets in Figure 4-1 for a blow-up of these regions). Based on these observations, we postulated that this side product was hemiacetal **70** formed from reaction between the aldehyde **69** and 2-propen-1-ol **68**. The hemiacetal **70** contains olefinic protons (H^6 and H^7) and an alcohol proton (H^3) that have almost identical chemical environments to the same protons found in the 2-propen-1-ol **68** starting material (H_C , H_D , H_A), explaining the chemical shift overlap of these protons in the NMR. As well, the hemiacetal **70** contains both a methylene and methyl group (H^2 and H^1 , respectively) that appear upfield from the methylene and methyl groups in the aldehyde product **69** (H_b and H_a) due to the absence of the carbonyl group in the hemiacetal **70**. We tentatively assigned the hemiacetal proton H^5 to the peak found at 4.5 ppm. The signal at 4.1 ppm, which we assigned to protons $H^4/H^{4'}$, has a unique splitting pattern because the chiral carbon center in hemiacetal **70** rendered the protons $H^4/H^{4'}$ diastereotopic. Thus, H^4 would be coupled by $H^{4'}$, H^7 , H^5 and H^6 , resulting in a doublet of doublet of doublet of triplets. $H^{4'}$ would also have the same complicated splitting pattern, which is consistent with the splitting observed in the NMR spectrum. In conclusion, the NMR evidence strongly suggests the formation of the side product hemiacetal **70** during the solvent-free isomerization of 2-propen-1-ol. We believe that the

solvent-free conditions encouraged the reaction between the aldehyde product and allylic alcohol starting material.

As a result of this finding, we decided to abandon primary allylic alcohols and focus on the isomerization of secondary allylic alcohols. In fact, in a preliminary reaction with secondary allylic alcohol 3-buten-2-ol **71** (0.025 mol% rhodium, 0.125 mol% AgBF₄, 70°C, solvent-free), the reaction was complete after 1.25 hours generating 2-butanone **72** as the sole detectable product (TON = 4000) (Scheme 4-8).

Scheme 4-8. Solvent-free isomerization of 3-buten-2-ol **71** catalyzed by rhodium catalyst-organic framework **41**.



Therefore, the formation of hemiacetal/hemiketal side products was successfully avoided by switching from primary to secondary allylic alcohol substrates.

Section B: The Effect of Silver Salts on the Catalytic Activity of the Polymer-Supported Rhodium Catalyst-Organic Framework 41

There are many factors that play a role in the activity of the polymer-supported COF **41**. Two of the more prominent factors include the extent of activation of the rhodium centers by removal of the bridging chlorides by the silver salt and the coordinating ability of the silver salt anion. We screened a variety of silver salts for the isomerization of 3-buten-2-ol **71** in order to determine which silver salt was the most effective in activating the rhodium metal centers. The results are presented in Table 4-1.

Table 4-1. Solvent-free isomerization of 3-buten-2-ol **71** using different silver salts.^a

Entry	Silver Salt	TON ^b			
		1 h	2 h	24 h	48 h
1	AgSbF ₆	6000	9200	25,600	28,800
2	AgBF ₄	6400	9600	31,200	35,200
3	AgOTf	3600	5200	17,200	22,400 ^c
4	AgClO ₄	1200	1800	20,800	34,000 ^c

^[a] All runs were performed under solvent-free conditions at 70°C with Sub/Ag/Rh = 40,000/5/1. ^[b] TON was determined by ¹H-NMR and by comparison to authentic samples. ^[c] These TONs are after 68 hours of reaction time.

The SbF_6^- and BF_4^- silver salts (entries 1 and 2) produced catalysts with higher activities than the OTf^- and ClO_4^- salts (entries 3 and 4). The BF_4^- silver salt effected the isomerization of 3-buten-2-ol **71** with the highest initial TON and highest TON after 48 hours (6400 and 35,200, respectively, entry 2). In addition, although the ClO_4^- silver salt resulted in the catalyst with the lowest initial activity (entry 4), after 24 hours this catalyst had provided more TOs than the OTf^- salt (entry 3).

The order of solubility of the silver salts in 3-buten-2-ol **71** was $\text{AgBF}_4 > \text{AgSbF}_6 > \text{AgOTf} > \text{AgClO}_4$ and this degree of solubility is in accordance with the catalytic activity with the exception of AgOTf and AgClO_4 . It is probable that the solubility in 3-buten-2-ol **71** affects the silver salt's ability to reach and activate the rhodium sites within the catalyst-organic framework. The solubility argument does not explain why the catalyst activated by AgClO_4 provided higher overall TONs than the catalyst activated by AgOTf . In this case, it is likely that the coordinating ability of the anion affected the overall catalytic activity. Specifically, rhodium(I)-triflate complexes are known¹⁶ and they are quite stable. It is likely that the rhodium centers are partially deactivated through relatively strong coordination by OTf^- . It should also be noted that rhodium(I)-hexafluoroantimonate, -tetrafluoroborate, and -perchlorate complexes are not known in the literature.

In addition to the solubility of the silver salt and the coordinating ability of the silver salt anion, there are other potential factors/interactions

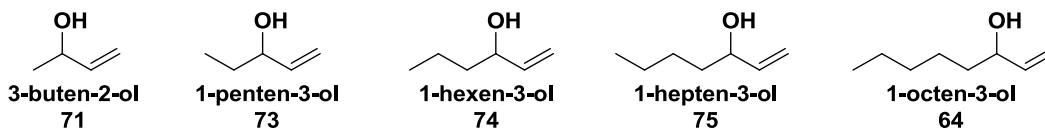
that could affect the overall catalytic activity of the COF **41**. For example, abstraction of the bridging chlorides will convert the COF **41** from a neutral framework (poly-[RhCl((*R*)-5,5'-dinorimido-BINAP)]₂) crosslinked at rhodium to a more open, charged framework (poly-[Rh((*R*)-5,5'-dinorimido-BINAP)]⁺). The nature of the silver salt anion could potentially influence the structure, and by extension the reactivity, of such a charged framework.

In conclusion, the nature of the silver salt and the resulting counterion have a definite effect on the catalytic activity of the COF **41**. In particular, we found that AgBF₄ was the best catalyst activator as this silver salt resulted in the highest TON for the solvent-free isomerization of 3-buten-2-ol **71** (Table 4-1, entry 2). As a result, AgBF₄ was used in all further experiments as the chloride abstractor.

Section C: Isomerization of Secondary Allylic Alcohols

The polymer-supported rhodium catalyst-organic framework **41** proved to be very active in the solvent-free isomerization of 3-buten-2-ol **71**, producing 2-butanone in 100% yield with no detectable side products. The results from the isomerization of a variety of different secondary allylic alcohols with varying alkyl chain lengths are shown in Figure 4-2.

Figure 4-2. Secondary allylic alcohol substrates chosen for the rhodium catalyst-organic framework **41** catalyzed solvent-free isomerization reactions.



In addition to preventing side product formation, these substrates would allow us to study the effect of chain length on the rate and extent of isomerization. This information is crucial in elucidating the nature and structure of the polymer-supported catalyst-organic framework. For example, the catalytic activity of a pore-channel catalyst-organic framework would be much more dependent on substrate size than a high surface area catalyst-organic framework.

The results from the solvent-free isomerization of secondary allylic alcohols are presented in Table 4-2.

Table 4-2. Solvent-free batch isomerization reactions of secondary allylic alcohols catalyzed by rhodium catalyst-organic framework **41**.^a

Entry	Sub	Sub/Ag/Rh	T (°C)	Time (h)	TON ^b (TOF, h ⁻¹)	% Yield ^b
1	71	4000/5/1	70	1.25	4000 (3200)	100
2	71	40,000/5/1	70	1	6400 (6400)	16
				2	9600 (4800)	24
				24	31,200 (1300)	78
				48	35,200 (733)	88
3	71^c	40,000/5/1	70	1	3600 (3600)	9
				24	30,000 (1250)	75
				48	38,000 (792)	95
4	73	5000/5/1	85	1.5	5000 (3333)	100
5	74	5000/5/1	85	1	5000 (5000)	100
6	75	5000/5/1	85	1.5	800 (533)	16
				17	3135 (184)	63
				48	4500 (94)	90
7	64	3000/5/1	100	22	2550 (116)	85

^[a] All runs were carried out under solvent-free conditions with AgBF₄ as an activator. ^[b] TON and % yield were determined by ¹H-NMR and by comparison to authentic samples. ^[c] Ba-L-tartrate, rather than BaSO₄, was used as the catalyst support for this run.

3-buten-2-ol **71** (entries 1-3) is the most active secondary allylic alcohol substrate. With a catalyst loading of 0.025 mol%, 3-buten-2-ol **71** was completely isomerized to the 2-butanone product after 1.25 hours at 70°C

(entry 1). Decreasing the catalyst loading by a factor of ten (0.0025 mol%) resulted in a TON of 35,200 after 48 hours at 70°C (entry 2). We also investigated the use of Ba-L-tartrate as a support for the COF **41** in the isomerization of 3-buten-2-ol (entry 3). The Ba-L-tartrate supported catalyst exhibited lower initial activity than the BaSO₄ supported catalyst (3600 vs 6400 TOs) but provided a higher overall TON (38,000 vs 35,200 TOs). These differences in activity may be due to Ba-L-tartrate/rhodium, Ba-L-tartrate/substrate and/or Ba-L-tartrate/framework interactions. These are the largest TONs and the lowest catalyst loadings reported to date in the isomerization of secondary allylic alcohols catalyzed by a rhodium-containing catalyst.

With the higher substrate loading runs (entries 2 and 3) the catalyst underwent significant deactivation over time. For example, after one hour of reaction time a TOF of 6400 h⁻¹ was obtained while after 48 hours the TOF decreased by almost a factor of ten to 733 h⁻¹. Product inhibition could be responsible for the catalyst deactivation if competitive binding of the allylic alcohol substrate and ketone product exists. If this were the case, as more substrate was converted into product then there would be more competition for binding sites on the rhodium metal centers, which would result in an eventual decrease in catalytic activity over time.

As shown in entries 4 and 5, the rate and extent of isomerization were nearly identical for 1-penten-3-ol **73** and 1-hexen-3-ol **74** with both reactions going to completion after 1.5 hours and 1 hour, respectively. The

rate and extent of isomerization of 1-hepten-3-ol **75** (entry 6) was significantly lower as after 1.5 hours the reaction had only proceeded by 16%. The isomerization had still not gone to completion (90%) after 48 hours. These results suggest that there exists a substrate size threshold that, if exceeded, results in a significant decrease in the catalytic activity of the COF **41**. For example, in the isomerization of substrates **71**, **73** and **74**, which all contained alkyl chains with three carbons or less, the rates and extents of isomerization were all quite similar, and did not seem to be significantly dependent on alkyl chain length. Although, it should be noted that higher temperature was required for 1-penten-3-ol **73** and 1-hexen-3-ol **74** (85°C) compared to 3-buten-2-ol **71** (70°C) suggesting a mild decrease in catalytic activity within these substrates. However, in the isomerization of substrate **75**, which contained an alkyl chain with more than three carbons, the rate and extent of reaction were significantly decreased.

As mentioned previously, the effect of substrate size on the rate and extent of reaction can help to elucidate the nature and structure of the supported catalyst-organic framework. Since there appears to be a size threshold, we postulated that the polymer-supported COF **41** likely adopts a pore-channel type of structure, similar to that of a metal-organic framework.¹⁷ In such a framework, considering only substrate size, substrates small enough to fit in the pores and travel down the channels to the catalytic active sites should have similar rates of reaction. Those

substrates that are too large or encounter unfavorable steric interactions during diffusion to the active sites should have significantly slower rates of reaction. That being said, this conclusion is speculation at this point and more in depth framework characterization is required to confirm the actual structure adopted by the COF **41** (refer to Chapter 6).

In order to confirm the possibility of a substrate size threshold within the rhodium catalyst-organic framework **41**, the solvent-free isomerization of 1-octen-3-ol **64**, which also contains an alkyl chain longer than three carbons, was investigated next (entry 7). In this case, the rate and extent of reaction were even lower than that obtained in the isomerization of 1-hepten-3-ol **75** (entry 6). As well, a higher temperature (100°C) was required to promote this reaction. This result lends support to the existence of a substrate size threshold within the COF **41**.

Despite these remarkable batch reactivity results, attempts at catalyst reuse were unsuccessful. This suggests that the COF **41** became deactivated during the course of the initial run or between catalytic runs. This deactivation could be due to catalyst decomposition or rhodium leaching from the framework. Neutron activation analysis (see Chapter 5 for an indepth discussion) of the catalyst before and after should be done to determine if rhodium leaching did occur.

In summary, we reported the largest TONs (up to 38,000) and the lowest catalyst loadings (0.03-0.0025 mol%) to date for the rhodium catalyzed isomerization of secondary allylic alcohols. These results are

particularly remarkable as typical rhodium catalyst loadings range from 0.2-5 mol% for these reactions.⁴ We were also successful in eliminating the use of organic solvents entirely, which is integral in the development of sustainable catalytic processes. In addition, we discovered that within the polymer-supported rhodium catalyst-organic framework exists a substrate size threshold that, if exceeded, results in a substantial decrease in catalytic activity.

Section D: Comparison of the Polymer-Supported Rhodium Catalyst-Organic Framework **41 to the Homogeneous Catalyst Analogue**

The COF **41** displayed remarkably high activity in the isomerization of secondary allylic alcohols compared to most other reported rhodium catalysts. We synthesized $[\text{RhCl}((R)\text{-BINAP})]_2$ according to literature procedures¹⁸ and tested the catalyst in the solvent-free isomerization of 3-buten-2-ol **71**. The results afforded by the homogeneous catalyst and the COF **41** are presented in Table 4-3.

Table 4-3. Comparison of the rhodium catalyst-organic framework **41** and the homogeneous $[\text{RhCl}((R)\text{-BINAP})]_2$ catalyst in the solvent-free isomerization of 3-buten-2-ol **71**.^a

Entry	Catalyst	TON ^b		
		1 h	2 h	24 h
1	rhodium catalyst-organic framework 41	6400	9600	31,200
2	$[\text{RhCl}((R)\text{-BINAP})]_2$	2000	3400	17,600

^[a] Both runs were carried out under solvent-free conditions at 70°C with Sub/AgBF₄/Rh = 40,000/5/1. ^[b] TON was determined by ¹H-NMR and by comparison to authentic samples.

Both the homogeneous and supported catalysts afforded the ketone as the only detectable product, however the COF **41** was almost twice as active as the homogeneous catalyst after 24 hours. Therefore, even though the supported catalyst could not be reused in high substrate loading runs, it still provided substantially more TOs than the homogeneous $[\text{RhCl}((R)\text{-BINAP})]_2$ catalyst. This result is consistent with the results from the 1,6-enyne cycloisomerization study (refer to Chapter 3, section D) and, therefore, we can conclude that the COF **41** is inherently more active than the homogeneous catalyst analogue. This is rare, if not unique, in the field of catalysis.

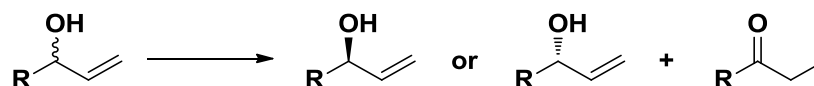
There are many possible factors that contribute to the high activity of the supported catalyst. These include catalyst/framework-support interactions (i.e. the BaSO₄ interaction with catalytic active sites and/or the framework, swellability, etc.) and framework-catalyst interactions (i.e.

cross-linking, size exclusion, etc.). Future research in the Bergens group is in part focused on understanding/determining the origins of this high activity and, as a result, a more in depth discussion will be presented in the conclusions and future work chapter of this dissertation (Chapter 6).

Section E: Kinetic Resolution of 3-Buten-2-ol

The secondary allylic alcohols that were chosen for our isomerization study (see Figure 4-2) were all racemic mixtures that were isomerized to the achiral ketone products. It was possible that a kinetic resolution occurred during these isomerizations as illustrated in Equation 4-2.

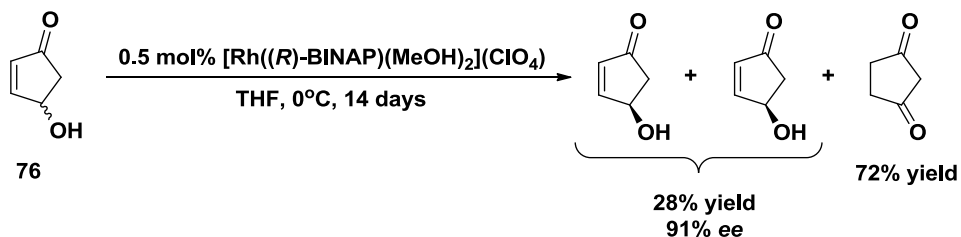
Equation 4-2. The kinetic resolution of secondary allylic alcohols.



To the best of our knowledge, there are only three reports on the kinetic resolution of allylic alcohols in the literature.¹⁹ The highest ee (91%) reported to date was obtained by Noyori and coworkers in the [Rh((*R*)-BINAP)(MeOH)₂](ClO₄) catalyzed (*R*)-enantio-enrichment of 4-hydroxy-2-cyclopentenone **76** (Scheme 4-9).^{19b} Despite the high enantioselectivity, a very long reaction time was required (14 days), a low temperature (0°C) had to be maintained throughout the process and only 28% yield of the

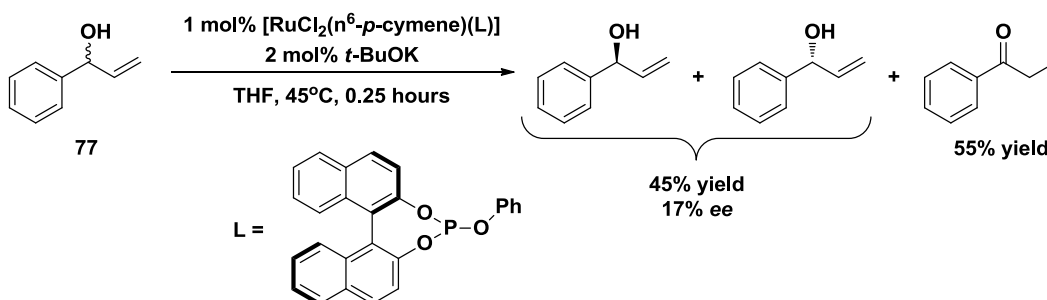
enantio-enriched allylic alcohol starting material was obtained, making this process impractical for large scale kinetic resolution of allylic alcohols.

Scheme 4-9. Noyori's kinetic resolution of 4-hydroxy-2-cyclopentenone **76**.



The most recent study by Gimeno and coworkers reported the use of $[\text{RuCl}_2(\eta^6\text{-arene})\{(R)\text{-PR}(\text{binaphthoxy})\}]$ -type catalysts in the (S)-enantio-enrichment of α -vinylbenzyl alcohol **77** and related allylic alcohols.^{19c} The best result obtained by Gimeno is outlined in Scheme 4-10.

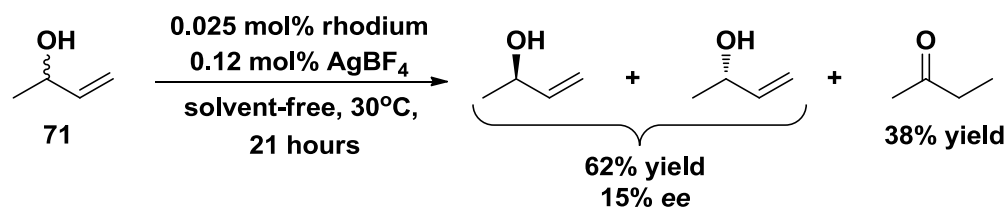
Scheme 4-10. Gimeno's kinetic resolution of α -vinylbenzyl alcohol **77**.



Here, a 45% yield of the enantio-enriched α -vinylbenzyl alcohol **77** was obtained, however the ee was only 17%. They attributed the low overall selectivity of the catalyst to the relative orientation of the chiral binaphthoxy unit to the arene ligand. In particular, the best enantioselectivities (up to 17%) were obtained with more sterically rigid arene ligands (i.e. *p*-cymene). As a result, Gimeno is currently focused on synthesizing more structurally rigid arene-ruthenium complexes containing chiral phosphate ligands in an attempt to increase the kinetic resolution enantioselectivity.

These previous reports highlight that both high enantioselectivity and high yield of the enantio-enriched allylic alcohol are required for practical, large scale kinetic resolution of allylic alcohols. As a result, we chose to study the kinetic resolution of 3-buten-2-ol **71** as this was the most active substrate with our COF **41** (see Table 4-2). The reaction conditions employed for the kinetic resolution and the results that we obtained are outlined in Scheme 4-11.

Scheme 4-11. The kinetic resolution of 3-buten-2-ol catalyzed by rhodium catalyst-organic framework **41**.



A 62% yield of the enantio-enriched 3-buten-2-ol **71** was obtained after 21 hours of reaction time under solvent-free conditions and had an ee of approximately 15%. Although relatively low, the enantioselectivity afforded by COF **41** was comparable to the aforementioned Gimeno arene-ruthenium catalyst system.^{19c} We are currently investigating different secondary allylic alcohol substrates and optimizing reaction conditions in an attempt to better the enantioselectivity of the kinetic resolution.

Conclusion

In summary, this is the first report of an immobilized catalyst utilized in the solvent-free isomerization of allylic alcohols, which is a prominent step forward in the development of sustainable chemical and catalytic processes. The polymer-supported rhodium catalyst-organic framework **41** provided the highest TONs to date (up to 38,000) for the rhodium catalyzed isomerization of secondary allylic alcohols, with catalyst loadings as low as 0.0025 mol%. The rhodium catalyst-organic framework also provided higher TONs than the parent homogeneous catalyst, which is rare, if not unique, in the field of catalysis. As well, we reported the kinetic resolution of secondary allylic alcohol 3-buten-2-ol **71** with enantioselectivity comparable to the most recent literature report published by Gimeno and coworkers^{19c} (15% ee vs 17% ee, respectively).

In addition to these results, some other notable discoveries and developments were made along the way. For example, we discovered that the solvent-free isomerization of primary allylic alcohol 1-propen-3-ol resulted in the formation of not only the isomerized aldehyde product but also a hemiacetal side product (formed from reaction between the aldehyde and the starting allylic alcohol). As well, it was discovered that the identity of the silver salt plays a substantial role in the catalytic activity of the polymer-supported rhodium catalyst-organic framework. Finally, we discovered that the framework appears to contain a substrate size

threshold that, if exceeded, significantly affects the rate and extent of reaction. These developments are very important in elucidating the factors that affect the catalytic activity of the rhodium catalyst-organic framework and can help us understand the overall structure of the framework, which is important for system optimization.

Experimental

General procedures and methods. $^1\text{H-NMR}$ spectra were recorded using Varian Inova (300, 400, 500 MHz) spectrometers. $^1\text{H-NMR}$ chemical shifts are reported in parts per million (δ) relative to TMS with the solvent as the internal reference.

Unless otherwise stated, all experiments were performed under an inert atmosphere using standard Schlenk and glove-box techniques. Argon and nitrogen gas (Praxair, 99.998%) were passed through a drying train containing 3Å molecular sieves and indicating DrieriteTM before use. All allylic alcohols and Mosher's acid chloride were obtained from Sigma-Aldrich Co. and the allylic alcohols were distilled under a nitrogen atmosphere.

Representative procedure for the isomerization of allylic alcohols catalyzed by the polymer-supported rhodium catalyst-organic framework 41. For these experiments, the allylic alcohols were bubbled with either nitrogen or argon gas for 30 minutes prior to use.

In a typical experiment, under nitrogen or argon atmosphere, a Schlenk flask equipped with a TeflonTM valve was charged with 0.0987 g of the polymer-supported rhodium catalyst-organic framework on BaSO_4 (1.16 mg of “[RhCl((*R*)-5,5'-dinorimido-BINAP)]₂”, 5.27×10^{-4} mmol) and 5.27×10^{-3} mmol of the desired Ag salt. Next, the desired amount of allylic

alcohol was added to the catalyst/Ag mixture and the Schlenk flask was sealed with the TeflonTM valve. The Schlenk flask was then placed in an oil bath set to the desired temperature. Conversion was monitored by ¹H-NMR of aliquots.

Homogeneous isomerization of 3-buten-2-ol 71. For this experiment, 3-buten-2-ol was bubbled with nitrogen gas for 30 minutes prior to use.

1.2 mg of [RhCl((*R*)-BINAP)]₂ (7.88×10^{-4} mmol) was weighed out in a glove box into an NMR tube equipped with a rubber septum. 1.5 mg (7.88×10^{-3} mmol) of AgBF₄ was weighed out in a glove box into a Schlenk flask equipped with a TeflonTM valve. The catalyst was then dissolved in 1 mL of 3-buten-2-ol and transferred to the Schlenk tube, followed by another 1 mL rinse of 3-buten-2-ol. The remainder of the substrate (4.55 g, 63.1 mmol, 5.45 mL total) was then added directly to the Schlenk flask. The flask was then sealed and stirred in an oil bath set to 70°C. Conversion was monitored by ¹H-NMR of aliquots.

Determination of ee from the kinetic resolution experiments.

For these experiments, the CDCl₃ and pyridine were distilled over CaH₂ prior to use.

1 equiv. of the 3-buten-2-ol reaction solution was weighed out into an NMR tube and sealed with a rubber septum. 0.7 mL of CDCl₃ was then

added to the NMR tube. Next, 6 equiv. of pyridine were added to the NMR tube and this was shaken for 5 minutes. Finally, 3 equiv. of Mosher's acid chloride ((S)-(+)- α -methoxy- α -trifluoromethyl-phenylacetyl chloride) (**78**) was added to the NMR tube and this was periodically shaken for 30 minutes before being analyzed by $^1\text{H-NMR}$ (Figure 4-3).

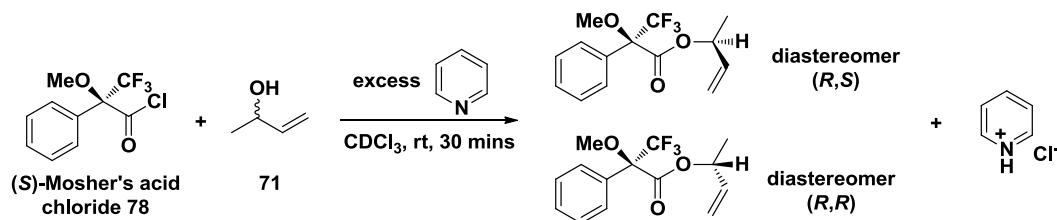
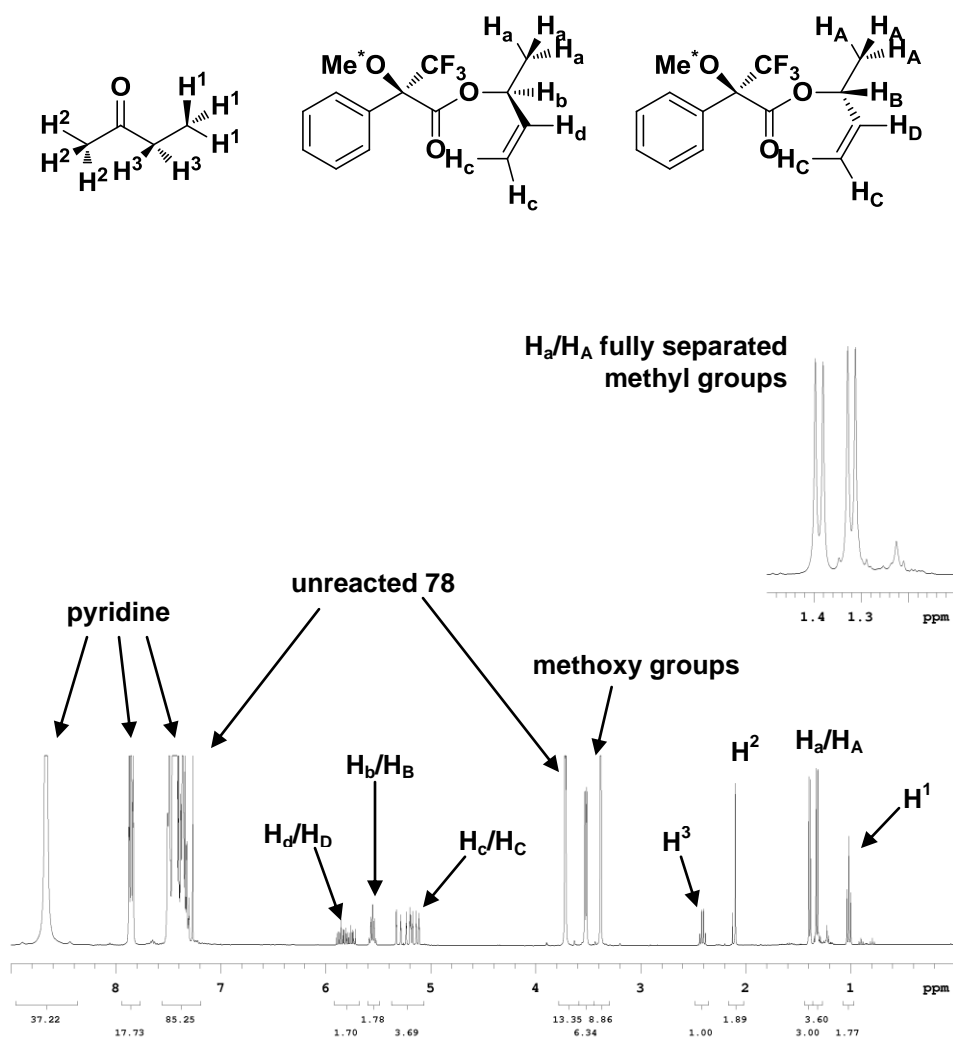


Figure 4-3. $^1\text{H-NMR}$ spectrum of the kinetic resolution reaction mixture mixed with Mosher's acid chloride **78**.



References

- (1) (a) Linthorst, J. A. *Found. Chem.* **2010**, *12*, 55. (b) Horváth, I. T.; Anastas, P. T. *Chem. Rev.* **2007**, *107*, 2169. (c) *Green Chemistry: Theory and Practice*; Anastas, P. T., Warner, J. C., Eds.; Oxford University Press, **1998**. (d) *Alternative Solvents for Green Chemistry*; Kerton, F. M., Ed.; Royal Society of Chemistry, **2009**.
- (2) (a) van der Drift, R. C.; Bouwman, E.; Drent, E. *J. Organomet. Chem.* **2002**, *650*, 1. (b) Uma, R.; Crévisy, C.; Grée, R. *Chem. Rev.* **2003**, *103*, 27. (c) Mantilli, L.; Mazet, C. *Chem. Lett.* **2011**, *40*, 341. (d) Cadierno, V.; Crochet, P.; Gimeno, J. *Synlett.* **2008**, 1105. (e) Fu, G. C. in *Modern Rhodium-Catalyzed Organic Reactions* **2005**, 75. (f) Varela-Álvarez, A.; Sordo, J. A.; Piedra, E.; Nebra, N.; Cadierno, V.; Gimeno, J. *Chem.-Eur. J.* **2011**, *17*, 10583.
- (3) (a) Tani, K.; Yamagata, T.; Otsuka, S.; Akutagawa, S.; Kumobayashi, H.; Taketomi, T.; Takaya, H.; Miyashita, A.; Noyori, R. *J. Am. Chem. Soc., Chem. Commun.* **1982**, 600. (b) Tani, K.; Yamagata, T.; Akutagawa, S.; Kumobayashi, H.; Taketomi, T.; Takaya, H.; Miyashita, A.; Noyori, R.; Otsuka, S. *J. Am. Chem. Soc.* **1984**, *106*, 5208.
- (4) Rhodium-containing catalysts: (a) Tanaka, K.; Qiao, S.; Tobisu, M.; Lo, M.-C.; Fu, G. C. *J. Am. Chem. Soc.* **2000**, *122*, 9870. (b)

- Tanaka, K.; Fu, G. C. *J. Org. Chem.* **2001**, *66*, 8177. (c) Reetz, M. T.; Guo, H. *Synlett.* **2006**, 2127.
- (5) Iridium-containing catalysts: (a) Mantilli, L.; Gérard, D.; Torche, S.; Besnard, C.; Mazet, C. *Chem.-Eur. J.* **2010**, *16*, 12736. (b) Mantilli, L.; Mazet, C. *Tetrahedron Lett.* **2009**, *50*, 4141. (c) Mantilli, L.; Mazet, C. *Chem. Commun.* **2010**, *46*, 445. (d) Mantilli, L.; Gérard, D.; Torche, S.; Besnard, C.; Mazet, C. *Angew. Chem. Int. Ed.* **2009**, *48*, 5143.
- (6) Ruthenium-containing catalysts: (a) Liu, P. N.; Ju, K. D.; Lau, C. P. *Adv. Synth. Catal.* **2011**, *353*, 275. (b) Martín-Matute, B.; Bogár, K.; Edin, M.; Kaynak, F. B.; Bäckvall, J.-E. *Chem.-Eur. J.* **2005**, *11*, 5832. (c) van der Drift, R. C.; Gagliardo, M.; Kooijman, H.; Spek, A. L.; Bouwman, E.; Drent, E. *J. Organomet. Chem.* **2005**, *690*, 1044. (d) Ito, M.; Kitahara, S.; Ikariya, T. *J. Am. Chem. Soc.* **2005**, *127*, 6172. (e) Sabitha, G.; Nayak, S.; Bhikshapathi, M.; Yadav, J. S. *Org. Lett.* **2011**, *13*, 382. (f) Takai, Y.; Kitaura, R.; Nakatani, E.; Onishi, T.; Kurosawa, H. *Organometallics* **2005**, *24*, 4729. (g) Crochet, P.; Fernández-Zúmel, M. A.; Gimeno, J.; Scheele, M. *Organometallics* **2006**, *25*, 4846.
- (7) Qiao, S.; Fu, G. C. *J. Org. Chem.* **1998**, *63*, 4168.
- (8) Tani, K. *Pure Appl. Chem.* **1985**, *57*, 1845.
- (9) (a) Ahlsten, N.; Lundberg, H.; Martín-Matute, B. *Green Chem.* **2010**, *12*, 1628. (b) Knight, D. A.; Schull, T. L. *Synth. Commun.*

- 2003**, 33, 827. (c) Leung, D. H.; Bergman, R. G.; Raymond, K. N. *J. Am. Chem. Soc.* **2007**, 129, 2746. (d) Cadierno, V.; García-Garrido, S. E.; Gimeno, J. *Chem. Commun.* **2004**, 232. (e) Lastra-Barriera, B.; Díez, J.; Crochet, P. *Green Chem.* **2009**, 11, 1681.
- (10) (a) Bianchini, C.; Meli, A.; Oberhauser, W. *New J. Chem.* **2001**, 25, 11. (b) Fekete, M.; Joó, F. *Catal. Commun.* **2006**, 7, 783. (c) Cadierno, V.; Crochet, P.; García-Garrido, S. E.; Gimeno, J. *Dalton Trans.* **2004**, 3635.
- (11) (a) Díaz-Álvarez, A. E.; Crochet, P.; Zablocka, M.; Dunhayon, C.; Cadierno, V.; Gimeno, J.; Majoral, J. P. *Adv. Synth. Catal.* **2006**, 348, 1671. (c) Cadierno, V.; García-Garrido, S. E.; Gimeno, J.; Varela-Álvarez, A.; Sordo, J. A. *J. Am. Chem. Soc.* **2006**, 128, 1360. (d) García-Álvarez, J.; Gimeno, J.; Suárez, F. J. *Organometallics* **2011**, 30, 2893.
- (12) Azua, A.; Sanz, S.; Peris, E. *Organometallics* **2010**, 29, 3661.
- (13) Crochet, P.; Díez, J.; Fernández-Zúmel, M. A.; Gimeno, J. *Adv. Synth. Catal.* **2006**, 348, 93.
- (14) García-Garrido, S. E.; Francos, J.; Cadierno, V.; Basset, J.-M.; Polshettiwar, V. *ChemSusChem* **2011**, 4, 104.
- (15) Menéndez-Rodríguez, L.; Crochet, P.; Cadierno, V. *J. Mol. Catal. A: Chem.* **2013**, 366, 390.

- (16) (a) Goikhman, R.; Milstein, D. *Chem. Eur. J.* **2005**, *11*, 2983. (b) O'Mahony, D. J. R.; Belanger, D. B.; Livinghouse, T. *Synlett* **1998**, 443.
- (17) (a) Corma, A.; García, H.; Llabrés i Xamena, F. X. *Chem. Rev.* **2010**, *110*, 4606. (b) Ma, L.; Abney, C.; Lin, W. B. *Chem. Soc. Rev.* **2009**, *38*, 1248.
- (18) Cramer, R. *Inorg. Synth.* **1990**, *28*, 86.
- (19) (a) Ohkubo, K.; Ohgushi, T.; Kusaga, T.; Yoshinaga, K. *Inorg. Nucl. Chem. Letters* **1977**, *13*, 631. (b) Kitamura, M.; Manabe, K.; Noyori, R.; Takaya, H. *Tetrahedron Lett.* **1987**, *28*, 4719. (c) Fernández-Zúmel, M. A.; Lastra-Barreira, B.; Scheele, M.; Díez, J.; Crochet, P.; Gimeno, J. *Dalton Trans.* **2010**, *39*, 7780.

Chapter 5

The Continuous-Flow, Asymmetric Hydrogenation of Olefins

Introduction

Section A: Rhodium-BINAP Catalyzed Asymmetric Hydrogenation

Reactions

Rhodium-catalyzed asymmetric hydrogenations are among the first asymmetric catalytic reactions to be successfully utilized in industry. In fact, the $[\text{Rh}((R,R)\text{-DIPAMP})(\text{sol})_2]^+$ (sol = solvent, $(R,R)\text{-DIPAMP}$ = 1,2-ethanediylbis[(2-methoxyphenyl)phenylphosphine]) catalyzed hydrogenation of (*Z*)-2-acetamido-3-(3,4-dihydroxyphenyl)acrylic acid **79** is the first industrial application of an asymmetric catalyst used to produce a highly enantiopure product.¹ This catalytic process is utilized by the Monsanto Company in the production of L-Dopa (Scheme 5-1), a treatment for Parkinson's disease, and Knowles received the 2001 Nobel Prize in chemistry for inventing this technology.^{2a} Knowles' synthesis of L-Dopa encouraged the development of numerous rhodium-based catalysts for the asymmetric hydrogenation of unsaturated substrates.³ In fact, there are a number of pharmaceuticals industrially synthesized using rhodium-catalyzed hydrogenation reactions (Figure 5-1).²

Scheme 5-1. The $[\text{Rh}((R,R)\text{-DIPAMP})(\text{sol})_2]^+$ catalyzed synthesis of L-Dopa.

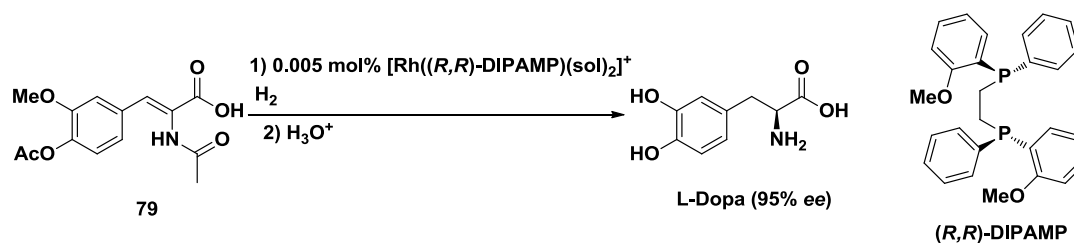
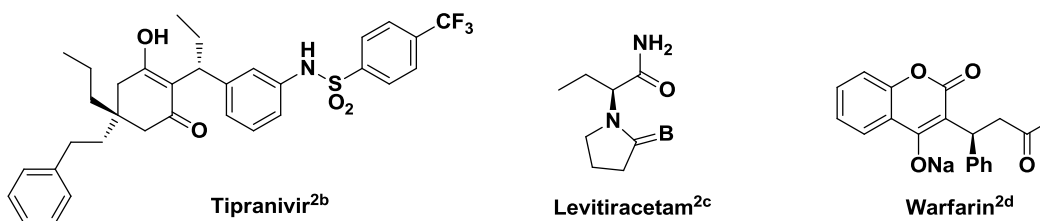
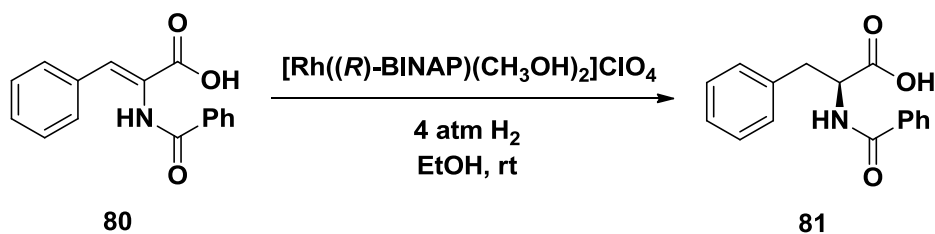


Figure 5-1. Pharmaceuticals synthesized utilizing rhodium-catalyzed hydrogenation reactions.



Noyori's $\text{Rh}(R)\text{-BINAP}/(S)\text{-BINAP}$ catalyst system is among the first rhodium catalysts for asymmetric hydrogenations. This system has potential pharmaceutical applications⁴ and is highly enantioselective in the asymmetric hydrogenation of dehydro amino acids. For example, in the asymmetric hydrogenation of $(Z)\text{-}\alpha\text{-benzamidocinnamic acid}$ **80** (S/C = 100:1), the $[\text{Rh}((R)\text{-BINAP})(\text{sol})_2]^+$ catalyst afforded the N-benzoylphenylalanine product **81** in 97% yield and in 99.9% ee (Scheme 5-2).⁵

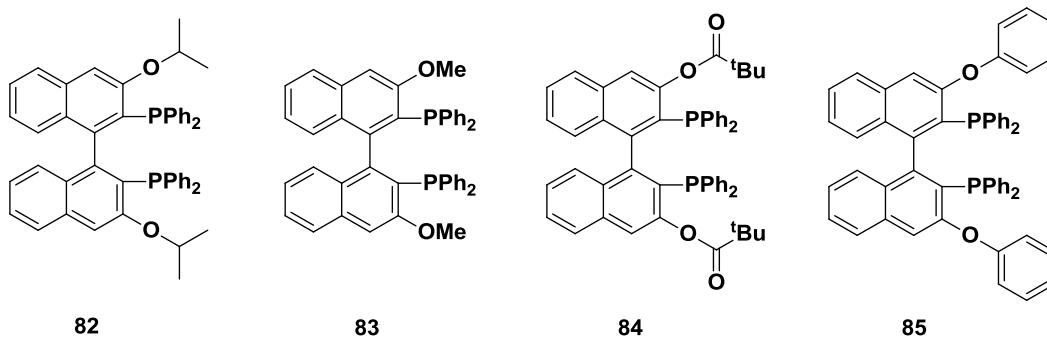
Scheme 5-2. Noyori's $[\text{Rh}((R)\text{-BINAP})(\text{sol})_2]^+$ catalyzed asymmetric hydrogenation of (*Z*)- α -benzamidocinnamic acid **80**.



Although this catalyst works well for the hydrogenation of dehydro amino acids, the overall substrate scope of this catalyst system is narrow, being limited to olefin containing substrates. In addition, the industrial application of this catalyst system is limited by Halpern and Brown's discovery that the asymmetric hydrogenation reactions must be conducted with a relatively low substrate concentration and under a low pressure of H_2 (< 4 atm). If these conditions are not met, both diastereomeric olefin/rhodium complexes are competitively hydrogenated, resulting in poor enantioselectivity. It should be noted that the mechanism for this reaction is well known and has been extensively studied.⁶

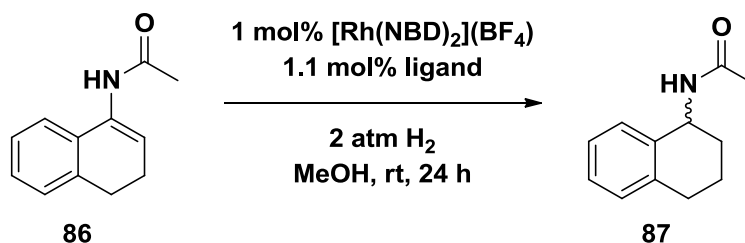
A significant amount of research has been focused on improving the enantioselectivity and efficiency of the $[\text{Rh}(\text{BINAP})(\text{sol})_2]^+$ catalyst system.⁷ The main approach that is employed is functionalization of the BINAP ligand.^{7,8} The interested reader is directed to a recent review on the subject.^{7c} As an example, Keay and coworkers synthesized a series of 3,3'-disubstituted BINAP ligands for use in rhodium catalyzed asymmetric hydrogenations (Figure 5-2).^{8a,b}

Figure 5-2. Keay's 3,3'-disubstituted BINAP ligands.



They postulated that these modifications would have a large effect on the steric and electronic properties of these ligands due to the proximity of these positions to the phosphorus atoms. Specifically, substitution at the 3 and 3' positions are thought to have the most effect on the electron density of the phosphorus donor atoms, due to the strong ortho-directing effect of the phosphine groups,^{8c} and on the steric environment around the catalytic site by sterically interacting with the R groups on the phosphorus atoms. In fact, exchange of BINAP for all of the 3,3'-disubstituted BINAP ligands, with the exception of ligand **82**, resulted in an increase in enantioselectivity in the hydrogenation of cyclic enamide **86** (Scheme 5-3).

Scheme 5-3. Asymmetric hydrogenation of **86** using 3,3'-disubstituted BINAP ligands **82-85**.



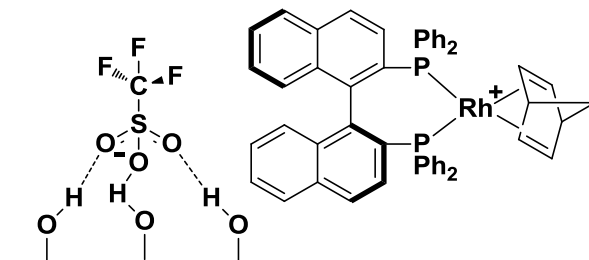
Ligand **85** provided the largest increase in enantioselectivity compared to BINAP (57% and 17%, respectively), however, despite these improvements, the overall enantioselectivity remained moderate at best. For a more detailed discussion on BINAP modification, refer to Chapter 2 of this dissertation.

In addition to improving the enantioselectivity and the substrate scope, significant research has been directed towards immobilizing the BINAP ligand. The interested reader is directed to the following review and the references therein.^{9a} Immobilization would allow for relatively easy recovery of the catalyst from the product mixture and catalyst reuse, thus improving the potential industrial applications of this catalyst system (refer to Chapter 1 for a more in depth discussion). Despite the obvious advantages of immobilization, there are surprisingly few reports involving $[\text{Rh}(\text{BINAP})(\text{sol})_2]^+$.^{9b,c,11,12} As an aside, biphasic solvent systems have been employed for $[\text{Rh}(\text{BINAP})(\text{sol})_2]^+$ catalyzed asymmetric hydrogenations as an additional method for catalyst recovery and reuse.¹⁰ However, as this dissertation is focused on the immobilization of rhodium-

BINAP based catalysts, the remaining examples will be focused on catalyst immobilization rather than the use of biphasic solvent systems.

The most common method of immobilizing the $[\text{Rh}(\text{BINAP})(\text{sol})_2]^+$ catalyst system for asymmetric hydrogenations involves grafting the catalyst to a silica support.^{11,12} As an example, Vizza and coworkers reported the synthesis of an immobilized $[\text{Rh}(\text{NBD})((S)\text{-BINAP})](\text{OTf})$ catalyst (NBD = norbornadiene, OTf = trifluoromethanesulfonate or triflate) on porous silica. Here, using the solvent impregnation method with CH_2Cl_2 , hydrogen-bonding between the triflate counter-ion and the silica support resulted in the immobilization of the $[\text{Rh}(\text{NBD})((S)\text{-BINAP})]^+$ complex (Figure 5-3).¹¹

Figure 5-3. Vizza's silica supported $[\text{Rh}(\text{NBD})((S)\text{-BINAP})](\text{OTf})$ catalyst.

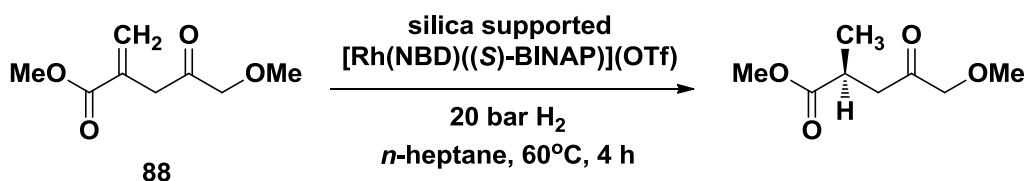


Based on ICP-AES (inductively coupled plasma atomic emission spectroscopy), the grafting procedure was complete and reproducible for metal loadings up to 1 wt%. Once immobilized, the $[\text{Rh}(\text{NBD})((S)\text{-BINAP})]^+$ complex could not be extracted back into CH_2Cl_2 solutions. It was also discovered that replacing the triflate counter-ion with a counter-ion

incapable of hydrogen-bonding, such as $(\text{BPh}_4)^-$, resulted in a complete lack of immobilization of the catalyst.

The immobilized catalyst was then tested in the asymmetric hydrogenation of dimethyl itaconate **88** (Scheme 5-4). With a S/C ratio of 100:1, **88** was hydrogenated in 99% yield with an ee of 32% after a period of four hours at 60°C in *n*-heptane. Although the enantioselectivity was quite low, this result was nearly identical to that obtained with the parent homogeneous catalyst, which hydrogenated **88** in a 100% yield with an ee of 33% in MeOH. It should be noted however that the use of solvents of different polarity (i.e. *n*-heptane and MeOH) rules out a reliable comparison between the immobilized and homogeneous catalysts.

Scheme 5-4. Hydrogenation of dimethyl itaconate **88** catalyzed by silica supported $[\text{Rh}(\text{NBD})((S)\text{-BINAP})](\text{OTf})$.

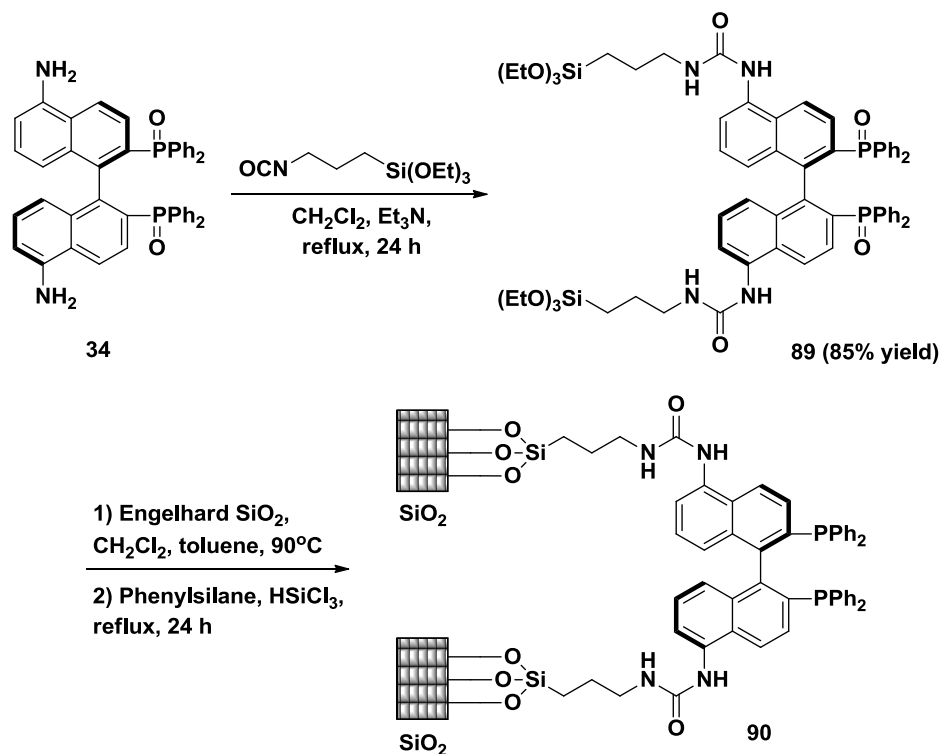


The immobilized catalyst was recovered and reused for three consecutive hydrogenation reactions with no loss in activity or selectivity and no detectable rhodium leaching (< 1 ppm). However, the choice of solvent is crucial as significant rhodium leaching was observed in CH_2Cl_2 , EtOH and MeOH under catalytic conditions. This observation suggests that the immobilized could sustain multiple reuses in the hydrogenation of **88** due

primarily to its insolubility in *n*-heptane rather than an intrinsic improvement to the catalyst itself. Therefore, although the immobilized catalyst system is comparable to homogeneous [Rh(NBD)((S)-BINAP)](OTf) catalyst, the overall low enantioselectivity, coupled with the high solvent dependence, limits the industrial application of this silica supported catalyst.

In another example, van Koten and coworkers synthesized a modified BINAP ligand **90** which was then immobilized on silica by covalent Si-O bonding (Scheme 5-5).¹²

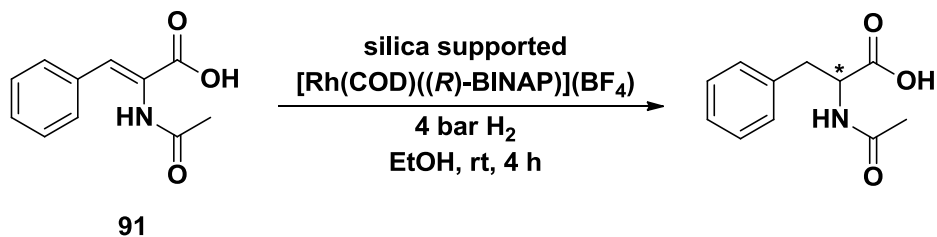
Scheme 5-5. van Koten's synthesis of a silica supported BINAP ligand **90**.



In this synthesis, 5,5'-diamino-BINAP-dioxide **34** was coupled with 3-(triethoxysilyl)propyl-1-isocyanate in the presence of triethylamine to give the di-ureyl compound **89**. This compound was then reacted with silica, followed by reduction of the phosphine-oxides with trichlorosilane in phenylsilane to give the silica immobilized BINAP ligand **90**. **90** was then metallated with $[\text{Rh}(\text{COD})_2](\text{BF}_4)$ (COD = 1,5-cyclooctadiene) to produce a silica immobilized rhodium-BINAP catalyst. Elemental analysis of the immobilized catalyst showed a phosphorus/rhodium ratio of 2:1, indicating that most, if not all, of the BINAP ligand sites were successfully metallated. As well, the silica support was only 0.20 wt% phosphorus by mass, suggesting that there was a relatively low overall loading of ligand.

The silica immobilized $[\text{Rh}(\text{COD})((R)\text{-BINAP})](\text{BF}_4)$ catalyst was evaluated with the asymmetric hydrogenation of *trans*- α -(acetamido)-cinnamic acid **91** (Scheme 5-6).

Scheme 5-6. Hydrogenation of *trans*- α -(acetamido)-cinnamic acid **91** catalyzed by silica supported $[\text{Rh}(\text{COD})((R)\text{-BINAP})](\text{BF}_4)$.



With a S/C ratio of 150:1, **91** was hydrogenated in 100% yield and in 85% ee after a period of four hours at room temperature. This is identical to the results obtained with the homogeneous catalytic reaction. Despite this promising result, the catalyst could not be reused without a significant decrease in yield (56%) and complete loss of selectivity. The poor reusability of the immobilized catalyst was attributed to catalyst instability during washing and recycling and decomposition from oxygen contamination.

The examples presented above represent many of the common challenges associated with $[\text{Rh}(\text{BINAP})(\text{sol})_2]^+$ catalyzed reactions. In particular, the enantioselectivity and substrate scope are limited for both homogeneous and heterogeneous catalyzed reactions. As well, the reported immobilized $[\text{Rh}(\text{BINAP})(\text{sol})_2]^+$ type catalysts suffer from poor reusability, instability and significant solvent dependence, rendering them unsuitable for industrial use (refer to Chapter 1 for a more in depth discussion). We reasoned that our polymer-supported rhodium catalyst-organic frameworks (COFs), having already shown remarkable reusability, batch reactivity and enantioselectivity (see Chapters 3 and 4), would be ideal for use in the asymmetric hydrogenation of olefinic substrates and could potentially address the limitations encountered with other immobilized $[\text{Rh}(\text{BINAP})(\text{sol})_2]^+$ type catalysts. As well, the modular structure of our COFs (i.e. the support, spacer monomer and catalyst

monomer) allows for easy modification if enantioselectivity enhancement is required.

Section B: Continuous-Flow Hydrogenation Reactions

Within the last 20 years, the requirement for environmentally friendly and sustainable chemical processes has increased exponentially due, in part, to concerns regarding the negative impact of industry on the environment. Specifically, environmentalists have been focused on minimizing industrial pollution and waste. As a result of these concerns, industry has been attempting to reduce chemical waste, maximize atom economy and increase production, all while minimizing the total energy input, utilizing safe chemical processes and maximizing catalytic efficiency.¹³ As a result of this initiative, a significant amount of research has been focused on developing continuous-flow catalytic reactors and processes that can be applied to industrial-scale preparations. The interested reader is directed to recent reviews on this subject.^{13,14}

Although often requiring time intensive initial equipment set-up and optimization of concentrations, temperatures, pressures and flow rates, continuous-flow catalytic processes, have the potential to address many of the environmental and industrial demands mentioned above.^{13,14} For example:

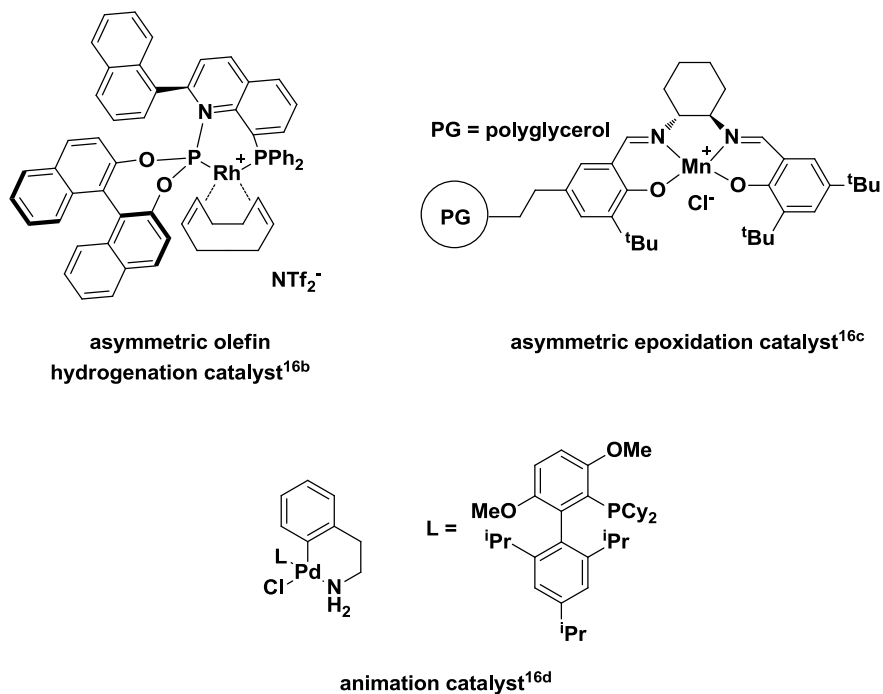
- 1) Parameters such as mixing speed, temperature, pressure and even reactor geometry can affect the overall product quality (e.g. enantioselectivity) and yield. In batch reactors these parameters can be quite difficult to control due to the large reactor size, however in smaller, continuous-flow reactors they can be strictly monitored and controlled, resulting in the production of a large volume of highly regular material.
- 2) Reactive species can be easily separated from the reaction mixture in continuous-flow processes, potentially minimizing the production of undesirable side products and increasing reaction yields. This in turn could perhaps eliminate the need for costly clean-up steps thus reducing chemical waste. For example, if the product reacts further with the catalyst (e.g. isomerization), then removing the product with a continuous-flow reactor will prevent the formation of undesired side products. If the same problem existed in a batch reactor, the reaction between product and catalyst could not be avoided and the reaction mixture would have to undergo clean-up to remove the undesired side product that was formed.
- 3) In continuous-flow reactors, the substrate is continuously percolating through a bed of an immobilized catalyst. This may improve the mass transport of the substrate to the catalyst thereby increasing the rate of the reaction and maximizing catalytic efficiency.

- 4) A continuous-flow reactor is ideal for substrate screening as a wide variety of substrates can be circulated through a single bed of immobilized catalyst at a fairly rapid rate. This has the potential to reduce screening time and minimize production costs while providing important information regarding the reactivity of the catalyst itself.
- 5) Continuous-flow operations can be utilized in the development of safe chemical process by consuming toxic or highly reactive compounds as they are formed or by generating the minimum amount of a particular toxic or reactive reagent required for complete consumption. The accumulation of such materials can thus be prevented and a potential accident can be avoided. For example, an industrial continuous-flow process has been developed for the generation and complete consumption of highly reactive diazomethane in the synthesis of HIV protease inhibitor drug intermediates. This process avoids the potentially hazardous accumulation of diazomethane thus minimizing the possibility for industrial accidents.^{14b}

For these reasons, many homogeneous and heterogeneous catalysts are being adapted for use in continuous-flow reactors and processes.¹³⁻¹⁶

Figure 5-4 shows some of the most recent catalysts that have been utilized in continuous-flow reactions.^{16b-d}

Figure 5-4. Recent examples of catalysts used in continuous-flow processes.



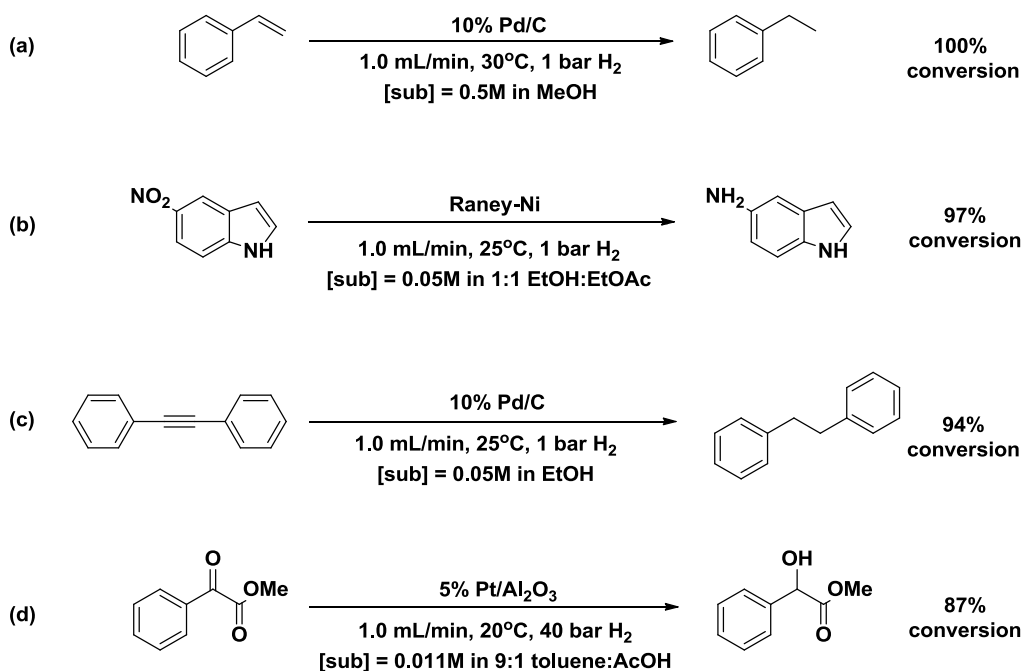
In addition to designing and adapting catalysts for continuous-flow processes, there has been a significant amount of research focused on the development of continuous-flow reactors themselves.¹⁴ Common lab scale continuous-flow reactors found in the literature include, (a) fixed-bed reactors,¹⁷ where immobilized catalysts are fixed in and the flowing substrate occupies the vacancies between the catalyst particles; (b) trickle-bed reactors,¹⁸ where, in a downward movement, a particular substrate is allowed to move over a packed bed of immobilized catalyst particles; and (c) tube reactors,¹⁹ where the homogeneous catalyst, combined with the substrate, is pumped through a tubular column of varying length to an outlet valve. At present, these continuous-flow

gas/solution mixture is passed through the bubble detector **D**, which determines if there is hydrogen in the reaction line, and then into the catalyst cartridge (CatCart®) heating unit **E**. The CatCart® itself (**F**) contains the immobilized catalyst and is situated within the CatCart® heating unit **E**. It should be noted that in addition to providing a variety of pre-packed CatCarts®, Thales Nanotechnology® also supplies empty CatCarts® allowing users to test their own immobilized catalysts in the H-Cube®. After the gas/solution mixture is exposed to the immobilized catalyst, it flows out of the CatCart® **F** and through the outlet pressure sensor **G** and the back-pressure regulator **H**. The back-pressure regulator **H** can restrict the flow of solvent/substrate through the system to maintain the desired hydrogen pressure throughout the system. Finally, the solution exits the H-Cube® through the hydrogenated product collector **I** and enters the collection reservoir.

The H-Cube®, like any other continuous-flow reactor, provides a significant number of benefits over the traditional batch reactors found in industry. These benefits have been discussed in detail previously in this chapter. In addition, the H-Cube® generates hydrogen through the electrolysis of water, thus removing the hydrogen cylinder from the hydrogenation equation. As well, all of the generated hydrogen is used *in situ*, preventing the unsafe build-up of hydrogen pressure within the instrument.

For the aforementioned reasons, the H-Cube® has been utilized in a wide variety of transition metal catalyzed hydrogenation/reduction reactions (Scheme 5-7).²⁰⁻²²

Scheme 5-7. Examples of transition metal catalyzed hydrogenation/reduction reactions performed in the H-Cube®.

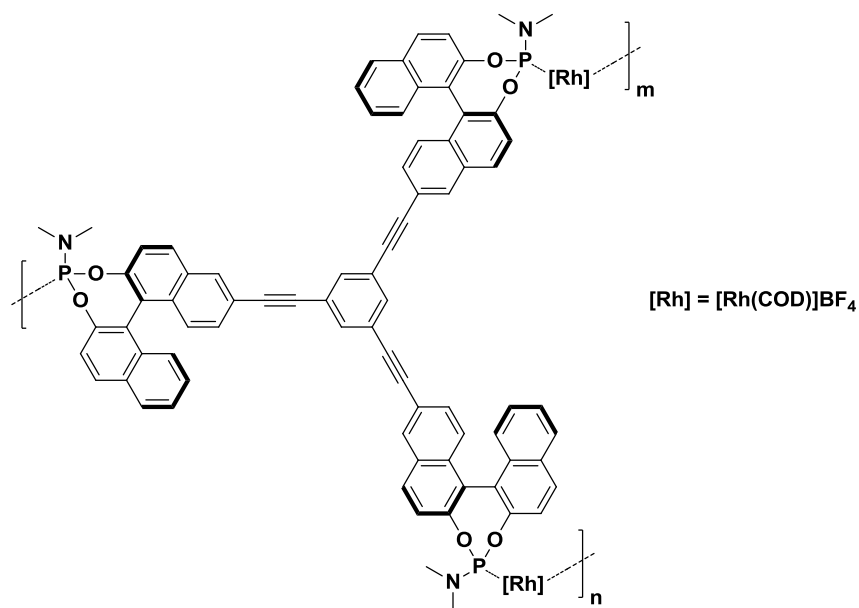


As illustrated in Scheme 5-7, common H-Cube® operating conditions are 1.0 mL/min flow rate, 20-30°C and 1 bar of H₂, although hydrogen pressures as high as 40 bar have been reported. Additionally, substrate solutions typically range from 0.5 – 0.01M in solvents such as MeOH or EtOH. Under such conditions, the immobilized catalysts performed quite well in the H-Cube® hydrogenation reactor affording the desired products in high yields. However, it should be noted that the majority of the

immobilized catalysts that have been tested for use in the H-Cube® (i.e. Pd/C, Pt/Al₂O₃, Raney-nickel, etc.) are high surface area, commercially available, achiral, metal nanoparticle catalysts. Nevertheless, these preliminary examples illustrate the versatility and potential of the H-Cube® in continuous-flow catalytic reactions.

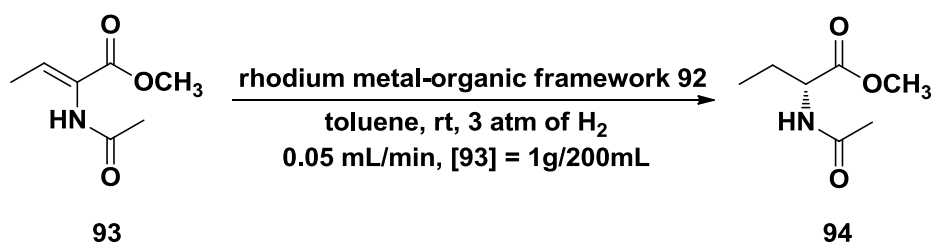
The H-Cube® technology is quite new and, as a result, there are very few reports of rhodium catalyzed asymmetric hydrogenations utilizing the H-Cube®.²⁴ However, the rhodium-based immobilized catalytic systems that have been reported are very promising. In one example, Ding and coworkers synthesized a self-supported rhodium metal-organic framework **92** by mixing a MonoPhos-based ligand with [Rh(COD)]BF₄ (Figure 5-6).²³

Figure 5-6. Ding's rhodium-MonoPhos metal-organic framework **92**.



The self-supported immobilized rhodium metal-organic framework **92** was then deposited on activated carbon and used in the asymmetric hydrogenation of (*Z*)-methyl-2-acetamidobut-2-enoate **93** (Scheme 5-8). Under continuous-flow conditions, the rhodium catalyst afforded the desired hydrogenated product **94** in 99% yield and in 97% ee over a period of 144 hours without a drop in activity or selectivity.

Scheme 5-8. Asymmetric hydrogenation of (*Z*)-methyl-2-acetamidobut-2-enoate **93** in continuous-flow.



This activity corresponds to a constant daily production of 0.36 g, giving an overall yield of 2.52 g of **94** after the 144 hours of reaction time. As well, ICP spectroscopy studies showed that only 1.7% (0.13 ppm) of the total rhodium content leached from the metal-organic framework over the course of the reaction.

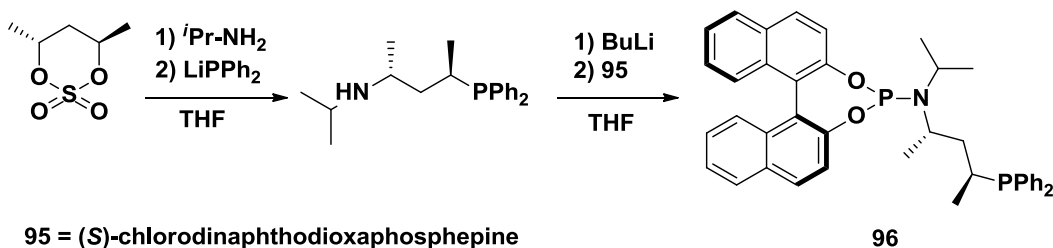
Despite these remarkable results, the overall activity of this system is quite low with only 15 mg of product being produced every hour. Moreover, the loading of catalyst used (60 mg of catalyst per 90 mg of activated carbon) was relatively high, considering the loading of our rhodium catalyst-organic framework **42** on BaSO₄ is 10 mg of catalyst per

1 g of support. In addition, it should be noted that the percent catalyst loading and total TONs are typically not included in continuous-flow literature reports, which is the case for this example. As well, the supported rhodium metal-organic framework **92** was only used in the one 144 hour long run and reuse was not reported. Furthermore, it was discovered that use of only the rhodium metal-organic framework **92** (i.e. in the absence of activated carbon) resulted in system blockage over time. Therefore, additional supports, such as MgSO₄, TiO₂ and activated carbon, were required to ensure that the metal-organic framework remained insoluble and to improve the flow properties of the packed catalyst. That being said, activated carbon was the only support that did not lead to a decrease in catalytic activity; in fact, the overall activity increased. The authors attribute this to improved dispersion of the immobilized metal-organic framework in the reaction mixture in the presence of activated carbon.

In a more recent example, Bakos and coworkers reported the synthesis of a phosphine-phosphoramidite ligand **96** (Scheme 5-9) that was reacted *in situ* with [Rh(COD)₂]BF₄ to generate the catalyst [Rh(COD)(**96**)]BF₄.^{24a} The [Rh(COD)(**96**)]BF₄ catalyst was then immobilized on an Al₂O₃ support using phosphotungstic acid (PTA) as an anchoring agent. The PTA, anchored to the alumina through hydrogen-bonding, is believed to interact with rhodium either covalently, through the formation of a direct rhodium-oxygen bond, or electrostatically where the

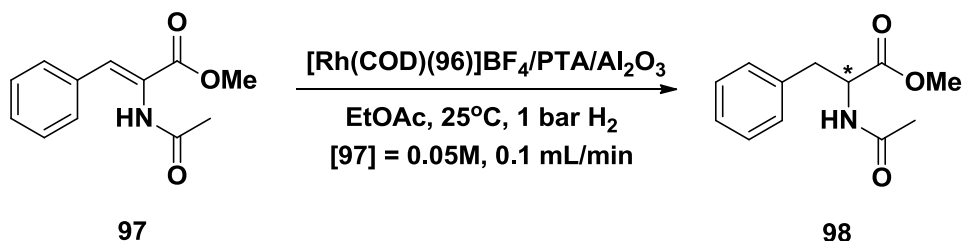
rhodium cation interacts with an oxygen anion on the PTA.^{24b} In this case, an electrostatic interaction is more likely as the rhodium complex is charged.

Scheme 5-9. Bakos' synthesis of phosphine-phosphoramidite ligand **96**.



Once immobilized, the $[\text{Rh}(\text{COD})(\mathbf{96})]\text{BF}_4$ catalyst was evaluated in the H-Cube® for the asymmetric hydrogenation of (*Z*)- α -acetamidocinnamic acid methyl ester **97** (Scheme 5-10). It should be noted that Bakos did not report the amount of Al_2O_3 support used in the immobilization process, therefore there is no way of determining the percent loading of catalyst used in the continuous-flow hydrogenation experiments and the overall TON obtained.

Scheme 5-10. The asymmetric hydrogenation of (*Z*)- α -acetamidocinnamic acid methyl ester **97** in the H-Cube®.



During the first six hours of reaction time, the immobilized rhodium catalyst afforded the desired hydrogenated product in 99% yield and in 99% ee. However, during the next six hours the activity and selectivity did decrease to 90% conversion and 93% ee. Although this is not a substantial decrease, these results, coupled with their batch reactivity/reuse data (70% drop in yield over 8 runs), suggest that a constant decrease in activity and selectivity over time occurred. Bakos attributed this decrease in activity to catalyst decomposition, however it is also possible that significant rhodium leaching could be a factor as the rhodium catalyst was immobilized through non-covalent, electrostatic interactions. Such systems are, by their very nature, cation exchange columns. Electrostatic interactions are typically quite weak and, as a result, the majority of immobilized catalysts that utilize these interactions typically experience significant metal leaching over time. However, as no rhodium leaching data was reported by Bakos, this theory is speculation at this point in time.

This review illustrates many of the industrial and academic benefits of continuous-flow reactors in the field of catalysis. As well, the examples that have been presented show that the commercially available H-Cube® can be and has been successfully used in continuous-flow catalytic hydrogenation reactions. That being said, there still remains a significant amount of research to be done on developing suitable immobilized, asymmetric catalysts for use in the H-Cube®. Currently, the existing catalytic systems have been plagued by low activity (TOF),

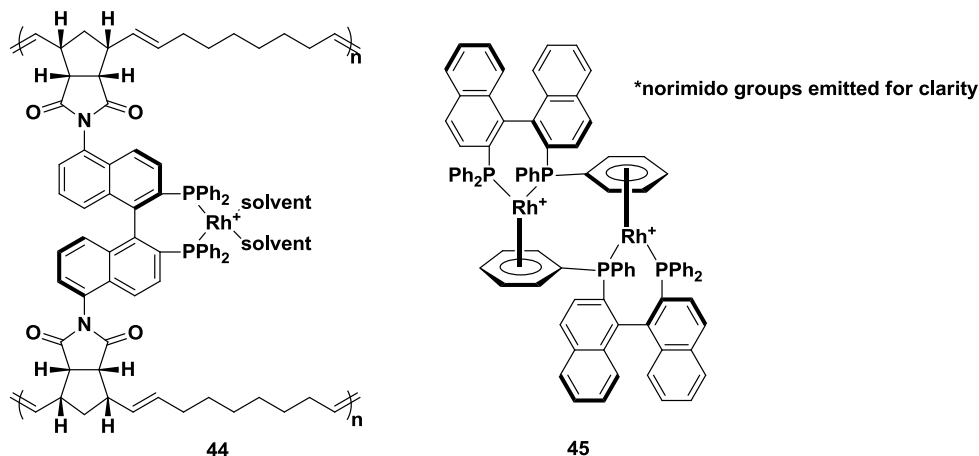
decreases in activity and selectivity over time and metal leaching. We reasoned that our polymer-supported rhodium catalyst-organic frameworks (COFs) could potentially resolve these problems as they have already shown remarkable batch and reuse activity in the intramolecular cycloisomerization of 1,6-enynes and allylic alcohol isomerizations (Chapters 3 and 4). As well, by utilizing the H-Cube® in the asymmetric hydrogenation of olefinic substrates, the industrial viability of the polymer-supported rhodium catalyst-organic frameworks will be realized. The remainder of this chapter discusses the continuous-flow reactivity of the polymer-supported rhodium catalyst-organic frameworks and efforts undertaken to understand the origin(s) of catalyst deactivation.

Results and Discussion

Section A: Activation of the Poly-[Rh(NBD)(N-BINAP)](SbF₆)/BaSO₄ Catalyst-Organic Framework 42 via Hydrogenation of 3-Buten-2-ol

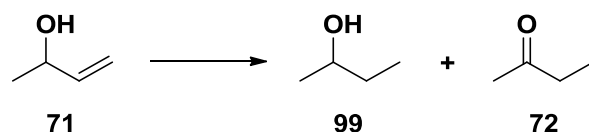
The COF poly-[Rh(NBD)((*R*)-5,5'-dinorimido-BINAP)](SbF₆)/BaSO₄ **42** was chosen for initial experiments in the H-Cube® continuous-flow hydrogenation reactor because this catalyst does not require a silver salt to generate the active catalyst. Rather, the NBD ligand is removed by hydrogenation during the catalytic hydrogenation reaction, generating the active catalytic species [Rh((*R*)-5,5'-dinorimido-BINAP)]⁺ **43**. Once generated, the active catalyst **43** most likely exists as a disolvento complex,^{25a} or perhaps forms bonds to the support or framework (e.g. η⁶-arene bonds), until substrate is present in the reaction mixture^{25b} (Figure 5-7). Refer to Chapter 2 for a more in depth discussion.

Figure 5-7. Possible catalyst resting states.



The COF **42** was first evaluated using 3-buten-2-ol (**71**) as an olefin substrate for the hydrogenation. We chose this substrate because, in a previous study, we found that 3-buten-2-ol was a highly active substrate for allylic alcohol isomerizations.²⁶ The high activity of this substrate suggests that adequate swelling of the catalyst-organic framework is achieved (refer to Chapter 4). Therefore, we reasoned that 3-buten-2-ol could act as a satisfactory activating agent for the catalyst. In addition to the high activity and suspected swelling properties, 3-buten-2-ol can undergo both olefin hydrogenation and isomerization (Equation 5-1), which would allow the activity of the COF to be evaluated for both hydrogenation and isomerization.

Equation 5-1. Olefin isomerization and hydrogenation of 3-buten-2-ol **71**.



The first experiments using the poly-[Rh(NBD)((*R*)-5,5'-dinorimido-BINAP)](SbF₆)/BaSO₄ COF in the H-Cube® are summarized in Table 5-1. It should be noted that the same CatCart® was used for all of these experiments. Here, entry 1 represents the first experiment that was performed in the H-Cube®. As a result, the reaction conditions for this run were essentially a starting point for optimization. Nevertheless, 54% conversion of the 3-buten-2-ol substrate was obtained under the following

conditions: S/C ratio of 2000/1, 30 bar H₂, 50°C, 0.8 mL/min flow rate and a concentration of substrate of 0.23 M in THF solvent.

Table 5-1. Catalyst activation with 3-buten-2-ol.^a

Entry	Loading (Sub/Rh)	[Sub]	H ₂ pressure (bar)	Conversion ^b (%)
1	2000/1	0.23 M	30	54
2	2000/1	0.077 M	30	100
3	1000/1	0.077 M	30	100
4	1000/1	0.077 M	60	100
5	1000/1	0.077 M	0	0
6	20,000/1	0.077 M	30	100
7	1000/1	0.077 M	30	100

^a The reactions were carried out in THF at 50°C with a flow rate of 0.8 mL/min. The same poly-[Rh(NBD)((*R*)-5,5'-dinorimido-BINAP)](SbF₆)/BaSO₄ CatCart® (30 x 4 mm) was used for every entry. ^b Conversion was determined by ¹H-NMR and by comparison to authentic samples.

In order to achieve 100% conversion, the concentration of the substrate solution was diluted by a factor of three, to 0.077 M in THF, while the other reaction conditions were kept constant (entry 2). The reaction conditions for entry 2 (30 bar H₂, 50°C, 0.8 mL/min flow rate, [substrate] = 0.077 M) were used as the standard H-Cube® operating conditions to activate the COF.

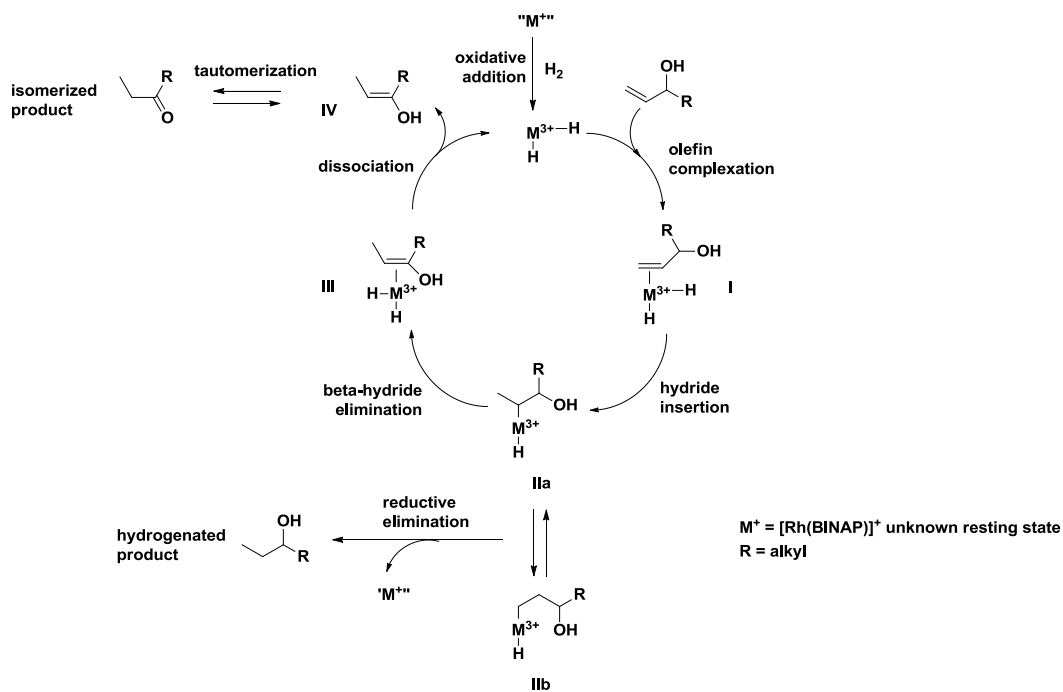
Once the catalyst was conditioned, the reaction was carried out under 60 bar (entry 4) and 0 bar (entry 5) to investigate the effect of

hydrogen pressure on the ratio of isomerized product **72** to hydrogenated product **99**. It was discovered that increasing the hydrogen pressure did not have any effect on the percent conversion (100%) or product distribution (7% isomerized product in both entries 3 and 4). Interestingly, there was 0% conversion in the absence of hydrogen (entry 5). While hydrogenation was not expected, the absence of isomerization suggests that when hydrogen is not present, the catalyst forms a relatively stable, catalytically inactive complex (or resting state). This discovery suggests that the catalyst can be stored in between catalytic runs without decomposing. However, this result is not consistent with the postulated catalyst resting states shown in Figure 5-7. The disolvento complex **44** contains a 16-electron Rh center, which would isomerize 3-buten-2-ol in the absence of hydrogen. The η^6 -arene complex **45** contains two 18-electron Rh centers, however, in the presence of coordinating solvents or substrates, this bonding interaction is disfavored.^{25b} Moreover, this complex should isomerize 3-buten-2-ol in the absence of hydrogen as well. Fortunately, solid state ^{31}P -NMR would help determine the COF resting state but was not within the scope of this project (see Chapter 6 for a discussion of future work).

From these results we speculated that the mechanism of hydrogenation and isomerization proceeds via metal hydride intermediates as shown in Figure 5-8. Here, the Rh resting state complex (\mathbf{M}^+) undergoes oxidative addition with hydrogen followed by olefin

complexation to form **I**. **I** then undergoes hydride insertion to form **II**, that can either reductively eliminate to produce the hydrogenated product or β -hydride elimination to form **III**. Dissociation gives the enol **IV**, that can either tautomerize or re-enter the catalytic cycle to give the isomerized product. In the absence of hydrogen, neither the hydrogenated nor the isomerized product would be produced, which is consistent with the results mentioned above.

Figure 5-8. Proposed mechanism for the isomerization and hydrogenation of olefins via metal hydride intermediates.



The COF **42** was tested in a large substrate loading run (S/C ratio of 20,000:1, 0.005 mol% catalyst, entry 6) using the standard operating conditions for the H-Cube, mentioned above. The catalyst achieved

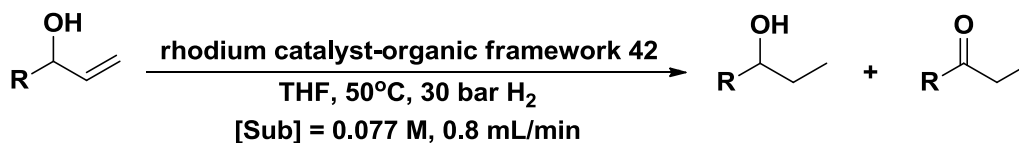
20,000 TOs (100% conversion) of the 3-buten-2-ol substrate in a total of 15 hours. This result is remarkable considering that most rhodium-BINAP catalyzed hydrogenation reactions are performed with 0.5 – 1 mol% of catalyst;⁷⁻¹² 100 – 200 times more catalyst than this run. The catalyst provided an additional 1000 TOs after the large substrate loading run (entry 7), indicating that the catalyst is still highly active and can sustain additional reuse in the H-Cube®.

Section B: Secondary Allylic Alcohol Size Effects

In a previous study on the isomerization of a series of allylic alcohols catalyzed by the poly-[RhCl((*R*)-5,5'-dinorimido-BINAP)]₂/BaSO₄ (+ AgSbF₆) COF,²⁶ we showed that increasing the chain length decreased the rate of isomerization. In particular, secondary allylic alcohols containing alkyl chains with more than three carbons resulted in a decrease in catalytic activity (see Chapter 4 for a more in depth analysis). The now activated poly-[Rh(NBD)((*R*)-5,5'-dinorimido-BINAP)](SbF₆)/BaSO₄ COF was used for the hydrogenation of a series of allylic alcohols to confirm/investigate the size effect.

The substrates that were chosen for this study include 3-buten-2-ol (**71**), 1-penten-3-ol (**73**), 1-hexen-3-ol (**74**) and 1-hepten-3-ol (**75**) and the results are summarized in Table 5-2.

Table 5-2. Continuous-flow hydrogenation/isomerization of allylic alcohol substrates catalyzed by rhodium catalyst-organic framework **42**.^a



R = CH₃ (**71**), C₂H₅ (**73**), C₃H₇ (**74**), C₄H₉ (**75**)

Sub	Loading (Sub/Rh)	Total Conversion ^b (%)	Product Distribution ^b (%)	
			Hydrogenated	Isomerized
71	2000/1	100	91	9
73	2000/1	100	75	25
74	2000/1	100	61	39
75	2000/1	70	-	-

^a The reactions were carried out in THF at 50°C under 30 bar H₂ with a flow rate of 0.8 mL/min and substrate concentrations of 0.077 M. The same poly-[Rh(NBD)((*R*)-5,5'-dinorimido-BINAP)](SbF₆)/BaSO₄ CatCart® (30 x 4 mm) was used for every entry. ^b Conversion and product distribution was determined by ¹H-NMR and by comparison to authentic samples.

Substrates **71**, **73** and **74** were converted in 100% yield into a mixture of hydrogenated and isomerized product by the COF **42**. However, under the same conditions, substrate **75** only underwent 70% conversion. This result is consistent with our previous findings in that the only substrate that was not fully converted into product contained an alkyl chain that was longer than three carbons, suggesting that larger allylic alcohols do in fact lead to a decrease in catalytic activity and rate of reaction. However, unlike the previous results, the substrates **71**, **73** and **74** were all fully converted into

product despite differences in alkyl chain length. This suggests that the rhodium catalyst-organic framework **42** has a substrate size threshold that should not be exceeded for optimal catalytic activity (refer to Chapter 4 for a more in depth discussion).

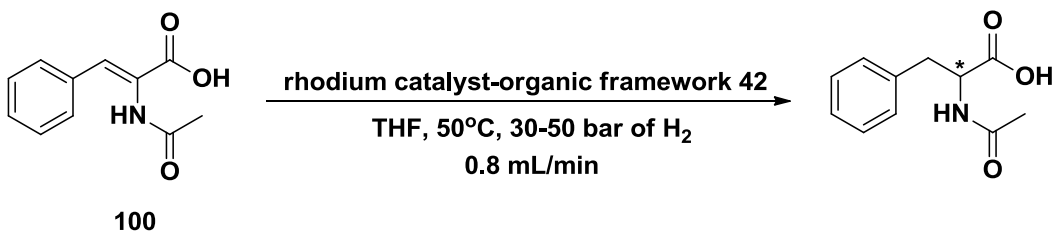
Interestingly, the product distribution (i.e. hydrogenation versus isomerization product) was also dependent on the length of the allylic alcohol hydrocarbon chain. From Table 5-2 it is apparent that increasing hydrocarbon chain length resulted in an increase in the amount of isomerized product obtained. From the metal hydride mechanism of hydrogenation/isomerization (see Figure 5-8) we postulated that β -hydride elimination is more favored (or occurs faster) than the reductive elimination step as the alkyl chain length increases. This theory is speculation and beyond the scope of this project, however deuterium labeling studies could perhaps elucidate the nature of this effect.

Section C: Hydrogenation of Dehydro Amino Acid Derivatives

As mentioned previously in the introductory section of this chapter, Noyori's homogeneous $[\text{Rh}((R)\text{-BINAP})(\text{sol})_2]^+$ catalyst system has shown remarkable activity and selectivity in the hydrogenation of certain dehydro amino acids. As a result, α -acetamidocinnamic acid **100** was chosen as the next substrate for this investigation.

Table 5-3 summarizes the results obtained from the hydrogenation of substrate **100** by COF **42** in the H-Cube®.

Table 5-3. Continuous-flow hydrogenation of α -acetamidocinnamic acid **100** catalyzed by rhodium catalyst-organic framework **42**.^a



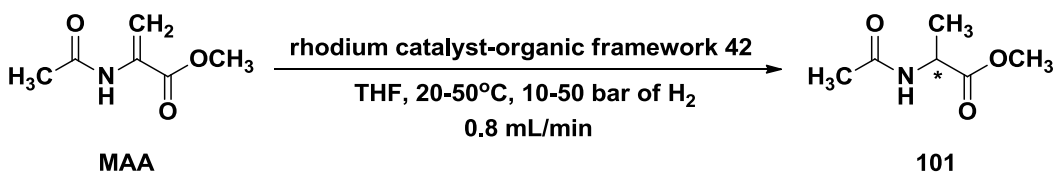
Entry	Temp (°C)	H ₂ Pressure (bar)	TON	Yield ^b (%)
1	50	30	22	11
2	50	50	46	23

^[a] These reactions were carried out with 0.028 M solutions of α -acetamidocinnamic acid in THF under the following conditions: Sub/Rh = 200/1, 0.8 mL/min flow rate. The same poly-[Rh(NBD)((*R*)-5,5'-dinorimido-BINAP)](SbF₆)/BaSO₄ CatCart® (30 x 4 mm) was used for both entries. ^[b] Yield was determined by ¹H-NMR and by comparison to authentic samples.

The yield was 11% (TON = 22) under our standard conditions (entry 1) and increased to only 23% (TON = 46) under 50 atm of H₂ (entry 2). Based on these results, we postulated that the poor reactivity was due to a substrate size effect; specifically, the COF **42** substrate size threshold was exceeded by the α -acetamidocinnamic acid substrate.

The results obtained from hydrogenation of the smaller substrate, methyl 2-acetamido acrylate (MAA), by COF **42** in the H-Cube® are summarized in Table 5-4.

Table 5-4. Continuous-flow hydrogenation of MAA catalyzed by rhodium catalyst-organic framework **42**.^a



Entry	Temp (°C)	H ₂ Pressure (bar)	Yield ^b (%)	ee ^c (%)
1	50	50	100	9.0
2	50	30	100	15
3	50	20	100	12
4	50	10	98	17
5	40	20	100	6.6
6	30	20	100	5.9
7	20	50	100	4.6
8	20	30	100	16

^[a] The reactions were carried out with 0.028 M solutions of MAA in THF under the following conditions: Sub/Rh = 200/1, 0.8 mL/min flow rate, 30 x 4 mm CatCart®. ^[b] Yield was determined by ¹H-NMR and by comparison to authentic samples. ^[c] ee was determined by chiral GC.

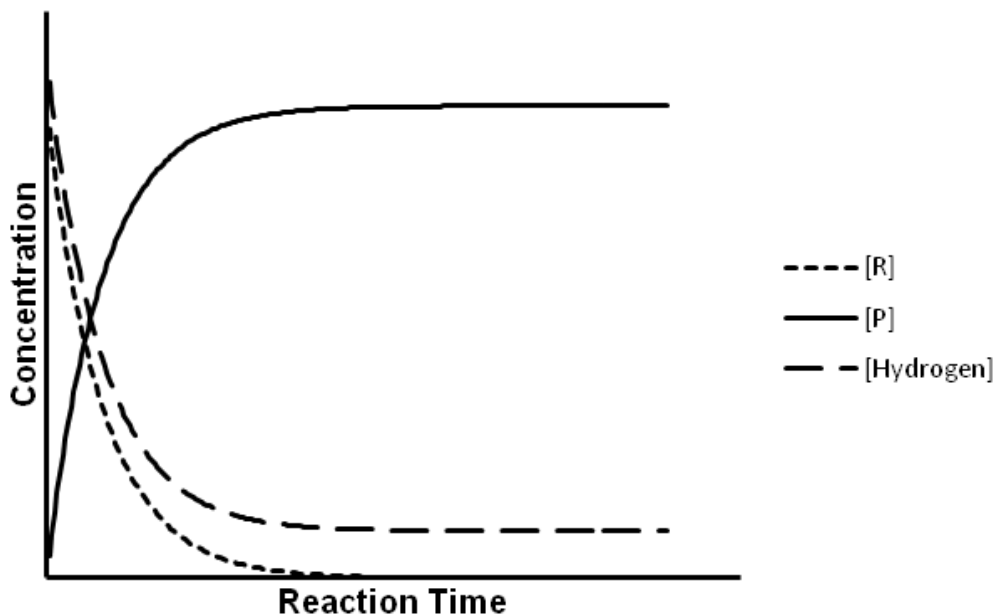
Unlike **100**, MAA was hydrogenated in 100% yield (TON = 200) under standard conditions and 50 atm of H₂ (entries 1 and 2). This result supports our hypothesis that the substrate size threshold within COF **42** was exceeded as the less bulky substrate (MAA) was hydrogenated at a higher rate and to a larger extent than the bulky α -acetamidocinnamic acid substrate **100**. This finding is of particular importance as it suggests that

the COF **42** could be used to selectively hydrogenate specific substrates within a given mixture based on substrate size exclusion; a feat not possible with homogeneous catalysts.

The temperature and H₂ pressure were systematically varied to investigate the effect these parameters have on the yield and ee (see Table 5-4 for the summarized results). Changes in these reaction parameters have little or no effect on the overall yield of this reaction. 100% yields were obtained over the temperature range 20-50°C and H₂ pressure range 10-50 bar for every run. We found the ee generally increased with decreasing pressure of H₂ (entries 1, 2 and 4) and with increasing temperature (entries 3, 5 and 6). The highest ee (17%, entry 4) was obtained with an H₂ pressure of 10 bar and temperature of 50°C. The ee values are not optimized as we could not eliminate overlap of the enantiomer peaks in GC experiments with a chiral column.

The likely reaction profile for hydrogenations in the H-Cube® is outlined in Figure 5-9. Initially, the concentration of reactant ([R]) and hydrogen ([H₂]) is high and the concentration of product ([P]) is low as very little, if any, of the reactant has been hydrogenated into product. As the substrate solution proceeds through the CatCart® (i.e. increased reaction time), the [P] will steadily increase while the [R] and [H₂] decrease until a point is reached where all of the reactant has been hydrogenated. At this point, the [P] and [H₂] remain constant and the product solution along with the remaining hydrogen exits the CatCart®.

Figure 5-9. Reaction profile for H-Cube® hydrogenations.



Traditional batch/homogeneous hydrogenations typically involve rapid stirring and a replenishing hydrogen source, rendering the $[H_2]$ essentially constant throughout the reaction. However, in a flow reactor, it is likely that the hydrogen is not replenished throughout the run, resulting in a decrease in the $[H_2]$ during the run and necessitating the need for higher H_2 pressures. As mentioned previously in the introduction of this chapter, the enantioselectivity of dehydro amino acid hydrogenations is very sensitive to H_2 pressure.⁶ Specifically, at low pressures (<4 atm), the minor olefin/rhodium diastereomer is hydrogenated much faster than the major diastereomer, resulting in high enantioselectivity. However, at high pressures, the major diastereomer is competitively hydrogenated resulting

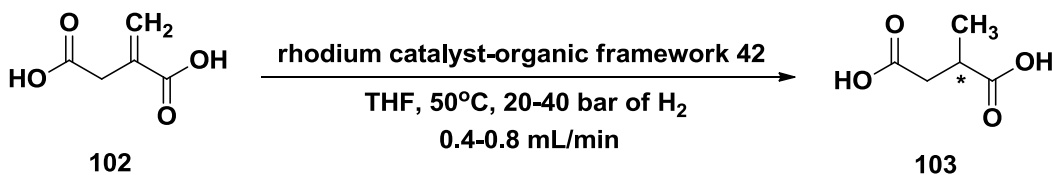
in poor enantioselectivity. Therefore, the low enantioselectivity obtained in the hydrogenation of MAA likely resulted from the H-Cube® higher H₂ pressure requirement. It is also possible that there exists an unfavorable substrate/framework or catalyst/framework interaction that is responsible for the low enantioselectivity.

As the reaction profiles of batch/homogeneous and continuous-flow catalysis are likely quite different, comparing results is quite difficult and many new factors need to be considered (i.e. [H₂], flow rate, etc.). Further, future investigations should focus on rapid screening of catalysts and substrates to find systems that are compatible with this new reaction profile. In fact, systems that are unsuitable for homogeneous or batch catalysis may be more suited for use in the H-Cube®.

Section D: Hydrogenation of Itaconic Acid

Itaconic acid (**102**) is known to give high enantioselectivities with a number of homogeneous rhodium-phosphine catalysts.²⁷ For example, Zhang and coworkers hydrogenated **102** in 99% ee with their [Rh(TangPhos)(NBD)](SbF₆) catalyst (TangPhos = (1*S*,1*S'*,2*R*,2*R'*)-1,1'-di-*tert*-butyl-(2,2')-diphospholane, S/C = 200, 20 psi H₂, 25°C).^{27a} The results obtained from the hydrogenation of itaconic acid **102** catalyzed by COF **42** in the H-Cube® are summarized in Table 5-5.

Table 5-5. Continuous-flow hydrogenation of itaconic acid **102** catalyzed by rhodium catalyst-organic framework **42**.^a



Entry	Flow Rate (mL/min)	H ₂ Pressure (bar)	Yield ^d (%) (TON)	ee ^e (%)
1	0.8	30	90 (180)	21
2	0.8	40	81 (162)	-
3 ^b	0.6	30	92 (184)	30
4 ^b	0.4	20	93 (186)	-
5 ^{a,c}	0.8	30	98 (196)	-

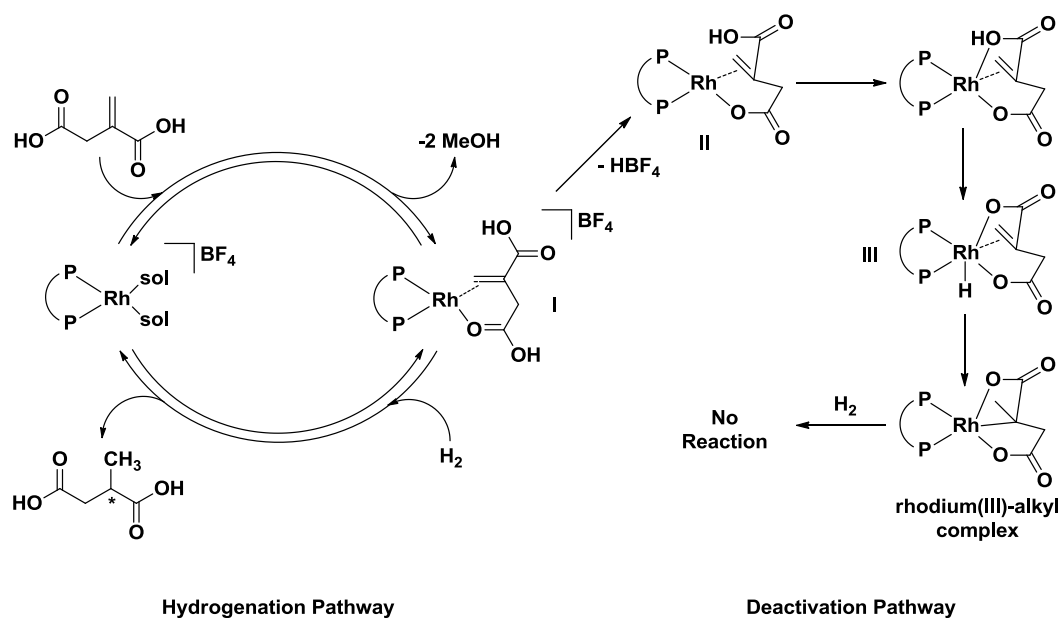
^[a] The reactions were carried out with 0.028 M solutions of itaconic acid in THF under the following conditions: Sub/Rh = 200/1, 50°C. The same poly-[Rh(NBD)((*R*)-5,5'-dinorimido-BINAP)](SbF₆)/BaSO₄ CatCart® (30 x 4 mm) was used for every entry. ^[b] The reactions were carried out with 0.014 M solutions of itaconic acid in THF under the following conditions: Sub/Rh = 200:1, 50°C. ^[c] The substrate solution was run through the H-Cube twice. ^[d] Yield was determined by ¹H-NMR and by comparison to authentic samples. ^[e] ee was determined by chiral HPLC.

In the first run (entry 1), under our standard H-Cube® conditions (30 bar H₂, 50°C and 0.8 mL/min flow rate), the hydrogenated product **103** was obtained in 90% yield (TON = 180). The yield actually dropped from 90% to 81% (TON = 162) when the pressure was increased to 40 bar (entry 2). This result indicates that the catalyst underwent some sort of decrease in activity from inhibition by itaconic acid. Reducing the flow rate and diluting the substrate concentration in half (entries 3 and 4) increased the yields to

92% (TON = 184) and 93% (TON = 186), respectively. The passing of the reaction mixture twice through the H-Cube® (entry 5) resulted in a yield of 98% (TON = 196).

In a recent study, Heller and coworkers reported that the homogeneous catalyst, $[\text{Rh}(\text{DIPAMP})(\text{MeOH})_2](\text{BF}_4)$, deactivates during the hydrogenation of itaconic acid.²⁸ Through extensive mechanistic studies, Heller postulated the *in situ* formation of a catalytically inactive rhodium(III)-alkyl complex (Figure 5-10). The itaconic acid displaces two MeOH solvento molecules to form the bis-chelating diastereomeric olefin-carbonyl complexes (I). Next, in the deactivation pathway, the β -carboxyl group undergoes deprotonation to form the rhodium(I) carboxylate complex II and eliminate HBF_4 . Coordination of the α -carboxyl group with protonation of the rhodium(I) metal center gives the rhodium(III) complex III. Olefin insertion gives the rhodium(III)-alkyl complex. This rhodium(III)-alkyl complex is proposed to be stable, resulting in the deactivation of the homogeneous $[\text{Rh}(\text{DIPAMP})(\text{MeOH})_2](\text{BF}_4)$ hydrogenation catalyst.

Figure 5-10. Catalyst deactivation through formation of a rhodium(III)-alkyl complex.

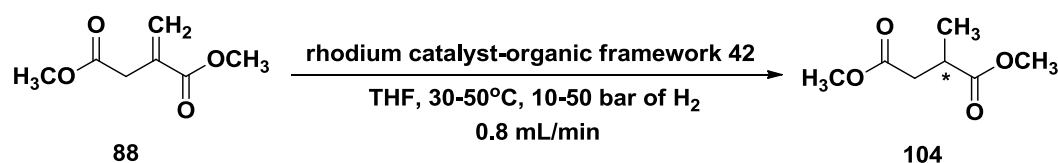


An interesting feature of this mechanism is the loss of the BF_4^- counter-ion as HBF_4 . In the COF **42**, SbF_6^- is the weakly coordinating counter-ion and, if the COF **42** does undergo deactivation via Heller's or a similar deactivation pathway, one would expect the loss of the SbF_6^- as HSbF_6 . In addition, as our reactions are performed in a continuous-flow reactor, the SbF_6^- that is lost should exit the reactor with the product solution. Therefore, quantifying the amount of antimony in the catalyst before and after use could potentially provide some insight into whether the COF **42** undergoes formation of rhodium-carboxylates similar to those proposed by Heller. The actual quantification of the antimony present in the catalyst before and after use will be discussed in more detail later in this chapter.

Section E: Hydrogenation of Dimethyl Itaconate

The results from the hydrogenation of dimethyl itaconate **88** catalyzed by the COF **42** in the H-Cube® are summarized in Table 5-6.

Table 5-6. Continuous-flow hydrogenation of dimethyl itaconate **88** catalyzed by rhodium catalyst-organic framework **42**.^a



Entry	Temp (°C)	H ₂ Pressure (bar)	Yield ^c (%)	ee ^d (%)
1	50	50	100	0.5
2	50	30	100	6.4
3	50	10	100	16
4	30	50	100	1.2
5	30	30	100	3.7
6	30	10	100	12
7 ^b	50	30	72	-
8 ^b	50	50	92	-

^[a] The reactions were carried out with 0.028 M solutions of dimethyl itaconate in THF under the following conditions: Sub/Rh = 200/1, 0.8 mL/min flow rate. The same poly-[Rh(NBD)((*R*)-5,5'-dinorimido-BINAP)](SbF₆)/BaSO₄ CatCart® (30 x 4 mm) was used for every entry. ^[b] The reactions were carried out with 0.077 M solutions of dimethyl itaconate in THF under the following conditions: Sub/Rh = 10,000:1. ^[c] Yield was determined by ¹H-NMR and by comparison to authentic samples. ^[d] ee was determined by chiral HPLC.

As shown in entries 1-6, changes in temperature (30-50°C) and H₂ pressure (10-50 bar) had no effect on the yield of the hydrogenated product **104**. In fact, every run went to 100% completion. The enantioselectivity increased with decreasing H₂ pressure (entries 1-3, 4-6). Also, the enantioselectivity increased with increasing temperature (entries 3 and 6). These trends are similar to those for the hydrogenation of MAA, suggesting that the optimal conditions for obtaining high enantioselectivities with the COF **42** involve the use of low H₂ pressures and high temperatures. The homogeneous analogue [Rh(NBD)((S)-BINAP)](BF₄) hydrogenated dimethyl itaconate in 67% ee (S/C = 100, 5 bar H₂, room temperature)²⁹ compared to the 16% ee obtained with the COF (entry 3). This again suggests that either the high H₂ pressures (>10 bar) or the existence of an unfavorable substrate/framework or catalyst/framework that is not present in the homogeneous systems is responsible for the lower enantioselectivity.

Due to the high activity exhibited by the COF **42** in the hydrogenation of dimethyl itaconate (entries 1-6), two large scale runs were performed to test the endurance of the catalyst. With a S/C ratio of 10,000:1, a TON of 7200 was achieved under the following conditions: 50°C, 30 bar of H₂, 0.8 mL/min flow rate with a concentration of dimethyl itaconate of 0.077 M in THF (entry 7). In an attempt to increase the total percent yield, the H₂ pressure was increased from 30 bar to 50 bar. This increase in H₂ pressure resulted in a 20% increase in the yield, which

corresponds to a total TON of 9200 (entry 8). We attributed this requirement for higher pressures to the relatively high concentration of the dimethyl itaconate solutions. For example, for the large 10,000:1 runs, a substrate concentration of 0.077 M was used, which is 2.75 times more concentrated than the smaller, 200:1 runs (0.028 M, entries 1-6). We decided to use a higher substrate concentration for the high loading runs as the experiment run times were a reasonable 8 hours. If the substrate concentration had been kept at 0.028 M, the run time would have increased to 22 hours. Thus, despite the requirement for higher H₂ pressure and the decrease in yield, the TOF for the 10,000:1 runs (entries 7 and 8) was actually 2.5 times faster than the 200:1 runs (entries 1-6).

In summary, the results for the hydrogenation of dimethyl itaconate catalyzed by the COF **42** also suggest that either the high H₂ pressure or the existence of an unfavorable substrate/framework or catalyst/framework interaction is responsible for the lower enantioselectivity. However, the activity, versatility and endurance of the COF **42** continued to be truly remarkable and unprecedented.

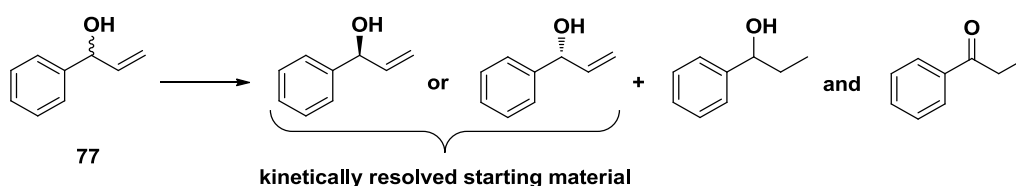
Section F: Kinetic Resolution/Hydrogenation of α -Vinylbenzyl

Alcohol

As the high activity of the COF **42** had been illustrated and verified with a variety of substrates, we decided to investigate whether the catalyst

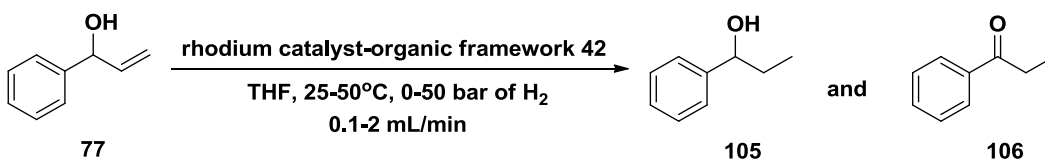
could be used for the kinetic resolution of racemic substrates. In this case, kinetic resolution would result from the preferential hydrogenation/isomerization of one enantiomer of the starting material over the other. α -Vinylbenzyl alcohol (**77**) was chosen as this substrate is known to provide good kinetic resolution of the starting allylic alcohol (up to 17% ee) (Equation 5-3).³⁰ Refer to Section E of Chapter 4 of this dissertation for a discussion on the kinetic resolution of this substrate.

Equation 5-3. The kinetic resolution of α -vinylbenzyl alcohol **77**.



The results from the hydrogenation of α -vinylbenzyl alcohol **77** catalyzed by the COF **42** are summarized in Table 5-7.

Table 5-7. Continuous-flow hydrogenation of α -vinylbenzyl alcohol **77** catalyzed by rhodium catalyst-organic framework **42**.^a



Entry	[Sub]	Flow Rate (mL/min)	Temp (°C)	H ₂ Pressure (bar)	Conversion ^c (%)
1	0.028 M	0.8	50	50	100
2	0.028 M	0.8	50	30	100
3	0.028 M	0.8	50	10	100
4	0.077 M	1.2	50	10	100
5	0.077 M	1.6	50	10	100
6	0.077 M	1.6	25	10	100
7	0.077 M	2.0	25	10	100
8	0.1 M	2.0	25	10	100
9	0.1 M	2.0	25	1	100
10	0.1 M	2.0	25	0	0
11 ^b	0.1 M	2.0	25	1	97

^[a] The reactions were carried out in THF with Sub/Rh = 200/1. The same poly-[Rh(NBD)((*R*)-5,5'-dinorimido-BINAP)](SbF₆)/BaSO₄ CatCart® (30 x 4 mm) was used for every entry. ^[b] This reaction was carried out in EtOH. ^[c] Conversion was determined by ¹H-NMR and by comparison to authentic samples.

Substrate **77** proved to be the most active substrate to date undergoing 100% conversion despite increasing the concentration (0.028-0.1M) and

flow rate (0.8-2.0 mL/min) and decreasing the temperature (25-50°C) and H₂ pressure (1-50 bar) (entries 1-9). In fact, TOFs as high as 4150 hour⁻¹ were obtained when flow rates of 2.0 mL/min were used (entries 8 and 9). These activities are even more remarkable considering that in typical asymmetric continuous-flow hydrogenation reactions, flow rates of <0.1 mL/min are used to ensure complete conversion^{23,24} (refer to the introduction of this chapter). Thus, the COF **42** is 20 times more active than most other reported continuous-flow chiral hydrogenation catalysts. As well, batch reactions having similar S/C ratios typically require a number of hours to achieve the same conversion that the COF **42** afforded in a matter of minutes. The one downside of this extremely high activity was that we were unable to detect any kinetic resolution that may have taken place. In fact, we purposefully manipulated the reaction conditions outlined in entries 1-9 to prevent the complete conversion of the substrate **77** and, despite our best efforts, we were unsuccessful.

As the kinetic resolution could not be analyzed we took this as an opportunity to confirm/investigate additional points of interest. We first decided to confirm the finding that in the absence of hydrogen the COF **42** is no longer catalytically active. As expected, under 0 bar of H₂ pressure, the catalyst was completely unsuccessful in converting substrate **77** into either product **105** or **106** (entry 10). This result is in accordance with our previous result (refer to Table 5-1, entry 5) and lends support to our claim that in the absence of hydrogen, the catalyst forms a relatively stable,

catalytically inactive complex. As mentioned previously, this property is significant in that it suggests that the catalyst can be stored in between catalytic runs without decomposing. As well, this confirms that the mechanism for hydrogenation occurs via rhodium-hydride formation (refer to Figure 5-8).

Next, we investigated if changes in solvent would affect the catalytic activity in the hydrogenation of substrate **77**. In preliminary batch studies, it was discovered that the COF **42** was completely inactive in EtOH and highly active in THF. This difference in activity was attributed to the difference in the swellability of the catalyst in these two solvents. Surprisingly, the rhodium catalyst-organic framework **42** exhibited nearly the same activity in EtOH as in THF with only a slight decrease in the percent conversion (entry 11, 97% conversion in EtOH and 100% conversion in THF). This result highlights the remarkable activity, versatility and flexibility of our catalyst system; attributes that are currently absent in the majority of reported continuous-flow catalysts but that are essential for any sustainable, industrially applicable catalyst system.

**Section G: Overall Summary of the Poly-[Rh(NBD)((*R*)-5,5'-
dinorimido-BINAP)](SbF₆)/BaSO₄ Catalyst-Organic Framework 42
Activity**

The preliminary results that have been discussed in sections A to F of this chapter were obtained using three different CatCarts® loaded with the poly-[Rh(NBD)((*R*)-5,5'-dinorimido-BINAP)](SbF₆)/BaSO₄ COF **42**. A summary of the catalyst longevity and the overall TONs obtained from the individual CatCarts® are illustrated in Table 5-8.

Table 5-8. Summary of the longevity and total TONs obtained from the CatCarts® loaded with the rhodium catalyst-organic framework **42**.

Entry	Longevity ^a (days)	Total TONs	# of Different Substrates Tested
1	25	36,500	7 (71, 73, 74, 75, MAA, 100, 102)
2	30 ^b	55,700	3 (71, MAA, 88)
3	27 ^b	17,600	2 (71, 77)

^[a] The longevity refers to the number of consecutive days that the catalyst was present in the H-Cube® and remained active. After the indicated period of time, the catalyst was removed from the H-Cube® and was not used in any further catalytic experiments. ^[b] The catalyst was still active upon removal from the H-Cube®.

The first CatCart® that was loaded with the COF **42** remained catalytically active in the H-Cube® for a period of 25 days and produced approximately 36,500 TOs (entry 1). These 36,500 TOs were obtained from the continuous-flow hydrogenation of seven different substrates. To the best

of our knowledge, this is the largest number of substrates that have been hydrogenated using the same CatCart®. These results indicate that a single CatCart®, and thus the H-Cube® itself, would be ideal for rapid substrate screening.

After the initial exploratory experiments performed with the first CatCart®, we were able to extend the lifetime of the catalyst to 30 days and obtained approximately 55,700 TOs with the second CatCart® (entry 2). It should be noted that the COF **42** was still catalytically active at the time of removal from the H-Cube®. However, after 30 days of continual use, the CatCart® itself began to degrade which resulted in system clogging and required the removal of the loaded CatCart® from the H-Cube®. Specifically, the rubber o-rings used for sealing the CatCart® degraded from the sheer volume of THF (approximately 4-5 liters) passed through the H-Cube®.

The third CatCart® was used for the completion of the preliminary substrate screening experiments and thus was not used as extensively as the first two CatCarts®. Regardless, the third CatCart® provided a total of approximately 17,600 TOs over a period of 27 days. Similar to the second CatCart®, the catalyst was still catalytically active at the time of removal from the H-Cube®.

In summary, the CatCarts® containing the poly-[Rh(NBD)((*R*)-5,5'-dinorimido-BINAP)](SbF₆)/BaSO₄ catalyst-organic framework provided total TONs as high as 55,700 and sustained reuse for a period of up to 30

days before the CatCart® itself began to degrade in the H-Cube®. To the best of our knowledge, these are the largest TONs and longest catalyst lifetimes reported for any chiral catalyst utilized in a continuous-flow reactor. As well, a variety of different substrates were hydrogenated using a single CatCart®, which illustrates the suitability of the H-Cube® for rapid screening purposes.

Section H: CatCart® Removal from the H-Cube®

Having demonstrated extraordinary catalytic activity and longevity with the COF **42** in the H-Cube®, it was imperative to characterize the catalyst before and after use. Such a comparison could potentially provide insight into the origin(s) of the high catalytic activity and sustainability/reusability. As well, this study could result in a better understanding of the origin(s) of catalyst deactivation. That being said, the method of removal of the CatCarts® from the H-Cube® was extremely important in maintaining the integrity and minimizing any changes to the catalysts themselves.

As shown in the previous section, the first CatCart® provided 36,500 TOs over a period of 25 days (Table 5-8, entry 1). At the end of that 25 day period, the COF **42** had lost a considerable amount of activity. The second CatCart® (Table 5-8, entry 2) gave the largest TONs and was still catalytically active when physical degradation of the CatCart® itself

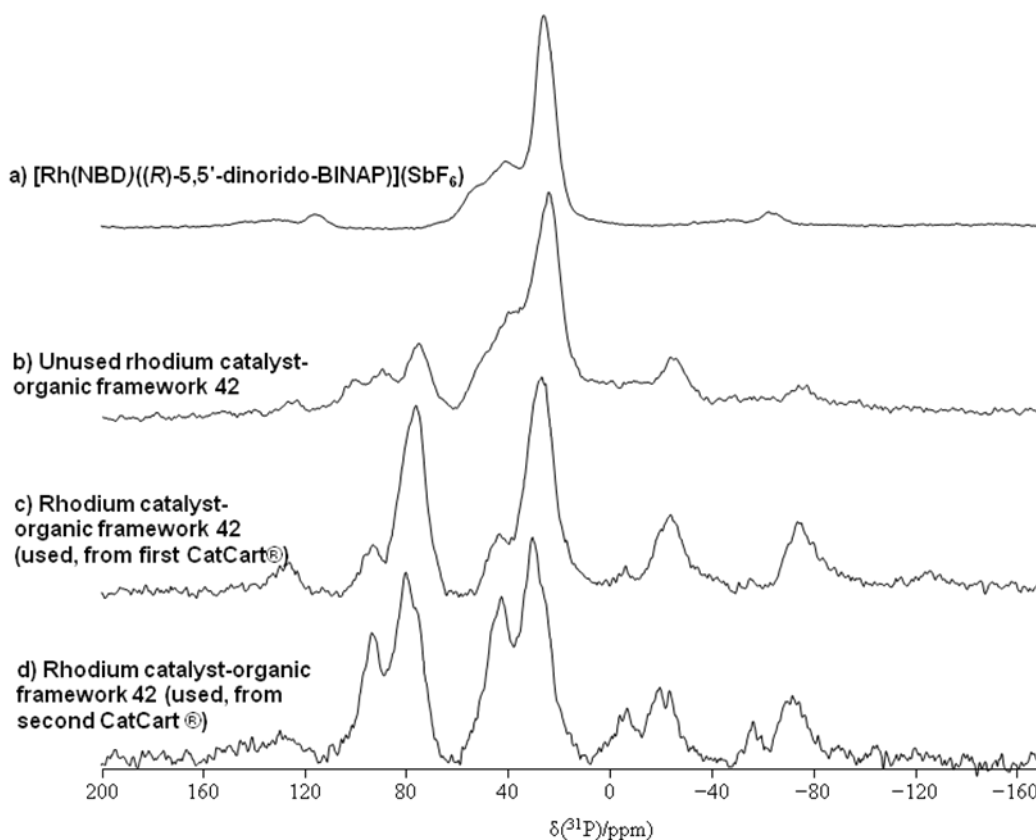
caused system clogging. Both of these CatCarts® were removed from the H-Cube® in air and quickly placed under a nitrogen atmosphere. The second CatCart® was first flushed with a solution of COD (100 equiv. per Rh, 0.028 M solution in THF, 0.2 mL/min, 0 bar H₂) in an attempt to store the catalyst as the [Rh(COD)((*R*)-5,5'-dinorimido-BINAP)]⁺ complex.

In the literature, catalyst decomposition and metal leaching are the most common reasons for poor catalytic activity and reusability (refer to Chapter 1). Therefore, we utilized solid state NMR to probe the chemical environment of the phosphines and neutron activation analysis (NAA) to quantify the amount of rhodium in the catalyst samples before and after use. Together, these analyses were used to determine whether catalyst decomposition and/or metal leaching occurred for our COF **42** in the H-Cube®. The results from these analyses are discussed in detail in the following sections of this chapter.

Section I: Solid State NMR Analysis

Solid state ³¹P-NMR spectra were acquired of the monomer unit [Rh(NBD)((*R*)-5,5'-dinorimido-BINAP)](SbF₆) **40**, the unused poly-[Rh(NBD)((*R*)-5,5'-dinorimido-BINAP)](SbF₆)/BaSO₄ COF **42** and the poly-[Rh(NBD)((*R*)-5,5'-dinorimido-BINAP)](SbF₆)/BaSO₄ COF **42** that was used in the first and second CatCarts®. The spectra are shown in Figure 5-11.

Figure 5-11. ^{31}P -NMR spectra of used and unused samples of the rhodium catalyst-organic framework **42**.^a



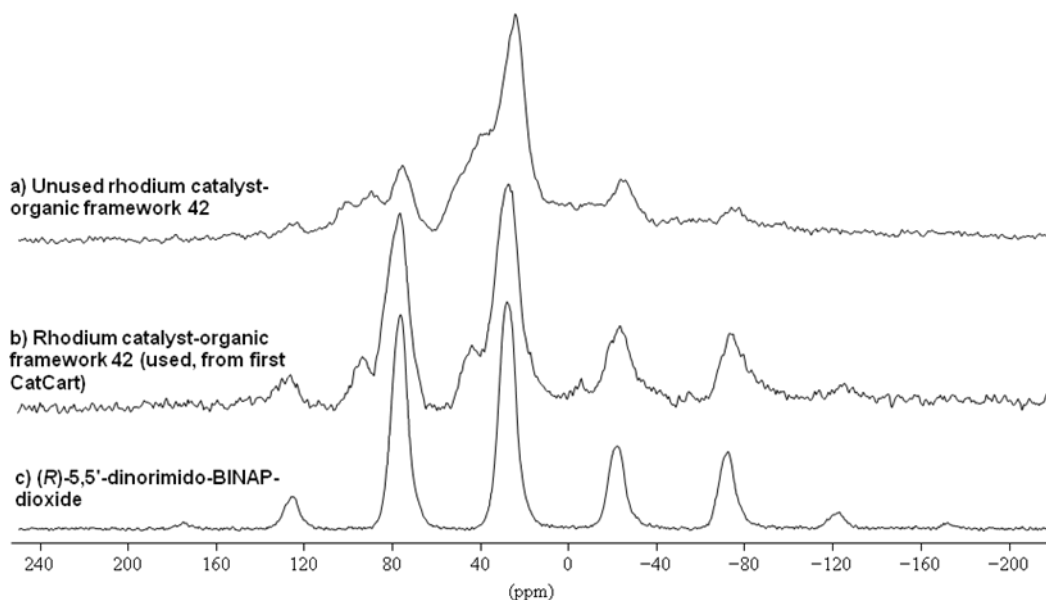
^[a] 500.3 MHz. For spectrum (a), a 2.5 mm probe and a magic angle spinning (MAS) frequency of 18 kHz (1820 scans) were used. For spectrum (b), a 4.0 mm probe and MAS frequency of 10 kHz (30144 scans) were used. For spectrum (c), a 4.0 mm probe and MAS frequency of 10 kHz (32724 scans) were used. For spectrum (d), a 4.0 mm probe and MAS frequency of 10 kHz (34124 scans) were used.

The ^{31}P -NMR spectrum for the monomer unit $[\text{Rh}(\text{NBD})((R)\text{-}5,5'\text{-dinorimido-BINAP})](\text{SbF}_6)$ (Figure 5-11a) contained one peak at ~30 ppm, due to the BINAP phosphines, and a smaller, broader side peak at ~40 ppm. The identity of the side peak remains unknown, however it is likely from the rotational isomers of the (*R*)-5,5'-dinorimido BINAP ligand (see Chapter 2). More importantly, the ^{31}P -NMR spectrum of the unused COF

42 (Figure 5-11b) was almost identical to that of the monomer. This confirms that the alternating ROMP assembly does not alter the electronic environment of the rhodium metal centers. The only difference between the two spectra is the emergence of three spinning side bands at ~80 ppm, ~-20 ppm and ~75 ppm in the unused COF **42** spectrum (Figure 5-11b), which were subsequently identified as phosphine oxide peaks (Figure 5-12). The presence of these oxides were attributed to handling as no oxide peaks were present in the solution ^{31}P -NMR spectrum (refer to Figures 2-9 and 2-10 in Chapter 2). Specifically, the NMR probe was packed with the COF and handled in air. Comparison of the ^{31}P -NMR spectra of the used COF **42** (Figure 5-11c) to the unused COF **42** shows that the intensity of the phosphine oxide peaks was greatly increased and that the peak located at ~30 ppm, from the BINAP, was still present, suggesting that some active rhodium centers are still present in the catalyst.

The solid state ^{31}P -NMR spectrum of oxidized (*R*)-5,5'-dinorimido-BINAP ligand is shown in Figure 5-12.

Figure 5-12. ^{31}P -NMR spectral comparison of the (*R*)-5,5'-dinorimido-BINAP-dioxide ligand with the used and unused poly-[Rh(NBD)((*R*)-5,5'-dinorimido-BINAP)](SbF_6)/ BaSO_4 catalyst-organic framework.^a



[a] 500.3 MHz. For spectrum (a), a 4.0 mm probe and MAS frequency of 10 kHz (30144 scans) were used. For spectrum (b), a 4.0 mm probe and MAS frequency of 10 kHz (32724 scans) were used. For spectrum (c), a 4.0 mm probe and MAS frequency of 8 kHz were used.

The spectra provided in Figure 5-12 confirm that there are phosphine oxides present in both the unused and used COF samples. As mentioned previously, the phosphine oxides present in the unused catalyst sample (Figure 5-12a) were attributed to sample handling. Comparison of the signal intensities in the unused and used catalyst spectra (Figures 5-12a and 5-12b) indicate that there are more oxides present in the used sample. This suggests that oxidation of the phosphines occurred in the H-Cube® and was at least partly responsible for catalyst deactivation. As well, it can be concluded that since deactivation occurred slowly over time,

the oxidation of the phosphines was probably quite slow over the 25 days of catalyst use in the H-Cube®. As an aside, it should be noted that both phosphine oxides and rhodium-phosphines have isotropic chemical shifts of ~ 30 ppm in the solid state ³¹P-NMR.³¹ However, the interaction of the phosphine-oxide with the external magnetic field results in the formation of spinning side bands, which are not present in samples containing unoxidized phosphines.^{31a} Therefore, the presence of the side bands in our spectra is diagnostic for the presence of phosphine oxides.

Solid state ³¹P-NMR analysis of the second CatCart® (Figure 5-11d), after addition of COD, shows two phosphorus environments present at ~45 ppm and ~35 ppm. The emergence of a new phosphorus environment could be due to the presence of COD, however more analysis is required. This spectrum also contains a very large spinning side band at ~80 ppm, which has been attributed to the formation of phosphine oxides in the H-Cube®.

In summary, the solid state ³¹P-NMR analysis suggests that slow phosphine oxidation is a contributing factor to catalyst deactivation in the H-Cube®. This analysis also confirmed that the alternating ROMP assembly does not alter the electronic environment of the rhodium metal centers.

Section J: Neutron Activation Analysis

Neutron activation analysis (NAA) is a technique used to determine the concentrations of specific elements in a given sample. In particular, bombardment with neutrons causes the elements in the sample to form radioactive isotopes. These isotopes will then decay via element specific radioactive decay paths that have been well studied and documented and that typically involve the emission of gamma radiation. The amount of emitted radiation can then be compared to an elemental standard and the concentration of the desired elements can be determined.³² In our case, NAA was performed on used and unused samples of the COF **42** in order to determine the amount of rhodium present. These values were then quantified through comparison with a rhodium standard and used to determine the amount of rhodium leaching that had occurred over the catalyst lifetime in the H-Cube®. In addition to quantifying the amount of rhodium, the amount of antimony was also determined to investigate whether anion exchange occurred (see section D of this chapter for an in depth discussion). A summary of the NAA data is presented in Table 5-9.

Table 5-9. Neutron activation analysis of the rhodium catalyst-organic framework **42** before and after use in the H-Cube®.

Entry	Catalyst	[Rh] ($\mu\text{g/g}$)	[Sb] ($\mu\text{g/g}$)
1	unused	544	439
2	first CatCart® after use	355	46
3	unused	653	534
4	second® CatCart after use	548	41
5 ^a	initial solution	84	109

^[a] This data was obtained from the initial solution that was collected from the H-Cube® at the beginning of the second catalyst cartridge's lifetime.

In the case of the first CatCart®, there was a difference of 188 $\mu\text{g/g}$ of rhodium between the unused and used COF samples (entries 1 and 2). Assuming a uniform distribution of rhodium throughout the catalyst samples, this corresponds to a loss of approximately 1.3 mg of rhodium (34%) over the course of 25 days. We analyzed the initial solution collected from the H-Cube® at the beginning of the catalyst lifetime for the second CatCart®. This consisted of THF (~ 10 mL) that had been run through the CatCart® at 0.8 mL/min before any addition of substrate. In total, 105 $\mu\text{g/g}$ of rhodium leached, corresponding to ~ 16% of the total rhodium originally present in the CatCart®. 84 $\mu\text{g/g}$ (~ 80%) of the total rhodium leached (105 $\mu\text{g/g}$) were lost in the initial fractions (entry 5). This result shows that the rhodium leaching is due to the loss of low molecular weight rhodium-containing polymer at the beginning of the catalyst lifetime

rather than gradual loss of rhodium throughout the entire lifetime of the catalyst. In fact, only 21 $\mu\text{g/g}$ of rhodium leached during the 30 days that the catalyst was utilized. Therefore rhodium leaching does not significantly contribute to the deactivation of the COF **42**. We attribute this to relatively strong rhodium/framework/support interactions that ultimately prevent leaching of rhodium from the framework. Refer to Chapters 1 and 2 for a discussion on our catalyst synthetic strategies.

We also quantified the amount of antimony in the unused and used COF samples. Recall that Heller postulated the deactivation of his catalyst through the formation of a rhodium(III)-alkyl complex in the presence of itaconic acid and that this deactivation pathway resulted in the loss of BF_4^- as HBF_4 (refer to section D for the complete mechanism). For our catalyst, such a pathway would result in loss of SbF_6^- as HSbF_6 . For both the first and second CatCarts[®], the loss in antimony was 90% (entries 1 and 2) and 72% (entries 3, 4 and 5), respectively. We note that acidic substrates were not used in the second CatCart[®] and a 72% loss in antimony still occurred. Although it is plausible that itaconic acid formed carboxylate intermediates, NAA experiments provide no information on this pathway. Additional causes for loss of SbF_6^- include catalyst decomposition by oxidation and exchange by trace anions in the solvent. However, it remains unclear at this point what is responsible for the loss of the majority of the antimony and more study is required.

In summary, the NAA results show that rhodium leaching from the CatCarts® was not significant and thus does not contribute to the deactivation of COF **42**. Conversely, the lack of rhodium leaching could be the main reason for the high activity and reusability of the COF **42**. As well, the results suggest that the use of acidic substrates could be a minor contributor to catalyst deactivation, however, we currently cannot explain the significant loss of antimony in our catalyst samples.

Section K: CatCart® Lifetime Assessment

The significant conclusion of the solid state ³¹P-NMR analysis is that catalyst deactivation primarily results from oxidation of the phosphines over the course of the 25-30 days of H-Cube® operation. Further, as shown by the NAA results, rhodium leaching is not significant over this operational time period. Taken together, these results strongly indicate that neither metal leaching nor intrinsic catalyst lifetime limits the lifetime of the COF **42** CatCarts®. Rather, slow oxidation of the catalyst occurs over the 25-30 days of operation when 4 to 5 liters of THF solvent are passed through the CatCart®. In fact, if the proper substrates are studied, i.e. no acidic substrates, and appropriate precautions are taken to reduce/eliminate dissolved oxygen in solvents and substrates, the CatCart® itself is what limits the lifetime of the catalyst. For example, the second CatCart® was still 100% active after 30 days and approximately

55,700 TOs (Table 5-8, entry 2). However, after encountering clogging problems with the H-Cube®, and subsequent removal of the CatCart® from the H-Cube®, we noticed that the rubber o-rings on the CatCart® had begun to degrade, likely due to the sheer volume of THF solvent that had been passed through the CatCart® over the course of the 30 days. Thus, the degradation of the CatCart® itself was most likely responsible for the clogging issues we experienced and for CatCart® removal, both of which limited the lifetime of the catalyst.

Section L: Utilization of the Poly-[RhCl((*R*)-5,5'-dinorimido-BINAP)]₂/Ba-L-tartrate **41 Catalyst-Organic Framework in the H-Cube®**

The achiral support BaSO₄ was replaced by Ba-L-tartrate and the chloro-bridged dimeric COF poly-[RhCl((*R*)-5,5'-dinorimido-BINAP)]₂/Ba-L-tartrate **41** was investigated in an effort to improve the *ee*'s of these hydrogenations. This COF had previously afforded remarkable enantioselectivity in the intramolecular cycloisomerization of 1,6-enynes (Chapter 3) and exhibited remarkable activity in the isomerization of allylic alcohols (Chapter 4). As well, we reasoned that the chiral Ba-L-tartrate support could potentially increase the enantioselectivity afforded by the catalyst.

The COF **41** was inherently more difficult to adapt to use in the H-Cube® as this catalyst requires a silver salt to abstract the bridging chlorides in order to generate the active “[Rh((*R*)-5,5'-dinorimido-BINAP)]⁺” catalyst. As a result, it was decided to pack the CatCart® with both the COF **41** and 25.5 equivalents of AgSbF₆ per rhodium center. 15.5 equivalents of AgSbF₆ were in the first layer of the CatCart® followed by a mixture of 10 equivalents of AgSbF₆ and the rhodium COF **41**. We reasoned that the THF solvent would dissolve the AgSbF₆ at the start of the CatCart® and trickle through the entire mixture of the rhodium catalyst-organic framework. At the same time, the AgSbF₆ mixed throughout the COF could potentially activate the more difficult to reach rhodium centers. Thus, by packing the CatCart® in such a way, we intended to activate a significant portion of the rhodium centers present in the framework.

Similar to the previously studied COF **42**, the Ba-L-tartrate supported COF **41** was first tested in the hydrogenation of 3-buten-2-ol. As a reminder, this substrate was found to be highly active (see Chapter 4) and we believe that it conditions the column. The results are given in Table 5-10.

Table 5-10. Continuous-flow hydrogenation of 3-buten-2-ol (**71**) catalyzed by rhodium catalyst-organic framework **41**.^a

Entry	Loading (Sub/Rh)	H ₂ pressure (bar)	Flow Rate (mL/min)	Conversion ^b (%)
1	1000/1	30	0.8	95
2	1000/1	30	0.8	91
3	5000/1	40	0.8	93
4	5000/1	40	0.6	95

^a The reactions were carried out with 0.077 M solutions of 3-buten-2-ol in THF at 50°C. The same poly-[RhCl((*R*)-5,5'-dinorimido-BINAP)]₂/Ba-L-tartrate CatCart® (30 x 4 mm) was used for every entry. ^b Conversion was determined by ¹H-NMR and by comparison to authentic samples.

The initial experiments (entries 1 and 2) were performed under our standard operating procedures: 50°C, 30 bar of H₂, 0.8 mL/min flow rate and a substrate concentration of 0.077 M in THF. Unlike the previous catalyst, which gave 100% conversion under these conditions (Table 5-1, entry 3), the Ba-L-tartrate supported COF **41** gave 95% and 91% conversion. In larger substrate runs (S/C = 5000), increasing the pressure to 40 bar (entry 3) and decreasing the flow rate to 0.6 mL/min (entry 4) did not appear to affect the % conversion at all (93% and 95% conversion, respectively). We attributed this difference in catalyst activity to the swellability of the COFs. The chloro-bridged COF **41** is inherently more rigid than COF **42** because of the extra crosslinking from the chloro-bridges (see Chapter 2). As a result, the Ba-L-tartrate supported COF **41** may require a longer swelling period than the BaSO₄ supported COF **42** to

ensure high activity. In addition, as a direct consequence of poor swelling, perhaps not all of the rhodium centers were activated by the AgSbF_6 , which would also negatively affect the overall catalytic activity.

Another difference between COFs **41** and **42** was the ratio of isomerized product **72** to hydrogenated product **99**. With the poly- $[\text{Rh}(\text{NBD})((R)\text{-5,5'-dinorimido-BINAP})](\text{SbF}_6)/\text{BaSO}_4$ catalyst, 7% of the product was isomerized. With the poly- $[\text{RhCl}((R)\text{-5,5'-dinorimido-BINAP})]_2/\text{Ba-L-tartrate}$ catalyst, only 1% of the product was isomerized. The reason for this difference in product distribution is unknown, however these results show that the isomerization pathway is not as competitive when the Ba-L-tartrate catalyst system is used.

Itaconic acid (**102**) was chosen for study with this catalyst system as this substrate provided the highest enantioselectivities from the previously studied COF **42** (refer to section D). The results from the hydrogenation of itaconic acid are provided in Table 5-11.

Table 5-11. Continuous-flow hydrogenation of itaconic acid **102** catalyzed by rhodium catalyst-organic framework **41**.^a

Entry	Loading (Sub/Rh)	Flow Rate (mL/min)	H ₂ Pressure (bar)	Yield ^c (%)	ee ^d (%)
1 ^b	200/1	0.6	30	62	>99.9
2	100/1	0.4	30	78	>99.9
3	100/1	0.4	50	91	>99.9

^[a] These reactions were carried out with 0.0071 M solutions of itaconic acid in THF at 50°C. The same poly-[RhCl((*R*)-5,5'-dinorimido-BINAP)]₂/Ba-L-tartrate CatCart® (30 x 4 mm) was used for every entry. ^[b] A 0.014 M solution of itaconic acid in THF was used for this run. ^[c] Yield was determined by ¹H-NMR and by comparison to authentic samples. ^[d] ee was determined by chiral HPLC.

In the first experiment, the hydrogenated product **103** was obtained in 62% yield and >99.9% ee (entry 1). Under identical conditions, the poly-[Rh(NBD)((*R*)-5,5'-dinorimido-BINAP)](SbF₆)/BaSO₄ catalyst gave the product **103** in a higher yield (92%) but with lower enantioselectivity (30%, refer to Table 5-5). The Ba-L-tartrate catalyst **41** is less active, but is much more selective, providing near perfect enantioselectivity in the hydrogenation of itaconic acid.

Dilution of the substrate by half from 0.014 M to 0.0071 M and lowering the flow rate from 0.6 mL/min to 0.4 mL/min (entry 2) resulted in an increase in yield from 62% to 78%, and the enantioselectivity remained high at >99.9%. Increasing the H₂ pressure from 30 to 50 bar (entry 3) increased the yield increased to 91% while the ee remained at >99.9%. It should be noted that 91% was the highest yield we were able to obtain

due to the likely equilibrium that exists between product and substrate Rh-carboxylate complexes (refer to Equation 5-2). Taken altogether, these results show that the poly-[RhCl((*R*)-5,5'-dinorimido-BINAP)]₂/Ba-L-tartrate COF is extremely selective in the hydrogenation of itaconic acid despite the requirement for higher pressures of H₂, relatively slow flow rates and dilute substrate solutions. We are currently investigating the use of other substrates with this catalyst in the H-Cube® continuous-flow reactor.

The origin(s) of the high enantioselectivity of the poly-[RhCl((*R*)-5,5'-dinorimido-BINAP)]₂/Ba-L-tartrate COF and the differences in enantioselectivity among seemingly similar COFs are currently unknown and are being investigated in our laboratories. That being said, there are some factors that we believe play a role in the enantioselectivity of the rhodium catalyst-organic frameworks. One such factor is the nature of the support. For example, the Ba-L-tartrate supported catalyst provided substantially higher ee values than the BaSO₄ supported catalyst in the hydrogenation of itaconic acid. This suggests that there exists a possible catalyst-support or substrate-support interaction that has the potential to enhance enantioselectivity. In addition, we believe the close proximity of the two rhodium metal centers in the poly-[RhCl((*R*)-5,5'-dinorimido-BINAP)]₂ COF may play a role in the high enantioselectivity exhibited by this catalyst. In fact, there may exist some cooperativity between the two rhodium metal centers in this catalyst that is not present in the poly-

[Rh(NBD)((*R*)-5,5'-dinorimido-BINAP)](SbF₆) COF, resulting in improved enantioselectivity.

Conclusion

In summary, we have shown that the poly-[Rh(NBD)((*R*)-5,5'-dinorimido-BINAP)](SbF₆)/BaSO₄ catalyst-organic framework is ideal for the continuous-flow hydrogenation of olefin-containing substrates. In particular, the catalyst showed remarkable activity in the hydrogenation of a variety of substrates, including allylic alcohols, dehydro amino acids, unsaturated dicarboxylic acids and unsaturated diesters, and sustained up to approximately 55,700 TOs over a period of 30 days in the H-Cube®. In addition, through solid state ³¹P-NMR and neutron activation analysis, it was determined that catalyst deactivation was due to oxidation from the sheer volume of solvent passed through the catalyst over a 30 day period rather than rhodium leaching or an intrinsic catalyst lifetime. This suggests that the catalyst lifetime can be extended past 30 days if the proper precautions are taken and if the CatCart® does not significantly degrade.

In addition to these remarkable results, we have obtained >99.9% ee in preliminary experiments involving the continuous-flow hydrogenation of itaconic acid catalyzed by the poly-[RhCl((*R*)-5,5'-dinorimido-BINAP)]₂/Ba-L-tartrate catalyst-organic framework. We are currently optimizing this catalyst and investigating additional substrates for use in highly enantioselective, continuous-flow hydrogenation reactions. In conclusion, these results truly highlight the industrial viability of the

rhodium catalyst-organic frameworks synthesized from alternating ROMP assembly and commercialization of this technology is currently underway.

Experimental

General procedures and methods. Gas chromatography analyses were carried out using a Hewlett-Packard 5890 chromatograph equipped with a flame ionization detector, a 3392A integrator, and a Supelco Beta Dex™ 120 fused silica capillary column (30m x 0.25mm x 0.25µm). HPLC analyses were performed using a Waters 600E multisolvent delivery system equipped with Waters 715 Ultra WISP sample processor, Waters temperature control system, Waters 990 photodiode array detector, Waters 410 differential refractometer, Waters 5200 printer plotter, and Daicel CHIRALPAK IB (4.6 mm i.d. x 250 mm) chiral column. HPLC grade hexanes (Min. 99.5%) and 2-propanol (Min. 99.5%) were obtained from Caledon Laboratories Ltd. Continuous-flow reactions were performed using an H-Cube® SS continuous-flow hydrogenation reactor equipped with a K-120 HPLC pump. CatCarts® and related packing products were obtained from ThalesNano Nanotechnology Inc.

Unless otherwise stated, all experiments were performed under an inert atmosphere using standard Schlenk and glove-box techniques. Argon and nitrogen gas (Praxair, 99.998%) were passed through a drying train containing 3Å molecular sieves and indicating Drierite™ before use. All solvents were dried and distilled under a nitrogen atmosphere using standard drying agents, unless otherwise noted. All allylic alcohol reagents and dimethyl itaconate were obtained from Sigma-Aldrich Co. and were

distilled under a nitrogen atmosphere prior to use. Methyl α -acetamido acrylate and itaconic acid were obtained from Sigma-Aldrich Co. and used without further purification. α -Acetamidocinnamic acid was synthesized according to literature procedures.³³

Representative procedure for packing a CatCart® with the poly-[Rh(NBD)((*R*)-5,5'-dinorimido-BINAP)](SbF₆)/BaSO₄ catalyst-organic framework 42. An empty CatCart® (30 x 4 mm) was brought into the glove box and weighed (8.5267 g). In ~ 50 mg increments, the BaSO₄ supported poly-[Rh(NBD)(N-BINAP)](SbF₆) was added to the empty CatCart® via scoopula. After each addition of catalyst, the CatCart® was tapped for ~ 3 minutes to ensure that all of the catalyst added was tightly and evenly packed in the CatCart®. Once the level of the catalyst reached the lip of the CatCart® (slightly below where the CatCart® “top” would be placed) no more catalyst was added and the full CatCart® was then weighed (8.9491 g, 0.4215 g of BaSO₄ supported catalyst in the CatCart®). The final loading of rhodium in the CatCart® was 4.16 mg (9.88 mg of rhodium per gram of BaSO₄ support). The packed CatCart® was stored in the glove box until required.

Representative procedure for packing a CatCart® with the poly-[RhCl((*R*)-5,5'-dinorimido-BINAP)]₂/Ba-L-tartrate catalyst-organic framework 41. An empty CatCart® (30 x 4 mm) was brought into the

glove box and weighed (8.4475 g). AgSbF_6 (0.0169 g, 4.92×10^{-2} mmol) was added initially to the CatCart® and the CatCart® was tapped for ~ 3 minutes to ensure even packing. Next, AgSbF_6 (0.0109 g, 3.17×10^{-2} mmol) was mixed evenly with the Ba-L-tartrate supported poly-[Rh(N-BINAP)Cl]₂. The catalyst/ AgSbF_6 mixture was then added to the CatCart® via scoopula in ~ 50 mg increments. After each addition of catalyst, the CatCart® was tapped for ~ 3 minutes to ensure that all of the catalyst added was tightly and evenly packed in the CatCart®. Once the level of the catalyst reached the lip of the CatCart® (slightly below where the CatCart® “top” would be placed) no more catalyst was added and the full CatCart® was then weighed (8.7362 g, 0.2609 g of Ba-L-tartrate supported catalyst in the CatCart®). The final loading of rhodium in the CatCart® was 3.09 mg (11.84 mg of rhodium per gram of Ba-L-tartrate support). The final number of equivalents of AgSbF_6 per rhodium center was 25.5 equivalents. The packed CatCart® was stored in the glove box until required.

Representative procedure for pressing a packed CatCart® loaded with a particular rhodium catalyst-organic framework. The packed CatCart® was removed from the glove box for pressing. The packed CatCart® opening was covered first with a piece of pre-cut filter paper, followed by a pre-cut metal screen. Next, a rubber o-ring followed by a thick rubber o-ring were placed on top of the metal screen. The thick

rubber o-ring was pressed down slightly with tweezers to keep all the components in place for pressing. Using an arbor press, the components were pressed into the CatCart® thus sealing the contents. The CatCart® was then immediately transferred to the H-Cube® CatCart® holder for use.

Representative procedure for operating the H-Cube. A packed and pressed CatCart® was inserted into the H-Cube® CatCart® holder and the H-Cube® water reservoir was filled with triply distilled water. The solvent and substrate were freshly distilled and bubbled with nitrogen gas for 30 minutes prior to use in the H-Cube®. A substrate solution of desired concentration was prepared in a purged round-bottom flask equipped with a side-arm.

In a typical experiment, the H-Cube® and the connected HPLC pump were first switched on. The H-Cube® water line was then purged for ~ 1 minute, followed by a purging of the HPLC pump inlet with the desired solvent to remove and prevent any air bubbles from entering the pump itself. Next, the desired parameters (i.e. temperature, H₂ pressure and flow rate) were programmed into the H-Cube® using the H-Cube® interface. The HPLC pump was then initiated and pure solvent was flushed through the H-Cube for ~ 10 minutes. The H-Cube® was then started and the internal pressures were allowed to build-up and stabilize over the course of ~ 10 minutes. Once the system was stable, pure H₂ and solvent were

flushed through the system for ~ 5 minutes before switching to the desired substrate solution. Once all the substrate solution had been added to the HPLC pump inlet reservoir, the reservoir was rinsed with ~ 3 x 10 mL of the selected solvent to ensure that all of the substrate solution was flushed through the H-Cube®. Next, the run was stopped by using the H-Cube® interface and either new parameters were entered and the next run was started or the H-Cube® was flushed with deoxygenated anhydrous ethanol and the H-Cube® and connected HPLC pump were shut down.

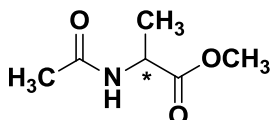
Solid state NMR acquisition. All ^{31}P -NMR spectra were acquired with magic angle spinning (MAS) and ramped cross-polarization (RAMP-CP) on a Bruker Avance 500 NMR spectrometer, operating at 500.3 and 202.5 MHz for ^1H and ^{31}P , respectively. The $[\text{Rh}(\text{NBD})((R)\text{-}5,5'\text{-BINAP})](\text{SbF}_6)$ sample was packed into a 2.5 mm outer diameter rotor and spun at MAS frequencies 8 or 18 kHz; this sample was used to optimize the experimental conditions for the RAMP-CP experiments for all samples. The ^1H 90° pulse for the $[\text{Rh}(\text{NBD})((R)\text{-}5,5'\text{-BINAP})](\text{SbF}_6)$ sample was 2.0 μs , the contact time was 3.0 ms, the acquisition time was 30 ms and the recycle delay was 3.0 s. All other ^{31}P -NMR spectra were acquired on the same instrument, but were packed in 4.0 mm outer diameter NMR rotors. Samples for the latter were spun at 8.0 or 10.0 kHz, with a ^1H 90° pulse of 4.0 μs . All other acquisition parameters were as outlined for the $[\text{Rh}(\text{NBD})((R)\text{-}5,5'\text{-BINAP})](\text{SbF}_6)$ sample above.

Neutron activation analysis acquisition. Instrumental neutron activation analysis (NAA) was used to determine the rhodium (Rh), barium (Ba), and antimony (Sb) contents of used, and unused, catalyst samples. Samples (each weighing ≤ 55 mg) and standards were accurately weighed (or pipetted) into polyethylene micro-centrifuge tubes (~ 175 μL volume), hermetically sealed and individually irradiated in the University of Alberta SLOWPOKE II nuclear reactor for 100 s at a nominal thermal neutron flux of 1×10^{11} $\text{n cm}^{-2} \text{s}^{-1}$. Following a measured decay period (of between 20 - 30 s) the irradiated samples were individually counted for 100 s live-time at a sample-to-detector distance of 3 cm to measure the induced Rh gamma-ray activity. The Rh measurements were performed in open geometry using a 22% relative efficiency ORTEC hyperpure Ge detector (full-width at half maximum, FWHM, of 1.95 keV for the 1332.5 keV full energy peak of ^{60}Co). The Ge detector was connected to a PC-based Aptec multichannel analyzer (MCA) card. Following a decay period of ~ 4 h the samples were recounted for 1800 s to determine their Ba and Sb contents on the end-cap of an ORTEC high-purity FX-Profile Ge detector (Model GEM-FX8530P4) with a relative efficiency of 40% and a FWHM of 1.75 keV (for the 1332.5 keV ^{60}Co photopeak) housed in a 10 cm Pb cave with Cu shield. The FX Profile detector was coupled to an ORTEC *DSPEC-Pro* digital spectrometer. Elemental analysis was performed by the semi-absolute method of activation analysis for Rh and Ba.³⁴ Antimony was determined by absolute instrumental NAA. The nuclear reactions and

relevant nuclear data for the quantification of the three elements measured are listed in the following table. A Sigma-Aldrich Fluka Analytical Rh AA standard solution (977.0 ug Rh/mL in 5% HCl) was used in quantifying Rh. Barium sulphate was used as comparator standard for the determination of the Ba. As noted above Sb was determined by absolute (*i.e.*, standard-less) NAA.

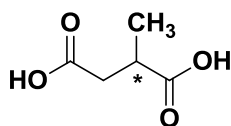
Nuclear Reaction	Half-life	Principal γ -ray(s)
$^{103}\text{Rh} (n,\gamma) ^{104}\text{Rh}$	42.3 s	555.8 keV
$^{138}\text{Ba} (n,\gamma) ^{139}\text{Ba}$	83.06 m	165.9 keV
$^{121}\text{Sb} (n,\gamma) ^{122}\text{Sb}$	2.7238 d	564.1 keV

Determination of enantiomeric excess. The products from the catalytic hydrogenations were concentrated under reduced pressure and an aliquot was flushed through a FluorosilTM plug using CH_2Cl_2 as an eluent to remove any catalyst residues. The retention times and chiral GC or HPLC conditions for the products are given below and the retention times were confirmed with racemic samples of the products. $^1\text{H-NMR}$ spectra recorded were identical to the authentic samples.



101

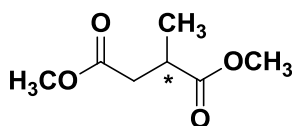
The enantiomeric excess of the product from the hydrogenation of MAA (**101**) was determined through chiral GC, however the peaks did not fully separate on the column. The product was concentrated under reduced pressure and a solution was prepared in CH₂Cl₂ at a concentration of 2 mg/mL. Next, 1 μL was injected into the GC under the following conditions: helium carrier gas (20 psig); constant temperature of 80°C; injector temperature of 220°C; detector temperature of 220°C. The retention times for the two enantiomers were 75.7 min and 77.6 min.



103

The enantiomeric excess of the product from the hydrogenation of itaconic acid (**103**) was determined through chiral HPLC and confirmed with the racemic methylated compound (dimethyl methyl succinate, **104**), which was obtained from Sigma-Aldrich. The product was first methylated by reaction with diazomethane. The methylated product was then concentrated under reduced pressure and a solution was prepared in THF at a concentration of 2 mg/mL. Next, 3 μL was injected into the HPLC under the following conditions: 30°C, 0.8 mL/min flow rate, mobile phase of 98:2 hexane: isopropanol. The retention times for the two enantiomers of the racemic methylated compound **104** were 7.6 min and 9.9 min. Methylated product from certain rhodium catalyst-organic framework

reactions only contained the enantiomer at 9.9 min. Therefore, the ee was determined to be >99.9%.



104

The enantiomeric excess of the product from the hydrogenation of dimethyl itaconate (**104**) was determined through chiral HPLC and confirmed with the racemic compound, which was obtained from Sigma-Aldrich. The product was concentrated under reduced pressure and a solution was prepared in THF at a concentration of 2 mg/mL. Next, 3 μ L was injected into the HPLC under the following conditions: 30°C, 0.8 mL/min flow rate, mobile phase of 98:2 hexane: isopropanol. The retention times for the two enantiomers were 7.5 min and 9.7 min.

References

- (1) (a) Knowles, W. S. *Acc. Chem. Res.* **1983**, *16*, 106. (b) Knowles, W. S. *Angew. Chem. Int. Ed.* **2002**, *41*, 1998. (c) *Asymmetric Catalysis on Industrial Scale*; Blaser, H. U., Schmidt, E., Eds.; Wiley-VCH: Weinheim, Germany, **2004**. (d) Knowles, W. S. *Acc. Chem. Res.* **1983**, *16*, 106.
- (2) (a) Ager, D. J.; de Vries, A. H. M.; de Vries, J. G. *Chem. Soc. Rev.* **2012**, *41*, 3340. (b) Hewitt, B. D.; Burk, M. J.; Johnson, N. B. *PCT Pat. Appl.* **2000**, WO0055150. (c) Surtees, J.; Marmon, V.; Differding, E.; Zimmermann, V. *PCT Pat. Appl.* **2001**, WO01/64637. (d) Robinson, A.; Li, H.-Y.; Feaster, J. *Tetrahedron Lett.* **1996**, *37*, 8321.
- (3) (a) *Modern Rhodium-Catalyzed Organic Reactions*; Evans, P. A., Ed.; Wiley-VCH: Weinheim, Germany, **2005**. (b) Tang, W.; Zhang, X. *Chem. Rev.* **2003**, *103*, 3029.
- (4) (a) Rossen, K.; Weissman, S. A.; Sager, J.; Reamer, R. A.; Askin, D.; Volante, R. P.; Reider, P. J. *Tetrahedron Lett.* **1995**, *36*, 6419. (b) Donate, P. M.; Frederico, D.; da Silva, R.; Constantino, M. G.; Del Ponte, G.; Bonatto, P. S. *Tetrahedron: Asymmetry* **2003**, *14*, 3253.
- (5) Miyashita, A.; Takaya, H.; Souchi, T.; Noyori, R. *Tetrahedron* **1984**, *40*, 1245.

- (6) (a) Noyori, R. *Angew. Chem. Int. Ed.* **2013**, *52*, 79. (b) Noyori, R.; Kitamura, M.; Ohkuma, T. *Proc. Natl. Acad. Sci.* **2004**, *101*, 5356. (c) Genet, J.-P. *Reduction of Functionalized Alkenes in Modern Reduction Methods (Chapter 1)*; Andersson, P. G., Munslow, I. J., Eds.; Wiley-VHC: Weinheim, Germany, **2008**. (d) Landis, C. R.; Halpern, J. *J. Am. Chem. Soc.* **1987**, *109*, 1746. (e) Brown, J. M.; Chaloner, P. A. *J. Am. Chem. Soc.* **1980**, *102*, 3040.
- (7) (a) Alamé, M.; Jahjah, M.; Pellet-Rostaing, S.; Lemaire, M.; Meille, V.; de Bellefon, C. *J. Mol. Catal. A: Chem.* **2007**, *271*, 18. (b) Alamé, M.; Jahjah, M.; Berthod, M.; Lemaire, M.; Meille, V.; de Bellefon, C. *J. Mol. Catal. A: Chem.* **2007**, *271*, 205. (c) Berthod, M.; Mignani, G.; Woodward, G.; Lemaire, M. *Chem. Rev.* **2005**, *105*, 1801.
- (8) (a) Rankic, D. A.; Hopkins, J. M.; Parvez, M.; Keay, B. A. *Synlett.* **2009**, *15*, 2513. (b) Hopkins, J. M.; Dalrymple, S. A.; Parvez, M.; Keay, B. A. *Org. Lett.* **2005**, *7*, 3765. (c) Cram, D. J.; Helgeson, R. C.; Peacock, S. C.; Kaplan, L. J.; Domeier, L. H.; Moreau, P.; Koga, K.; Mayer, J. M.; Chao, Y.; Siegel, M. G.; Hoffman, D. H.; Sogah, G. D. Y. *J. Org. Chem.* **1978**, *43*, 1930.
- (9) (a) Saluzzo, C.; Lemaire, M. *Adv. Synth. Catal.* **2002**, *344*, 915. (b) Shimazu, S.; Ro, K.; Sento, T.; Ichikuni, N.; Uematsu, T. *J. Mol. Catal. A: Chem.* **1996**, *107*, 297. (c) Guerreiro, P.;

- Ratovelomanana-Vidal, V.; Genêt, J.-P.; Dellis, P. *Tetrahedron Lett.* **2001**, *42*, 3423.
- (10) (a) She, J.; Ye, L.; Zhu, J.; Yuan, Y. *Catal. Lett.* **2007**, *116*, 70. (b) Bayardon, J.; Holz, J.; Schäffner, B.; Andrushko, V.; Verevkin, S.; Preetz, A.; Börner, A. *Angew. Chem. Int. Ed.* **2007**, *46*, 5971. (c) Yinghuai, Z.; Carpenter, K.; Bun, C. C.; Bahnmüller, S.; Ke, C. P.; Srid, V. S.; Kee, L. W.; Hawthorne, M. F. *Angew. Chem. Int. Ed.* **2003**, *42*, 3792. (d) Altinel, H.; Avsar, G.; Yilmaz, M. K.; Guzel, B. *J. Supercrit. Fluids* **2009**, *51*, 202.
- (11) Bainchini, C.; Barbaro, P.; Dal Santo, V.; Gobetto, R.; Meli, A.; Oberhauser, W.; Psaro, R.; Vizza, F. *Adv. Synth. Catal.* **2001**, *343*, 41.
- (12) McDonald, A. R.; Müller, C.; Vogt, D.; van Klink, G. P. M.; van Koten, G. *Green Chem.* **2008**, *10*, 424.
- (13) Wiles, C.; Watts, P. *Green Chem.* **2012**, *14*, 38.
- (14) (a) Anderson, N. G. *Org. Process Res. Dev.* **2012**, *16*, 852. (b) Proctor, L. D.; Warr, A. J. *Org. Process Res. Dev.* **2002**, *6*, 884.
- (15) Chinnusamy, T.; S, S. Y.; Hager, M.; Kreitmeier, P.; Reiser, O. *ChemSusChem* **2012**, *5*, 247.
- (16) (a) Irfan, M.; Glasnov, T. N.; Kappe, C. O. *ChemSusChem* **2011**, *4*, 300. (b) Noël, T.; Naber, J. R.; Hartman, R. L.; McMullen, J. P.; Jensen, K. F.; Buchwald, S. L. *Chem. Sci.* **2011**, *2*, 287. (c) Hintermair, U.; Höfener, T.; Pullmann, T.; Franciò, G.; Leitner, W.

- ChemCatChem*. **2010**, 2, 150. (d) Beigi, M.; Haag, R.; Liese, A. *Adv. Synth. Catal.* **2008**, 350, 919.
- (17) (a) Al Herz, M. A.; Tsoligkas, A. N.; Simmons, M. J. H.; Wood, J. *Appl. Catal. A: Gen.* **2011**, 396, 148. (b) Stephenson, P.; Licence, P.; Ross, S. K.; Poliakoff, M. *Green Chem.* **2004**, 6, 521. (c) Kunzle, N.; Soler, J. W.; Baiker, A. *Catal. Today* **2003**, 79-80, 503.
- (18) Ruta, M.; Yuranov, I.; Dyson, P. J.; Laurenczy, G.; Kiwi-Minsker, L. *J. Catal.* **2007**, 247, 269.
- (19) (a) Johnson, M. D.; May, S. A.; Clavin, J. R.; Remacle, J.; Stout, J. R.; Diserod, W. D.; Zaborenko, N.; Haeberle, B. D.; Sun, W.-M.; Miller, M. T.; Brennan, J. *Org. Process Res. Dev.* **2012**, 16, 1017. (b) de Bellefon, C.; Lamouille, T.; Pestre, N.; Grenouillet, P.; Hessel, V. *Adv. Synth. Catal.* **2003**, 345, 190. (c) Newton, S.; Ley, S. V.; Arcé, E. C.; Grainger, D. M. *Adv. Synth. Catal.* **2012**, 354, 1805.
- (20) Jones, R. V.; Godorhazy, L.; Varga, N.; Szalay, D.; Urge, L.; Darvas, F. *J. Comb. Chem.* **2006**, 8, 110.
- (21) Bryan, M. C.; Wernick, D.; Hein, C. D.; Petersen, J. V.; Eschelbach, J. W.; Doherty, E. M. *Beilstein J. Org. Chem.* **2011**, 7, 1141.
- (22) (a) Szöllősi, G.; Hermán, B.; Fülöp, F.; Bartók, M. *React. Kinet. Catal. Lett.* **2006**, 88, 391. (b) Szöllősi, G.; Makra, Z.; Fülöp, F.; Bartók, M. *Catal. Lett.* **2011**, 141, 1616.

- (23) Shi, L.; Wang, X.; Sandoval, C. A.; Wang, Z.; Li, H.; Wu, J.; Yu, L.; Ding, K. *Chem. Eur. J.* **2009**, *15*, 9855.
- (24) (a) Balogh, S.; Farkas, G.; Madarász, J.; Szöllősy, Á.; Kovács, J.; Darvas, F.; Urge, L.; Bakos, J. *Green Chem.* **2012**, *14*, 1146. (b) Augustine, R. L.; Tanielyan, S. K.; Mahata, N.; Gao, Y.; Zsigmond, A.; Yang, H. *Appl. Catal., A.* **2003**, *256*, 69.
- (25) (a) Preetz, A.; Fischer, C.; Kohrt, C.; Drexler, H.-J.; Baumann, W.; Heller, D. *Organometallics* **2011**, *30*, 5155. (b) Miyashita, A.; Yasuda, A.; Takaya, H.; Toriumi, K.; Ito, T.; Souchi, T.; Noyori, R. *J. Am. Chem. Soc.* **1980**, *102*, 7932.
- (26) Corkum, E. G.; Kalapugama, S.; Hass, M. J.; Bergens, S. H. *RSC Advances* **2012**, *2*, 3473.
- (27) (a) Tang, W.; Liu, D.; Zhang, X. *Org. Lett.* **2003**, *5*, 205. (b) Wu, S.; Zhang, W.; Zhang, Z.; Zhang, X. *Org. Lett.* **2004**, *6*, 3565. (c) Schwarze, M.; Milano-Brusco, J. S.; Stempel, V.; Hamerla, T.; Wille, S.; Fischer, C.; Baumann, W.; Arlt, W.; Schomäcker, R. *RSC Advances* **2011**, *1*, 474. (d) Burgemeister, K.; Franciò, G.; Hugl, H.; Leitner, W. *Chem. Commun.* **2005**, 6026. (e) Almena, J.; Monsees, A.; Kadyrov, R.; Riermeier, T. H.; Gotov, B.; Holz, J.; Börner, A. *Adv. Synth. Catal.* **2004**, *346*, 1263.
- (28) (a) Schmidt, T.; Drexler, H.-J.; Sun, J.; Dai, Z.; Baumann, W.; Preetz, A.; Heller, D. *Adv. Synth. Catal.* **2009**, *351*, 750. (b)

- Schmidt, T.; Baumann, W.; Drexler, H.-J.; Heller, D. *J. Organomet. Chem.* **2011**, 696, 1760.
- (29) Botman, P. N. M.; Fraanje, J.; Goubitz, K.; Peschar, R.; Verhoeven, J. W.; van Maarseveen, J. H.; Hiemstra, H. *Adv. Synth. Catal.* **2004**, 346, 743.
- (30) Fernández-Zúmel, M. A.; Lastra-Barrera, B.; Scheele, M.; Díez, J.; Crochet, P.; Gimeno, J. *Dalton Trans.* **2010**, 39, 7780.
- (31) (a) Bemis, L.; Clark, H. C.; Davies, J. A.; Fyfe, C. A.; Wasylishen, R. E. *J. Am. Chem. Soc.* **1982**, 104, 438. (b) Wu, G.; Wasylishen, R. E. *Inorg. Chem.* **1992**, 31, 145.
- (32) (a) *Neutron Activation Analysis*; Soete, D., Gijbels, R., Hoste, J., Eds.; Wiley-Interscience, **1972**. (b) Byrne, A. R. *Fresenius J. Anal. Chem.* **1993**, 345, 144.
- (33) Shinkai, H.; Toi, K.; Kumashiro, I.; Seto, Y.; Fukuma, M.; Dan, K.; Toyoshima, S. *J. Med. Chem.* **1988**, 31, 2092.
- (34) Bergerioux, C.; Kennedy, G.; Zikovosky, L. *J. Radioanal. Chem.* **1979**, 50, 22.

Chapter 6

Concluding Remarks

Homogeneous asymmetric catalysis is arguably the most attractive method for the production of enantiopure compounds,¹ however, there are some inherent challenges that ultimately hinder its practical application. Specifically, the catalysts themselves are typically quite expensive and toxic,² and product contamination caused by metal leaching is often encountered.³ As a result, immobilization of homogeneous chiral catalysts is often pursued as these catalysts can potentially be quantitatively recovered from the product mixture and reused.^{1,4} However, the majority of these attempts have failed, resulting in immobilized catalysts that display lower activities and selectivities than their homogeneous catalyst analogues. Further, the ideal immobilized homogeneous asymmetric catalyst should be applicable to a wide variety of reactions, easily recovered from the reaction mixture, sustain multiple reuses with constant activity and selectivity, which are comparable or better than the homogeneous analogue, and limit the amount of metal leached into the reaction mixture. As well, the immobilization technique should be adaptable to a variety of homogeneous catalysts. The research presented in this dissertation is thus a major step forward towards achieving these goals.

Section A: Synthesis of Polymer-Supported Rhodium Catalyst-Organic Frameworks via AltROMP Assembly

In this work, the previously synthesized ring-opening metathesis polymerization (ROMP) active BINAP ligand, (*R*)-5,5'-dinorimido-BINAP (**36**),⁵ was utilized to prepare the metal containing monomers (MCMs) [RhCl((*R*)-5,5'-dinorimido-BINAP)]₂ (**38**) and [Rh(NBD)((*R*)-5,5'-dinorimido-BINAP)](SbF₆) (**40**) through reaction with [RhCl(C₂H₄)₂]₂ (**37**) and [Rh(NBD)₂](SbF₆) (**39**), respectively. As was the case for **36**, monomers **38** and **40** were formed as mixtures of three diastereomeric atropisomers, two with a C₂-axis of rotation and one without. The origin of the three NMR-distinct atropisomers was the relative rotameric orientations of the norimido groups about the aryl-N bond. Interestingly, it was shown that interconversion of the atropisomers was influenced by the electron density of the rhodium metal center and the binaphthyl framework. Specifically, the [Rh(I)Cl] moiety of **38** was discovered to be a poorer π-donor than the [Rh(I)(NBD)]⁺ moiety of **40**, resulting in a decrease in the rate of interconversion between the atropisomers of **38** compared to **40**. Future investigations of these compounds should focus on determining the rates of interconversion and studying the effect of interconversion on the alternating ROMP (altROMP) assembly and the catalytic properties of the resulting catalyst-organic frameworks.

The previously developed altROMP assembly^{5,6} was employed to prepare the polymer-supported catalyst-organic frameworks **41** and **42**. By design, altROMP between COE and the norbornyl groups in either **38** or **40**, in the presence of the Grubbs 1st generation catalyst (**23**), resulted in the assembly of extended, three-dimensional catalyst-organic frameworks with the catalyst complex as the crosslinking units. Although more characterization of frameworks **41** and **42** is required (see Section E of this chapter), NMR studies suggest that the electronic environment of the rhodium metal center was not significantly altered during polymerization. Moreover, we showed that the altROMP methodology, previously utilized in the preparation of ruthenium hydrogenation catalysts,^{5,6} can be easily adapted and applied to other homogeneous catalysts. The frameworks were deposited on either BaSO₄ or Ba-L-tartrate to improve mass transport to the catalytic active sites and improve mechanical stability toward rapidly stirred batch reactions and were then tested in the intramolecular cycloisomerization of 1,6-enynes, isomerization of allylic alcohols and continuous-flow hydrogenation reactions.

Section B: Intramolecular 1,6-Enyne Cycloisomerizations

In this work, the newly prepared catalyst-organic framework **41** was tested in the intramolecular cycloisomerization of 1,6-enynes **53** and **46**. **41** sustained six reuses with no loss in activity or selectivity (total TON =

620, >95% ee) in the cycloisomerization of **53** and four reuses (total TON = 360, >99.9% ee) in the cycloisomerization of **46** (S/C/AgSbF₆ = 20/1/2 for the first run and S/C = 100/1 for all subsequent runs). The difference in activity between the two substrates was attributed to competitive η⁶-binding of the aromatic ring on the substrate or cycloisomerized product of **46** to the rhodium metal center, which is not present in substrate **53**.

In batch studies, **41** sustained up to 800 TOs (S/C/AgSbF₆ = 1000/1/5, >95% ee) and 890 TOs (S/C/AgSbF₆ = 1600/1/5, >99.9% ee) in the cycloisomerization of **53** and **46**, respectively. To the best of our knowledge, these are the highest TONs reported for any cycloisomerization reaction. It was also discovered that the coordinating ability of the solvent has a significant effect on the reusability and batch reactivity of the catalyst, however choice of solvent has no effect on the overall enantioselectivity. Thus, the catalyst-organic framework can be tailored for reuse or batch reactions simply by selecting an appropriate solvent.

Comparison to the homogeneous analogue, [RhCl((*R*)-BINAP)]₂, showed that **41** was not only more active but also more selective in the cycloisomerization of **53** as a mixture of isomerized products was obtained with the homogeneous catalyst. This is the first example of a polymer-supported catalyst that is both more active and selective than the homogeneous catalyst analogue. Future work should be focused on determining the origins of the high activity and selectivity of **41** (see

Section E of this chapter). Framework **41** was also utilized in the production of a key intermediate of the pharmaceutical (+)-pilocarpine (S/C/AgSbF₆ = 300/1/5, TON = 285, >99.9% ee), illustrating the potential industrial application of the polymer-supported rhodium catalyst-organic framework.

Section C: Solvent-Free Allylic Alcohol Isomerizations

In this work, framework **41** was tested in the 100% atom economic, solvent-free isomerization of primary and secondary allylic alcohols. **41** provided the highest TONs to date (up to 38,000) for the rhodium catalyzed isomerization of secondary allylic alcohols, with catalyst loadings as low as 0.0025 mol%. **41** also proved to be more active than the homogeneous catalyst analogue in the isomerization of 3-buten-2-ol (**71**). As well, we reported the kinetic resolution of **71** with enantioselectivity comparable to the most recent literature report published by Gimeno and coworkers⁷ (15% ee vs 17% ee, respectively). Future work should be focused on determining the origins of the high activity (see Section E of this chapter) and optimizing the conditions for the kinetic resolution.

Interestingly, we discovered that the solvent-free isomerization of primary allylic alcohol 1-propen-3-ol resulted in the formation of not only the isomerized aldehyde product but also a hemiacetal side product (formed from reaction between the aldehyde and the starting allylic

alcohol). As well, it was discovered that the identity of the silver salt plays a substantial role in the catalytic activity of the framework. Specifically, the solubility and coordinating ability of the silver salt appear to dictate the extent of catalyst activation and, by extension, the catalytic activity of the framework. There are, however, many more factors that could be at play and future work should be focused on determining what these factors are and their effects on catalytic activity. Finally, we discovered that the framework appears to contain a substrate size threshold that, if exceeded, significantly affects the rate and extent of reaction. Future investigations should be done on elucidating the structure and determining the size of the pores within the framework, which would allow for better system optimization.

Section D: Continuous-Flow Hydrogenations

In this work, frameworks **41** and **42** were adapted for use in the H-Cube® continuous-flow hydrogenation reactor and then tested in the asymmetric hydrogenation of olefin-containing substrates. Framework **42** exhibited remarkable activity in the hydrogenation of a variety of substrates, including allylic alcohols, dehydro amino acids, unsaturated dicarboxylic acids and unsaturated diesters, and sustained up to approximately 55,700 TONs over a period of 30 days in the H-Cube®. Through solid state ³¹P-NMR and neutron activation analysis, it was

determined that catalyst deactivation was due to oxidation from the sheer volume of solvent passed through the catalyst over a 30 day period rather than rhodium leaching or an intrinsic catalyst lifetime. This suggests that the catalyst lifetime can be extended past 30 days if the proper precautions are taken and if the CatCart® itself does not significantly degrade around the catalyst. As well, in preliminary experiments, framework **41** supported on Ba-L-tartrate gave >99.9% ee in the hydrogenation of itaconic acid.

Interestingly, it was discovered that **42** was completely inactive in the absence of hydrogen, suggesting that the mechanism of hydrogenation proceeds via the initial formation of metal-hydrides. As well, we discovered that high concentrations of hydrogen are required for high catalytic activity in the H-Cube® as hydrogen is continually lost throughout each continuous-flow run preventing the regeneration of the catalytic metal-hydride complex.

As this was a preliminary study, future investigations should be focused on optimizing the frameworks and reaction conditions and investigating additional substrates. As well, the *trans*-[RuCl₂((*R*)-5,5'-dinorimido-BINAP)((*R,R*)-dpen)] framework (**26**), previously synthesized by Corbin Ralph,⁵ should be adapted for use in the H-Cube® continuous-flow reactor and tested in the asymmetric hydrogenation of ketones, imines, etc.

Section E: Future Directions

As was shown in this dissertation, the polymer-supported rhodium catalyst-organic frameworks **41** and **42** have not only exhibited remarkable reusability, but have also shown to be more active and selective than their homogeneous catalyst analogues. We believe that the possible origins of this enhanced activity and selectivity include catalyst/framework-support interactions (i.e. the BaSO₄ interaction with catalytic active sites and/or the framework, swellability, etc.) and framework-catalyst interactions (i.e. cross-linking, size exclusion, etc.), but have yet to confirm these suspicions. To this end, future efforts should be focused on extensive catalyst characterization. Scanning Electron Microscopy (SEM) and Transmission Electron Microscopy (TEM) of the polymers before and after deposition onto the barium salt support would be useful in obtaining the morphology of the polymers as well as providing information on the density/location of the catalytic active sites within the frameworks. Dynamic Light Scattering (DLS) and Gel Permeation Chromatography (GPC) would probe the poly-dispersity of the polymers and provide a rough estimate of molecular weight. As well, solid state ³¹P-NMR and ¹⁰³Rh-NMR spectroscopy would be useful in probing the environment of the metal centers in the polymers, supported-polymers and active catalysts.

In addition to catalyst characterization, the modular nature of the frameworks (i.e. the support, spacer monomer and catalyst monomer) allows for relatively easy modification. By changing the support and introducing spacer monomers with varying lengths, functional groups and stereochemistry we may be able to identify the features of the frameworks that dictate the overall activity of the catalyst. As well, these modifications could potentially result in frameworks with even better selectivity, activity and reusability.

As was demonstrated in this work, the altROMP methodology is a superior method for preparing highly active, selective and reusable polymeric catalysts and can be adapted quite easily to different homogeneous catalysts. In addition, our utilization of solvent-free and continuous-flow catalysis has highlighted the industrial viability of the frameworks and the commercialization of this technology is currently underway. It is our hope that this work will continue to contribute to the development of more sustainable, cost-effective applications of asymmetric catalysis.

References

- (1) (a) *Fundamentals of Asymmetric Catalysis*; Walsh, P. J., Kozlowski, M. C., Eds.; University Science Books: Sausalito, California, **2009**.
(b) Noyori, R. *Asymmetric Catalysis in Organic Synthesis*; Wiley and Sons, Inc.: New York, **1994**. (c) Noyori, R. *Angew. Chem. Int. Ed.* **2002**, *41*, 2008. (d) Farina, C.; Reeves, J. T.; Senanayake, C. H.; Song, J. H. J. *Chem. Rev.* **2006**, *106*, 2734.
- (2) (a) Garrett, C. E.; Prasad, K. *Adv. Synth. Catal.* **2004**, *346*, 889. (b) Hawkins, J. M.; Watson, T. J. N. *Angew. Chem. Int. Ed.* **2004**, *43*, 3224.
- (3) Cole-Hamilton, D. J. *Science* **2003**, *299*, 1702.
- (4) (a) *Chiral Catalyst Immobilization and Recycling*; De Vos, D. E., Vankelecom, I. F. J., Jacobs, P. A., Eds.; Wiley-VHC: Weinheim, Germany, **2000**. (b) Heitbaum, M.; Glorius, F.; Escher, I. *Angew. Chem. Int. Ed.* **2006**, *45*, 4732.
- (5) Ralph, C. K.; Bergens, S. H. *Organometallics* **2007**, *26*, 1571.
- (6) Ralph, C. K.; Akotsi, O. M.; Bergens, S. H. *Organometallics* **2004**, *23*, 1484.
- (7) Fernández-Zúmel, M. A.; Lastra-Barreira, B.; Scheele, M.; Díez, J.; Crochet, P.; Gimeno, J. *Dalton Trans.* **2010**, *39*, 7780.